BUCKLING OF SHORT, THIN-WALLED CYLINDERS, AS APPLIED TO STORAGE TANKS.

Geraldine Touche du Poujol

University of Natal

Durban

This thesis is submitted in fulfilment of the academic requirements for the Degree of Master of Science in Engineering in the School of Mechanical Engineering, University of Natal.

December 2001

Supervisors :

Professor S. Adali

Mr R Bodger

Acknowledgements

I would like to thank my supervisors Mr R. Bodger and Professor S. Adali for their guidance and encouragement.

Financial assistance from SASOL and the National Research Foundation of South Africa is gratefully acknowledged.

Declaration

I, Geraldine Touche du Poujol, student number 961078017, hereby declare that this dissertaion is my own unaided work, unless otherwise stated. It is submitted for the Degree of Master of Science in Engineering, to the University of Natal in Durban. Neither this dissertation, nor part thereof, has been submitted before for any degree or examination at any other university.

As the candidate's supervisors we have/have not approved this thesis/dissertation for submission

Signed : ..... Name : ..... Date : .....

Signed : ..... Name : ..... Date : .....

Abstract

This is an investigation of the buckling characteristics of short, thin-walled cylinders. This study was required as large storage tanks, which were converted from floating roof to fixed roofed tanks, were found to buckle when severe atmospheric temperature drops and thus pressure differentials occurred. These severe ambient temperature changes are characteristic of the Highveld in South Africa where the tanks in question are situated. Since this modification is an uncommon procedure, codes of practice for storage vessels do not cover this type of cylinder. For the same reason, research performed in this field is limited.

Buckling due to axial loading, lateral external pressure, hydrostatic pressure and a combination of axial loading and hydrostatic pressure are explored in this study. To compare with and verify theory, existing research for each case is examined, and the Finite Element Analysis package MSC Nastran used to determine trends. In some cases, to the best of the author's knowledge, no research exists and numerical analysis is performed to establish the relationships present in those cases. The study is extended to include the design of imperfect cylinders, as defined in the tank code AD Merkblatter where it is stated as being dependant on the major and minor diameters of the imperfect section. The study is also extended to the case of variable wall thickness cylinders, where the thickness variation is symmetrical about the axis of the cylinder.

Contents

List of Figures

List of symbols used

α	Angle of taper [^{0}]
β	Change in curvature
χ	$= \frac{\pi r}{l}$
ϵ	Strain [MPa]
ε	Non-dimensional parameter indicating the thickness non-uniformity, where $\varepsilon = -\frac{l}{2t_0}\tan\alpha$
$\phi = \phi_1$	$= \frac{qr(1-\nu^2)}{Et}$
ϕ_2	$= -\frac{q(1-\nu^2)}{Et}$
γ	Shear Strain, and a free parameter
κ	$= \frac{t^2}{12r^2}$
λ	Eigenvalue
ν	Poisson's ratio
θ	Angle of displacement
σ	Stress [MPa]
τ	Shear stress
Ω	Thickness variation parameter [%]
∇^2	Operator where $\nabla^2 = \frac{\partial^2}{\partial x^2} + \frac{\partial^2}{\partial x^2}$
∇^4	Operator where $\nabla^4 = \frac{\partial^4}{\partial x^4} + 2\frac{\partial^4}{\partial x^2 \partial y^2} + \frac{\partial^4}{\partial x^4}$
A	Amplitude of imperfection [m] $A = e$

$\bar{A}$ Magnitude of imperfection relative to the shell thickness $\bar{A} = \dfrac{A}{t}$

D Flexural rigidity where $D = \dfrac{Et^3}{12(1-\nu^2)}$

e Eccentricity [m] $e = A$

E Young's modulus

G Shear Modulus [MPa]

k Stiffness of element

K Stiffness of element

k_d Stiffness of system

K_d Differential stiffness of system

l Length/height of cylinder [m]

M Moment [Nm]

m Number of lobes in the longitudinal direction

N Parameter where $N = \left(\dfrac{l}{r}\right)^2 \left(\dfrac{r}{t}\right)$

n Number of lobes in the circumferential direction

$\bar{n}$ Number of lobes in the initial deformation pattern

N_x, N_y, N_{xy}, N_{yx} Resultant force per unit length

P Axial load [N]

P_a Applied load

$\bar{P}$ Total axial load [N]

P_{cl} Classical buckling load, ie. P_{cr} for a perfect cylinder

P_{cr} Critical buckling axial load

PE	Potential energy
$\widetilde{P}$	Load parameter where $\widetilde{P} = \frac{Pr^2}{Et^2}\sqrt{3(1-\nu^2)}$
Q	Parameter where $Q = \left(\frac{l}{r}\right)^2 \left(\frac{r}{t}\right)^3 \frac{q_{cr}}{E}$
q	External pressure [Pa]
$\widetilde{q}$	Pressure parameter where $\widetilde{q} = \frac{qr^2}{Et^2}\sqrt{3(1-\nu^2)}$
q_{cl}	Classical buckling pressure, ie. q_{cr} for a perfect cylinder
q_{cr}	Critical buckling external pressure
Q_x, Q_y	Shear forces per unit length
r	Radius of cylinder [m]
r_{max}	Maximum (major) diameter of an ellipse [m]
r_{mean}/r_m	Mean radius, or equivalent perfect circle radius [m]
r_{min}	Minimum (minor) diameter of an ellipse [m]
R_p	Parameter where $R_p = \frac{q_{cr}}{q_{cl}}$
R_x	Parameter where $R_p = \frac{P_{cr}}{P_{cl}}$
S_U	Ultimate tensile strength [MPa]
S_Y	Yield strength [MPa]
ΔT	Work
t	Cylinder wall thickness [m]
t_m	Cylinder mean wall thickness taken at the mid-length [m]
$\{u\}$	Vector of displacement
u	Imperfection [%], given by $u = 2\frac{r_{max} - r_{min}}{r_{max} + r_{min}} \times 100\%$

U, U_t, U_b, U_s Total strain energy, strain energy due to twisting, bending, and stretching respectively

u,v,w Displacement in the x,y and z-directions respectively

u', v', w' $\frac{\partial u}{\partial x}$, $\frac{\partial v}{\partial x}$ and $\frac{\partial w}{\partial x}$ respectively

$\dot{u}$, $\dot{v}$, $\dot{w}$ $\frac{\partial u}{\partial \theta}$, $\frac{\partial v}{\partial \theta}$ and $\frac{\partial w}{\partial \theta}$ respectively

w_0 Initial deflection

Z Batdorf parameter where $Z = \frac{l^2}{rt}\sqrt{1-\nu^2}$

z Distance to the neutral axis [m]

Chapter 1

THE THEORY OF BUCKLING

1.1 Stability theory

The phenomenon of buckling can be illustrated using a simple example of an idealised structure, shown in figure 1-1.

Member AB is a rigid bar that is pinned at the base end and supported by a spring at the top, with a stiffness of k. This stiffness is also known as the spring constant. An axial force P is centrally applied to the beam such that it is perfectly aligned with the axis of the beam. In this state the spring has no force in it. Suppose then that the beam is then disturbed by an external force, such that it rotates through an angle θ about support A. If the force P is small,

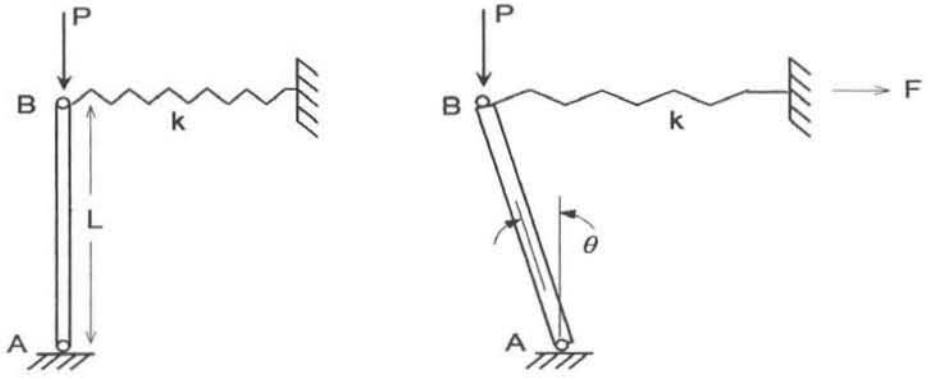

Figure 1-1: Simple rigid bar. Reproduced from Timoshenko [62].

the system will return to its initial position when the disturbing external force is removed. Thus this system is stable. But if the force P is large, when the external disturbing force is removed, the system will continue to rotate and the system will collapse. Thus this latter system is unstable. This system can be analysed in more detail if its static equilibrium is considered. If the bar is rotated slightly, the spring elongates to a length θL, where L is the length of the beam. The force in the spring is therefore

$$F = k\theta L \tag{1.1}$$

This force creates a moment about A of FL, which is $k\theta L^2$, in the clockwise direction. Because this force is the spring tension, the tendency of this moment is to return it to its original position. Therefore, $k\theta L^2$ is known as the restoring moment. The force P tends to overturn the bar by creating a moment of $P\theta L$. Thus this moment is known as the overturning moment. Generally, if the restoring moment is larger than the overturning moment, then the system is stable and the bar returns to the initial vertical position. The converse is obviously also true. Therefore the following conditions exist :

If $P\theta L < k\theta L^2$, or $P < kL$, the system is stable.

If $P\theta L > k\theta L^2$, or $P > kL$, the system is unstable.

The shift from a stable system to an unstable system occurs at $P = kL$, and this value of loading is known as the critical load. So, one can see that a system is stable when $P < P_{cr}$, and unstable when $P > P_{cr}$. Even when P is greater than P_{cr}, and the beam is in the vertical position (thus in equilibrium), this equilibrium is unstable and cannot be maintained. Even the slightest disturbance will cause the beam to collapse. At the critical load, the overturning and returning moments are equal at small values of θ. Thus the beam is in equilibrium at the critical load for small values of θ, and this equilibrium is known as neutral equilibrium.

These equilibrium relationships are shown in figure 1-2, on graphs of P versus θ. The two heavy lines represent the equilibrium conditions. At point B, where

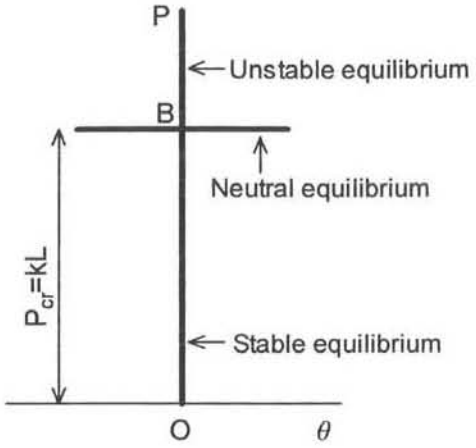

Figure 1-2: Figure showing the bifurcation point. Reproduced from [62].

the equilibrium lines branch, is the bifurcation point. The neutral equilibrium condition extends as a horizontal line because the angle θ may be clockwise or anti-clockwise. One can see that the line only extends a short distance, as our analysis is based on the assumption that the angle θ is small. This assumption of the angle being small is valid, because the angle is small when buckling begins and the bar departs from the vertical position.

If we consider a shell carrying a certain load (basic load), it produces a basic stress and basic displacements. A small deformation then disturbs the elastic equilibrium, which is produced by certain external forces. When these forces are removed, if the disturbance vanishes the equilibrium is stable. When the basic load is increased, less force may be required to produce the same disturbance until, a point is reached where the disturbance is produced without any external forces. In this particular case, the equilibrium is neutral. The smallest basic load at which the system is in neutral equilibrium is called the critical or buckling load. A disturbance may then occur, which results in the bucking of a shell. When the basic load is increased beyond the critical point, the equilibrium becomes unstable, and any external disturbance causes the shell to entirely leave its initial position of equilibrium, hence the shell buckles.

To find the buckling load the differential equations for the disturbed equilibrium

are formulated for the disturbed equilibrium without an external disturbing load. These equations contain terms with the additional stresses for the disturbing load as well. These terms are very small, since the disturbance is supposed to be very small. One must also remember that the basic load now acts on a slightly deformed element. Since the conditions of equilibrium are satisfied and Hooke's law expresses the stress resultants in terms of the displacements, a set of homogeneous linear differential equations for the displacements u, v and w result. Looking at a simple example of a column shown in figure 1-3 force P is the basic load and the basic stress system, N, consists only of the axial load. Therefore $N = -P$. If the equilibrium is then disturbed by a lateral deflection

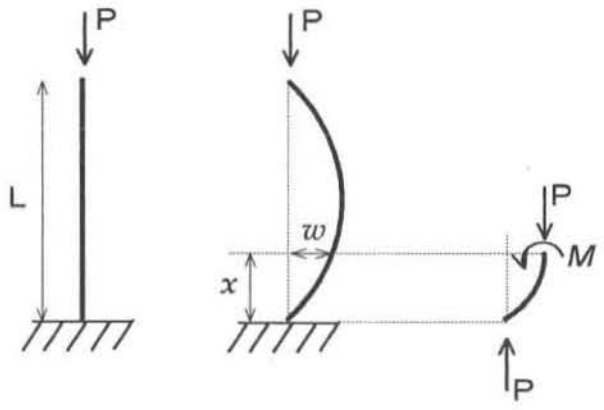

Figure 1-3: Figure showing the Euler column. Reproduced from Flügge [18].

w, the equation of moments is

$$M - Pw = 0. \tag{1.2}$$

Comparing this to a cylinder by using the basic differential equation of the deflection curve of a beam,

$$M = -EI\frac{d^2w}{dx^2} \tag{1.3}$$

and substituting this into equation 1.2

$$EI\frac{d^2w}{dx^2} + Pw = 0 \tag{1.4}$$

The solution of this equation is a homogeneous linear differential equation of the second order with constant coefficients. For convenience, let

$$k^2 = \frac{P}{EI}$$

therefore equation 1.4 becomes

$$\frac{d^2w}{dx^2} + k^2w = 0 \tag{1.5}$$

The general solution of this equation is

$$w = A_1 \sin kx + A_2 \cos kx \tag{1.6}$$

where A_1 and A_2 are constants determined by the boundary conditions. It is found that no deflection is possible unless

$$kL = m\pi$$

$$\text{or} \qquad P = \frac{m^2\pi^2 EI}{L^2} \qquad\qquad m = 1, 2, 3 \ldots$$

whereby

$$w = A \sin \frac{m\pi x}{L}. \tag{1.7}$$

1.2 Numerical analysis of buckling

Classical shell theories can be over complicated for the needs of the designer. Therefore analysis of non-simple buckling cases are generally executed by numerical methods, which have been found to achieve a good characterisation of the shell behaviour. The most versatile and well known is the finite element method, or FEM. FEM is a method of analysis whereby three main operations are performed. The first step is to divide the shell up into small finite elements. The second step involves computing the stiffness properties of each element and putting them into a matrix. The final step is to solve the matrix for a particular applied load. The solution gives the displacements at the nodes, which, together

with the element stiffnesses, is used to calculate the element forces at the nodes and thus element stresses. These operations are executed by FEM software packages, and the package used in this study is MSC Nastran version 4.5.1.

Prior to performing a stability analysis with any finite element analysis software it is necessary to establish that the model contains a mesh density fine enough to yield accurate predictions of the buckling load. A convergence study was performed and an appropriate mesh selected for use to optimise both accuracy and reduced analysis time as a large number of analyses were to be performed.

Two kinds of buckling analyses are available in MSC Nastran, namely linear and non-linear. A linear buckling analysis assumes small deformations and a linear material whereas in a non-linear buckling analysis geometric non-linear effects and non-linear materials are considered. In the case of thin cylinders, the buckling loads obtained from the linear analysis are higher than the true bucking loads because the non-linear geometric effects are not included.

In this study the Nastran software that was available did not have the non-linear buckling solution sequence, but only the linear one. Therefore, it will be seen that the buckling results obtained numerically are notably higher than those obtained theoretically. Although there are discrepancies, the trends are continuous.

In 1995, M. H. Schneider, R. J. Feldes, J. R. Halcomb and C. C. Hoff [58] performed numerical analyses on the buckling of cylinders subjected independently to axial compression and hydrostatic pressure. In this research, among other FEM software packages, MSC Nastran was implemented and the non-linear solution sequence used. The results of the numerical analyses where then compared to bucking pressures obtained experimentally. Excellent agreement was found between the numerical and experimental results. In the case of axial loading the maximum deviation was found to be 4.7%, and 10.9% in the case of hydrostatic pressure.

Imperfect cylinders were also included in the study conducted by Schneider et

al whereby experimental models were fabricated and then measured using a scanning measuring system. These imperfect cylinders were then modelled in MSC Nastran and non-linear buckling analyses performed. The buckling pressure due to asymmetric imperfections was found to be reduced by 1.5% by experiment, but increased by 7.3% by numerical analysis.

Numerical buckling analysis takes the effect of the differential stiffness into account, which includes relationships that are functions of the geometry, element type and applied loads. Physically, the differential stiffness represents a linear approximation of the reduction of the stiffness matrix for a compressive load. In buckling analysis the eigenvalues calculated are scale factors that multiply the applied load in order to produce the buckling load. Usually only the lowest eigenvalue is of interest since the cylinder will fail before reaching any of the higher-order buckling loads. Therefore, in this study only the lowest eigenvalue was computed.

To expand, the element stiffness and differential stiffness matrices are $\left[k\right]_i$ and $\left[k_d\right]_i$ respectively. The system stiffness and differential stiffness are then

$$\begin{aligned} \left[K\right] &= \left[\sum_i^j k_i\right] \\ \left[K_d\right] &= \left[\sum_i^j k_{di}\right] \end{aligned} \tag{1.8}$$

respectively, where j is the number of elements. In order for the system to have static equilibrium the total potential energy, PE, must have a stationary value. In other words the following relationship should hold true

$$\frac{\partial\left[PE\right]}{\partial u_i} = \left[K\right]\left\{u\right\} + \left[K_d\right]\left\{u\right\} = \left\{0\right\} \tag{1.9}$$

where $\left\{u\right\}$ is the displacement vector and u_i the displacement of the i-th degreee of freedom. Equation 1.9 can be rewritten as

$$\left[\left[K\right] + P_a\left[K_d\right]\right]\left\{u\right\} = \left\{0\right\} \tag{1.10}$$

where $[K_d] = P_a[\bar{K}_d]$ and P_a the applied load. In order for equation 1.10 to have a non-trivial solution, the following relationship must be true

$$|[K] + P_a[\bar{K}_d]| = \{0\}. \tag{1.11}$$

Only particular values of P_a render equation 1.11 true, these values are the critical buckling loads.

A real structure has an infinite number of degrees of freedom. The finite element method approximates the system with a finite number of degrees of freedom. The number of buckling loads obtainable for the model in question is equal to the number of degrees of freedom of the model. In other words

$$P_{cr} = \lambda_i P_a. \tag{1.12}$$

Therefore equation 1.11 can be rewritten as

$$|[K] + \lambda_i[\bar{K}_d]| = \{0\}. \tag{1.13}$$

This is now in the form of an eigenvalue problem. Once the eigenvalues are obtained using equation 1.13, the buckling loads can be found using equation 1.12.

Chapter 2

PERFECT CYLINDRICAL SHELLS OF CONSTANT WALL THICKNESS

2.1 Introduction

The buckling of perfect cylindrical shells due to various forms of loading has been thoroughly studied for over a century, beginning with Euler's initial investigation of columns in the 18th century. In past research however, when the theoretical trends were compared with experimental data, a discrepancy always resulted. It was later found that these discrepancies were due to imperfections arising during the manufacture of the model which will be investigated later. In this chapter, the ideal cylinder is considered - one with no imperfections. The basis of the theory will be outlined, and equations determining the buckling loads produced. These equations are compared to equations obtained from other independent studies. Finally, the buckling loads are obtained for a number of cylinders of a limited range, namely with the range of ratios $0.923 \leq \frac{r}{l} \leq 1.626$, and $600 \leq \frac{r}{t} \leq 2166.7$ using the FEM analysis package Nastran. The numerical analyses are performed where the material is assumed to be carbon steel with a Young's modulus, E of 200GPa and a Poisson's Ratio, ν, of 0.32. These results are then compared with the numerous theoretical models available.

2.2 The Energy Method

When structures consist of elastic materials, ie. the material is assumed to follow Hooke's law and the stresses within the structure do not exceed the elastic limit, the equations of equilibrium can be replaced partially, or entirely, by considerations of elastic strain energy.

The law of virtual work states that during a small change in displacements, the work done by the loads (by all the external forces on the body) equals the change in elastic strain energy. It should be noted that displacements may be large, but the change in them must be small. Therefore, the law of virtual work is a simple application of the general law of conservation of energy, limited to mechanical work.

The law of virtual work can also be derived from the equations of equilibrium. For example, consider a body replaced by a system of particles interconnected by massless elastic springs. On each particle acts part-loads and the forces due to the springs. If the displacement of each particle in the x, y and z directions are u, v and w respectively, then the change in displacements are du, dv and dw. The equations of equilibrium are then applied to each particle, multiplied by du, dv and dw, and then all the equations added together. In the resulting expression, the products of the load components with the displacement components add up to the work done by the loads, while corresponding products with forces due to springs add up to the negative change in elastic strain energy, the sum of both being zero.

In practice application of the energy methods involves the assumption of a shape or mode of displacement, which approximates the actual shape. This assumption is based on general experience or experiments, or the displacements can be described by a series of component displacements with unknown magnitudes. Taken together the exact displacement can be approached with the component magnitudes being determined by the law of virtual work. Theoretically, this can

give exact solutions. This method has been found to be accurate for deflections of beams, buckling strengths, and other conditions which depend upon the state of the whole structure.

In the proceeding sections, the above procedure will be outlined. Initially for the simple case of thin flat plates and, then extended to thin cylindrical shells.

2.3 Thin flat plates

The theory of the bending of plates is similar to the theory of the bending of beams but the effect of bending in two directions instead of one, needs to be taken into account. Consider a thin flat plate subjected to pure bending as shown in figure 2-1a below.

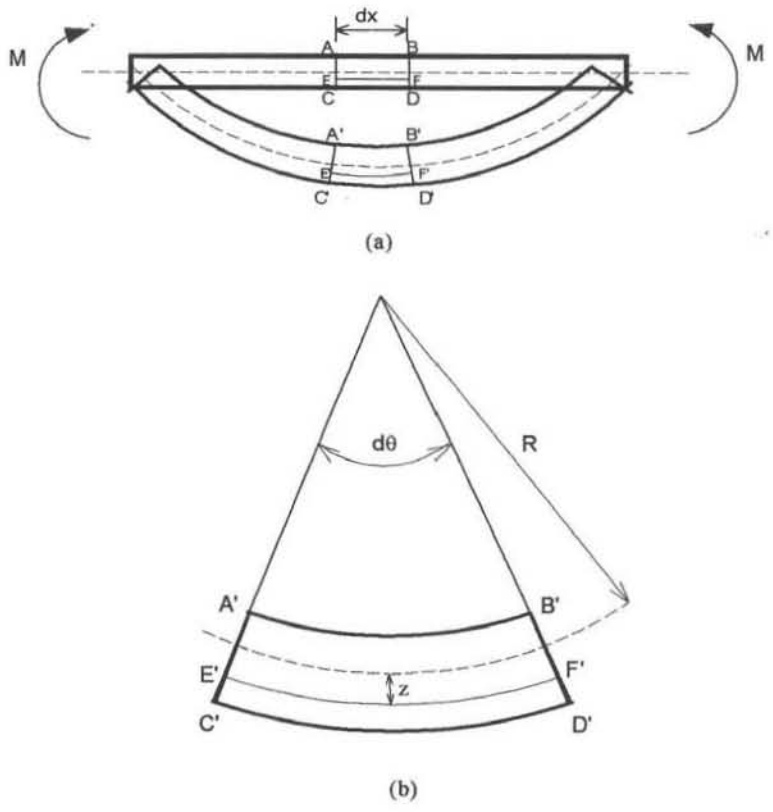

Figure 2-1: Bending of a thin flat plate. Reproduced from Benham & Crawford[64].

The element $ABCD$ deforms to $A'B'C'D'$, and the length along the neutral axis

in this deformed element is $rd\theta$. The length of the element $E'F'$ is $(R+z)d\theta$. The longitudinal strain can be found by using the change in length and the original length:

$$\epsilon_x = \frac{(r_x + z)d\theta - r_x d\theta}{r_x d\theta}. \tag{2.1}$$

Therefore,

$$\epsilon_x = \frac{z}{r_x}, \tag{2.2}$$

and similarly for the y-direction

$$\epsilon_y = \frac{z}{r_y}. \tag{2.3}$$

Consider a small element of this plate as shown in figure 2-2 with the variables as shown. When the plate deflects due to an external load, the plate will bend to have radii of curvature in the yz and zx planes. The curvature in the yz plane

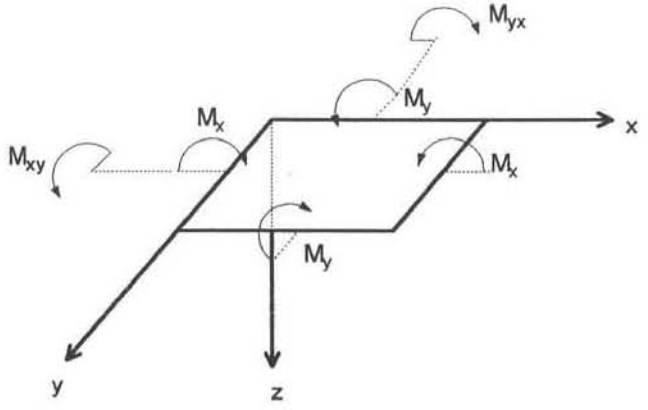

Figure 2-2: Small element of a plate. Reproduced from Benham & Crawford[64]

changes as the distance from the y-axis increases in the x-direction; similarly the curvature in the xz plane changes with increasing distance from the x-axis in the y-direction. Therefore the four corners of the element will each deflect a different amount in the z-direction. In order to adopt this shape, the element must twist as well as bend. The resistance of the plate to the external loads must therefore take into account the twisting of elements, as well as their curvatures.

There are basic assumptions to be made when using bending analysis:

- the deflections are small
- the middle plane of the plate does not stretch during bending
- plane sections rotate during bending to remain normal to the neutral surface and do not distort
- the loads are entirely resisted by bending and twisting of the plate element
- the thickness of the plate is small in comparison with other dimensions.

Now consider that this element is subjected to pure bending, where bending moments M_x and M_y per unit length are positive when acting on the middle of the plate. This plane is the neutral plane as it is unstressed, therefore the material above it is in compression and in tension below. The stress-strain relationships by elastic theory are

$$\epsilon_x = \frac{\sigma_x}{E} - \frac{\nu\sigma_y}{E}$$
$$\epsilon_y = \frac{\sigma_y}{E} - \frac{\nu\sigma_x}{E}. \tag{2.4}$$

Using these equations together with equations 2.2 and 2.3 to solve for σ_x and σ_y yields

$$\sigma_x = \frac{Ez}{1-\nu^2}\left(\frac{1}{r_x} + \frac{\nu}{r_y}\right)$$
$$\sigma_y = \frac{Ez}{1-\nu^2}\left(\frac{1}{r_y} + \frac{\nu}{r_x}\right). \tag{2.5}$$

The internal moments, due to the bending stresses acting on the edges of the element, are in equilibrium with the applied moments M_x and M_y per unit length. This equilibrium can be written as

$$\int_{-t/2}^{t/2} \sigma_x z dy dz = M_x dy$$
$$\int_{-t/2}^{t/2} \sigma_y z dx dz = M_y dx. \tag{2.6}$$

Substituting equations 2.5 and into equations 2.6 in turn yields

$$\begin{aligned} M_x dy &= \int_{-t/2}^{t/2} \frac{Ez}{1-\nu^2}\left(\frac{1}{r_x}+\frac{\nu}{r_y}\right) z dy dz \\ \therefore M_x &= \frac{E}{1-\nu^2}\left(\frac{1}{r_x}+\frac{\nu}{r_y}\right)\int_{-h/2}^{h/2} z^2 dz \\ \therefore M_x &= \frac{Et^3}{12(1-\nu^2)}\left(\frac{1}{r_x}+\frac{\nu}{r_y}\right) \end{aligned} \tag{2.7}$$

Similarly

$$M_y = \frac{Et^3}{12(1-\nu^2)}\left(\frac{1}{r_y}+\frac{\nu}{r_x}\right) \tag{2.8}$$

For simplification flexural rigidity, denoted as D, is introduced such that equations 2.7 and 2.8 reduce to

$$\begin{aligned} M_x &= D\left(\frac{1}{r_x}+\frac{\nu}{r_y}\right) \\ M_y &= D\left(\frac{1}{r_y}+\frac{\nu}{r_x}\right) \end{aligned} \tag{2.9}$$

where flexural rigidity is defined as

$$D = \frac{Et^3}{12(1-\nu^2)}. \tag{2.10}$$

This flexural rigidity of a plate corresponds to the stiffness, EI, of a beam. If w is the deflection in the z-direction, the principal curvatures are given by

$$\begin{aligned} \frac{1}{r_x} &= -\frac{\partial^2 w}{\partial x^2} \\ \frac{1}{r_y} &= -\frac{\partial^2 w}{\partial y^2} \end{aligned} \tag{2.11}$$

and therefore equations 2.9 become

$$\begin{aligned} M_x &= -D\left(\frac{\partial^2 w}{\partial x^2}+\nu\frac{\partial^2 w}{\partial y^2}\right) \\ M_y &= -D\left(\frac{\partial^2 w}{\partial y^2}+\nu\frac{\partial^2 w}{\partial x^2}\right) \end{aligned} \tag{2.12}$$

The shear strain in the element can be related to the shear stress by using Hooke's law in shear, which is

$$\tau_{xy} = G\gamma_{xy} \tag{2.13}$$

where G is the shear modulus of elasticity. This shear modulus of elasticity is related to the modulus of elasticity by the following equation

$$G = \frac{E}{2(1+\nu)}. \tag{2.14}$$

To obtain an expression for shear strain, consider the lamina *abcd* shown in figure 2-3.

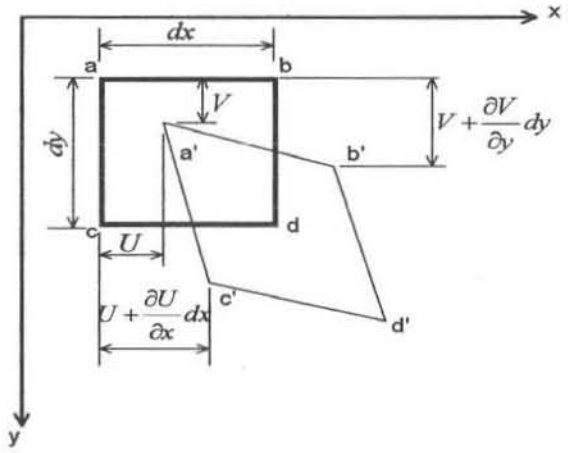

Figure 2-3: Lamina subjected to shear strain. Reproduced from Timoshenko[16]

During bending the points a, b, c and d experience small displacements. The components of the displacement of point a in the x and y directions are U and V respectively. The displacements of points b and c in the x and y directions are $U + (\partial U/\partial x)dx$ and $V + (\partial U/\partial y)dy$ respectively. The shearing strain owing to these displacements is

$$\gamma_{xy} = \frac{\partial U}{\partial x} + \frac{\partial V}{\partial y} \tag{2.15}$$

and the corresponding shear stress, using equation 2.13 is

$$\tau_{xy} = G\left(\frac{\partial U}{\partial x} + \frac{\partial V}{\partial y}\right). \tag{2.16}$$

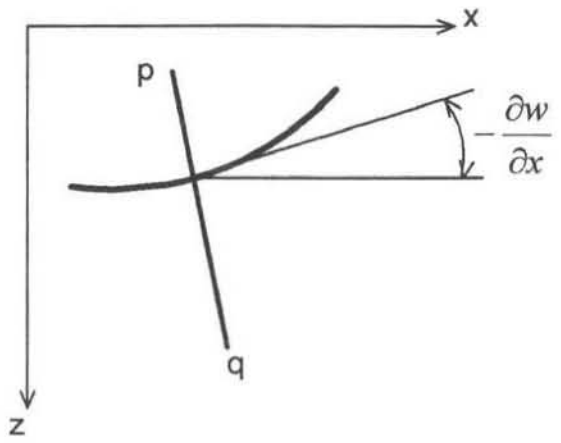

Figure 2-4: Section of the neutral surface. Reproduced from Timoshenko[16]

Figure 2-4 represents a section of the neutral surface, with a perpendicular (to the neutral surface) pq. One can see that the perpendicular pq has rotated in a counterclockwise direction through an angle of $-\partial w/\partial x$. A point of the element at distance z from the neutral axis has a displacement in the x-direction, due to this rotation, equal to

$$U = -z\frac{\partial x}{\partial x}. \tag{2.17}$$

The same point has a displacement in the y-direction of

$$V = -z\frac{\partial x}{\partial y}. \tag{2.18}$$

Substituting these values into equation 2.16 yields the following equation for strain

$$\tau_{xy} = -\frac{E}{1+\nu}\frac{\partial^2 w}{\partial x \partial y}z. \tag{2.19}$$

If this is then integrated across the element, and equated to the twisting moments, the following expression is obtained

$$M_{xy}dxdy = \int_{-t/2}^{t/2} \tau_{xy} z dx dy dz$$

which, after solving reduces to

$$M_{xy} = -\frac{Et^3}{12(1+\nu)}\frac{\partial^2 w}{\partial x \partial y}. \tag{2.20}$$

The twisting moments are illustrated together with the bending moments, on an element as in figure 2-2.

Multiplying through by

$$\frac{(1-\nu^2)}{(1-\nu^2)}$$

can further reduce this expression to

$$M_{xy} = -D(1-\nu)\frac{\partial^2 w}{\partial x \partial y} \tag{2.21}$$

By employing the principle of conservation of energy, the strain energy stored in the system is equated to the work done by the applied loads. An expression for the strain energy, U, can now be derived. The strain energy stored in a plate element is the sum of the work done by the bending moments M_x, M_y, and by the twisting moments M_{xy} and M_{yx}. The work done by the shear force and by the stretching of the middle plane are neglected by beam theory, which states that strain energy due to compression or tension along an axis, or due to shear distortion is neglected.

Since the sides of the elements remain plane, the work done by the bending moments is $\frac{1}{2}$ × moment × angle between the corresponding sides of the element after bending. Since $-(\partial^2 w/\partial x^2)$ and $-(\partial^2 w/\partial y^2)$ represent the curvatures in the xz and yz planes respectively, the angle is $-(\partial^2 w/\partial x^2)dx$ in the xz plane, and $-(\partial^2 w/\partial y^2)dy$ in the yz plane. The angles are negative because there is a downward (sagging) curvature. Therefore, the energy stored due to bending, U_b, is given by

$$dU_b = -\frac{1}{2}\left(M_x\frac{\partial^2 w}{\partial x^2} + M_y\frac{\partial^2 w}{\partial y^2}\right)dxdy. \tag{2.22}$$

In deriving the expression for the strain energy due to the twisting moment, $M_{xy}dy$, we note that the angle of twist is equal to the rate of change of the slope $\partial w/\partial y$ as x varies, multiplied with dx. The same applies to the moment $M_{yx}dx$. Therefore, the strain energy due to twist, U_t, is given by

$$dU_t = \frac{1}{2}\left(M_x \frac{\partial^2 w}{\partial x^2} + M_y \frac{\partial^2 w}{\partial y^2} \right) dxdy. \tag{2.23}$$

The couple $M_{yx}dx$ will produce the same amount of energy as $M_{xy}dy$. The above equation therefore reduces to

$$dU_t = M_{xy} \frac{\partial^2 w}{\partial x \partial y} dxdy. \tag{2.24}$$

Since the twist does not affect the strain energy due to bending, the total energy can be found by adding U_b and U_t, such that

$$dU = \left(M_{xy} \frac{\partial^2 w}{\partial x \partial y} - \frac{1}{2} M_x \frac{\partial^2 w}{\partial x^2} - \frac{1}{2} M_y \frac{\partial^2 w}{\partial y^2} \right) dxdy. \tag{2.25}$$

When the expressions for M_x, M_y and M_{xy} are substituted in, the following equation is obtained

$$dU = \frac{1}{2} D \left[(\nabla^2 w)^2 - 2(1-\nu) \left[\frac{\partial^2 w}{\partial x^2} \frac{\partial^2 w}{\partial y^2} - \left(\frac{\partial^2 w}{\partial x \partial y} \right)^2 \right] \right] dxdy \tag{2.26}$$

where

$$\nabla^2 w = \frac{\partial^2 w}{\partial x^2} + \frac{\partial^2 w}{\partial y^2}. \tag{2.27}$$

The expression derived by Bryan in 1891 for the total strain energy stored by a plate in pure bending can be found by integrating equation 2.26 over the entire surface, and is given by

$$dU = \frac{1}{2} D \iint \left[(\nabla^2 w)^2 - 2(1-\nu) \left[\frac{\partial^2 w}{\partial x^2} \frac{\partial^2 w}{\partial y^2} - \left(\frac{\partial^2 w}{\partial x \partial y} \right)^2 \right] \right] dxdy. \tag{2.28}$$

2.4 Thin cylindrical shells

A small shell element is considered, as in figure 2-5, which is formed by the intersection of two pairs of adjacent planes perpendicular to the surface. The x and y axes are taken as tangents to the element at O and z is perpendicular to the surface. The principle radii of curvature in the xz and yx planes are r_x and r_y respectively. When the element deforms due to an external load, the radii of curvature change to r'_x and r'_y. A fundamental assumption is now made that says

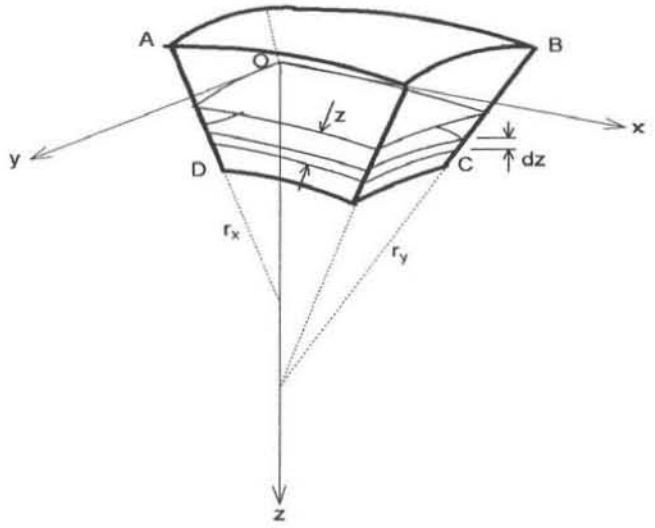

Figure 2-5: A small shell element. Reproduced from Bulson & Allen[37]

that the faces of the element rotate with respect to their lines of intersection with the middle surface. In addition to this, the sides of the element are displaced due to the middle surface straining in the x and y directions.

The equation for strain energy of a thin shell is derived directly from the expression for flat plates (equation 2.28), with the substitution of $\partial^2 w/\partial x^2$, $\partial^2 w/\partial y^2$, and $\partial^2 w/\partial x \partial y$ for the change in curvatures, for example $(\frac{1}{r'_x} - \frac{1}{r_x})$ is substituted for $\partial^2 w/\partial x^2$. So the equation becomes

$$U_b = \frac{1}{2} D \int_0^{\ell} \int_0^{2\pi r} \left[\left(\frac{1}{r'_x} - \frac{1}{r_x} + \frac{1}{r'_y} - \frac{1}{r_y} \right)^2 - 2(1-\nu) \left(\left(\frac{1}{r'_x} - \frac{1}{r_x} \right) \left(\frac{1}{r'_y} - \frac{1}{r_y} \right) - \left(\frac{1}{r'_{xy}} - \frac{1}{r_{xy}} \right)^2 \right) \right] dx dy \quad (2.29)$$

where $\left(\frac{1}{r'_{xy}} - \frac{1}{r_{xy}}\right)$ represents the twist of the element during bending, and $\left(\frac{1}{r'_{xy}} - \frac{1}{r_{xy}}\right)dx$ is the rotation of the edge BC relative to Oz [45]. The change in curvatures will be denoted as β_x, β_y and β_{xy} such that

$$U_b = \frac{D}{2}\int_0^{\ell}\int_0^{2\pi r}\left[\left(\beta_x + \beta_y\right)^2 - 2(1-\nu)\left(\beta_x\beta_y - \beta_{xy}^2\right)\right]dxdy. \tag{2.30}$$

In considering the bending of the shell, it is assumed that linear elements, such as AD and BC in figure 2-5 which are normal to the middle surface of the shell, remain straight and normal to the middle plane, even if deformed. This is known as the Love-Kirchhoff approximation [49]. During bending, the lateral faces of the element $ABCD$ rotate with respect to their lines of intersection with the middle surface only. The errors due to this approximation are negligible for thin shells of a homogeneous material. A shell is classified as thin when the thickness is small in comparison with the radius of curvature and corresponding 'radius of twist'.

Therefore, the unit elongations of a thin lamina at distance z are:

$$\begin{aligned}\epsilon_x &= -\frac{z}{1-\frac{z}{r_x}}\left(\frac{1}{r'_x} - \frac{1}{r_x}\right)\\ \epsilon_y &= -\frac{z}{1-\frac{z}{r_y}}\left(\frac{1}{r'_y} - \frac{1}{r_y}\right)\end{aligned} \tag{2.31}$$

Since we are dealing with thin walled shells, z will be small in comparison with r_x and r_y. Therefore the above equations reduce to

$$\begin{aligned}\epsilon_x &= z\beta_x\\ \epsilon_y &= z\beta_y.\end{aligned} \tag{2.32}$$

The middle surface is also stretched due to the lateral sides of the element displacing parallel to themselves, as seen in figure 2-6. If the length of the curved neutral surface of the element in the x-direction is ds and if we then denote the unit elongations of the middle surface in the x and y directions by ϵ_1 and ϵ_2 respectively, the elongation of the middle surface in the x-direction is:

$$\epsilon_x = \frac{l_2 - l_1}{l_1}. \tag{2.33}$$

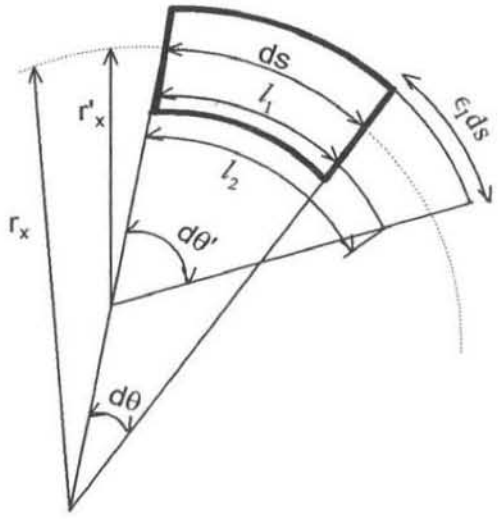

Figure 2-6: Figure showing the middle surface. Reproduced from [16].

It can be seen that $ds = r_x d\theta$, and $l_1 = d\theta(r_x - z)$, and by combining these expressions one obtains

$$l_1 = ds\left(1 - \frac{z}{r_x}\right). \tag{2.34}$$

Similarly, it can be seen that $(ds + \epsilon_1 ds = r'_x d\theta')$ and $(l_2 = d\theta'(ds - z))$, and by combining these expressions, one obtains

$$l_2 = ds(1 + \epsilon_1)\left(1 - \frac{z}{r'_x}\right). \tag{2.35}$$

By substituting these expressions for l_1 and l_2 into equation 2.33, the following equation for strain in the lamina in the x-direction, ϵ_x, is obtained

$$\epsilon_x = \frac{\epsilon_1}{1 - \frac{z}{r_x}} - \frac{z}{1 - \frac{z}{r_x}}\left[\frac{1}{(1 - \epsilon_1)r'_x} - \frac{1}{r_x}\right]. \tag{2.36}$$

A similar expression can be obtained for ϵ_y. Again, since we are dealing with thin shells where t, and therefore z, is small in comparison with the radii of curvature, the quantities z/r_x, z/r_y, z/r'_x and z/r'_y can be neglected. The effect of the elongations, ϵ_1 and ϵ_2, shall also be neglected (it can be shown in [62]p370 that this is justifiable if the depth of the cross section is small in comparison with the radius). Then, equation 2.36 can be reduced to

$$\epsilon_x = \epsilon_1 - z\beta_x \tag{2.37}$$

and silimarly

$$\epsilon_y = \epsilon_2 - z\beta_y. \tag{2.38}$$

By using the equations for stresses [64] which are

$$\begin{aligned} \sigma_x &= \frac{Ez}{1-\nu^2}\left[\epsilon_x + \nu\epsilon_y\right] \\ \sigma_y &= \frac{Ez}{1-\nu^2}\left[\epsilon_y + \nu\epsilon_x\right] \end{aligned} \tag{2.39}$$

and substituting in the values for the strains, the following expressions are attained:

$$\begin{aligned} \sigma_x &= \frac{Ez}{1-\nu^2}\left[\epsilon_1 - z\beta_x + \nu\left(\epsilon_2 - z\beta_y\right)\right] \\ \sigma_y &= \frac{Ez}{1-\nu^2}\left[\epsilon_2 - z\beta_y + \nu\left(\epsilon_1 - z\beta_x\right)\right]. \end{aligned} \tag{2.40}$$

Looking at the lamina in figure 2-7, with the edge forces per unit distance indicated, the resultant forces per unit length of the normal sections are:

$$\begin{aligned} N_x &= \int_{-t/2}^{t/2} \sigma_x \left(1 - \frac{z}{r_y}\right) dz \\ N_y &= \int_{-t/2}^{t/2} \sigma_y \left(1 - \frac{z}{r_x}\right) dz \\ N_{xy} &= \int_{-t/2}^{t/2} \tau_{xy} \left(1 - \frac{z}{r_y}\right) dz \\ N_{yx} &= \int_{-t/2}^{t/2} \tau_{yx} \left(1 - \frac{z}{r_x}\right) dz. \end{aligned} \tag{2.41}$$

But as before, the radius is large in comparison with the wall thickness. If the values for σ_x, σ_y, and τ_{xy} are also then substituted into equations 2.41, the equations obtained are:

$$\begin{aligned} N_x &= \int_{-t/2}^{t/2} \sigma_x dz = \frac{Et}{1-\nu^2}(\epsilon_1 + \nu\epsilon_2) \\ N_y &= \int_{-t/2}^{t/2} \sigma_y dz = \frac{Et}{1-\nu^2}(\epsilon_2 + \nu\epsilon_1) \\ N_{xy} = N_{yx} &= \int_{-t/2}^{t/2} \tau_{xy} dz = \frac{Et}{1-\nu}\gamma_{xy} \end{aligned} \tag{2.42}$$

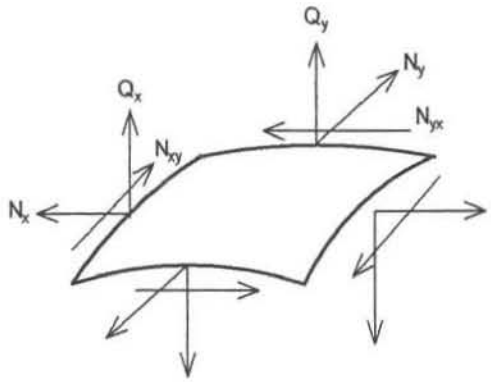

Figure 2-7: Figure showing a lamina. Reproduced from [16].

where γ_{xy} is the shear strain in the middle surface of the shell. The strain energy due to the stretching, U_s, of the middle surface is given by [37]:

$$U_s = \int_0^{\ell} \int_0^{2\pi r} \frac{1}{2}(N_x\epsilon_1 + N_y\epsilon_2 + N_{xy}\gamma_{xy})dxdy. \tag{2.43}$$

If the above expressions for N_x, N_y and N_{xy} are then substituted into this equation, the following is obtained:

$$\begin{aligned} U_s &= \frac{Et}{2(1-\nu^2)} \iint \left[(\epsilon_1 + \nu\epsilon_2)\epsilon_1 + (\epsilon_2 + \nu\epsilon_1)\epsilon_2 + \frac{(1-\nu)}{2}\gamma_{xy}^2 \right] dA \\ &= \frac{Et}{2(1-\nu^2)} \iint \left[(\epsilon_1^2 + \epsilon_2^2 + 2\nu\epsilon_1\epsilon_2 + \frac{(1-\nu)}{2}\gamma_{xy}^2 + 2\epsilon_1\epsilon_2 - 2\epsilon_1\epsilon_2 \right] dA \\ &= \frac{Et}{2(1-\nu^2)} \iint \left[(\epsilon_1 + \epsilon_2)^2 - 2(1-\nu)\left(\epsilon_1\epsilon_2 - \frac{\gamma_{xy}^2}{4}\right) \right] dA. \end{aligned} \tag{2.44}$$

The total strain energy is the sum of the strain energy due to stretching, U_s, and the strain energy due to bending, U_b. The total strain, U, energy is therefore:

$$\begin{aligned} U = \frac{Et}{2(1-\nu^2)} \int_0^{\ell} \int_0^{2\pi r} \Bigg[\frac{t^2}{6} \Big[(\beta_x + \beta_y)^2 - 2(1-\nu)(\beta_x\beta_y - \beta_{xy}^2) \Big] \\ + \Big[(\epsilon_1 + \epsilon_2)^2 - 2(1-\nu)(\epsilon_1\epsilon_2 - \frac{\gamma_{xy}^2}{4}) \Big] \Bigg] dA \end{aligned} \tag{2.45}$$

This method is generally used for the investigation of the buckling of a thin-walled cylinder subjected to axial compression.

2.4.1 The differential equations of equilibrium

The energy method, which did not involve the development of the differential equations of equilibrium, can be used in the case of cylinders subjected to axial loading. But cylindrical shells subjected to external pressure, or axial loading and external pressure, must be examined using differential equations using assumed functions for the displacements in the ordinate directions.

If the equilibrium of a shell element is considered in a similar fashion to that of a flat plate, it is possible to establish relationships between shear forces, edge forces and edge moments, as shown in figure 2-8.

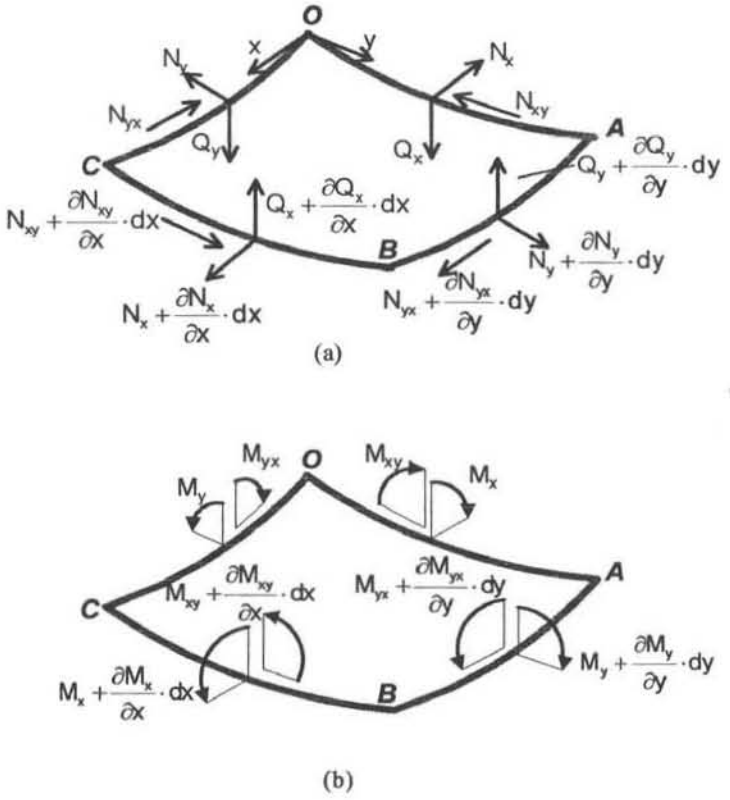

Figure 2-8: Bending of a thin flat plate. Reproduced from [37].

The displacements in the x, y and z directions will be denoted by u, v and w respectively as before. Before deformation, the x and y-axes are tangents to the element in an axial direction and circumferential direction respectively. After

deformation, which is assumed to be very small, these directions are altered slightly. The z-axis is then taken to be normal to the middle plane, the x-axis tangent to the element, and the y-axis perpendicular to the xz plane. In order for the equations of equilibrium for element $OABC$ to be established, the angular displacements of the sides BC and AB with reference to sides OA and OC respectively, need to be established.

The rotation of side BC with respect to OA can be resolved into the three components. The displacements v and w cause the rotations of sides OA and BC with respect to the x-axis. Since the displacement v represents motion of the sides OA and BC in the tangential (circumferential) direction (see figure 2-8), the corresponding rotation of side OA about the x-axis is v/r. Therefore, the rotation of side BC is

$$\frac{1}{r}\left(\nu + \frac{\partial \nu}{\partial x}dx\right). \tag{2.46}$$

Thus, owing to the displacement ν, the relative angular rotation of BC with respect to OA about the x-axis is:

$$\frac{1}{r}\frac{\partial \nu}{\partial x}dx. \tag{2.47}$$

Similarly, because of the displacement w, the side OA rotates about the x-axis through an angle of $\partial w/(r\partial\theta)$, and side BC through an angle of

$$\frac{\partial w}{r\partial\theta} + \frac{\partial}{\partial x}\left(\frac{\partial w}{r\partial\theta}\right)dx. \tag{2.48}$$

Therefore, because of displacement w, the relative angular displacement is

$$\frac{\partial}{\partial x}\left(\frac{\partial w}{r\partial\theta}\right)dx. \tag{2.49}$$

Therefore, by combining equations 2.47 and 2.49, the relative angular displacement of side BC with respect to side OA about the x-axis is

$$\frac{1}{r}\left(\frac{\partial \nu}{\partial x} + \frac{\partial^2 w}{\partial x \partial\theta}\right)dx. \tag{2.50}$$

The rotation of side BC with respect to the side OA about the y-axis is caused by the bending of the axial plane and is equal to

$$-\frac{\partial^2 w}{\partial x^2}dx. \tag{2.51}$$

The rotation of side BC with respect to side OA about the z-axis is caused by the bending of the tangential plane and is equal to

$$\frac{\partial^2 v}{\partial x^2}dx. \tag{2.52}$$

These last three expressions give the three components of rotation of the side BC with respect to the side OA.

The corresponding formulae for the angular displacement of side AB with respect to OC now needs to be established. Due to the curvature of the shell, the initial angle between the axial sides of the element $OABC$ is $d\theta$. But, because of the displacements v and w, this angle will change. The rotation of the side OC about the x-axis can be expressed as

$$\frac{\nu}{r}+\frac{\partial w}{rd\theta}. \tag{2.53}$$

The corresponding rotation for the other axial side AB is

$$\frac{\nu}{r}+\frac{\partial w}{rd\theta}+\frac{d}{d\theta}\left(\frac{\nu}{r}+\frac{\partial w}{rd\theta}\right)d\theta. \tag{2.54}$$

To calculate the angle of rotation of the side AB with respect to the side OC about the y-axis the expression for twist is used, and this gives the required angular displacement as

$$-\left(\frac{\partial^2 w}{\partial\theta\partial x}+\frac{\partial v}{\partial x}\right)d\theta. \tag{2.55}$$

Rotation of the side AB with respect to OC about the z-axis is caused by the displacements v and w. The angle of rotation of the side OC is $\partial v/\partial x$, because of the displacement v, and that of side AB is

$$\frac{\partial v}{\partial x}+\frac{\partial}{r\partial\theta}\left(\frac{\partial v}{\partial x}\right)rd\theta, \tag{2.56}$$

so the relative angular displacement is therefore

$$\frac{\partial}{r\partial\theta}\left(\frac{\partial v}{\partial x}\right)rd\theta. \tag{2.57}$$

Due to the displacement w, the side AB rotates in the axial plane by the angle $\partial w/\partial x$. The component of this rotation with respect to the z-axis is

$$-\frac{\partial w}{\partial x}d\theta. \tag{2.58}$$

By combining these last two expressions, the relative angular displacement of the side AB with respect to the side OC about the z-axis is given by

$$\left(\frac{\partial^2 v}{\partial\theta\partial x}-\frac{\partial w}{\partial x}\right)d\theta. \tag{2.59}$$

With these formulae for the angles, the three equations of equilibrium of the element $OABC$ can be obtained. This is done by projecting all forces onto the x, y and z-axes. The x-components of those forces parallel to the resultant forces N_x and N_{xy} are:

$$\begin{gathered}\frac{\partial N_x}{\partial x}dxrd\theta \\ \\ \frac{\partial N_{yx}}{\partial y}dydx\theta.\end{gathered} \tag{2.60}$$

Due to the angle of rotation, equation 2.59, the forces parallel to N_y give a component in the x-direction equal to

$$N_y\left(\frac{\partial^2 v}{\partial\theta\partial x}-\frac{\partial w}{\partial x}\right)d\theta dx. \tag{2.61}$$

Due to the rotation represented by equation 2.52, the forces parallel to N_{yx} has an x component of:

$$-N_{xy}\frac{\partial^2 v}{\partial x^2}dxrd\theta. \tag{2.62}$$

Finally, due to the angles expressed by equations 2.51 and 2.55, the forces parallel to Q_x and Q_y have the following x component:

$$-Q_x\frac{\partial^2 w}{\partial x^2}dxrd\theta-Q_y\left(\frac{\partial^2 w}{\partial\theta\partial x}+\frac{\partial v}{\partial x}\right)d\theta dx. \tag{2.63}$$

By summing all the projections calculated above, the first equilibrium equation is obtained. Similarly the other equation are obtained and after simplification are as follows:

$$r\frac{\partial N_x}{\partial x}+\frac{\partial N_{yx}}{\partial \theta}-rQ_x\frac{\partial^2 w}{\partial x^2}-rN_{xy}\frac{\partial^2 v}{\partial x^2}-Q_y\left(\frac{\partial v}{\partial x}+\frac{\partial^2 w}{\partial x\partial\theta}\right)-N_y\left(\frac{\partial^2 v}{\partial x\partial\theta}-\frac{\partial w}{\partial x}\right)=0$$

$$\begin{aligned}\frac{\partial N_y}{\partial \theta}+r\frac{\partial N_{xy}}{\partial x}+rN_x\frac{\partial^2 v}{\partial x^2}-Q_x\left(\frac{\partial v}{\partial x}+\frac{\partial^2 w}{\partial x\partial\theta}\right)\\ +N_{yx}\left(\frac{\partial^2 v}{\partial x\partial\theta}-\frac{\partial w}{\partial x}\right)-Q_y\left(1+\frac{\partial v}{r\partial\theta}+\frac{\partial^2 w}{r\partial\theta^2}\right)=0\end{aligned}\quad(2.64)$$

$$\begin{aligned}r\frac{\partial Q_x}{\partial x}+\frac{\partial Q_y}{\partial\theta}+N_{xy}\left(\frac{\partial v}{\partial x}+\frac{\partial^2 w}{\partial x\partial\theta}\right)+rN_x\frac{\partial^2 w}{\partial x^2}\\ +N_y\left(1+\frac{\partial v}{r\partial\theta}+\frac{\partial^2 w}{r\partial\theta^2}\right)+N_{yx}\left(\frac{\partial v}{\partial x}+\frac{\partial^2 w}{\partial x\partial\theta}\right)+qr=0\end{aligned}$$

For long equations such as these, the use of Flügge's notation of primes and dots for derivatives with respect to the axial and circumferential co-ordinates respectively will be convenient. The following relations illustrate this notation:

$$\begin{aligned}\frac{\partial u}{\partial x}&=u'\\ \frac{\partial u}{\partial\theta}&=\dot{u}\end{aligned}\quad(2.65)$$

Therefore, the preceeding three equations reduce to

$$\begin{aligned}0&=rN_x'+\dot{N}_{yx}-rQ_xw''-rN_{xy}v''-Q_y(v'+\dot{w}')-N_y(\dot{v}'-w')\\ 0&=\dot{N}_y'+rN_{xy}'+rN_xv''-Q_x(v'+\dot{w}')+N_{yx}(\dot{v}'-w')-Q_y\left(1+\frac{\dot{v}}{r}+\frac{\ddot{w}}{r}\right)\\ 0&=rQ_x'+\dot{Q}_y+N_{xy}(v'+\dot{w}')+rN_xw''\\ &\quad+N_y\left(1+\frac{\dot{v}}{r}+\frac{\ddot{w}}{r}\right)+N_{yx}(v'+\dot{w}')+qr\end{aligned}\quad(2.66)$$

This first set of equations relates edge forces to shears. A second set relates edge moments to shears. The second set of relations is the moment equilibria with respect to the x, y and z-axes. Again, the small angular displacements of the

sides BC and AB with respect to OA and OC are taken into consideration. The equations are:

$$\begin{aligned}
0 &= rM'_{xy} - \dot{M}_y - rM_x v'' - M_{yx}(\dot{v}' - w') + rQ_y \\
0 &= \dot{M}_{yx} + rM'_x + rM_{xy} v'' - M_y(\dot{v}' - w') + rQ_x \\
0 &= M_x(v' + \dot{w}') + rM_{xy} w'' + M_{yx}\left(1 + \frac{\dot{v}}{r} + \frac{\ddot{w}}{r}\right) \\
&\qquad - M_y(v' + \dot{w}') + r(N_{xy} - N_{yx})
\end{aligned} \tag{2.67}$$

These are the general equations for the deformation of a cylindrical shell subjected to external pressure. But, note that the displacement v is not involved when distortion of the element due to relative rotation of its opposite edges is considered. Therefore, eliminating Q_x and Q_y can reduce the above six equations.

The axial loading and external pressure which will be imposed on cylinders in this analysis, will be imposed in a manner which is symmetric with respect to the axis of the cylinder. Then, in both cases, all points of the middle surface of the shell, lying in the same cross section perpendicular to the axis of symmetry, will have the same displacement. It is then sufficient to consider an elemental strip ab of unit width as shown in figure 2-9, cut out from the shell by two axial sections. This width will be considered very small in comparison with the radius. Therefore the cross section of this strip can then be considered rectangular. An element, dx, of this strip is subjected to the forces N_x and $N_y dx$ in the middle surface of the shell, and qdx normal to the surface of the shell, where q is the intensity of the load acting on the shell. Let us assume that the axial load is constant, and therefore N_x is constant. The force N_y is dependent on the radial displacements, w, of the points of the strip during deformation of the shell. The strain of the middle surface of the shell in the circumferential direction is w/r. By using equations 2.42, expression for the forces are obtained

$$\begin{aligned}
N_x &= \frac{Et}{1-\nu^2}\left(\epsilon_1 - \nu\frac{w}{r}\right) \\
N_y &= \frac{Et}{1-\nu^2}\left(-\frac{w}{r} + \nu\epsilon_1\right).
\end{aligned} \tag{2.68}$$

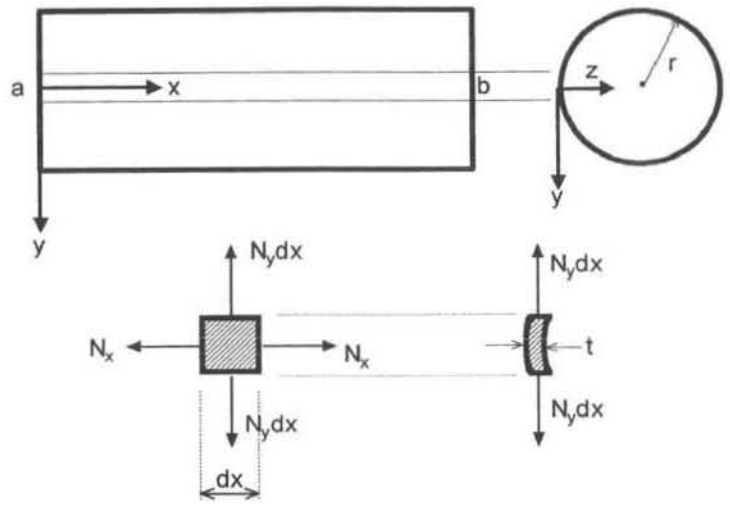

Figure 2-9: Figure showing an elemental strip. Reproduced from [8].

From the above equations, we can see that N_x and N_y are related by the following relation

$$N_y = \nu N_x - \frac{w}{r} Et. \tag{2.69}$$

These forces give a component in the radial direction, per unit length, of

$$\frac{N_y}{r} = \frac{1}{r}\left(\nu N_x - \frac{w}{r} Et\right). \tag{2.70}$$

Due to the curvature of the strip, the longitudinal force, N_x, also gives a radial component of

$$N_x w''. \tag{2.71}$$

By summing up all these transverse loads, we obtain the differential equation for the deflection of the strip:

$$Dw'''' = q + \frac{v}{r} N_x - \frac{w}{r^2} Et + N_x w''. \tag{2.72}$$

2.5 Axial loading of the cylinder

2.5.1 Literature survey

When a perfect cylinder of uniform wall thickness is subjected to axial loading, buckling symmetrical with respect to the axis of the cylinder can occur at a certain value of load in two possible modes. In the first of these two modes, radial displacements are in the form of longitudinal waves along the length of the cylinder, with these displacements being constant around the perimeter at any point. This form of buckling is known as symmetric, or ring buckling. In the second of these two modes, waves form in both the longitudinal and transverse directions. This results in a 'chessboard' effect, where there is a pattern of rectangular depressions and bulges all over the surface. If loading is continued during this second mode of buckling, the cylinder snaps through to another state of equilibrium associated with a smaller axial load. The rectangular shaped depressions and bulges now become a depressed diamond shape. This is known as Yoshimura buckling. An illustration of these forms of buckling can be seen in figure 2-10. Due to the well-known difficulties of solving nonlinear differential

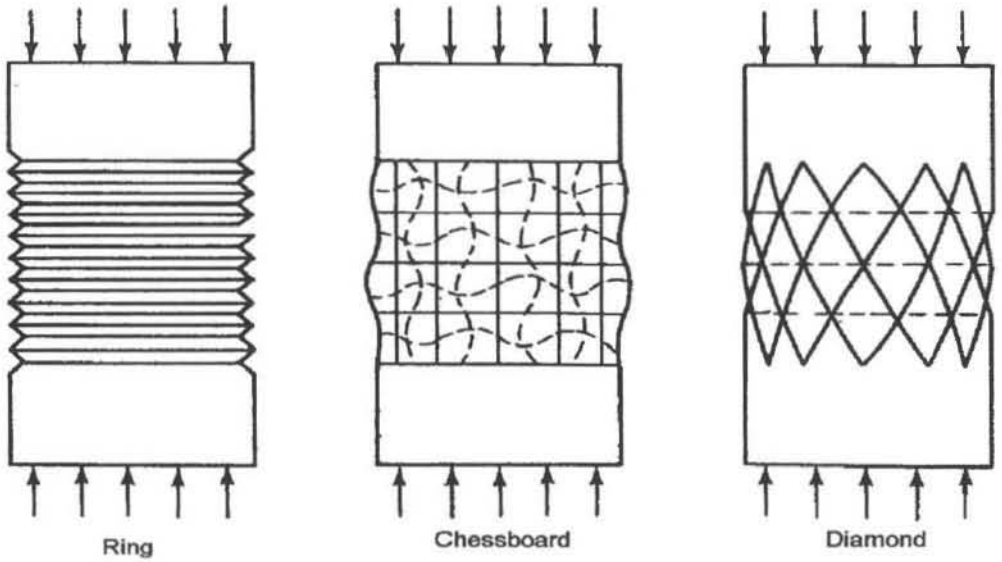

Figure 2-10: Ring, chessboard and diamond buckling forms. From [37]

equations, the critical value of the axial load, P_{cr}, will be found using the energy method. As long as the shell remains cylindrical, the total strain energy is the energy of axial compression. But, once buckling begins, the strain of the middle surface in the circumferential direction must also be considered. Therefore, the strain energy of the shell is increased. At the critical load value, this increase in energy must be equal to the work done by the compressive load as the cylinder shortens. As shown in chapter 1.1, equation 1.7, the radial displacement for ring buckling is considered to be

$$w = -A \sin \frac{m\pi x}{l}.$$

The strains ϵ_1 and ϵ_2, in the axial and circumferential directions respectively are found by assuming that the axial load remains constant during the buckling. The axial strain of the unbuckled cylinder, ϵ_0, at the critical load is given by

$$\epsilon_0 = -\frac{\sigma_{cr}}{E}. \tag{2.73}$$

From equation 2.42, the axial strain after buckling is $(\epsilon_1 + \nu\epsilon_2)/(1 - \nu^2)$, and therefore

$$\epsilon_1 + \nu\epsilon_2 = (1 - \nu^2)\epsilon_0. \tag{2.74}$$

The circumferential strain in any section due to radial deflection is w/r, and there is also a further circumferential strain due to Poisson's ratio. Therefore, the circumferential strain is:

$$\epsilon_2 = -\nu\epsilon_0 - \frac{w}{r}. \tag{2.75}$$

Similarly, the axial strain is:

$$\epsilon_1 = \epsilon_0 - \nu\frac{w}{r}. \tag{2.76}$$

Due to the complete symmetry of the deformation, there is no shear strain, no change in curvature in the y-direction, and no twist of an element of the shell wall. In terms of their variables:

$$\gamma_{xy} = \beta_y = \beta_{xy} = 0. \tag{2.77}$$

The change of curvature in the axial plane is

$$\beta_x = w'' = A\frac{m^2\pi^2}{l^2}\sin\frac{m\pi x}{l}. \tag{2.78}$$

When these expressions are substituted into the equation for strain energy due to bending and stretching, equation 2.45, the following is obtained

$$U = DA^2\pi rl\frac{\pi^4 m^4}{2l^4} + \pi rlEt\epsilon_0^2 - 2\pi tE\nu\epsilon_0\int_0^\ell A\sin\frac{m\pi x}{l}dx + \frac{Et\pi lA^2}{2r}. \tag{2.79}$$

The strain energy in the cylinder before buckling, U_{0c}, is given by

$$U_{0c} = \iint \frac{1}{2}N_x\epsilon_0 dA = \pi rlEt\epsilon_0^2 \tag{2.80}$$

and therefore, the change in strain energy during the actual buckling is

$$\Delta U = U - \pi rlEt\epsilon_0^2. \tag{2.81}$$

By substituting in equation 2.79,

$$\Delta U = DA^2\pi rl\frac{\pi^4 m^4}{2l^4} - 2\pi tE\nu\epsilon_0\int_0^\ell A\sin\frac{m\pi x}{l}dx + \frac{Et\pi lA^2}{2r}. \tag{2.82}$$

The work done by the external axial load during buckling is equal to the end-load on the cylinder multiplied by the shortening of the axial length due to bending, and to the change in axial strain, $\epsilon_1 - \epsilon_0$. The work is denoted by ΔT, and is given by

$$\begin{aligned}\Delta T &= \sigma_{cr}t\cdot 2\pi r\left[\frac{A^2}{4}\cdot\frac{m^2\pi^2}{l} - (\epsilon_1 - \epsilon_0)\right] \\ &= \sigma_{cr}t\cdot 2\pi r\left[\frac{A^2}{4}\cdot\frac{m^2\pi^2}{l} - \left(-\nu\frac{w}{r}\right)\right] \\ &= \sigma_{cr}t\cdot 2\pi r\left[\frac{A^2}{4}\cdot\frac{m^2\pi^2}{l} + \frac{\nu}{r}\int_0^\ell A\sin\frac{m\pi x}{l}dx\right].\end{aligned} \tag{2.83}$$

Equating the increase in strain energy, ΔU, to the work done by the compressive load, ΔT, and substituting in the expression for ϵ_0 yields

$$\sigma_{cr} = D\frac{m^2\pi^2}{l^2 t} + \frac{El^2}{r^2 m^2\pi^2}. \tag{2.84}$$

Assuming there are many waves formed along the length of the cylinder during buckling, and also considering P_{cr} as a continuous function of π/l:

$$\frac{d\sigma_{cr}}{d(m\pi/l)} = 0 \tag{2.85}$$

which occurs at

$$\frac{m\pi}{l} = \sqrt[4]{\frac{Et}{r^2 D}}. \tag{2.86}$$

Substituting this into equation 2.84 yields a minimum buckling load of

$$\sigma_{cr} = \frac{2}{rt}\sqrt{EDt} = \frac{Et}{r\sqrt{3(1-nu^2)}}. \tag{2.87}$$

This form of the equation was given in [37], but numerous other references ([55],[65]) quoted this equation as

$$P_{cr} = \frac{Et^2}{r\sqrt{3(1-\nu^2)}} \tag{2.88}$$

where P_{cr} is the critical buckling load. Clearly, in this form, the units for the load are incorrect. However, in [8], it is stated that this critical load is in fact the 'critical value of the compressive force per unit length of the edge of the shell.' This was not stated explicitly in [55] and [65], and some confusion arose. Therefore, as given in [24] and [36], the critical value of the buckling load is

$$P_{cr} = \frac{Et^2 2\pi}{\sqrt{3(1-\nu^2)}}. \tag{2.89}$$

This relationship is shown in figure 2-11.

The expression for radial displacement in initial chessboard buckling, to take account of circumferential as well as longitudinal waves, is assumed as

$$w = -A \sin\frac{m\pi x}{l} \cdot \sin n\theta \tag{2.90}$$

where w is as shown in figure 2-12. Proceeding as before, it can be shown that if m, and therefore $m^2\pi^2 r^2/l^2$ is a large number,

$$\sigma_{cr} = \frac{D}{t}\left[\frac{\left(n^2 + (m\pi r/l)^2\right)^2}{r^2(m\pi r/l)^2}\right] + \frac{E(m\pi r/l)^2}{\left(n^2 + (m\pi r/l)^2\right)^2}. \tag{2.91}$$

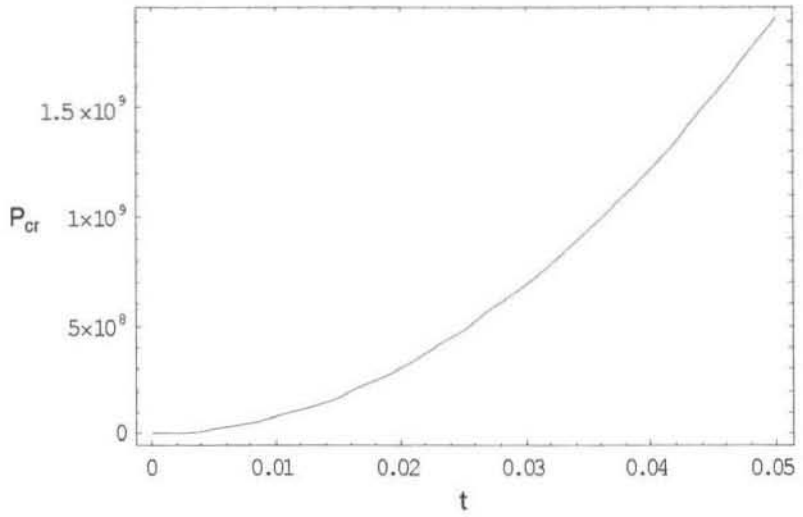

Figure 2-11: Graph showing the relationship between the buckling load and radius to wall thickness ratio.

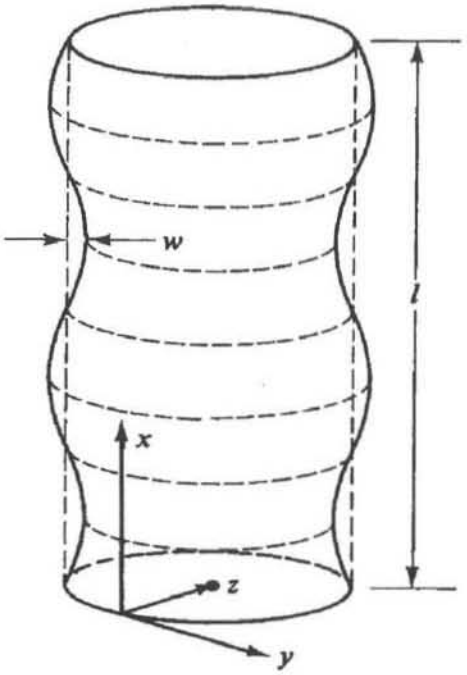

Figure 2-12: Figure showing the definition of variable w. From [37]

To check this expression, if $n = 0$ (ie. no circumferential waves as for ring buckling), this expression coincides with equation 2.84. As before, minimising to find the lowest value of P_{cr}, yields

$$\sigma_{cr} = \frac{Et}{r\sqrt{3(1-\nu^2)}} \tag{2.92}$$

where $P_{cr} = \sigma_{cr} 2\pi r t$, and this occurs at

$$\frac{n^2 l^2 + m^2 \pi^2 r^2}{m\pi r l} = \left(\frac{Et}{r^2 D}\right)^{\frac{1}{4}}. \tag{2.93}$$

These two equations were used in references [37],[8] and [43].

Instead of using the energy method as above, it can be shown that the differential equations for symmetrical deflection can also be used in calculating the critical load. This development can be seen in appendix A.

Since predictability of initial buckling is sought, postbuckling loads and stresses are not investigated.

2.5.2 Numerical Analysis

Simulations were run on MSC Nastran for Windows v4.5.1 to compare numerical testing with the presented theory. The analyses were conducted on cylinders with a mesh of 120 elements along the circumference and 12 elements along the axis. Such a model of a cylinder is shown in figure 2-13. Finer meshes were used, but the improvement was very limited. This is discussed in chapter 1.2.

Cylinders of radius 11.43m (37.5ft), corresponding to SASOL's F7110 tanks, were used with various wall thicknesses for various lengths, and the buckling loads were determined.

The trends of increasing critical pressure with increasing wall thickness to radius ratio can be clearly seen in figure 2-14, where numerical results are compared with the theoretical curve from equation 2.89.

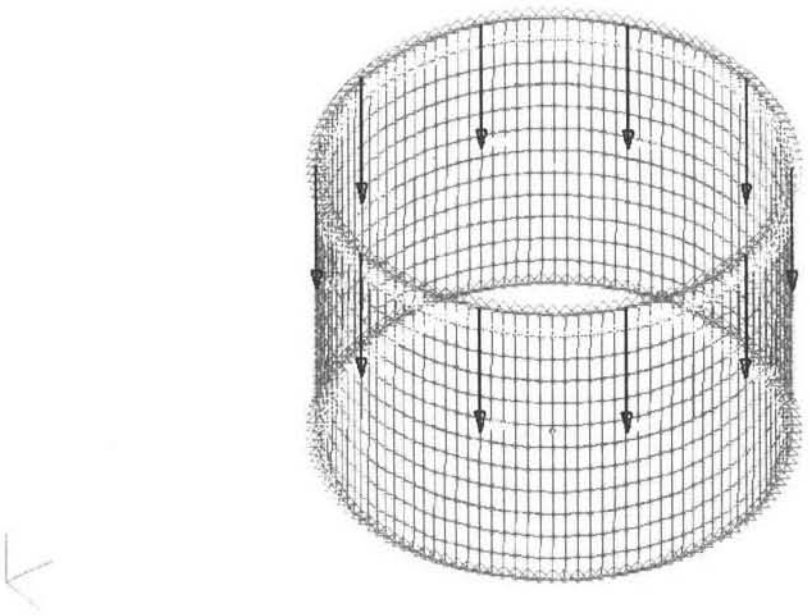

Figure 2-13: The initial model for numerical analysis of perfect cylinders.

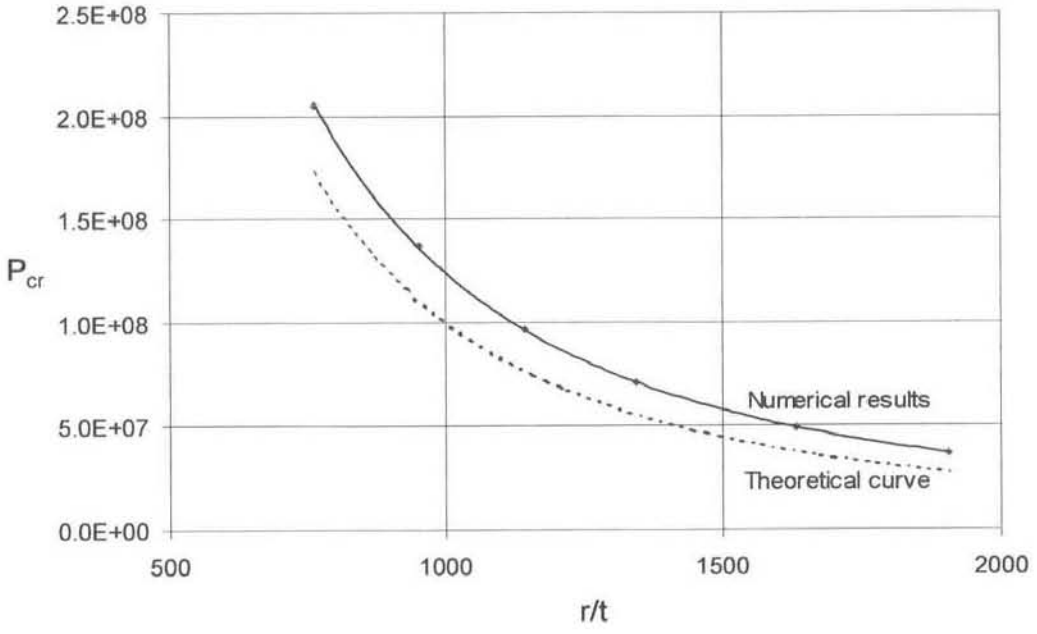

Figure 2-14: Figure showing the numerical results compared with theory.

In the above graph, the experimental values are compared with the theory developed, and they co-relate fairly closely. A table showing the exact cylinder dimensions used in the simulations is shown in appendix B.

An exaggerated chessboard buckling form can be seen in figure 2-15.

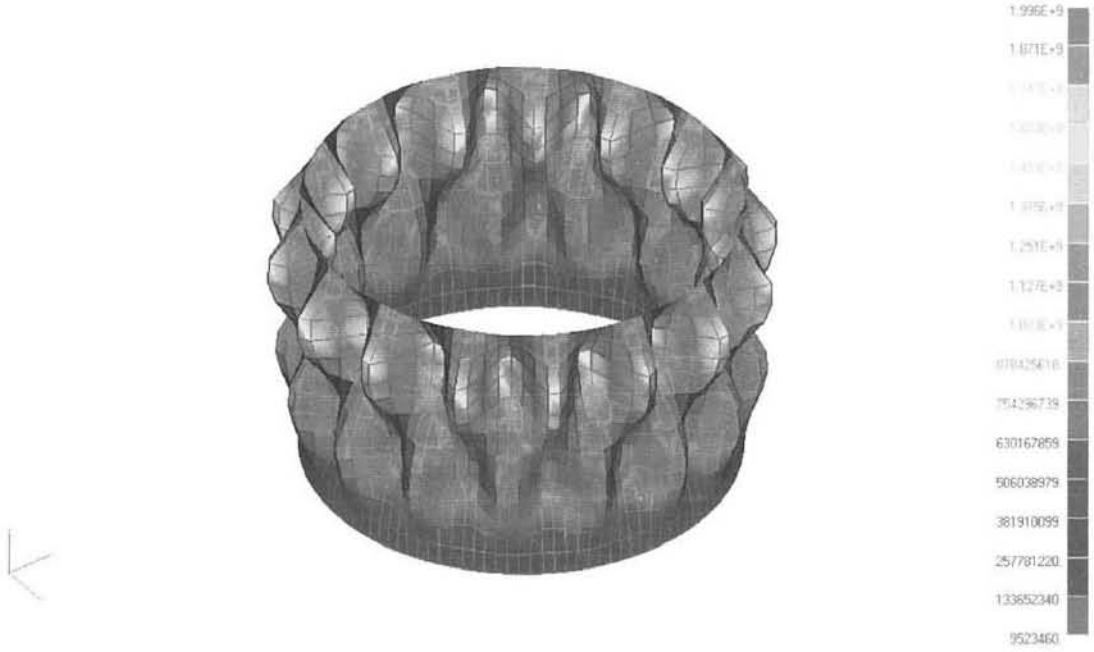

Figure 2-15: Chessboard buckling pattern.

According to Donnell [7] the experimental tests reflect that, except for very short cylinders, the exact degree to which the ends are fixed has little effect on the buckling strength. His tests indicate that the end conditions can be neglected even when the length to radius ratio is considerable less than one, and this study includes cylinders down to a length to radius ratio of only 0.769.

2.6 Lateral external pressure

2.6.1 Literature survey

As stated before, the external pressure and combined loading problems are best examined using differential equations, using assumed functions for the displacements u, v and w. In order for the equilibrium equations for external pressure to be examined, it is assumed that all the edge forces except N_y are small, and the products of these terms with the derivatives of displacements may be neglected. Equations 2.64 then reduce to

$$\begin{aligned} 0 &= rN'_x + \dot{N}_{yx} - N_y(\dot{v}' - w') \\ 0 &= \dot{N}_y + rN'_{xy} - Q_y \\ 0 &= rQ'_x + \dot{Q}_y + N_y\left(1 + \frac{\dot{v}}{r} + \frac{\ddot{w}}{r}\right) + qr \end{aligned} \tag{2.94}$$

It is then also assumed that all bending and twisting moments are small and the products of these with the derivatives of displacements may also be neglected. Since we are dealing with external pressure, which is in the z-direction, Q_x and Q_y can also be eliminated. Equations 2.67 are then reduced to

$$\begin{aligned} Q_x &= \frac{\dot{M}_{yx}}{r} + M'_x \\ Q_y &= \frac{\dot{M}_y}{r} - M'_{xy} \end{aligned} \tag{2.95}$$

By substituting equations 2.95 into 2.94, we reduce the initial six differential equations to the following three

$$\begin{aligned} 0 &= rN'_x + \dot{N}_{yx} - N_y(\dot{v}' - w') \\ 0 &= \dot{N}_y + rN'_{xy} - \frac{\dot{M}_y}{r} + M'_{xy} \\ 0 &= \dot{M}'_{yx} + rM''_x + \frac{\ddot{M}_y}{r} - \dot{M}'_{xy} + N_y\left(1 + \frac{\dot{v}}{r} + \frac{\ddot{w}}{r}\right) + qr \end{aligned} \tag{2.96}$$

As for flat plate analysis, the relationships between M_x, M_y and M_{xy}, and the curvature changes (β_x, β_y and β_{xy}), are derived from equations 2.12 and 2.21

$$\begin{aligned} M_x &= -D(\beta_x + \nu\beta_y) \\ M_y &= -D(\beta_y + \nu\beta_x) \\ M_{xy} = -M_{yx} &= -D(1-\nu)\beta_{xy} \end{aligned} \tag{2.97}$$

The middle surface strains and curvature changes are linked to the ordinate displacements, u v and w, by the following relations:

$$\begin{aligned} \epsilon_1 &= u' \\ \epsilon_2 &= \frac{\dot{v}}{r} - \frac{w}{r} \\ \gamma &= \frac{\dot{u}}{r} + v' \\ \beta_x &= w'' \\ \beta_y &= \frac{1}{r^2}(\dot{v} + \ddot{w}) \\ \beta_{xy} &= \frac{1}{r^2}(v' + \dot{w}') \end{aligned} \tag{2.98}$$

If these are substituted together with the relationships found in equations 2.42, through equations 2.97, into equations 2.96, the equations of equilibrium are

$$\begin{aligned} 0 &= r^2u'' + \frac{(1+\nu)}{2}r\dot{v}' - \nu r w' + qr^2\frac{(1-\nu^2)}{Et}(\dot{v}' - w') + \frac{(1-\nu)}{2}\ddot{u} \\ 0 &= \frac{(1+\nu)}{2}r\dot{u}' + \frac{(1-\nu)}{2}r^2v'' + \ddot{v} - \dot{w} + \kappa(\dot{v} + \dddot{w} + r^2\dot{w}'' + r^2(1-\nu)v'') \\ 0 &= r\nu u' + \dot{v} - w - \kappa\big(\ddot{v} + (2-\nu)r^2\dot{v}'' + r^4w'''' + \ddot{w} + 2r^2\ddot{w}''\big) \\ &\qquad - q^2\frac{(1-\nu^2)}{Et}(w + \ddot{w}) \end{aligned} \tag{2.99}$$

Donnell showed that these equilibrium equations could be simplified, with very little loss of accuracy. Remembering that $r\partial\theta = \partial y$ for cylinders, the equations then become:

$$\begin{aligned} 0 &= u'' + \frac{(1-\nu)}{2}\frac{\partial^2 u}{\partial y^2} + \frac{1+\nu}{2}\frac{\partial v'}{\partial y} + \frac{\nu}{r}w' \\ 0 &= \frac{\partial^2 v}{\partial y^2} + \frac{(1-\nu)}{2}v'' + \frac{(1+\nu)}{2}\frac{\partial u'}{\partial y} + \frac{1}{r}\frac{\partial w}{\partial y} \\ 0 &= D\nabla^4 w + qr\frac{\partial^2 w}{\partial y^2} \end{aligned} \tag{2.100}$$

where $\nabla^4(\cdots)$ is the usual operator of $\dfrac{\partial(\cdots)}{\partial x^4} + \dfrac{2\partial^4(\cdots)}{\partial x^2 \partial y^2} + \dfrac{\partial^4(\cdots)}{\partial y^4}$.

By manipulation of these equations, a single relationship can be obtained:

$$D\nabla^8 w + \frac{Et}{r^2} w'''' + \nabla^4 \frac{q}{r} \ddot{w} = 0. \tag{2.101}$$

Therefore, the problem of determining the critical external pressure is reduced to solving the above three differential equations, and satisfying boundary conditions. If, for example, the ends of the cylinder are simply supported, the boundary conditions require that w and $\partial^2 w/\partial x^2$ become zero at the ends. Also, if the length of the cylinder is l and the axes of reference are taken at the middle cross section, the following expressions are assumed for u v and w :

$$\begin{aligned} u &= A \sin n\theta \sin \frac{\pi x}{l} \\ v &= B \cos n\theta \cos \frac{\pi x}{l} \\ w &= C \sin n\theta \cos \frac{\pi x}{l} \end{aligned} \tag{2.102}$$

These expressions show that during buckling, the shell deflects to half a sine curve wave while the circumference is subdivided into $2n$ half waves. When these are substituted into equations 2.99, the following equations emerge

$$\begin{aligned} 0 &= A\left(-\chi^2 - \frac{(1-\nu)}{2} n^2\right) + B\left(\frac{(1+\nu)}{2} n\chi + n\chi\phi\right) + C(\nu + \phi)\chi \\ 0 &= A\left(\frac{(1+\nu)}{2} n\chi\right) - B\left(\frac{(1-\nu)}{2}\chi^2 + n^2 + n^2\kappa + \kappa(1-\nu)\chi^2\right) \\ &\qquad - C(n + \kappa n^3 + \kappa n\chi^2) \\ 0 &= A\nu\chi - B\left(n + \kappa n^3 + (2-\nu)\kappa n\chi^2\right) \\ &\qquad - C\left(1 + \kappa\chi^4 + \kappa n^4 2\kappa n^2\chi^2 + \phi(1-n^2)\right) \end{aligned} \tag{2.103}$$

where the variables χ, κ and ϕ are defined as

$$\begin{aligned} \chi &= \frac{\pi r}{l} \\ \kappa &= \frac{t^2}{12r^2} \\ \phi &= \frac{qr(1-\nu^2)}{Et} \end{aligned} \tag{2.104}$$

Thus, simultaneous equations in A, B and C result, and these yield non-trivial solutions if their determinant is zero. In this manner the equation for determining the critical load is obtained. This is shown in Timoshenko's work [8]. The small terms, which have very little effect on the magnitude of the critical pressure, are omitted. The following expression is then obtained for the buckling of a perfect cylinder

$$q_{cr} = \frac{E}{12(1-\nu^2)}\left(\frac{t}{r}\right)^3\left[n^2 - 1 + \frac{2n^2-1-\nu}{(\frac{nl}{\pi r})^2 - 1}\right] + \frac{Et}{r}\left[\frac{1}{(n^2-1)\left(1+(\frac{nl}{\pi r})^2\right)^2}\right]. \tag{2.105}$$

where n is the number of lobes or waves in a complete circumferential belt at collapse.

This formula was developed by Von Mises in 1914 [2]. The accuracy of this formula was confirmed by Windenburg and Trilling in 1934 [6], where Von Mises' formula was compared to other approximations and experiments. Thus, it forms the theory on which modern literature on buckling of thin cylinders is based. Windenburg and Trilling also note that in formulae in which n appears, the integral value of n which makes q_{cr} a minimum must be used. The minimising of n can be determined by the usual method of differentiation with respect to either n or some function of n. The calculated value of n may be fractional, thus, the correct value of n should be the closest integer. However, von Mises recognised that not all buckling formulae could be treated in this manner, and he used an iterative method to develop a chart to determine the number of nodes which yields the lowest buckling pressure. An example of this method will be illustrated in the next section, where hydrostatic pressure is considered.

If, as an alternative, Donnell's equations are used, the solution is

$$q_{cr} = \frac{E}{12(1-\nu^2)}\left(\frac{t}{r}\right)^3\left[\frac{\left(1+(nl/\pi r)^2\right)^2}{\frac{n^2l^4}{\pi^4r^4}}\right] + \frac{Et}{r}\left[\frac{1}{n^2\left(1+(nl/\pi r)^2\right)^2}\right]. \tag{2.106}$$

Windenburg and Trilling [6] state that the formula developed by Southwell [1] was derived as an approximation to von Mises' formula (equation 2.105) and it

is as follows

$$q_{cr} = \frac{E}{12(1-\nu^2)}\left(\frac{t}{r}\right)^3 (n^2-1) + \frac{Et}{r}\left[\frac{1}{(nl/\pi r)^4(n^2-1)}\right]. \tag{2.107}$$

Windenburg and Trilling found in 1934 [6] that this formula gives values of collapsing pressure which are about six percent lower than those obtained by equation 2.105. Southwell obtained his formula independently, before von Mises' research publication appeared. Equation 2.107 gives distinctly separate curves for successive integral values of n when q_{cr} is plotted against l/r for a constant t/r. Southwell later showed that a single hyperbola could be found that represented the envelope of family of curves very closely for the various values of n with t/r constant [3]. The equation of the hyperbola he found was

$$q_{cr} = \frac{16\pi\sqrt{6}}{27}\frac{E}{(1-\nu^2)^{\frac{3}{4}}}\frac{\left(\frac{t}{2r}\right)^{\frac{5}{2}}}{\left(\frac{l}{r}\right)}. \tag{2.108}$$

Figure 2-16 illustrates the dependance of q_{cr} on the wall thickness to radius, and length to radius ratios. Southwell also proved that this formula can be used

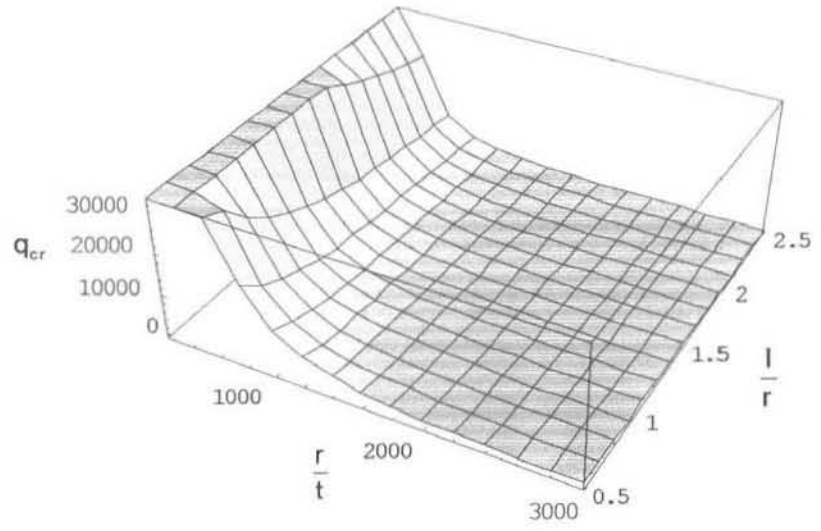

Figure 2-16: Figure showing the relationships of Southwell's hyperbola 2.108.

safely to determine the bucking pressure of short tubes, as it errs on the side of safety. An alternative form of the previous plot of q_{cr} can be seen in figure 2-17,

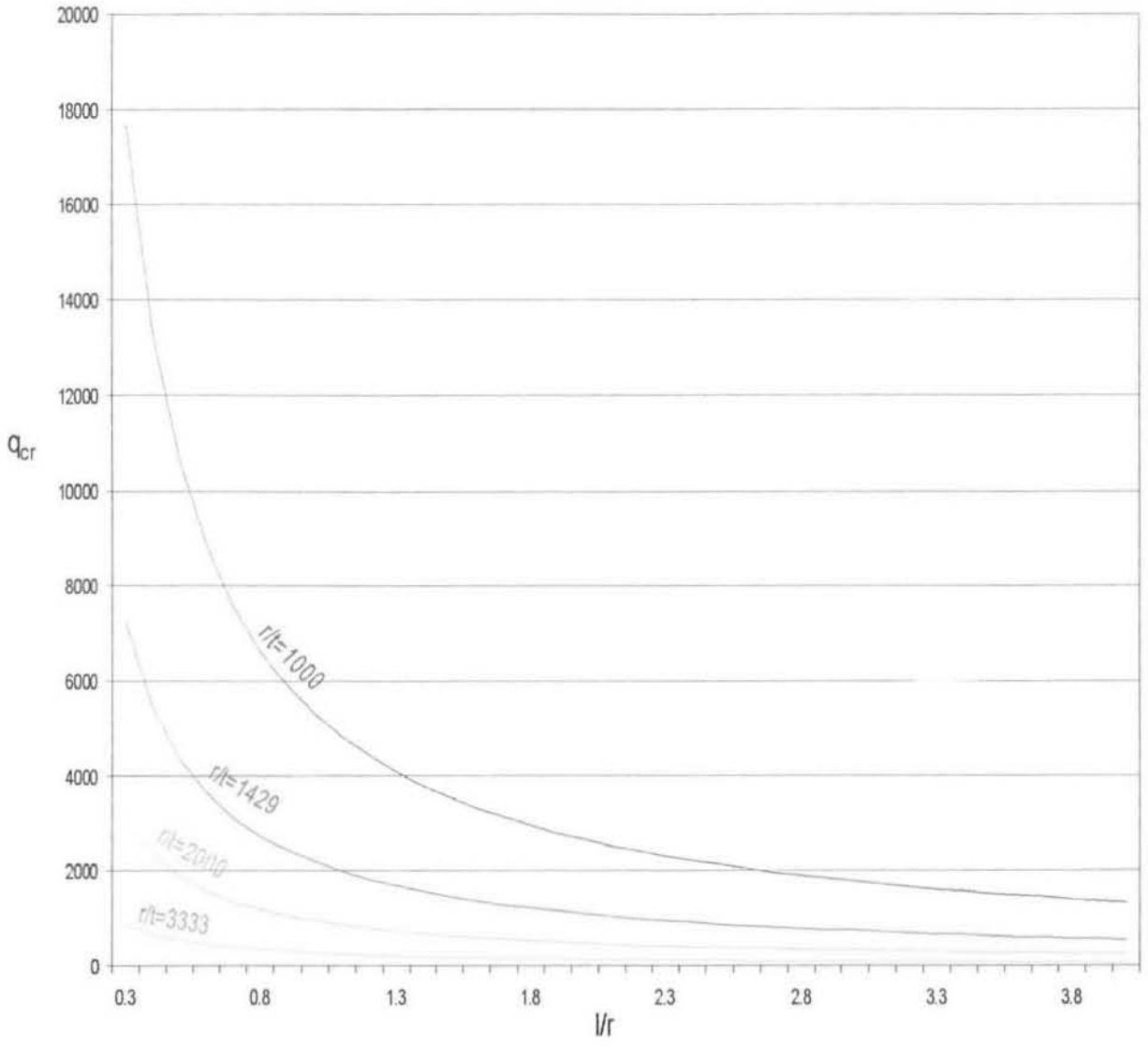

Figure 2-17: Plot showing Southwell's hyperbola in equation 2.108 for various intregral values of t/r.

for various integral values of t/r for carbon steel. Armenkas and Herrmann [19] took the effect of the change, during deformation, of the magnitude and direction of the buckling load into account, unlike all the previous investigations. Their expression for the value of the critical buckling external pressure is

$$q_{cr} = \frac{\pi^2 Et}{l^2 r}\left[\frac{\left(\frac{nl}{\pi}\right)^2}{1+\left(\frac{nl}{\pi r}\right)^2}\right] + \frac{\pi^2 Et^3}{12(1-\nu^2)l^2 r}\left[\frac{\left(\frac{r\pi}{nl}\right)^2 + 4 - 2\nu}{1+\left(\frac{nl}{r\pi}\right)^2}\right]. \tag{2.109}$$

Unlike equation 2.105, Southwell's formula (equation 2.107) is differentiable, and

the equation obtained after differentiation is

$$n^6 \frac{(n^2-1)^2}{(n^2-2/3)^2} = \frac{36(1-\nu^2)\left(\frac{\pi r}{l}\right)^4}{\left(\frac{t}{r}\right)^2} = \frac{36(1-\nu^2)\pi^4}{\left(\frac{t}{r}\right)^2\left(\frac{l}{r}\right)^4}. \tag{2.110}$$

The author would like to note that this formula is incorrect in Windenburg and Trilling's study [6], whereby the denominator in the first term was not squared. However, they correctly went on to show that a good approximation for the minimising of n is obtained by neglecting unity and $2/3$ in comparison with n^2, and it is given by

$$n = \sqrt[4]{\frac{6\sqrt{(1-\nu^2)}\pi^2}{(l/r)^2(t/r)}}. \tag{2.111}$$

Again, the nearest integral number should be used. The different theories are compared in figure 2-18.

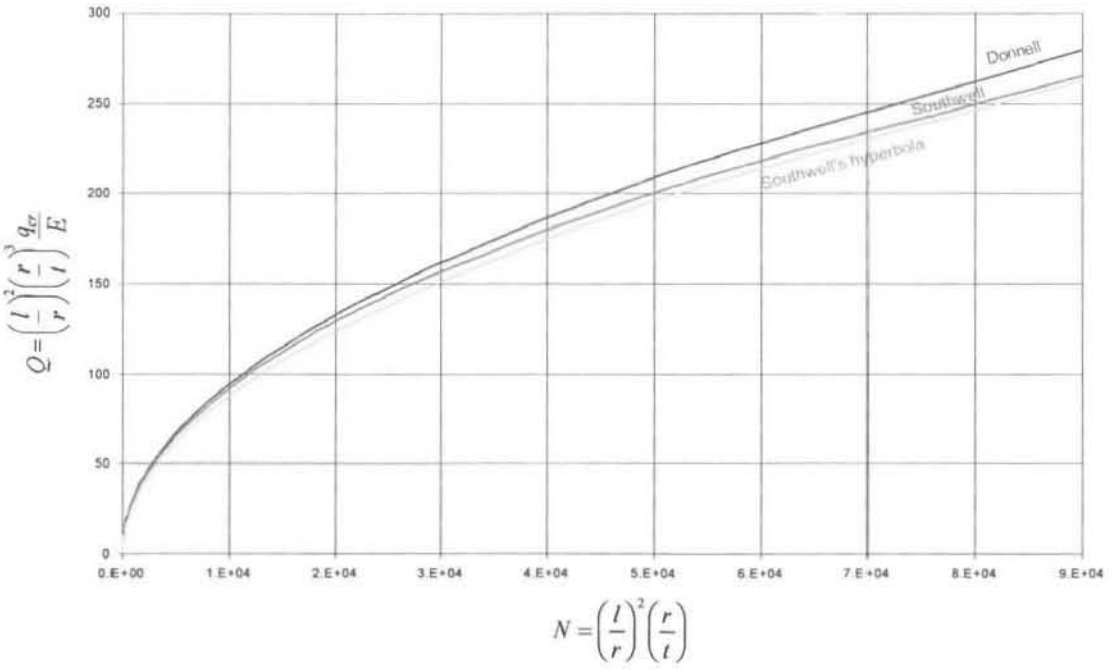

Figure 2-18: Figure showing a comparison of the various theories for lateral external pressure.

The relationship between n and l/r and t/r can be seen as a 3-D plot in figure 2-19 or more specifically, for integral values of t/r, the dependance can be more clearly

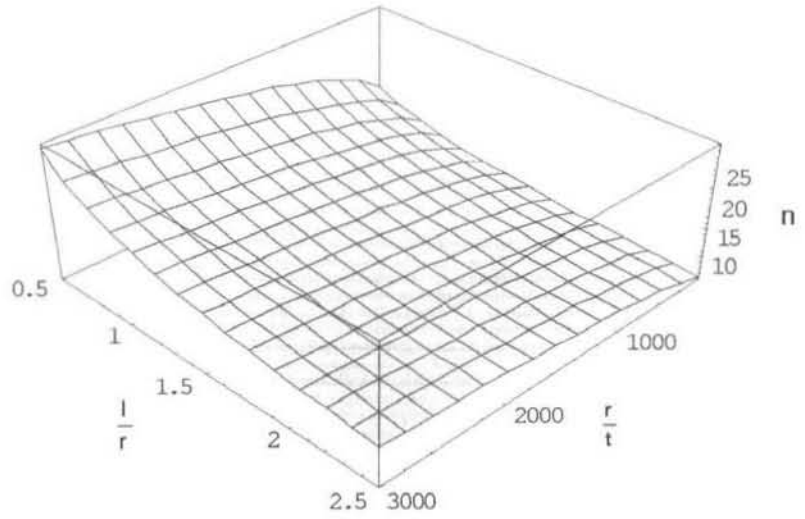

Figure 2-19: 3-D Plot of the relationships in equation 2.111.

seen in figure 2-20. As the length of the cylinder increases the number of lobes into which the cylinder buckles decreases, and as the wall thickness decreases the number of lobes increases.

In 1931, Saunders and Windenburg [5] compared the values of n obtained by the above equation and by equation 2.107, with the number of lobes obtained by experiment. The respective values are shown as a bar graph in figure 2-21.

2.6.2 Numerical Analysis

Using the same variables to represent the results as in Showkati and Ansourian's research [63], the results of the lateral external pressure buckling analyses as compared with the theoretical curve obtained from Von Mises' equation (equation 2.105) are shown in figure 2-22. The discrepancy between theory and the results obtained in Nastran can be mainly attributed to the linear buckling analysis mode (discussed in chapter 1.2). From figure 2-23, one can see that as the cylinder radius to wall thickness ratio increases this discrepancy increases too. Therefore it becomes more inaccurate as the wall thickness reduces.

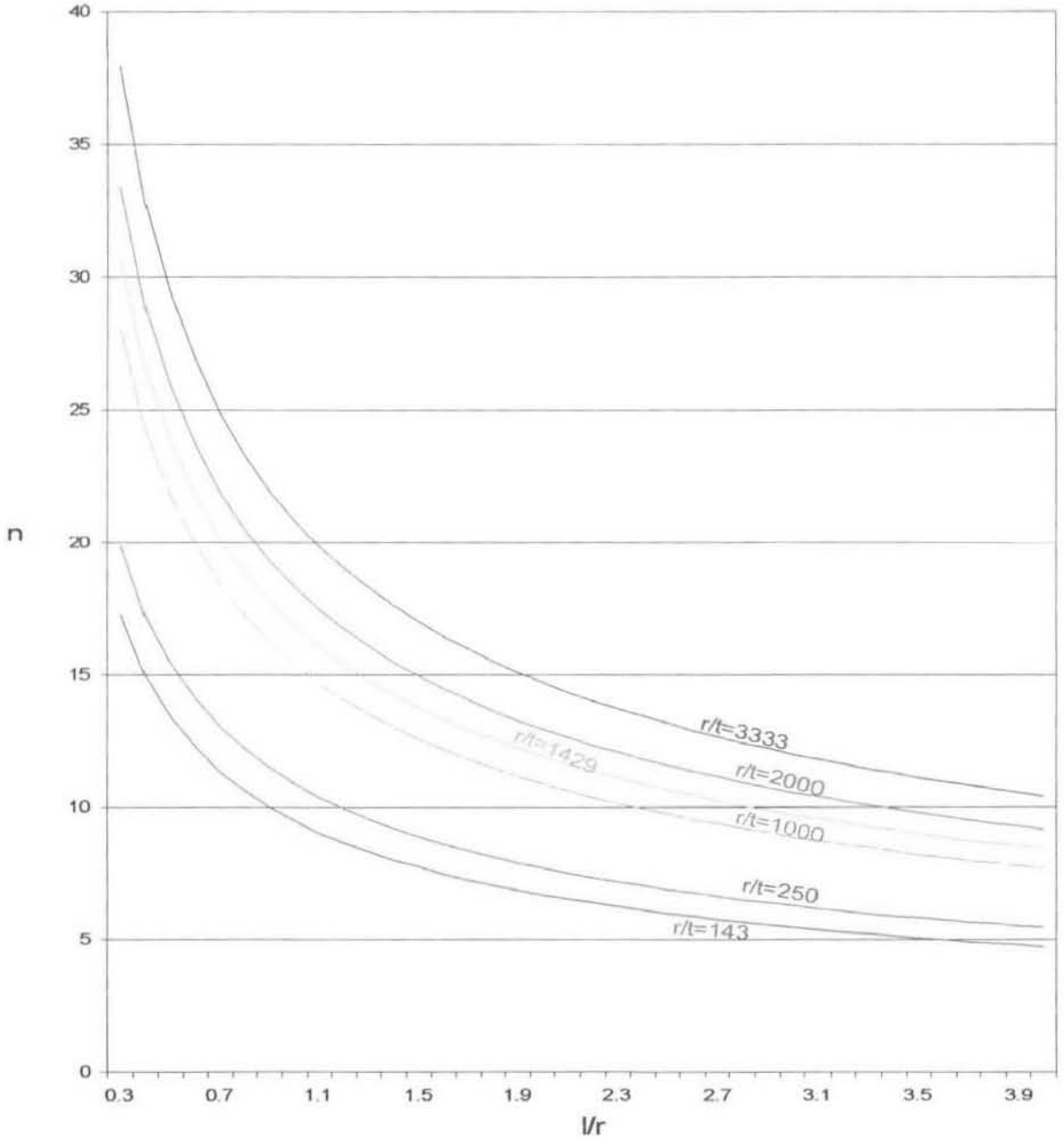

Figure 2-20: Figure showing the relationship between the length, thickness and radius ratios and the number of lobes into which the cylinder buckles.

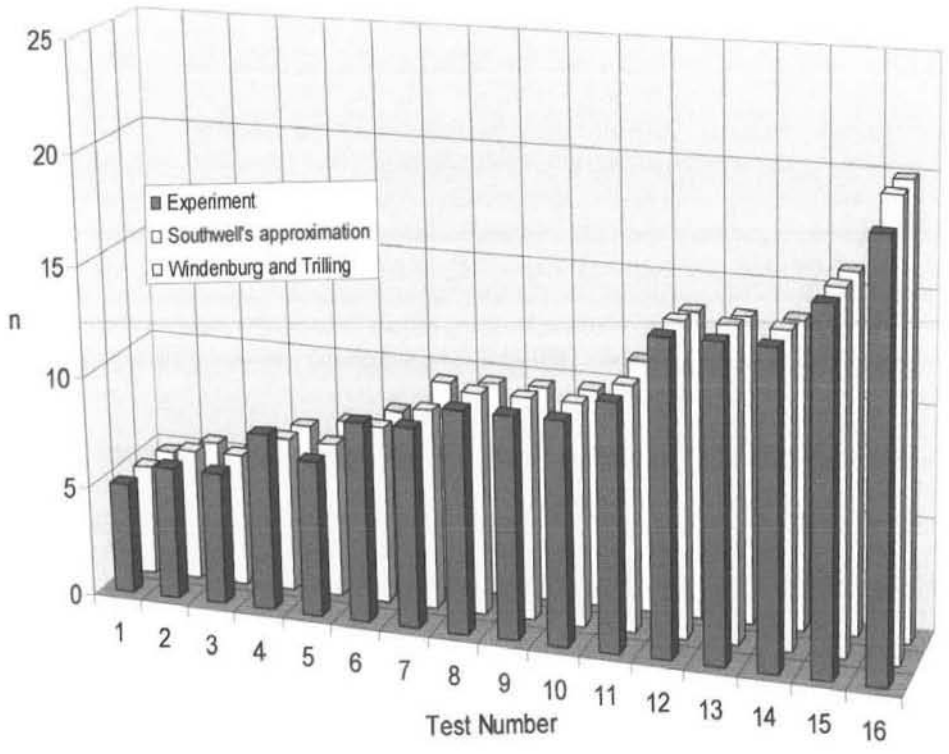

Figure 2-21: Graph showing the results of Southwell's investigation of theoretical and experimental values for n.

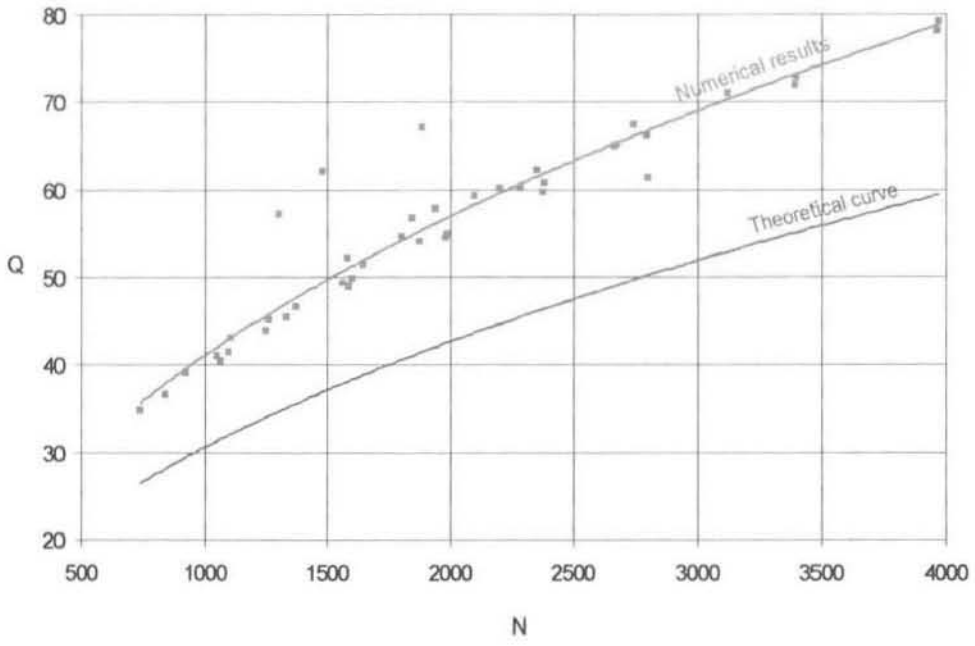

Figure 2-22: Lateral external pressure numerical analysis results compared to Von Mises' theory.

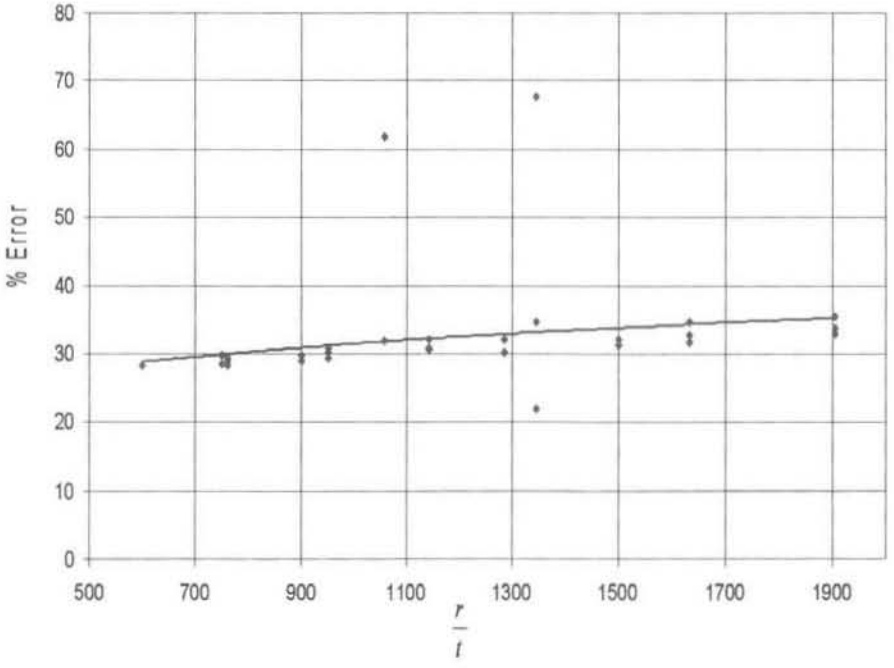

Figure 2-23: Figure showing the disprepancy between numerical analysis results and theory.

2.7 External Pressure - Both lateral and axial

2.7.1 Literature survey

There are many cases where thin cylindrical shells are subjected to an external pressure both axially and laterally (hydrostatically), and this will be investigated in this section.

The three differential equations of equilibrium for determining the three ordinate displacements can be written using equations 2.100 for the case of external pressure and equations A–4 for the case of axial compression. Using the notation for the lateral and axial effect respectively

$$\phi_1 = \frac{qr(1-\nu^2)}{Et} \qquad \phi_2 = -\frac{q(1-\nu^2)}{Et} \tag{2.112}$$

the differential equations are

$$\begin{aligned}
0 &= r^2u'' + \frac{(1+\nu)}{2}r\dot{v}' - \nu r w' + r\phi_1(\dot{v}' - w') + \frac{(1-\nu)}{2}\ddot{u} \\
0 &= \frac{(1+\nu)}{2}r\dot{u}' + \frac{1-\nu}{2}r^2v'' + \ddot{v} - \dot{w} + \kappa(\ddot{v} + \dddot{w} \\
&\qquad + r^2\dot{w}'' + r^2(1-\nu)v'') - r^2\phi_2 v'' \\
r\nu u' + \dot{v} - w - \kappa(\dddot{v} + (2-\nu)r^2\dot{v}'' + r^4\dot{w}'''' + \dddot{w} + 2r^2\ddot{w}'') &= \\
&\qquad \phi_1(w + \ddot{w}) + \phi_2 r^2 w''
\end{aligned} \tag{2.113}$$

By taking the same expressions for displacements as for axial compression (equation A–5), and substituting these into equation 2.113, we obtain three linear equations

$$\begin{aligned}
0 = A\left[m^2\chi^2 + \frac{1-\nu}{2}n^2(1+\kappa) - \phi_1 n^2 + \phi_2 m^2\chi^2\right] + B\left[-\frac{1+\nu}{2}m\chi n\right] \\
+ C\left[-\nu m\chi - \kappa\left(m^3\chi^3 - \frac{1-\nu}{2}n^2 m\chi\right) - \phi_1 m\chi\right]
\end{aligned}$$

$$0 = A\left[-\frac{1+\nu}{2}nm\chi\right] + B\left[n^2 + \frac{1-\nu}{2}m^2\chi^2(1+3\kappa) - \phi_1 n^2 + \phi_2 m^2\chi^2\right] + C\left[n + \frac{3-\nu}{2}\kappa n m^2\chi^2 - \phi_1 n\right] \quad (2.114)$$

$$0 = A\left[-\nu m\chi - \kappa\left(m^3\chi^3 - \frac{1-\nu}{2}n^2 m\chi\right) - \phi_1 m\chi\right] + B\left[n + \frac{3-\nu}{2}\kappa n m^2\chi^2 - \phi_1 n\right] + C\left[1 + \kappa(m^4\chi^4 + 2n^2m^2\chi^2 + n^4 - 2n^2 + 1) - \phi_1 n^2 + \phi_2 m^2\chi^2\right]$$

As before, the critical value of pressure is obtained by equating the determinant to zero, and can be written in the following form [8]

$$C_1 + C_2\kappa = C_3\phi_1 + C_4\phi_2 \quad (2.115)$$

where the coefficients are :

$C_1 = (1-\nu^2)m^4\chi^4$

$C_2 = \left(m^2\chi^2 + n^2\right)^4 - 2\left[\nu m^6\chi^6 + 3m^4\chi^4 n^2 + (4-\nu)m^2\chi^2 n^4 + n^6\right] + 2(2-\nu)m^2\chi^2 n^2 + n^4$

$C_3 = n^2\left(m^2\chi^2 + n^2\right)^2 - \left(3n^2m^2\chi^2 + n^4\right)$

$C_4 = m^2\chi^2\left(m^2\chi^2 + n^2\right)^2 + m^2\chi^2 n^2$

Equation 2.115 represents a linear relation between the quantities ϕ_1 and ϕ_2. If m were kept constant, a system of straight lines would result for the different integer value pairs of n and m, as shown in figure 2-24. The portions of these lines can be used to determine the critical pressure. The origin represents the unloaded shell. As the shell is gradually loaded, the corresponding diagram point moves along some path (shown by the finely dotted line in figure 2-24). As long as it does not meet any of the curves, the shell is in stable equilibrium. But as soon as one of the curves is reached, the equilibrium becomes neutral, with the buckling mode being defined by the parameters n and m.

Any axial pressure makes the critical value of the lateral pressure decrease, and any lateral pressure makes the critical value of the axial pressure decrease.

From equation 2.115, the critical pressure, as given by Von Mises in 1929 [4] is

$$q_{cr} = \frac{Et}{r}\left(\frac{1}{n^2 + \frac{1}{2}(\pi r/l)^2}\right)\left[\frac{1}{\left(n^2(\chi^{-1})^2+1\right)^2} + \frac{\kappa}{(1-\nu^2)}(n^2+\chi^2)^2\right] \tag{2.116}$$

This equation was found to be very accurate when compared to experimental data, and was deemed the best instability formula for vessels subjected to both radial and axial pressure by Windenburg and Trilling in 1934 [6]. A graphical representation of this relation can be seen in figure 2-25 for n=15.

At the US Experimental Model Basin, a formula was developed which is a close approximation to equation 2.116 :

$$q_{cr} = \frac{2.42E}{(1-\nu^2)^{3/4}} \frac{\left(\frac{t}{2r}\right)^{5/2}}{\left(\frac{l}{2r} - 0.45\sqrt{\frac{t}{2r}}\right)} \tag{2.117}$$

A graphical representation of equation 2.117 can be seen in figure 2-26.

It is a very simple formula, independent of n, but it still coincides closely to equation 2.116, the average deviation being about one percent.

Armenkas and Herrmann [19], as before in the case of lateral external pressure, took the effect of the change of the magnitude and direction of the buckling load during deformation into account. Their expression for the value of the critical hydrostatic pressure is

$$q_{cr} = \frac{\pi^2 Et}{l^2 r}\left[\frac{\left(\frac{nl}{\pi}\right)^2}{1-\left(\frac{nl}{\pi r}\right)^2}\right] + \frac{\pi^2 Et^3}{12(1-\nu^2)l^2 r}\left[\frac{\left(\frac{r\pi}{nl}\right)^2 + 4 - 2\nu}{1-\left(\frac{nl}{r\pi}\right)^2}\right]. \tag{2.118}$$

This problem can also be solved using the famous Donnell equations, yielding

$$q_{cr} = \frac{\pi^2 Et^3}{12(1-\nu^2)l^2 r}\left[\frac{\left(1+\left(\frac{nl}{\pi r}\right)^2\right)^2}{\frac{1}{2}+\left(\frac{nl}{\pi r}\right)^2} + \frac{12\left(\frac{l^2}{rt}\right)\sqrt{1-\nu^2}}{\pi^4\left(1+\left(\frac{nl}{\pi r}\right)^2\right)^2\left(\frac{1}{2}+\left(\frac{nl}{\pi r}\right)^2\right)}\right]. \tag{2.119}$$

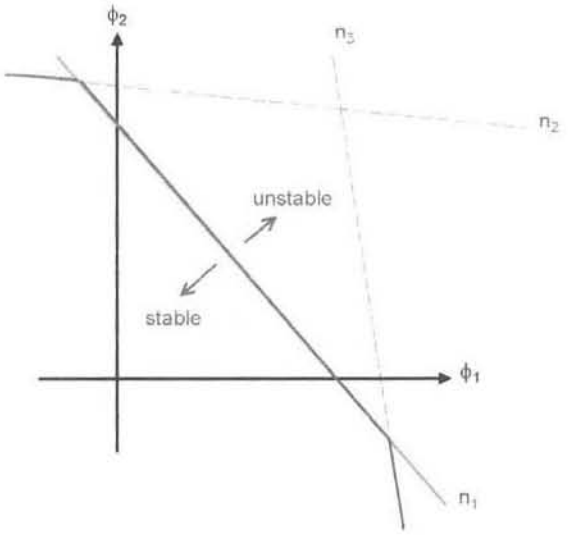

Figure 2-24: Figure showing ϕ_1 and ϕ_2. Reproduced from [18].

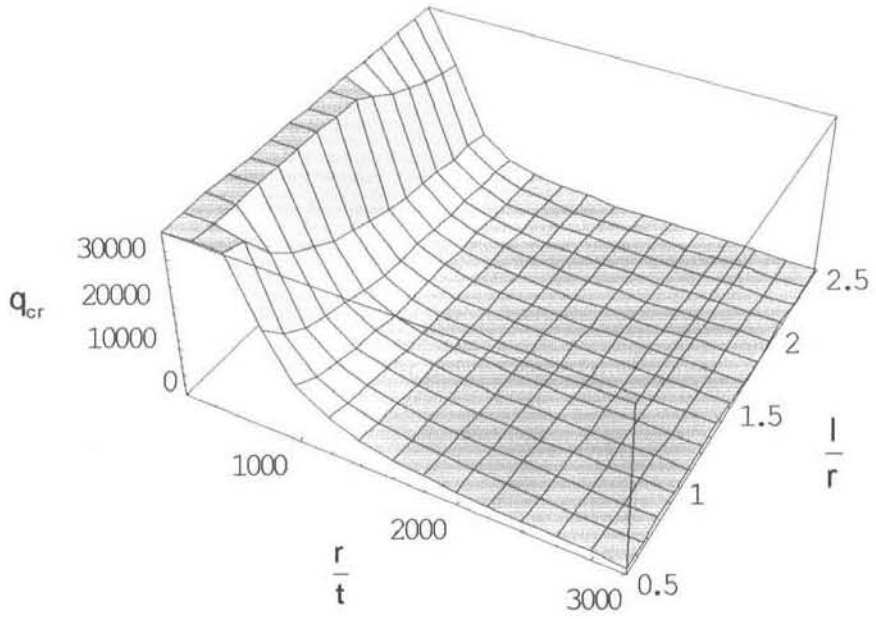

Figure 2-25: 3-D Plot of equation 2.116.

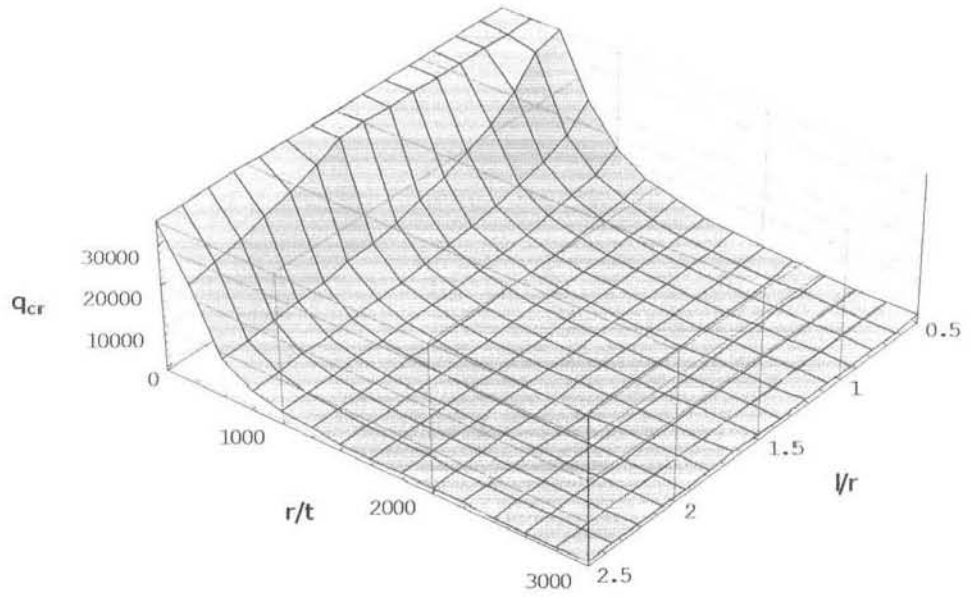

Figure 2-26: Figure showing the relation obtained by the US Experimental Model Basin.

Allen and Bulson [37] showed this to compare closely with Windenburg and Trilling's test results of 1934, except at a low Batdorf parameter, Z, where $Z = (l^2/rt)\sqrt{1-\nu^2}$.

In their research, Windenburg and Trilling also devise a chart from which the value of n must be taken to ensure that the critical pressure is a minimum and this chart is shown in figure 2-27.

This chart was also compared to experimental data and found to be the best known theoretical value for n. From figure 2-27, it can be seen that the number of circumferential lobes into which the cylinder buckles increases as the length and thickness of the shell decrease.

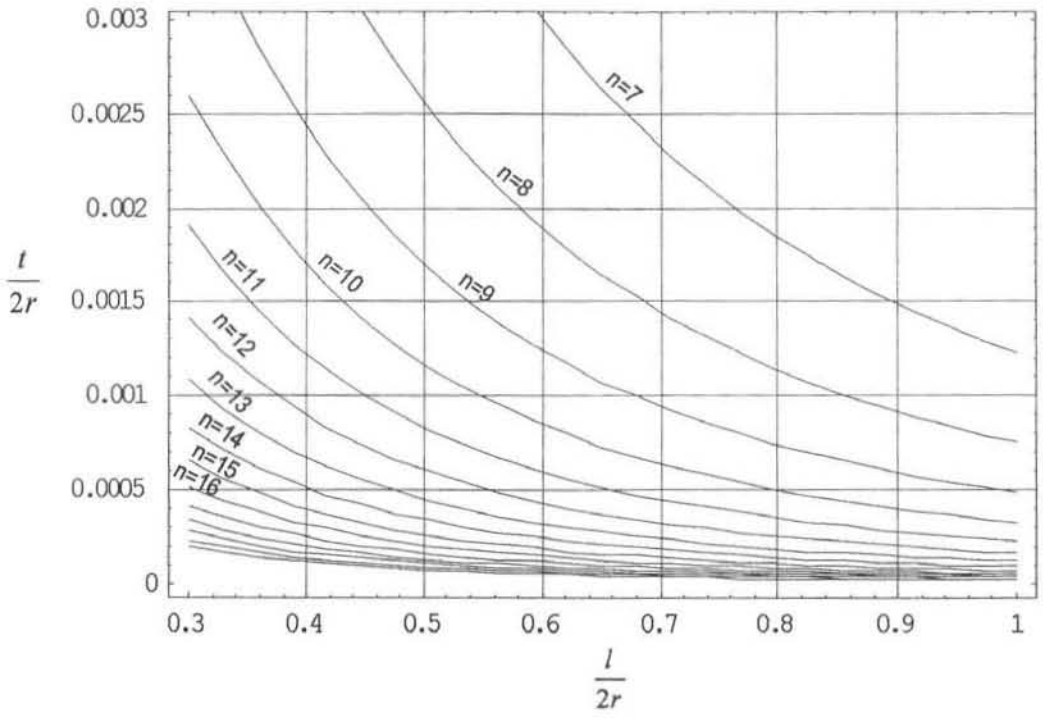

Figure 2-27: Chart reproduced as descibed in Windenburg and Trilling's research [6].

2.7.2 Numerical analysis

As before, experiments were run on a range of cylinders with varying radii, lengths and wall thicknesses. The results of the tests as compared with theory of the US Model basin (equation 2.117) can be seen in fig 2-28. As N and therefore Z, increases the error increases too.

The number of circumferential lobes into which the cylinder buckled is compared with Windenburg and Trilling's chart and is shown in table 2.1.

The number of waves into which the cylinder buckles as calculated by Nastran is higher than the theoretical values as presented by Windenburg and Trilling. This is continuous with the error of the buckling pressure.

l	r	t	n Theory	n Numerical Analysis
12	9	0.006	13	16
12	9	0.007	12	15
12	9	0.0085	12	15
12	9	0.01	11	14
12	9	0.012	11	13
12	9	0.015	10	12
12	11.43	0.006	15	19
12	11.43	0.007	15	18
12	11.43	0.0085	14	17
12	11.43	0.01	13	17
12	11.43	0.012	13	16
12	11.43	0.015	12	15
12	13	0.006	17	21
12	13	0.007	16	20
12	13	0.0085	15	19
12	13	0.01	15	17
12	13	0.012	14	17
12	13	0.015	13	16
14.63	9	0.006	12	15
14.63	9	0.007	11	14
14.63	9	0.0085	12	13
14.63	9	0.01	10	13
14.63	9	0.012	10	12
14.63	9	0.015	9	11
14.63	11.43	0.006	14	17
14.63	11.43	0.007	13	17
14.63	11.43	0.0085	13	16

Table 2.1: Table showing the number of lobes as calculated from theory and found numerically.

2.8 Combined hydrostatic pressure and axial loading

2.8.1 Literature survey

The loading case of hydrostatic pressure in conjunction with an axial load has not been extensively researched, yet it is an important consideration when vacuum tanks with a superstructure or holding tanks with an insufficient venting system subjected to sudden temperature changes are in question. Hutchinson investigated this loading condition for cylinders under external pressure [24] and internal pressure [23], and extended his investigation to deal with imperfect cylinders, which will be dealt with later. This investigation will be concerned with determining the critical external (hydrostatic) pressure while in the presence of a constant axial load.

Hutchinson [23] showed that the *large-deflection Donnell* equations yield a simple solution for this loading condition. Bifurcation from the pre-buckling solution occurs at a certain value of external pressure (for a given axial load). The load-deflection curve falls after bifurcation. Therefore, this bifurcation value is the buckling load.

The eigenvalue equation, modified from [23] for the case of perfect cylinders is

$$\left(1-\frac{\bar{P}}{P_{cl}}\right)^2\left[\frac{\left(1+\gamma^2\right)^2}{4}+\frac{4}{\left(1+\gamma^2\right)^2}-2\widetilde{q}\gamma^2-\frac{2\bar{P}}{P_{cl}}\right]=0 \tag{2.120}$$

where $\widetilde{q}=\frac{qr^2\sqrt{3(1-\nu^2)}}{Et^2}$, $\bar{P}$ is the total axial load (ie. hydrostatic pressure on the top as well as the axial load), γ a free parameter chosen such that q is minimised and P_{cl} is the buckling load of a cylinder subjected to purely axial loading (classical buckling load). To find the upper bound estimate of the external pressure for a given value of axial load, one must solve equation 2.120 for q and then minimise q with respect to γ.

Differentiating q with respect to γ yields ten roots of γ. To obtain the critical

buckling pressure, these roots of γ would then have to be substituted into the equation for q which is

$$q = \frac{Et^2(-8P(1+\gamma^2)^2 + P_{cl}(17 + 4\gamma^2 + 6\gamma^4 + 4\gamma^6 + \gamma^8)}{8r^2(1+\gamma^2)^2(Et^2\pi + P_{cl}\gamma^2\sqrt{3(1-\nu^2)})} \tag{2.121}$$

and the minimum value of q is calculated selected. These roots, which can be seen in appendix D, were found using Mathematica v4.1.

Tennyson, Booton et al [36] determined an interactive equation for the buckling of cylinders subjected to both axial load and hydrostatic pressure. The equation they developed in 1978 was

$$R_p + 1.5R_x - 0.5R_x^2 + R_pR_x = 1 \tag{2.122}$$

where

$$R_p = \frac{\text{Buckling pressure}}{\text{Buckling pressure with no axial load}} = \frac{q_{cr}}{q_{classical}}$$

$$R_x = \frac{\text{Axial load}}{\text{Buckling load with no pressure}} = \frac{P}{P_{classical}} \tag{2.123}$$

This relationship was confirmed by performing tests on spin-cast plastic cylinders.

However, this relationship was disproved for steel by Galletly and Pemsing in 1982 [40]. Tennyson, Booton et al equation was found to be inapplicable to steel cylinders, while accurate for appropriate epoxy plastics. Sharman [17] found that the interaction curve approaches a straight line, and is given by

$$R_x + R_p = 1 \tag{2.124}$$

These relations can be seen in figure 2-29.

Galletly and Pemsing showed that this relation is true, but only for steel cylinders with large values of Z (for Z >200), as seen in figure 2-30. The cylinders in this study had Batdorf parameters ranging approximately from 1000 to 4000, which

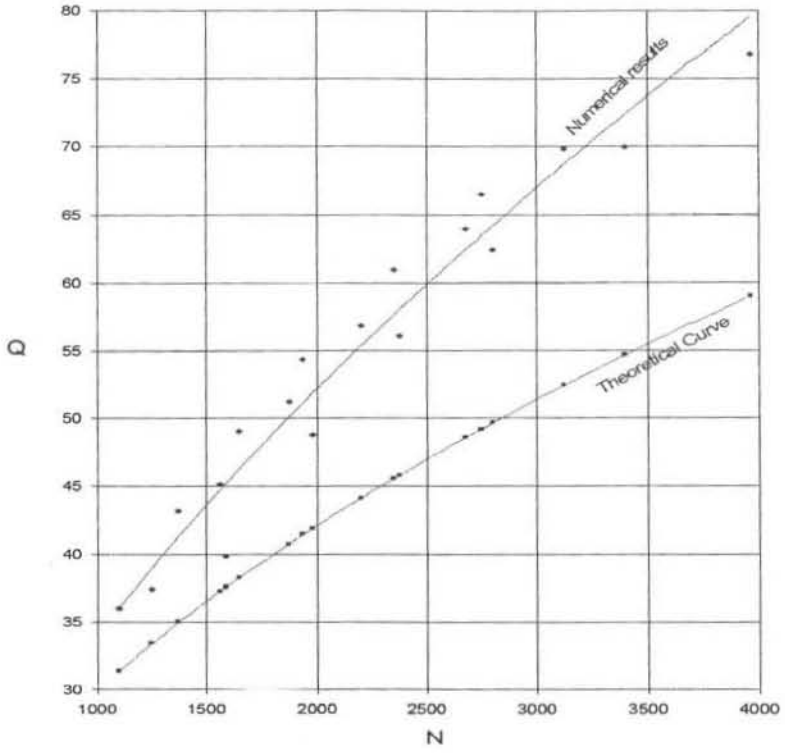

Figure 2-28: Figure showing the results of the tests as compared to the relation obtained from the US Experimental Model Basin.

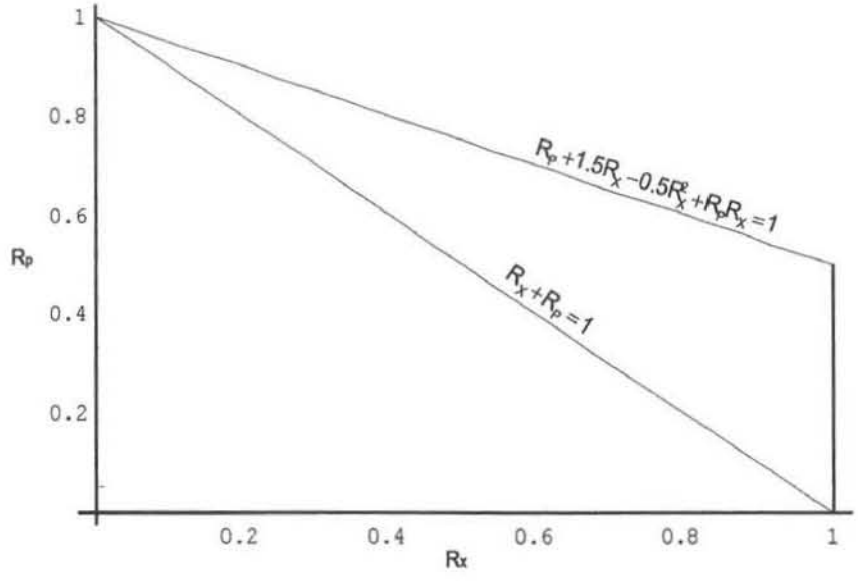

Figure 2-29: Interaction curves

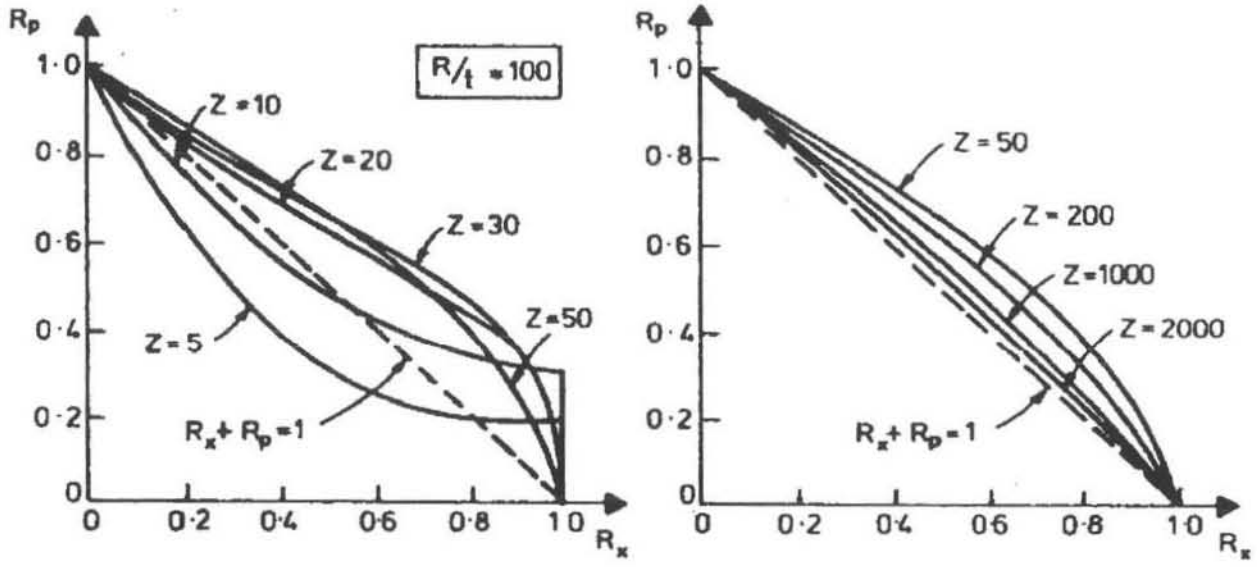

Figure 2-30: Experimental interaction curves for various cylinders. Obtained from [40]

when looking at figure 2-30, can be seen to closely approximate the straight line. Substituting in the expressions for R_x and R_p yields

$$\frac{P + q_{cr}\pi r^2}{P_{cl}} + \frac{q_{cr}}{q_{cl}} = 1 \tag{2.125}$$

Therefore, for a constant axial load, the critical hydrostatic pressure is

$$q_{cr} = \frac{P_{cl}q_{cl} - Pq_{cl}}{\pi r^2 q_{cl} + p_{cl}} \tag{2.126}$$

where the classical buckling axial load and pressure are determined by equations 2.89 and 2.117 respectively.

This relationship is also clearly evident in Shen and Chen [50] in their plots for the perfect cylinder case, where it is pointed out that for a large Batdorf parameter, the interaction curve approaches a straight line.

2.8.2 Numerical Analysis

Analyses were performed on the usual range of cylinders. An axial load was applied to the cylinder, and the hydrostatic buckling pressure determined. The

axial load for SASOL's F7101B tank was used which was reported to be 30000kg. This tank is a 75ft (22.86m) diameter tank, which corresponds to the mid-range of this study. The axial load comprises of the superstructure as well as the roof plating. This axial load forms 0.4% of the classical axial buckling load for the cylinder of dimensions l=12m, r=11.43m t=0.01m.

The numerical analysis results compared with equation 2.126 can be seen in figure 2-31. where, again, at lower values of N and therefore Z the discrepancy

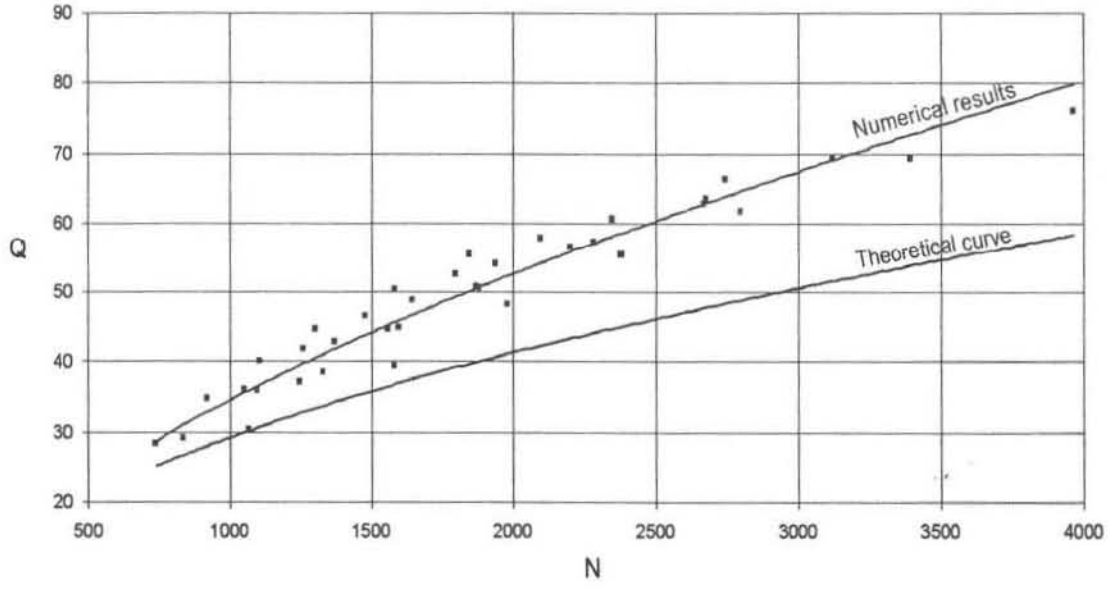

Figure 2-31: Combined loading buckling results for a perfect cylinder.

is smallest.

When these buckling results are compared with pure hydrostatic pressure buckling, one can see that the axial load reduces the buckling load by a very small margin, as seen in figure 2-32.

If this axial load is then varied, as the axial load increases the critical buckling pressure decreases as expected. Various axial loads were tested for a particular cylinder, and the results can be seen in figure 2-33.

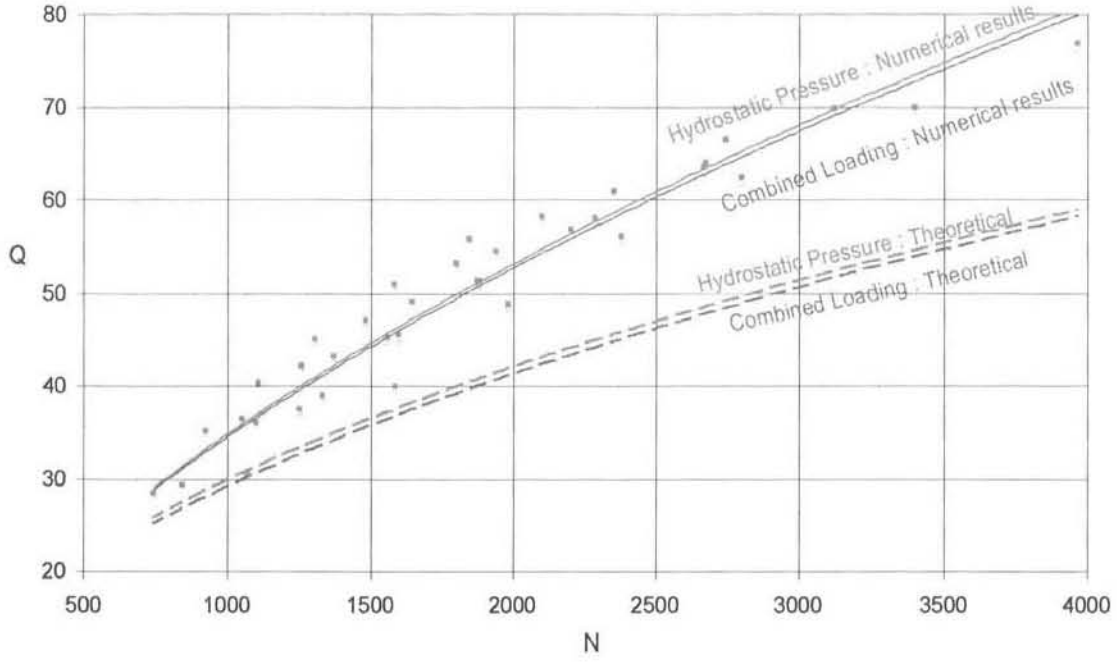

Figure 2-32: Comparison of hydrostatic nad combined loading buckling values.

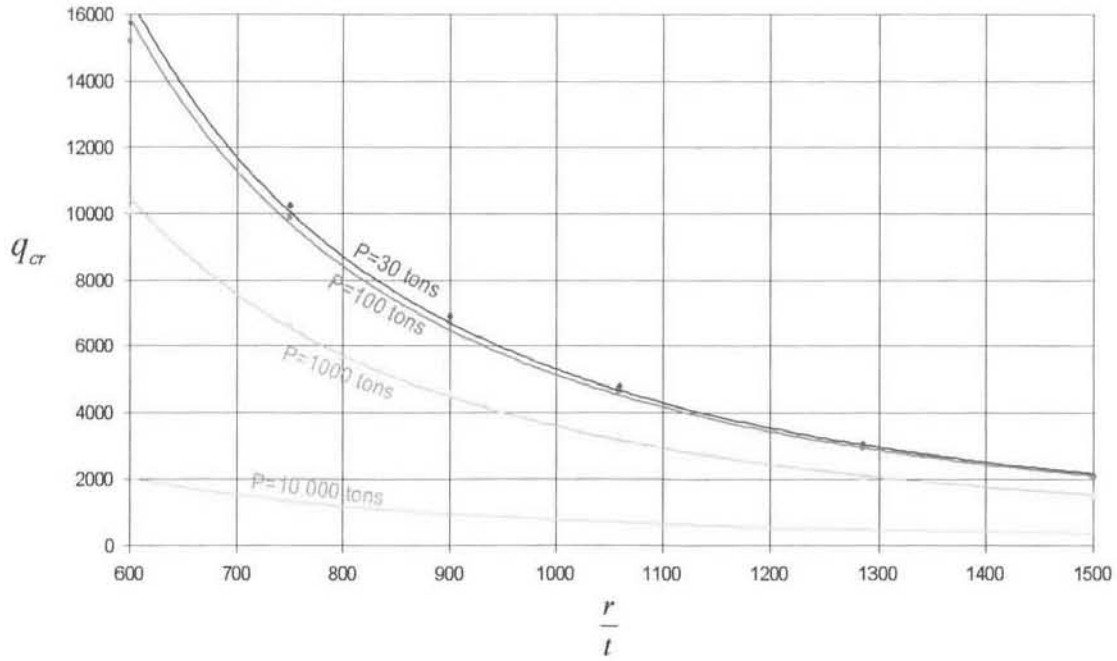

Figure 2-33: Graph showing the decrease of pressure bearing capability with increasing axial load.

Plotted as in Showkati & Ansourian [63] and comparing to hydrostatic pressure buckling analysis values, this relation is clearly evident in figure 2-34.

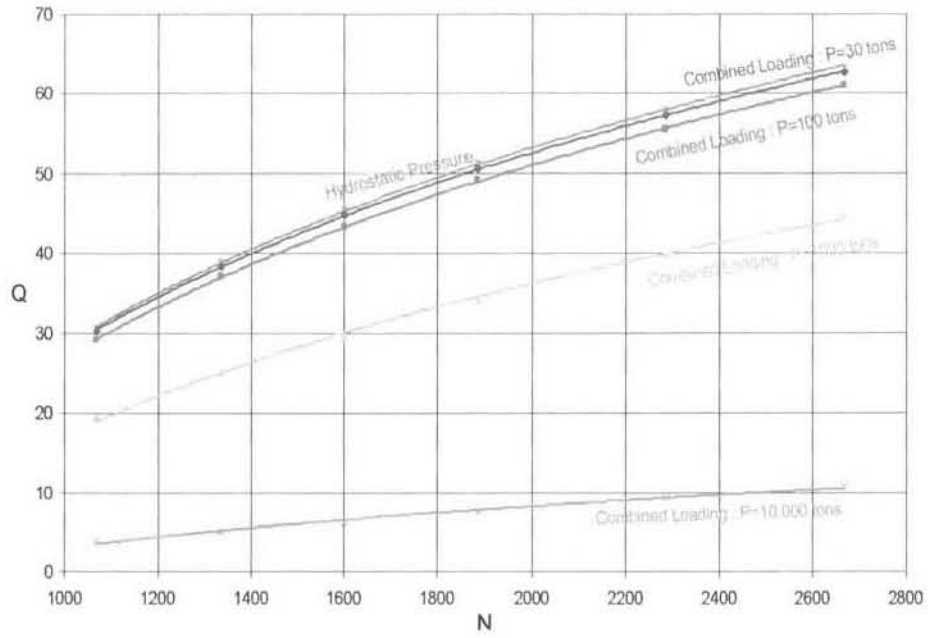

Figure 2-34: Graph showing the comparison of hydrostatic loading with varius cases of combined loading.

The buckling results of the three forms of loading (namely lateral pressure, hydrostatic pressure, and combined loading) can be seen in figure 2-35.

The expected trend of decreasing pressure loading capacity is clearly evident as one progresses from pure lateral external pressure, to pure hydrostatic external pressure, through to the case of combined loading.

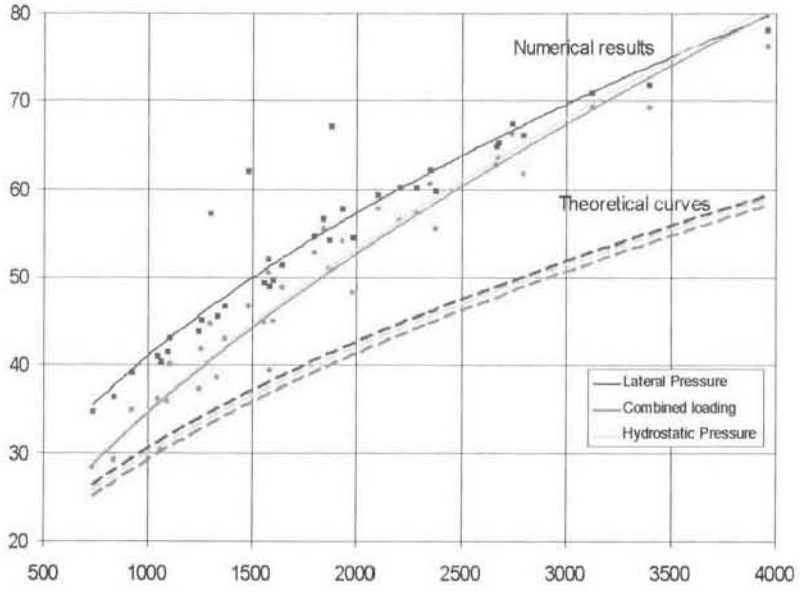

Figure 2-35: Graph showing a comparison of all loading conditions for perfect cylinders.

Chapter 3

IMPERFECT CYLINDRICAL SHELLS

3.1 Introduction

The study of buckling of real cylinders must take into account the fact that all constructions, however carefully made, do have defects sufficiently large to initiate buckling and affect buckling load. The design of vessels subjected to external pressure is different to the design of vessels subjected to internal pressure because of the buckling instability external pressure produces. This factor is evident in all research of buckling of cylinders whereby the correlation of actual bucking tests with theory has been poor with seemingly similar test specimens and techniques. These discrepancies were the subject of widespread controversy but, now it is generally accepted that initial imperfections are the principle cause of this disagreement. The imperfection, such as out-of-roundness, grows as the external pressure is introduced and increased, whereas it is 'cancelled out' in the case of internal pressure. The effect of small local geometric imperfections is small in stiff structures such as thick-walled cylinders and it is therefore not necessary to take them into account. However in more flexible structures such as thin-walled vessels, these imperfections can dramatically reduce the buckling load.

Deformation curves and critical stresses of the cylindrical shells, taking into

account initial imperfections, was first explored by Donnell and Wan in 1950[10] . However, this analysis assumed that the initial imperfection has the same shape as the buckling configuration. Since shape varies during buckling, this assumption of similarity in shape is theoretically wrong. This was shown in the general theory of Koiter [27] and [20]. Nevertheless, if it were true that in the case of an imperfection that has the same shape as the buckled shape was the most oppressive case, then this approach could furnish the critical buckling load correctly.

One trend that is obviously prevalent, as is shown in Kollar and Dulácska's publication [43] which looks at previous research in this field, is that the critical loads of imperfect cylinders decrease sharply with the increasing initial imperfection.

In this chapter, available theory will be reviewed. But, as will be shown, the nature of the imperfection considered throughout previous research varies greatly. Therefore, charts will be presented based almost exclusively on numerical analysis results. Since SASOL's interest lies in out-of-round tanks as defined in the tank code AD Merkblatter B6, out-of-roundness will be expressed as a percentage, and is defined as :

$$u = 2\left[\frac{r_{max} - r_{min}}{r_{max} + r_{min}}\right] \times 100\% \tag{3.1}$$

For the purposes of the numerical analysis, the imperfect cylinders are assumed to have an elliptical cross-section at mid-length. Figure 3-1 shows the variables used and the characteristics of the imperfection. Therefore, the imperfection has the form around the circumference of $e\sin(2\theta)$. For the numerical analyses, the material is assumed to be carbon steel with the material properties shown in appendix B.

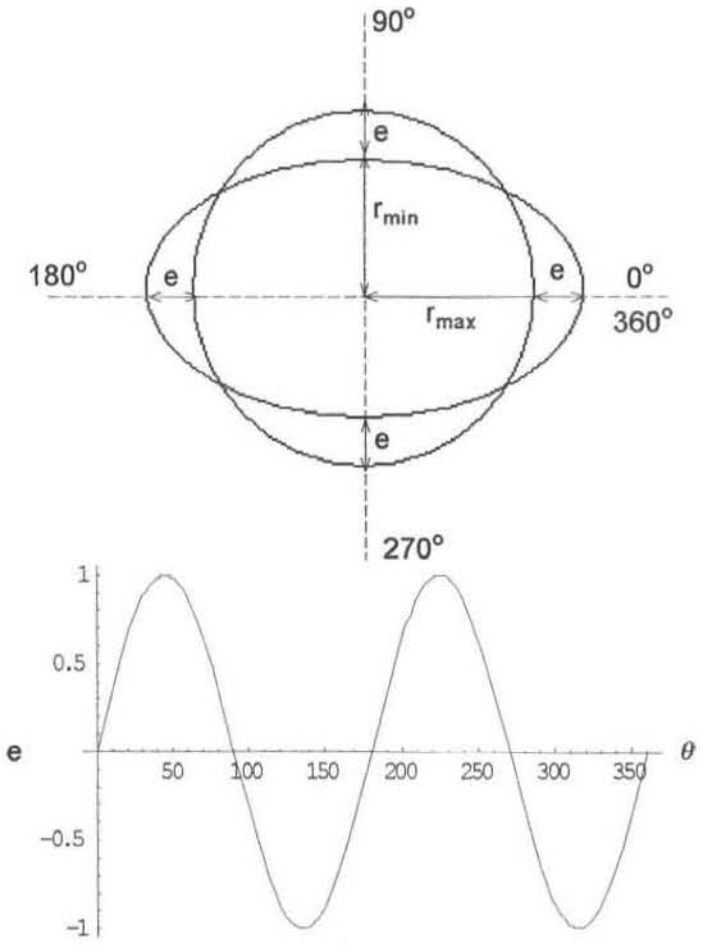

Figure 3-1: Figure showing the definitions of the variables used in the imperfect cylinder study.

3.2 Axial loading

3.2.1 Literature survey

The first documented investigation into the buckling of imperfect cylindrical shells is reported to have been by Donnell in 1934 [7] and then later by Donnell and Wan in 1950 [10]. In these publications an 'unevenness factor', U in the latter and α in the former, are adopted and assumed to depend only on the method of fabrication. It is also assumed here that the worst-case scenario is the case where the initial deflection has the same general form as the buckled form. The

expression for the initial deviation from the perfect cylinder was considered to be

$$w_0 = At\left(\cos\frac{mnx}{r}\cos\frac{ny}{r} + b\cos\frac{2mnx}{r} + c\cos\frac{2ny}{r} + d\right) \tag{3.2}$$

where A is the amplitude of the cylinder deviation and is given by $A = \left(U/\pi^2\right)l_x l_s/t^2$, m is the wave shape ratio, n is the number of circumferential waves and a, b, c, d are other arbitrary parameters to make this equation true. This expression for the initial amplitude of deviation is derived in the paper [7] from the case of actual columns. The variables l_x and l_s are the half wave lengths of the deviations in the axial and circumferential directions of the cylinder wall respectively. It was then shown that because most thin-walled cylinders in tests and applications are made by bending flat sheets and this bending into a cylinder tends to flatten out waves which are long in the circumferential direction (see figure 3-2a) more than those which are long in the axial direction (figure 3-2b), the initial amplitude becomes $A = \left(U/\pi^2\right)l_x^{0.5}l_s^{0.5}/t^2 = Ur^2/(m^{1.5}n^2t^2)$.

Donnell and Wan also went on to show that the value of the unevenness coefficient, U, which is found to explain most experimental cylinder strengths can be given as 0.00015. In figure 3-3, the results obtained by Donnell and Wan for $U = 0.00015$

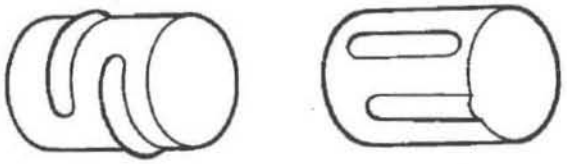

Figure 3-2: Figure showing the effect of bending on the initial defects. From [10]

are superimposed on their test results. The theoretical curve fits the average of the test group quite well. Unfortunately, this paper identifies the fact that these curves are true for a specific value of b, c, and d, and that the initial deviation from true is assumed to be idealised. It is apparent that in order to predict the influence of the actual initial imperfections that occur in practice, one must consider these real imperfections.

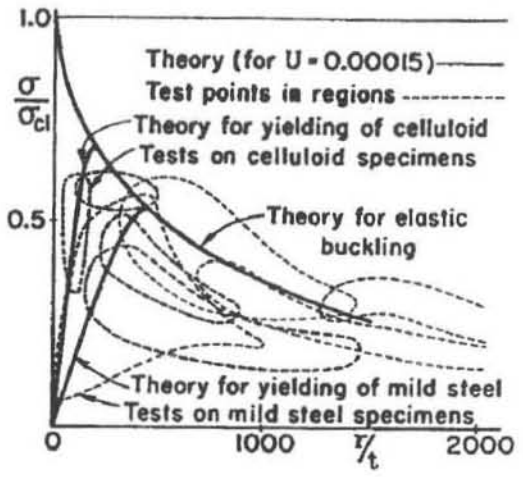

Figure 3-3: Donnell's results for U=0.00015. Obtained from [10]

In a move towards a more generalised curve, in 1965 Weingarten and Seide[21] proposed an equation for a lower bound to the data obtained from experiments. This method was introduced to overcome the increasingly sophisticated analyses that were being developed. It was found that a good representation of a lower bound curve for cylinders in the range $100 < \frac{r}{t} < 4000$, $0.031 < \frac{l}{r} < 5$ is given by

$$\frac{P}{2\pi Et^2} = 0.606 - 0.546\left[1 - e^{-\frac{1}{16}\sqrt{r/t}}\right] + 0.9\left(\frac{r}{l}\right)^2\left(\frac{t}{r}\right) \tag{3.3}$$

In 1969, Arbocz and Babcock[28] reported on buckling tests which for the first time were based on manufactured cylinders. The imperfections were measured by means of an automated scanning mechanism. These imperfections were then harmonically analysed and represented mathematically by Fourier series. This study also showed that asymmetric imperfections made the cylinder more sensitive to axial loading, therefore asymmetry had to be considered as well as modes other than buckling modes had to be considered. This immediately reduces the amount of viable research performed in this field, as numerous researchers based their research entirely on axisymmetric imperfections. Arbocz then went on to publish an Imperfection Data Bank in 1982 [39] which reviews imperfections surveys performed for various different fabrication methods. This publication proves useful for weight critical, low margin of safety applications such as the aerospace industry where the high cost of such an analysis can be absorbed.

This was then refined in 1995 by Arbocz and Hol[59], where they attempted to develop an 'improved shell design criteria' for cylinders subjected to axial loading. The improvements with respect to the existing shell design procedure was sought by the definition of a 'knock-down' (reduction) factor, applicable to a particular fabrication method. A full-scale model was produced to accurately ascertain the imperfections particular to that fabrication method. A stochastic (a random variable having a probability distribution) stability analysis was also performed to develop a method for checking the reliability of shells using statistical measures of the imperfections involved. Arbocz and Hol then concluded that in order for this approach to work, the companies involved in the production of shell structures must carry out complete imperfection surveys on a small representative sample of their shells. Again, this is viable in industries where the high cost of this can be absorbed.

Jamal, Midani et al[65] found analytically that the reduction in critical load due to a localised imperfection was proportional to $A^{2/3}$ where A is the amplitude of the imperfection. They also went on to propose formulae to predict the reduction in the critical load, as well as a correction of this formula once it was found to underestimate the reduction. The formula they proposed (simplified) was

$$\frac{P_{cr}}{P_{cl}} = 1 - \sqrt[3]{\frac{Et}{P_{cl}}}\sqrt[3]{\frac{9\left(0.14(1-\beta^2)^2(\delta_a^2+\delta_c^2)+0.8(1+\beta^2)\delta_b^2\right)}{8(1+\beta^2)^2}}\left(\frac{A}{t}\right)^{2/3} \tag{3.4}$$

where

$$
\begin{aligned}
\beta &= \frac{\text{axial wavelength}}{\text{circumferential wavelength}} \\
\beta &= \frac{\sqrt{\frac{r}{k}} \pm \sqrt{\frac{r}{k} - 4n^2}}{2n} \\
k^2 &= \frac{t^2}{12(1-\nu^2)} \\
\delta_a &= -\frac{\sqrt{12\pi(1-\nu^2)}}{8(1-\beta^2)} \frac{C}{r} \left[1 + e^{-\left(\frac{nC}{\beta r}\right)^2} + e^{-\left(\frac{n(1+\beta^2)C}{2\beta r}\right)^2} + e^{-\left(\frac{n(1-\beta^2)C}{2\beta r}\right)^2} \right] \\
\delta_b &= -\frac{\sqrt{12\pi(1-\nu^2)}}{8} \frac{C}{r} \left[1 + e^{-\left(\frac{n(1+\beta^2)C}{\beta r}\right)^2} \right] \\
\delta_c &= -\frac{\sqrt{12\pi(1-\nu^2)}}{8(1-\beta^2)} \frac{C}{r} \left[1 + e^{-\left(\frac{n\beta C}{r}\right)^2} + e^{-\left(\frac{n(1+\beta^2)C}{2\beta r}\right)^2} + e^{-\left(\frac{n(1-\beta^2)C}{2\beta r}\right)^2} \right]
\end{aligned}
$$

and C is the width of the imperfection.

For practical purposes, Croll [60] proposed in 1995 that the reduced stiffness method for the analysis of shell buckling could be used. Croll theorised that this method had reached the stage where it could be profitably adopted as a basis for improved shell buckling design methodology. This method was first introduced by Weingarten and Seide, and is outlined on page 69.

In 1999, Yamada and Croll [66] theoretically demonstrated the physically based theory of the reduced stiffness method. It was shown that the reduced stiffness was relevant even for initial imperfections having very different wave lengths. Therefore, the modified expression for the reduced stiffness lower bound to elastic buckling is given by

$$\frac{P_{cr}}{P_{cl}} = \frac{1-\nu^2}{2-\nu^2-\nu+\frac{\nu}{\pi}\sqrt{2Z\sqrt{3}}} \tag{3.5}$$

and is shown in figure 3-4. The dominant buckling mode having a single axial half-wave and a characteristic circumferential half wave number, was shown to conform closely with that predicted from a reduced stiffness analysis. The lowest recorded non-linear buckling loads were shown to be accurately predicted by the

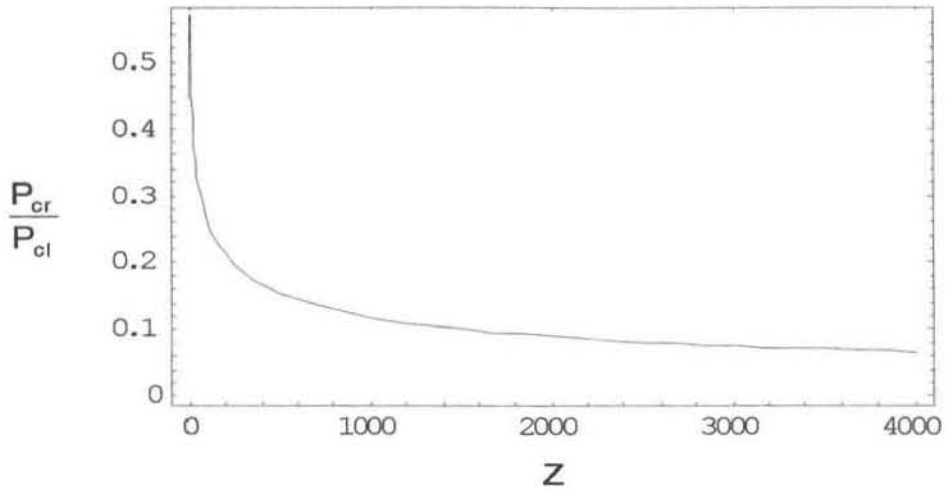

Figure 3-4: Plot showing the relationships in equation 3.5.

modified form of the reduced stiffness critical load. The authors concluded that the modified form of the reduced stiffness method provides a simple yet safe basis for the design of axially compressed cylinders, particularly for the design of cylinders where weight is not an issue.

A very useful contribution according to Allen and Bulson [37], has come from Koiter who examined the peak stress in cylinders with initial displacements. He showed that the following relation existed between the reduction in buckling load and the cylinder parameters:

$$\frac{P_{cr}}{P_{cl}}\frac{A}{t} = \left(1 - \frac{P_{cr}}{P_{cl}}\right)^2 \sqrt{\frac{4}{27(1-\nu^2)}} \tag{3.6}$$

This relationship is shown in figure 3-5.

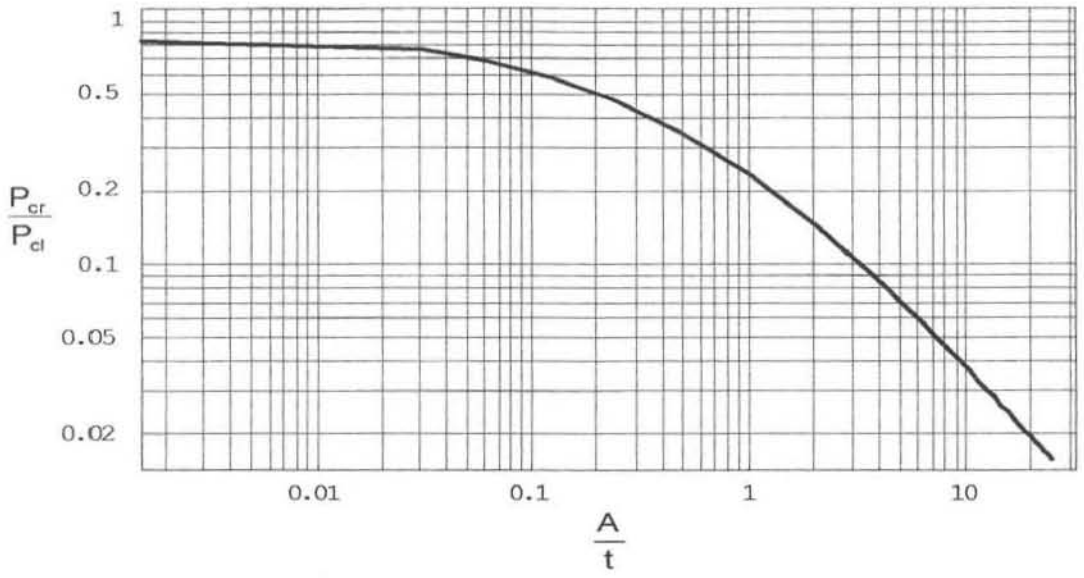

Figure 3-5: Plot showing Koiter's relationship for the reduction of buckling load.

3.2.2 Numerical analysis

Cylinders of the same basic dimensions as those simulated for the case of perfect cylinders were analysed here, but with a mid-length elliptic cross-section instead of a circular one. An exaggerated view of an imperfect cylinder can be seen in figures 3-6 to 3-8.

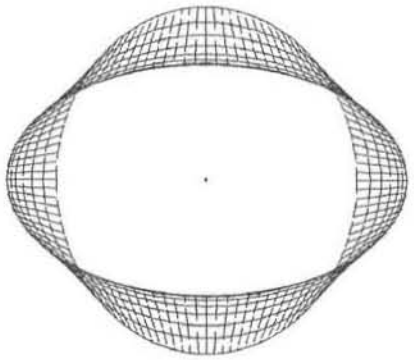

Figure 3-6: Top view of exaggerated imperfect cylinder.

Imperfections in the range 0.5%-2% were analysed, and the results recorded. Imperfections in this range were considered because in the appendix to AD-Merkblatt B6 : Cylindrical shells subjected to external overpressure, it is stated

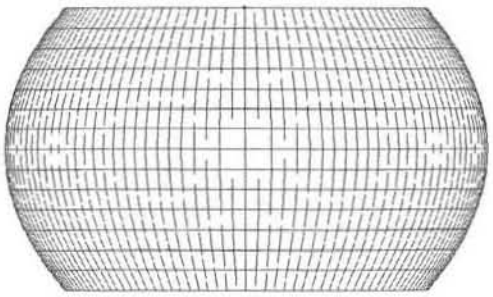

Figure 3-7: Side view of exaggerated imperfect cylinder.

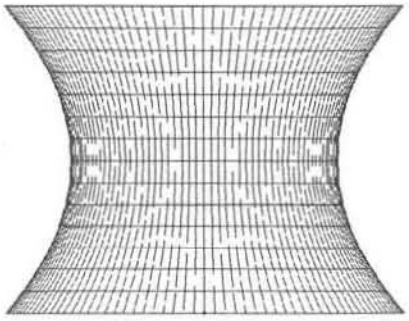

Figure 3-8: Side view of exaggerated imperfect cylinder rotated 90^o to figure 3-7.

that : "According to AD-Mekblatt HP1 Table 1, out-of-roundness may not usually exceed 1.5% in the presence of external pressure stresses and where the $(t/2r)$ ratio does not exceed 0.1." Numerical testing was then performed in MSC Nastran as before.

The buckling pattern was found to be asymmetric, with pronounced waves along the minor axis of the ellipse. The buckling pattern can be seen in figure 3-9.

The results of the numerical analysis under axial loading for various degrees of imperfection for the cylinders examined are shown in figure 3-10.

The decrease in load carrying capability due to the increase in imperfection can be clearly seen. It is also important to note that the effect of the imperfection becomes more pronounced as the thickness decreases.

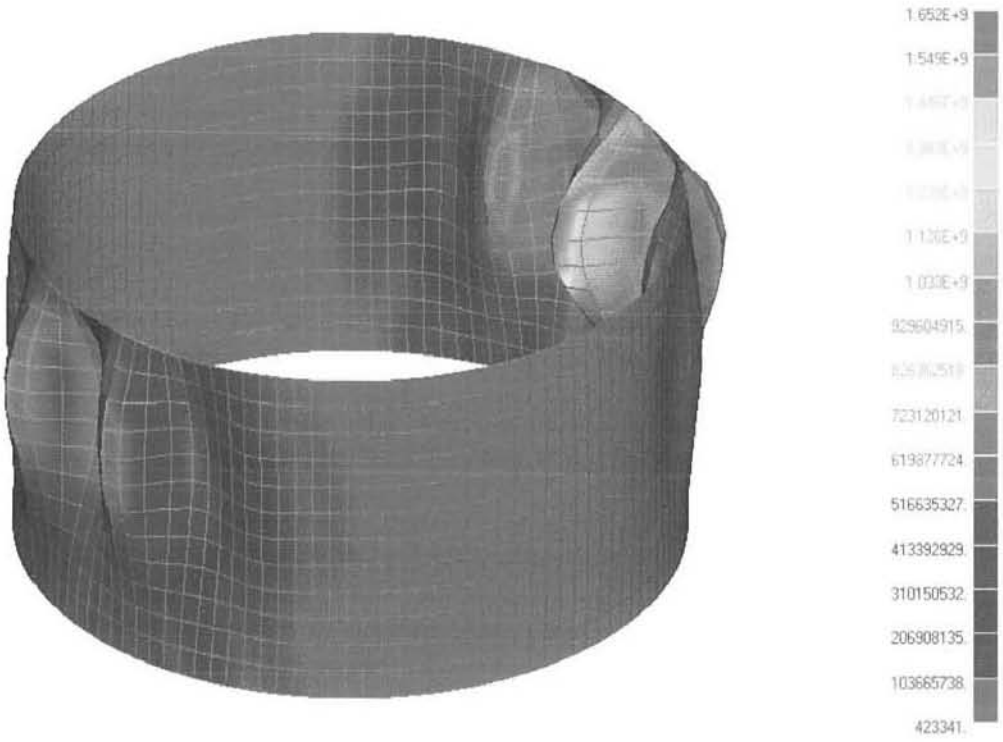

Figure 3-9: Buckled imperfect cylinder l=14.63m, r=11.43m, t=0.015m and u=2%

The dependence of the buckling load on the eccentricity can also be seen in figure 3-11, where the buckling load sharply decreases as the eccentricity increases.

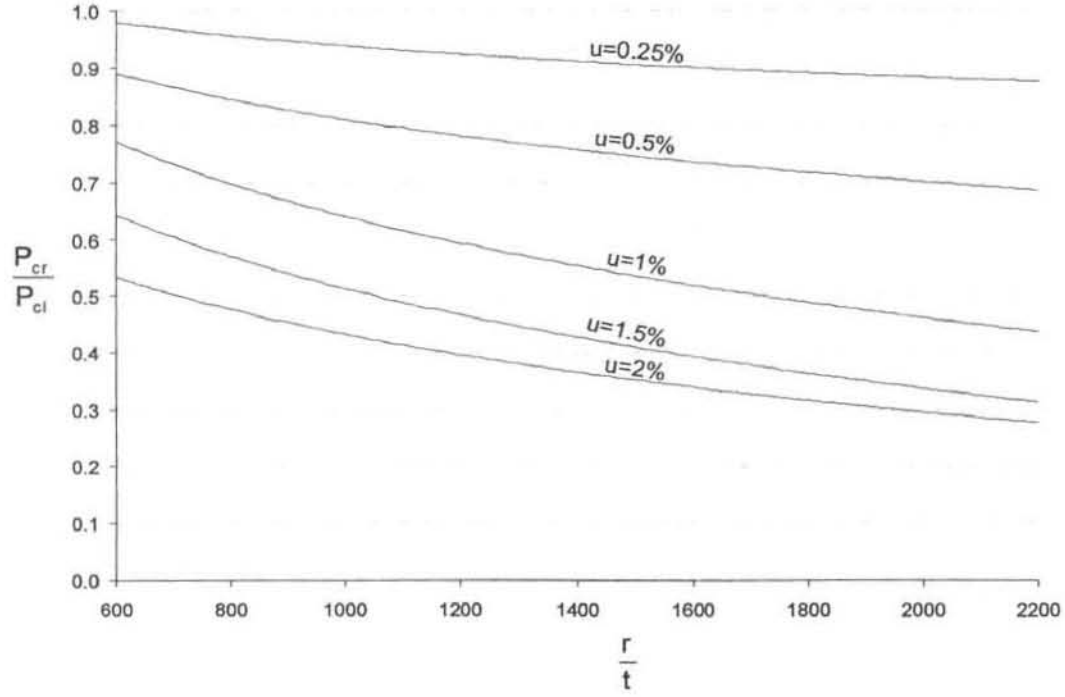

Figure 3-10: Numerical analysis results for the reduction in buckling load for various degrees of imperfection.

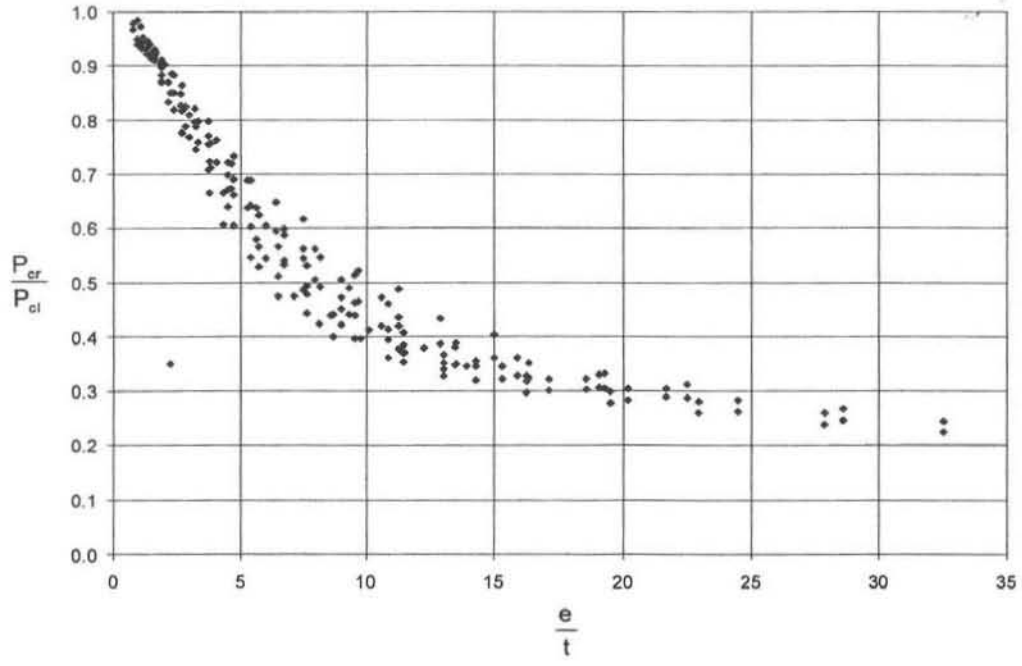

Figure 3-11: Plot showing the reduction in buckling load for varying eccentricity ratios.

3.3 Lateral external pressure

3.3.1 Literature survey

No previous research was found that concentrated solely on pure lateral external loading of imperfect circular cylindrical shells. Since, in practice, pressure is exerted on all faces, only hydrostatic pressure loading of imperfect cylindrical shells was considered. The survey of this form of loading is considered in the next section.

3.3.2 Numerical analysis

An exaggerated view of the buckling pattern can be seen in figure 3-12, which is seen to be non-axisymmetrical. The results for the numerous buckling analyses

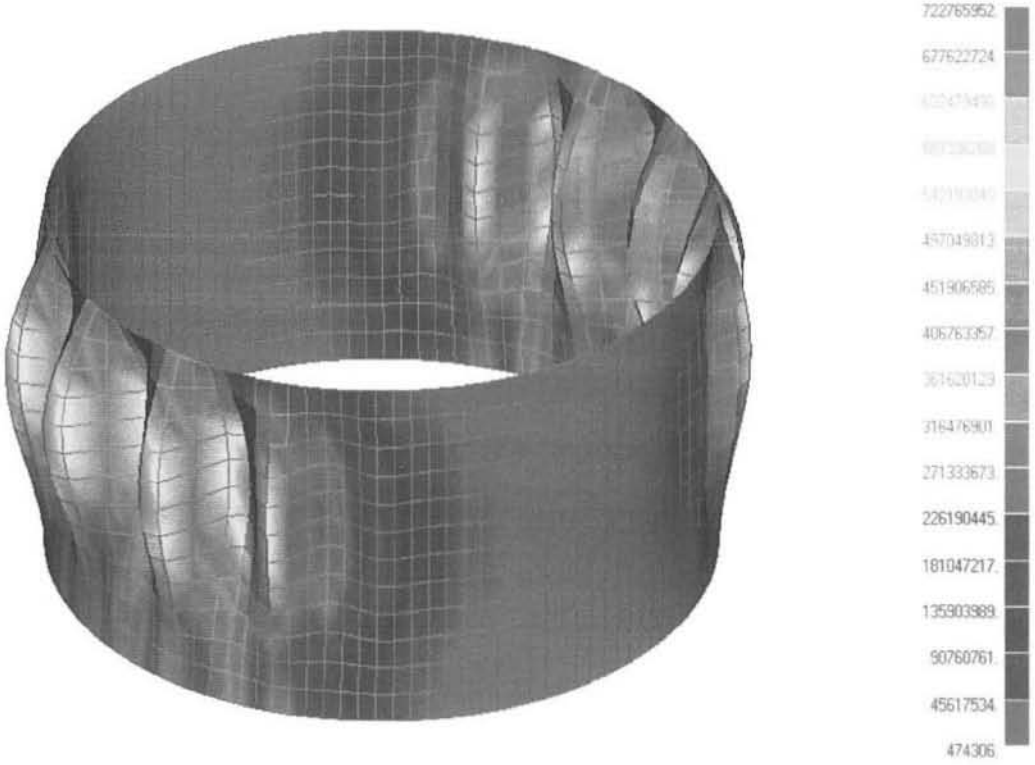

Figure 3-12: Deformed cylinder l=14.63m, r=11.43m, t=0.15m and u=2%

performed are plotted in figure 3-13. It can be seen that the buckling pressure decreases as the imperfection increases.

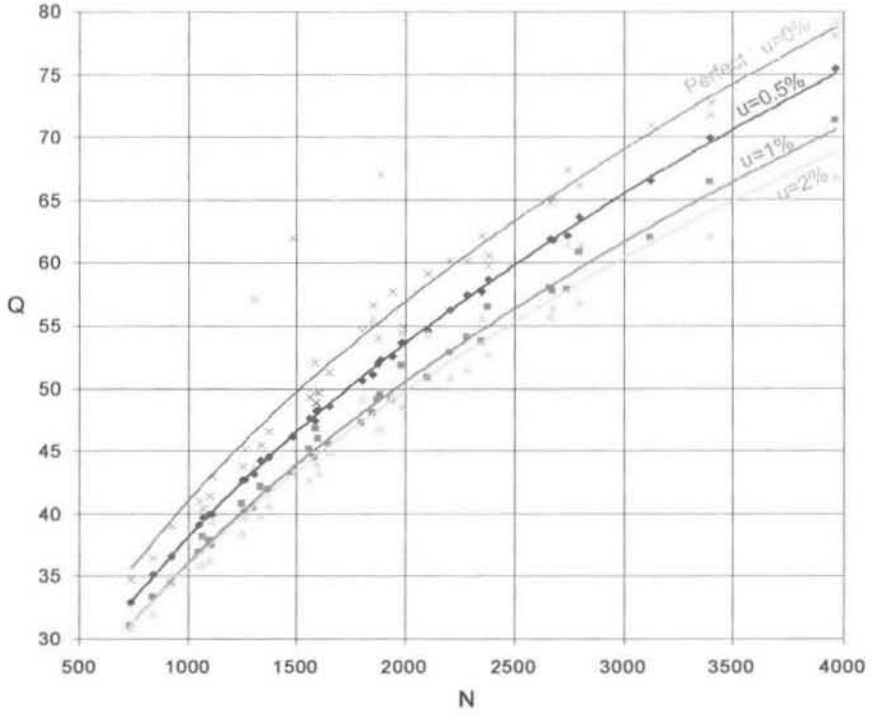

Figure 3-13: Results of numerical testing for various values of imperfection.

However, as the out-of-roundness increases to 2%, it can be seen that at low values of N, the buckling pressure does not decrease significantly from that of out-of-roundness of 1%. It was actually found that beyond some critical out-of-roundness the strength of the cylinder tends to increase again. This behaviour of decreasing sensitivity for increasing out-of-roundness beyond a critical level of imperfection was also found by Guggenberger in 1995 [61], and his results are reproduced in figure 3-14.

This trend in the results can be more clearly seen in figure 3-15 where the reduction in external buckling pressure is plotted versus the eccentricity to wall-thickness ratio.

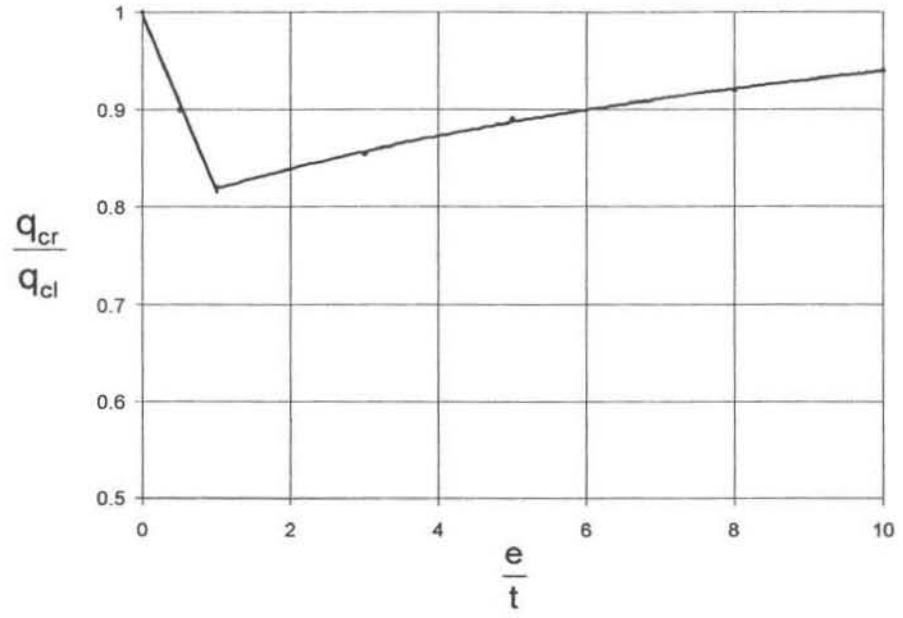

Figure 3-14: Results of Guggenberger's tests. Reproduced from [61].

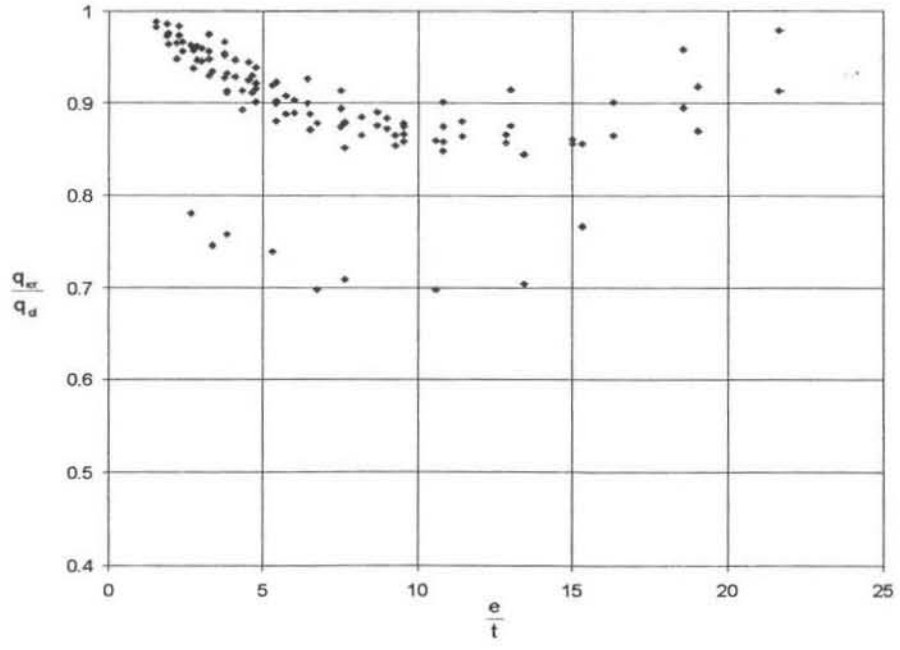

Figure 3-15: Behaviour of the reduction in buckling load as compared with the eccentricity to wall thickness ratio.

3.4 External hydrostatic pressure

3.4.1 Literature survey

In 1952, Holt [11] developed a procedure for computing the allowable out-of-roundness of a circular cylindrical shell subjected to external pressure. In this paper it was reported that the equation for computing the strength of an out-of-round cylinder is

$$q_{cr} = \frac{S_U \frac{t}{r}}{1 + \frac{A}{2t} \frac{E\left(\bar{n}^2 - 1 + \nu \frac{\pi^2 r^2}{l^2}\right) \frac{t^3}{r^3}}{\left(1-\nu^2\right)\left(q_{cl} - q_{cr}\right)}} \tag{3.7}$$

where $\bar{n}$ is the number of lobes in the initial out-of-roundness pattern, which can be seen in figure 3-1. Holt also developed an equation for the maximum amplitude which is applicable to conditions with elevated temperatures but, this will not be explored in this study.

Along with Holt's equation, another simpler equation was proposed for the reduced buckling load in [26], where the reduced buckling load is found to be

$$q_{cr} = \frac{S_U \frac{t}{r}}{1 + \frac{1.5u(1-0.4\frac{r}{l})}{50\frac{t}{r}}} \tag{3.8}$$

and is shown in figure 3-16.

Galletly and Bart [13] derived an equation for the reduction in buckling pressure for the case of external hydrostatic pressure in 1956. It was assumed that the initial imperfection in the cylinders were similar to one of the modes of buckling. But, actual shells never satisfy this condition. The equation they derived which expressed the initial pressure was

$$\frac{e}{t} = \left(1 - \frac{q_{cr}}{q_{cl}}\right)\left(\frac{-3 + \sqrt{9 - 4(1 - \beta + \beta^2)H}}{4(1 - \beta + \beta^2)K}\right) \tag{3.9}$$

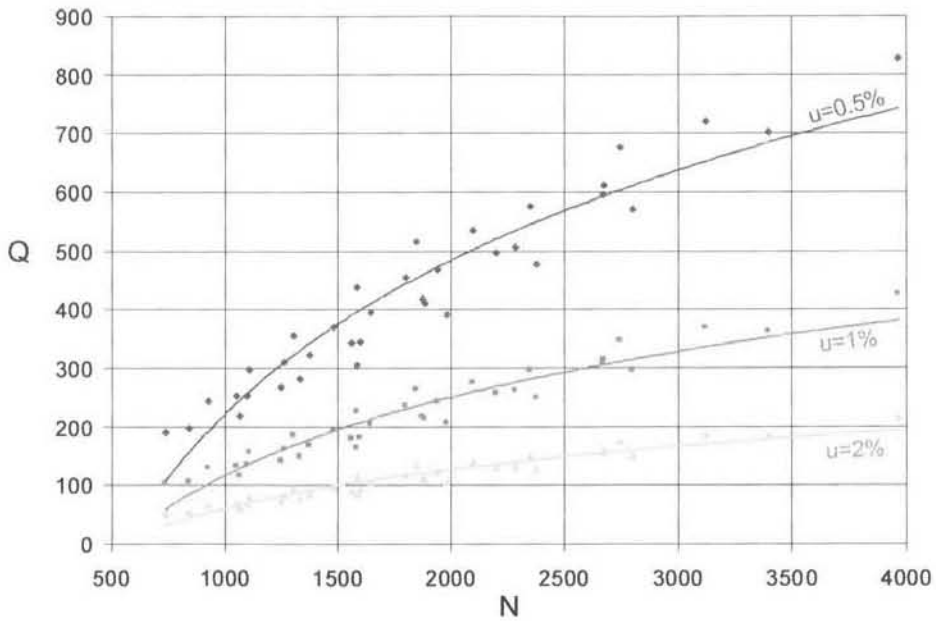

Figure 3-16: Plot showing the relationships in Holt's equation.

where

$$H = 3 - \left(\frac{2tS_Y}{rq_{cr}}\right)^2$$

$$\beta = \frac{\nu m^2 + \chi^2 + 2(1-\nu^2)\frac{r}{t}\frac{m^2\chi^2}{(m^2+\chi^2)})^2}{m^2 + \nu\chi^2 + 2(1-\nu^2)\frac{r}{t}\frac{\chi^4}{(m^2+\chi^2)^2}}$$

$$K = \frac{m^2 + \nu\chi^2 + 2(1-\nu^2)\frac{r}{t}\frac{\chi^4}{(m^2+\chi^2)^2}}{\frac{2q_{cl}(1-\nu^2)}{E}\left(\frac{r}{t}\right)^3}$$

$$S_Y = \text{Yield strength of the material.}$$

In the derivation of this expression, it was also assumed that the initial imperfection is small (with an order of magnitude of the shell wall thickness), which is limited in the context of this study.

When Donnell [14] initially explored the effects of imperfections of cylinders subjected to external hydrostatic pressure in 1956, he assumed the same unevenness factor as in his previous collaborated study [10] of cylinders subjected

to axial compression in 1950 with Wan, outlined in chapter (3.2) on page 67. But this study was inconclusive in respect of the fact that a reduction formula was not found.

Lunchick and Short [15] focussed their research on the buckling of imperfect shells with an 'accordion' initial deflection in 1957. This nature of imperfection occurs in stiffened cylinders and is caused by shrinkage of frame weld-joints. The imperfection equation they used was

$$w_0 = \frac{4}{l} e \left(x - \frac{x^2}{l} \right) \tag{3.10}$$

This expression for the initial imperfection does not hold true for the present study, as the imperfection is considered to be axisymmetric.

Abdelmoula et al [51] studied the buckling of imperfect cylinders due to external hydrostatic loading in great detail in 1992. Distributed imperfections, localised imperfections and combinations thereof where considered and reduction formulae for each case obtained. They even considered the separate cases of a localised imperfection and distributed imperfections being in phase and out of phase. This study was limited to applications where the Batdorf parameter (Z) was large $(Z \geq 500)$. The reduction formula they calculated for the case of distributed imperfections is

$$\frac{q_{cr}}{q_{cl}} = 1 - 4.7511 \frac{\sqrt[3]{1-\nu^2}}{\sqrt[3]{Z}} \sqrt[3]{\left(\frac{A}{t} \right)^2} \tag{3.11}$$

and is shown in figure 3-17. Thus the reduction formulae for both axial loading and hydrostatic pressure are proportional to $\left(\frac{A}{t}\right)^{2/3}$ using the same method.

Yamada and Croll analysed imperfection sensitivity in cylindrical panels in 1989 [46] and cylinders in 1993 [54]. In both cases the equations of equilibrium were formulated using the principle of total potential energy. The imperfection distribution was represented by the harmonic expression

$$w_0 = A \cos \frac{ny}{r} \sin \frac{\pi x}{l} \tag{3.12}$$

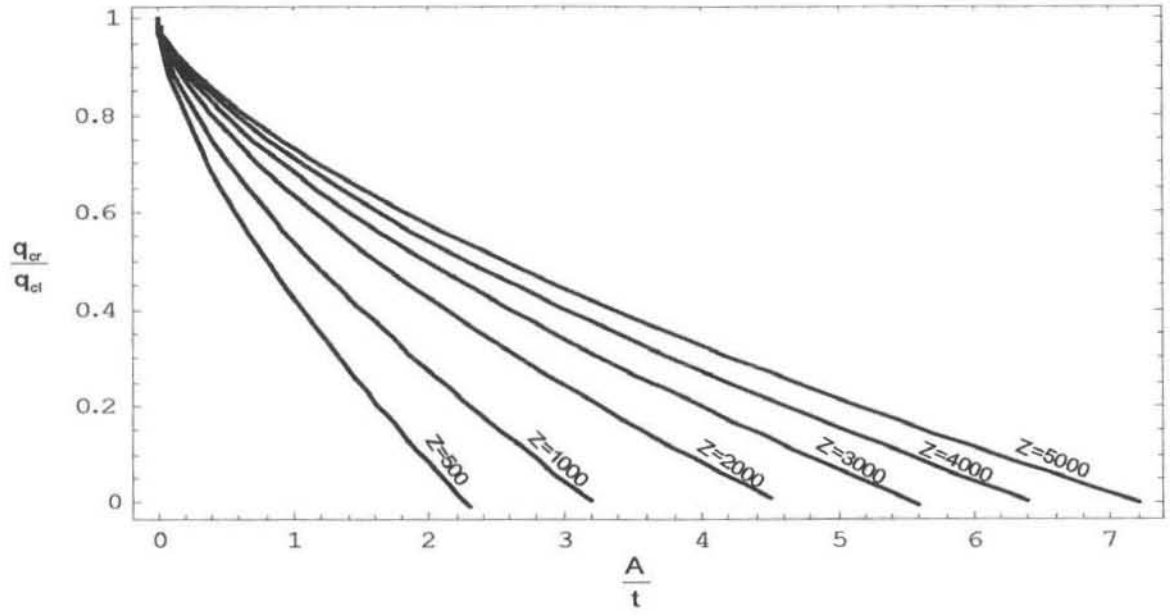

Figure 3-17: Graph showing Abdelmoula et al [51] relation for the case of distributed imperfections.

where the origin of the co-ordinate system was taken to be on the surface of the cylinder at mid-length. The 1989 study concluded that the complexity of the buckling behaviour displayed by this shape of shell was shown by the use of numerical experiments using various levels of geometric imperfection. Both studies noted that classical buckling analysis provided an unreliable upper bound to buckling pressures due to imperfections and that the reduced stiffness analysis provided a close lower bound to cases where imperfection sensitive loads are applied. Although no conclusive relation between the reduced buckling load, cylinder parameters and imperfection parameters was acquired in either study, these papers aided to enhance the understanding of buckling of cylinders subjected to imperfection sensitive loading case of external pressure.

Croll [60] later reviewed the developments of the reduced stiffness method for both axial loading and external pressure, from its early developments onward in 1995. By comparing numerical experiments and experiments performed by others, Croll concluded that this method is shown to provide a safe prediction of buckling loads, without the need of mathematically examining the imperfection

itself.

The ASME Boiler and Pressure Vessel Code UG-80(b)(1) [38] requires that the difference between the minimum and maximum diameters does not exceed 1% of the nominal diameter. Also, in code UG-80(b)(2), in order to detect flat spots and bulging caused by fabrication, a second requirement is that the maximum deviation from a true circle does not exceed that given in figure 3-18 when

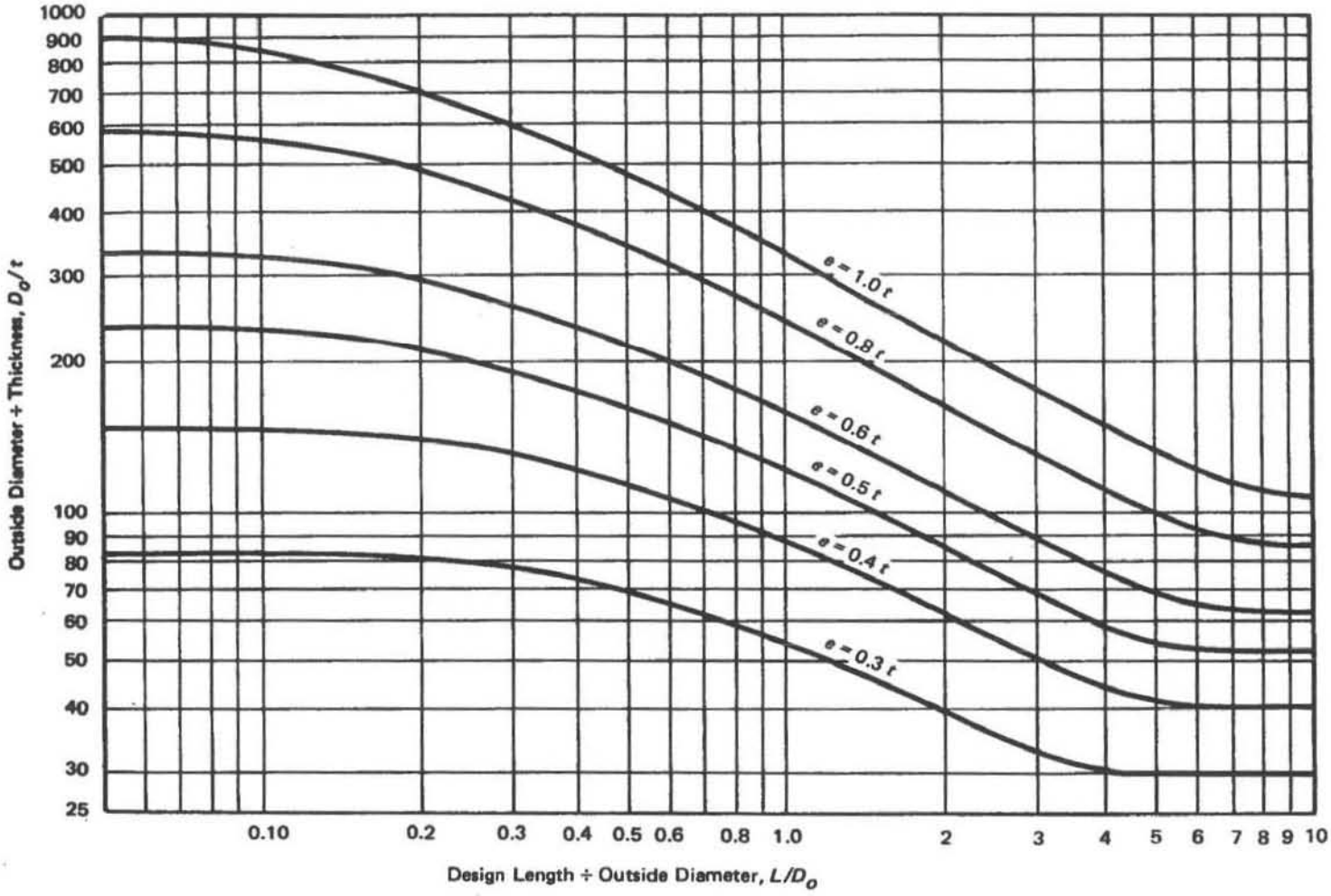

Figure 3-18: Figure obtained from 1980 ASME code [38].

measured over twice the arc length given in figure 3-19.

Jawad and Farr [47] identified that the curves in figure 3-18 are based on the

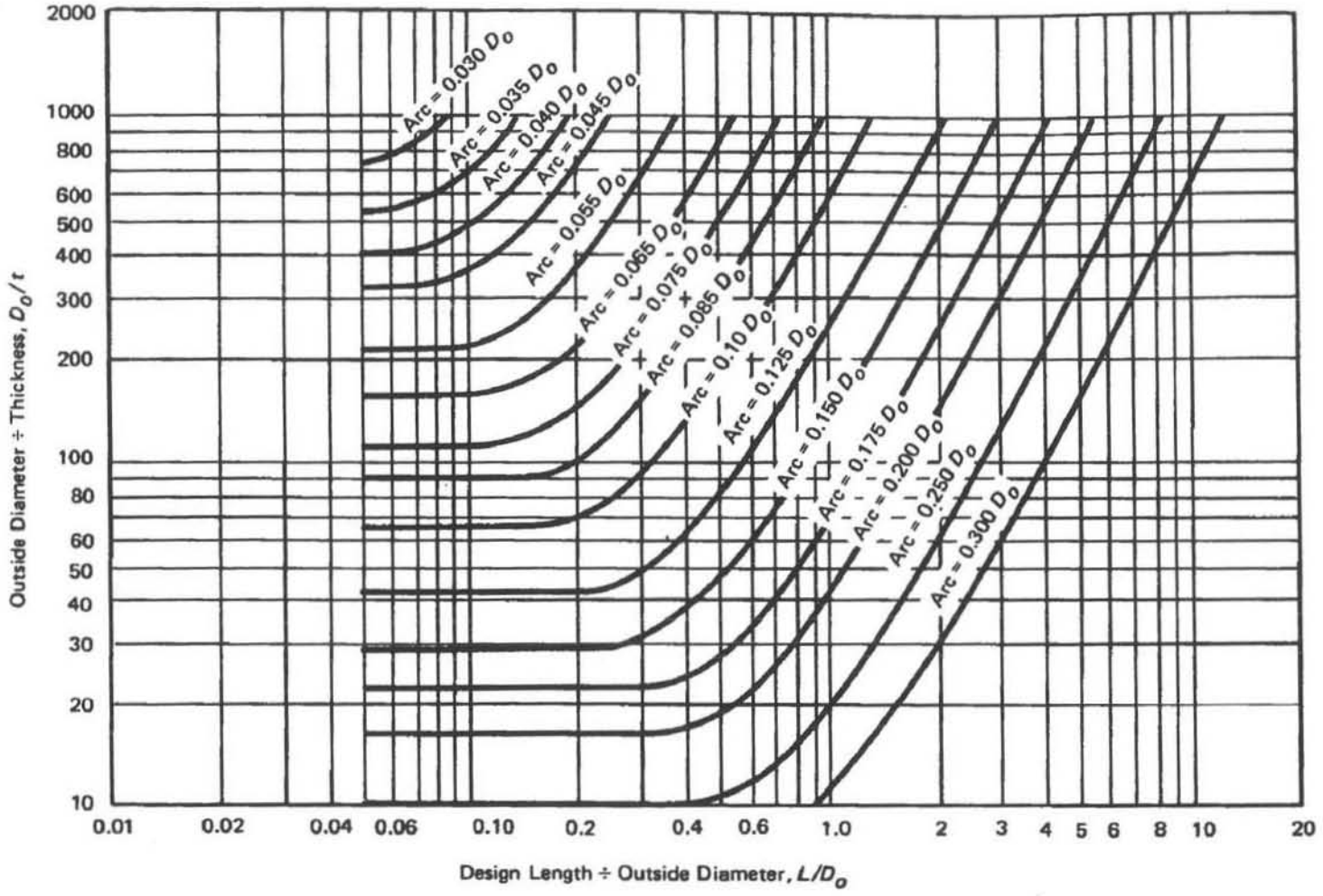

Figure 3-19: Figure obtained from 1980 ASME code [38].

formula

$$\frac{e}{t} = \frac{0.018}{n\left(\frac{t}{2r}\right)} + 0.015n. \tag{3.13}$$

This formula is based on an analogy between a cylindrical pressure vessel and a column by considering the cylinder to be made up of a series of columns. Harvey [44] then went on to show how this formula was derived, and showed that the equation for intermediate length cylinders was

$$\frac{e}{t} = \frac{\text{constant}}{n\left(\frac{t}{2r}\right)}. \tag{3.14}$$

It was noted that it was found by experiment that a certain eccentricity has less effect on the collapse pressure of a long cylinder than on a shorter one, of the same

thickness and diameter. This means that the allowable out-of-roundness decreases with decreasing length until a certain limit is reached and the e/t curve flattens out and continues parallel to the l/D_o axis, where here D_o is the nominal diameter. Likewise, the allowable out-of-roundness increases with increasing length until a critical length is reached and the e/t curve flattens and continues parallel to the l/D_o axis. Therefore, the basic equation 3.14 is modified to reflect this behaviour

$$\frac{e}{t} = \frac{a}{n\left(\frac{t}{2r}\right)} + bn \tag{3.15}$$

The values of a and b are then obtained such that the equation satisfies experimental results.

The control of imperfection, including eccentricity, ovality, bulges, dents and flat spots is vital if buckling under external pressure is to be avoided. It has been shown that collapse finally occurs at the location where the initial deviation from perfect is the greatest. Therefore, safety codes and regulations have established allowable deviations in overall out-of-roundness and local eccentricities. It is also required that these be verified by measurements taken around the circumference and at intervals along the length, which is the purpose of figure 3-18.

3.4.2 Numerical analysis

Cylinders were simulated in MSC Nastran as before and the buckling pressures noted. The buckled form of a cylinder subjected to hydrostatic external pressure is shown in figure 3-20.

As expected, since the axial load is quite low, the buckled form similar to that of lateral pressure.

When the reduction of buckling load is plotted versus the eccentricity to wall-thickness ratio as in figure 3-21, a similar trend to that shown in figure 3-15 for the case of lateral external pressure where the strength of the cylinder eventually increases with increasing eccentricity.

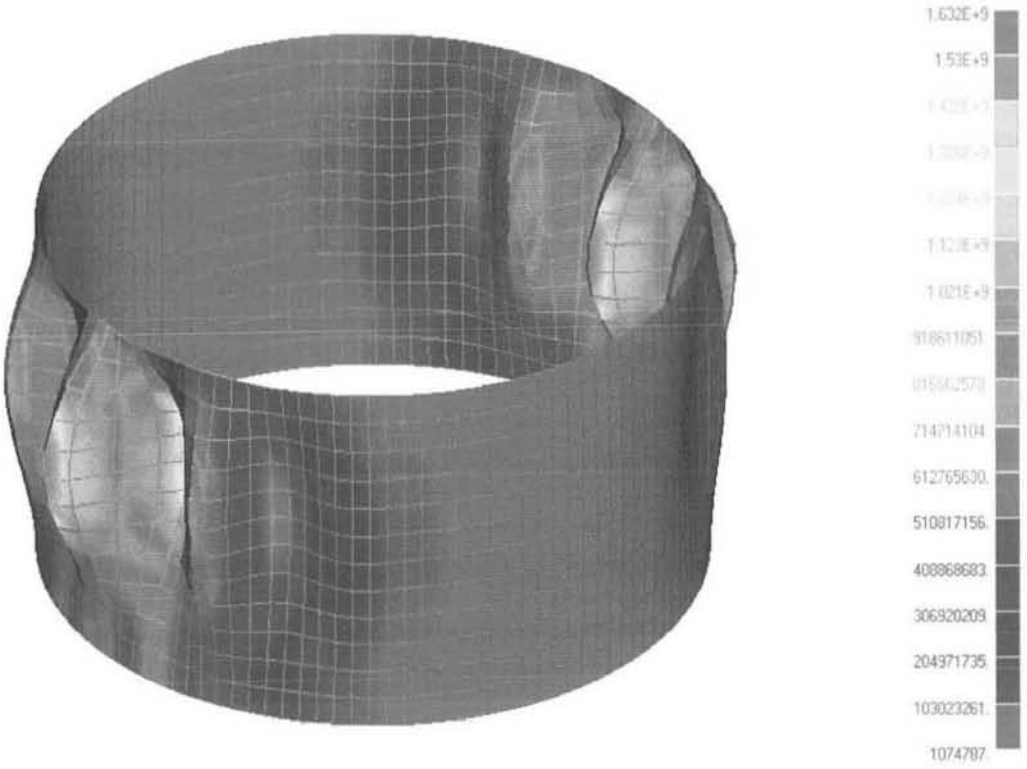

Figure 3-20: Deformed cylinder which is subjected to hydrostatic pressure. l=12m, r=11.43m, t=0.01m and u=2%.

The reduction in buckling load for increasing out-of-roundness is clearly seen in figure 3-22.

3.5 Combined loading

3.5.1 Literature survey

Very little research has been published on the topic of buckling of imperfect cylinders subjected to combined loading. Hutchinson considered the simultaneous action of internal pressure and axial loading [23] and then modified this study to include external pressure and axial loading [24]. Unfortunately for the purposes of this study, the initial imperfection was considered to be in the form of the axisymmetric buckling mode. However, as this is the only available research

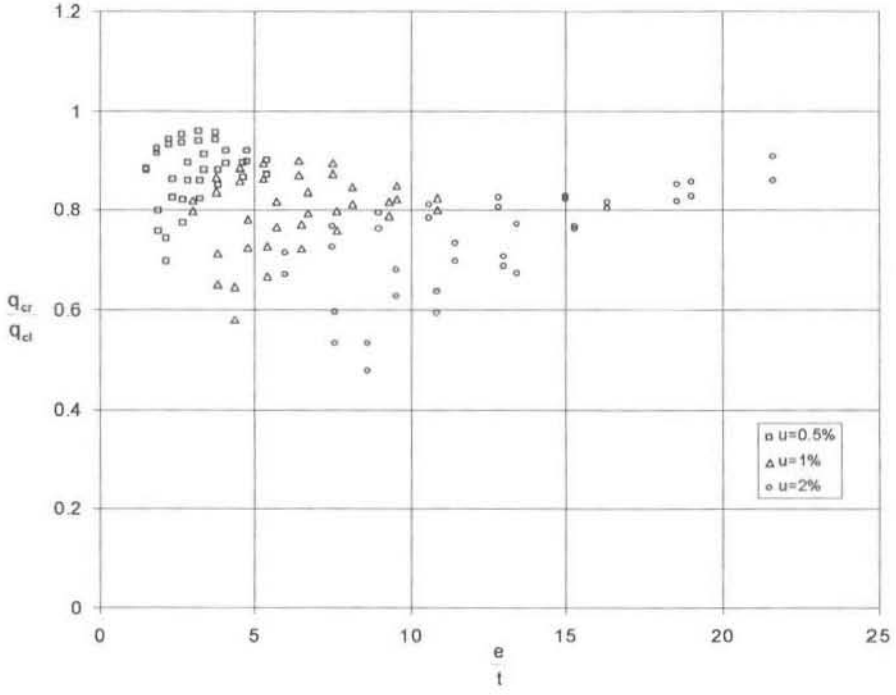

Figure 3-21: Hydrostatic pressure buckling results for imperfect cylinders.

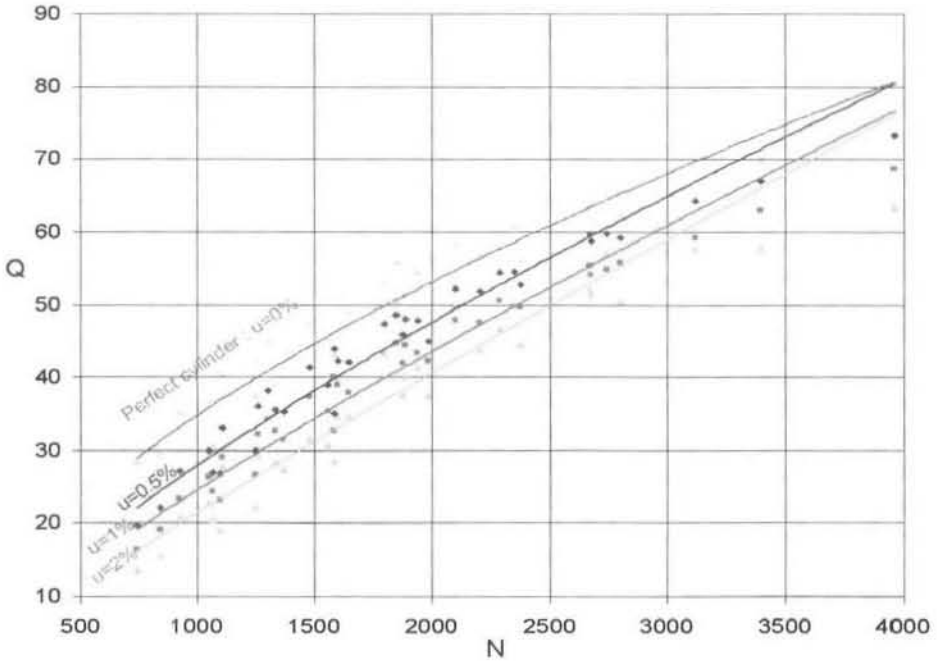

Figure 3-22: Plot of Q versus N showing the reduction of hydrostatic buckling load for increasing imperfection.

conducted for combined loading, it will be explored. The imperfection was considered to have the form

$$w_0 = \bar{A}t \cos q_0 \frac{x}{r} \tag{3.16}$$

where $\bar{A}$ is the magnitude of the imperfection relative to the shell thickness ($\bar{A}t$ is therefore the amplitude of the imperfection) and

$$q_0^4 = 12(1-\nu^2)\left(\frac{r}{t}\right)^2.$$

As explained by Hutchinson [24], bifurcation from the pre-buckling solution occurs at a certain value of external pressure (for a given axial load). The load-deflection curve falls subsequent to bifurcation, and this bifurcation value is therefore the buckling load.

The eigenvalue equation obtained in [23] which was shown to be applicable to the case of external pressure is

$$\left(1-\frac{\bar{P}}{P_{cl}}\right)^2\left[\frac{(1+\gamma^2)^2}{4}+\frac{4}{(1+\gamma^2)^2}-2\widetilde{q}\gamma^2-\frac{2\bar{P}}{P_{cl}}\right]-\sqrt{3(1-\nu^2)}\gamma^2\bar{A}$$
$$\left(1-\frac{\bar{P}}{P_{cl}}\right)\left[\frac{\bar{P}}{P_{cl}}+\frac{8}{(1+\gamma^2)^2}\right]+4\left[\sqrt{3(1-\nu^2)}\gamma^2\bar{A}\right]^2\cdot$$
$$\left[\frac{1}{(1+\gamma^2)^2}+\frac{1}{(9+\gamma^2)^2}\right]=0 \tag{3.17}$$

where γ is a free parameter to be chosen such that the upper bound value is minimised, $\bar{P}$ is the total axial load $P + q\pi r^2$, and $\widetilde{q} = \sqrt{3(1-\nu^2)}qr^2/Et^2$.

This equation for a perfect cylinder (ie. $\bar{A} = 0$) was identified in section 2.8.1.

Solving for $\widetilde{q}$ using the software Mathematica yields

$$\widetilde{q} = \frac{1}{2\left(1-\frac{\bar{P}}{P_{cl}}\right)^2\gamma^2}\left[\left(1-\frac{\bar{P}}{P_{cl}}\right)^2\left(-2\frac{\bar{P}}{P_{cl}}+\frac{4}{(1+\gamma^2)^2}+\frac{1}{4}(1+\gamma^2)^2\right)\right.$$
$$-\sqrt{3}\bar{A}\left(1-\frac{\bar{P}}{P_{cl}}\right)\gamma^2\left(\frac{\bar{P}}{P_{cl}}+\frac{8}{(1-\gamma^2)^2}\right)\sqrt{1-\nu^2}$$
$$\left.+12\bar{A}^2\gamma^4\left(\frac{1}{(1+\gamma^2)^2}+\frac{1}{(9+\gamma^2)^2}\right)(1-\nu^2)\right] \tag{3.18}$$

Minimising γ with respect to $\widetilde{q}$ yields

$$\Bigg[P_{cl}^2\Bigg(-\frac{1}{2}+\frac{4\bar{P}^3}{P_{cl}}-\frac{16\gamma^2}{(1+\gamma^2)^3}-\frac{8}{(1+\gamma^2)^2}+\frac{\bar{P}^2(-33-99\gamma^2-50\gamma^4-14\gamma^6+3\gamma^8+\gamma^{10})}{2P_{cl}^2(1+\gamma^2)^3}$$
$$+\frac{96\bar{A}^2\gamma^6(365+123\gamma^2+15\gamma^4+\gamma^6)(-1+\nu^2)}{(1+\gamma^2)^3(9+\gamma^2)^3}$$
$$+\gamma^4\Bigg(\frac{1}{2}+\frac{32\bar{A}\sqrt{3-3\nu^2}}{(-1+\gamma^2)^3}-\frac{48\bar{A}^2(41+10\gamma^2+\gamma^4)(-1+\nu^2)}{(1+\gamma^2)^2(9+\gamma^2)^2}\Bigg)$$
$$+\frac{\bar{P}\left(5+\frac{32\gamma^2}{(1+\gamma^2)^3}+\frac{16}{(1+\gamma^2)^2}+\gamma^4\left(-1-\frac{32\bar{A}\sqrt{3-3\nu^2}}{(-1+\gamma^2)^3}\right)\right)}{P_{cl}}\Bigg)\Bigg]/(2(\bar{P}-P_{cl})^2\gamma^3)=0 \tag{3.19}$$

Solving for γ yields 21 roots for γ, which are shown in appendix E. By substituting the values of γ obtained from equation 3.19 into the expression for $\widetilde{q}$ in equation 3.18 and the lowest value of q selected, the value for the buckling pressure of imperfect cylinders subjected to simultaneous external pressure and a constant axial load can be obtained.

Hutchinson pointed out that the assumed imperfection pattern has essentially no effect on the buckling load, so this equation is still valid for other harmonic initial imperfection distribution assumed, as is the case in this study.

3.5.2 Numerical analysis

The results of the numerical analyses performed can be seen plotted in figure 3-23. As before, the buckling pressure decreases as the out-of-roundness increases.

As in the other imperfect cylinders examined, beyond a critical eccentricity to wall thickness ratio the buckling pressure begins to increase. This is shown in figure 3-24.

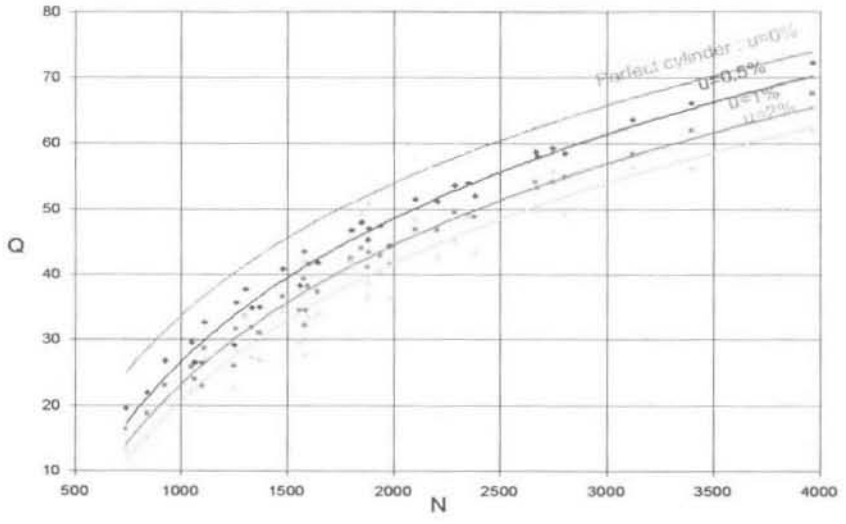

Figure 3-23: Plot of Q versus N showing the reduction of hydrostatic buckling pressure under combined loading for increasing imperfection.

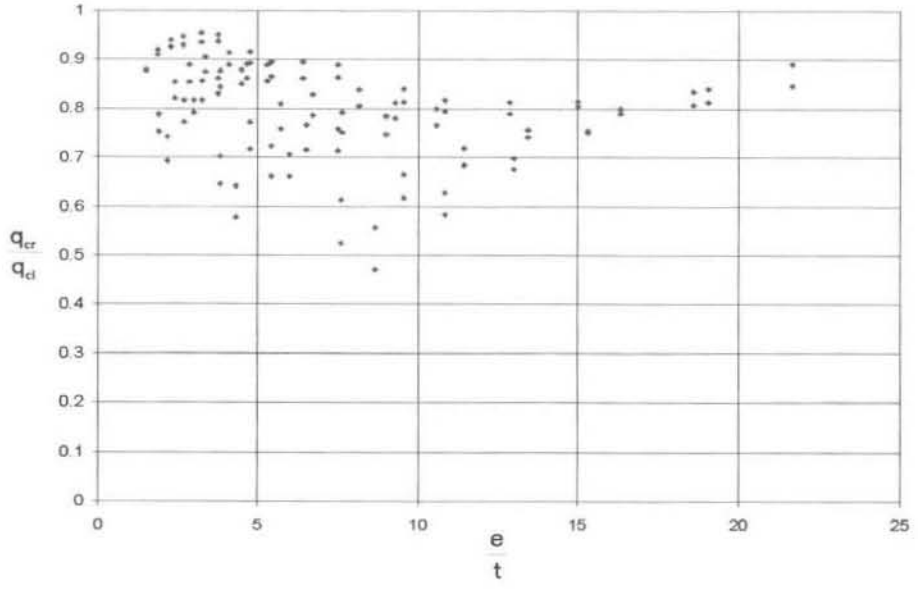

Figure 3-24: Graph showing the numerical results for increasing eccentricity to wall thickness ratios.

Chapter 4

VARIABLE WALL THICKNESS CYLINDERS

4.1 Introduction

Storage vessels are often made of expensive materials and therefore it is desired that the amount of material used in the construction of the vessel is minimised. One method of decreasing the structural weight of these vessels is to vary the wall thickness such that more material is present where the stresses are highest. Alternatively, a fixed roof storage vessel may have been converted from a floating roof tank where the walls are tapered. In this case, under drastic changes of atmospheric conditions, the tapered wall tank could be subjected to a negative pressure if the venting system is insufficient.

In this study cylinders with a taper, α, of the range 0.002^o to 0.04^o are considered, where the wall thickness at mid length, t_m, is considered to have similar values equal to those considered in the study of constant wall thickness cylinders. Figure 4.1 shows the assignment of the various variables used in this section.

Hardly any research has been conducted on the buckling of variable wall thickness cylinders and even less on axisymmetric thickness variations in particular. The influence of thickness variation on the buckling load has gained little attention thus far from researchers of this field. This specific form of buckling

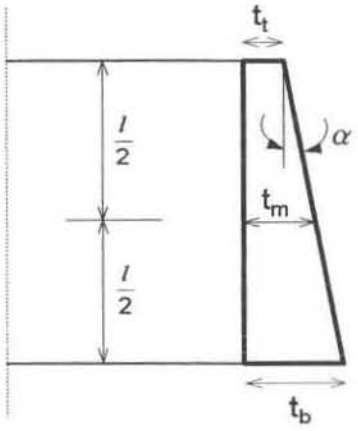

Figure 4-1: Exaggerated view showing the variables used in the study of tapered cylinders.

will be investigated here, whereby the limited available research is reviewed and numerical tests performed in order to establish trends between selected parameters. As before only carbon steel will be considered.

4.2 Axial loading

4.2.1 Literature survey

Koiter, Elishakoff et al [55] explored axial loading of inconsistent cylinders, but limited the thickness variation to an axisymmteric periodic variation. This research paper later goes on to derive reduction formulae based on parameters defined in the thickness variation formula.

The thickness is assumed to vary according to the relationship

$$t = t_m \left[1 - \varepsilon \cos \frac{2px}{r} \right] \tag{4.1}$$

where t_m is the nominal thickness of the shell, ε and p are non-dimensional parameters indicating the magnitude and wave of the thickness variation. Since the reduction formulae depend on ε, the parameter indicating the magnitude of the variation, one could assume a value of ε that is applicable to a tapered wall,

such that a relation similar to 4.1 holds. The following is such a relation

$$t = t_m\left(1 - \varepsilon\left(\frac{2}{l}x - 1\right)\right) \tag{4.2}$$

where $\varepsilon = -\frac{l}{2t_m}\tan\alpha$, and t_m is the thickness at mid-length of the cylinder.

Koiter et al [55] finally determined the reduction factor due to thickness variation by the use of a hybrid perturbation-weighted residuals method, and was found to be

$$\frac{P_{cr}}{P_{cl}} = 1 - \frac{1}{2}\nu\varepsilon - \frac{832 + 464\nu - 23\nu^2}{512}\varepsilon^2 \tag{4.3}$$

in the case of buckling with equal wave numbers in the axial and circumferential directions (Case A) and

$$\frac{P_{cr}}{P_{cl}} = 1 - \varepsilon - \frac{25}{32}\varepsilon^2 \tag{4.4}$$

in the case of axisymmetric buckling (Case B). The theoretical relationship between the reduction in buckling load and the magnitude parameter can be seen graphically in figure 4-2, for both cases A and B.

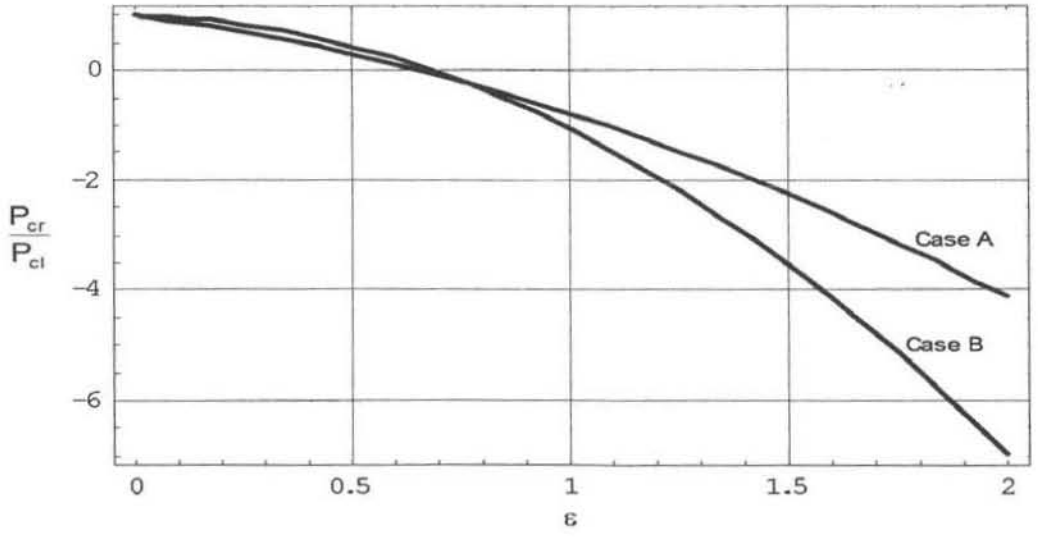

Figure 4-2: Plots of case A and case B.

Therefore, for case A, the buckling load is

$$P_{cr} = \left(1 - \frac{1}{2}\nu\varepsilon - \frac{832 + 464\nu - 23\nu^2}{512}\varepsilon^2\right)\frac{2\pi E t_m}{\sqrt{3(1-\nu^2)}} \tag{4.5}$$

and for case B is

$$P_{cr} = \left(1 - \varepsilon - \frac{25}{32}\varepsilon^2\right) \frac{2\pi E t_m}{\sqrt{3(1-\nu^2)}} \tag{4.6}$$

However, neither of these relationships were confirmed by experimental data.

4.2.2 Numerical analysis

The results of the numerical analyses are plotted in figure 4-3 for various tapers.

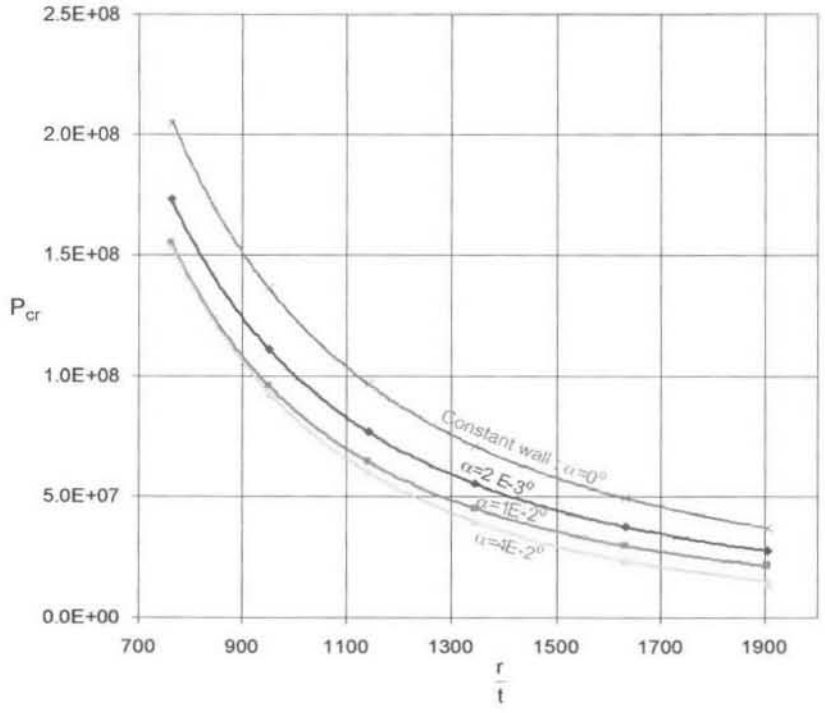

Figure 4-3: Numerical results for axial laoding for various tapers.

The reduction of the buckling load was found to behave in a predictable manner, whereby it decreases for increasing taper.

A comparison between numerical results and the theoretical curve from equation 4.5 is shown in figure 4-4.

4.3 Lateral external pressure

4.3.1 Literature survey

No previous research was found that investigated the buckling of tapered cylinders loaded by lateral external pressure.

4.3.2 Numerical analysis

A trend that runs through all the tests conducted with perfect variable wall cylinders is how the buckling pattern moves up the cylinder as the taper increases. This is shown in figures 4-5 and 4-6 where the tapers differ.

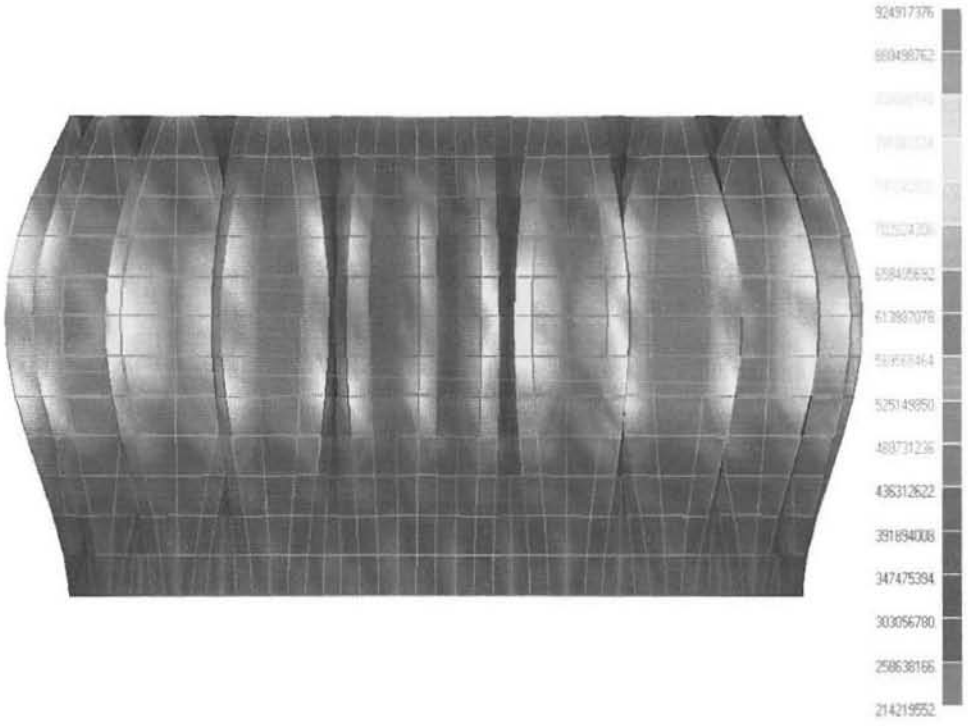

Figure 4-5: Buckled cylinder with a taper of $\alpha = 0.002^o$

During the numerical analyses of tapered cylinders subjected to lateral external pressure, it was found that as the taper was introduced and increased, the strength of the cylinder decreased from that of a constant wall. This trend is shown in

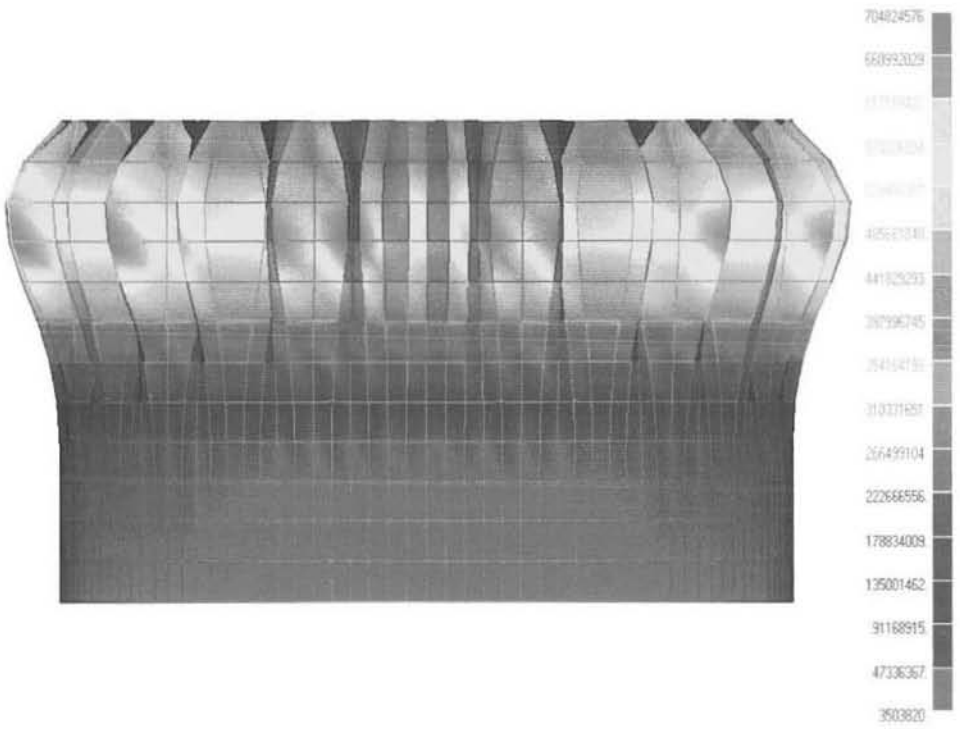

Figure 4-6: Buckled cylinder with a taper of $\alpha = 0.04^o$

figure 4-7, where the buckling pressures for a constant wall thickness cylinder is compared to cylinders with various tapers.

Another trend is shown in figure 4-8 where the reduction of buckling load for cylinders of various Batdorf parameters are compared. It can be seen that as the Batdorf parameter increases, the sensitivity to taper increases too.

4.4 External hydrostatic pressure

4.4.1 Literature survey

Pioneers in the investigation of buckling of variable wall thickness cylinders, Biezeno and Koch [9] explored this for cylinders subjected to hydrostatic external pressure in as early as 1938. But, they considered the general case of varying thickness too complicated and decided to replace the tapered wall cylinder with a cylinder built up of a finite number of rings, each of constant thickness. They then deduced that buckling of a cylinder of this form is similar to the buckling of a bar composed of a finite number of segments, as long as $\frac{r}{t} \ll 1$ and the radius and length of the cylinder were of the same order of magnitude. They then solved for the buckling of the bar. Although inconclusive for cylinders, this paper identifies the need for further study in this field.

4.4.2 Numerical analysis

As expected, similar trends to that found in lateral external pressure loading is exhibited in hydrostatic pressure loading. Figure 4-9 shows that as the Batdorf parameter increases, the effect of the increased taper is more pronounced.

Figure 4-10 shows how the reduction in buckling load increases as the taper increases.

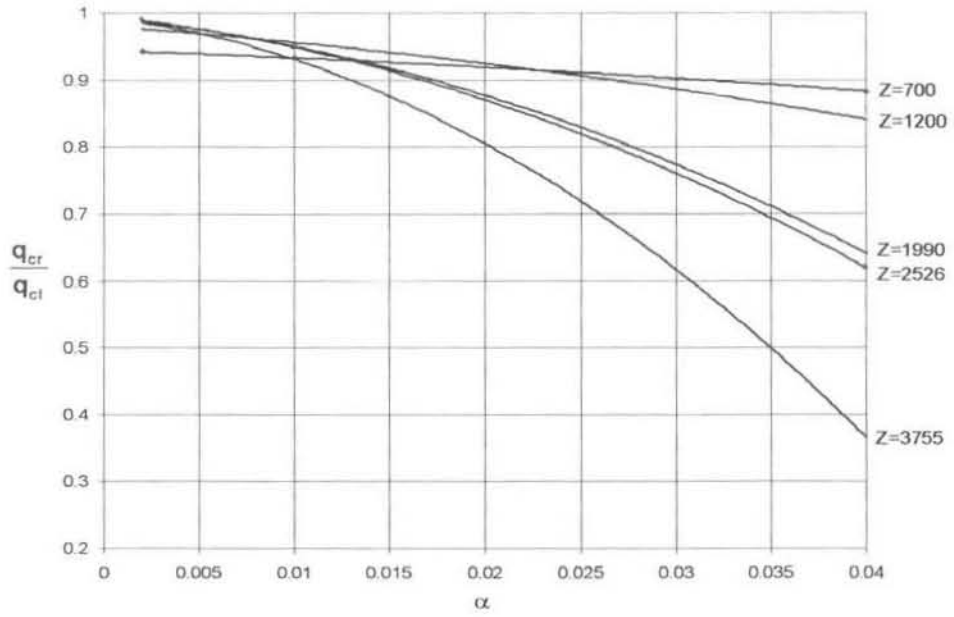

Figure 4-9: Graph showing the reduction in buckling load versus taper for various cylinders, subjected to hydrostatic external pressure.

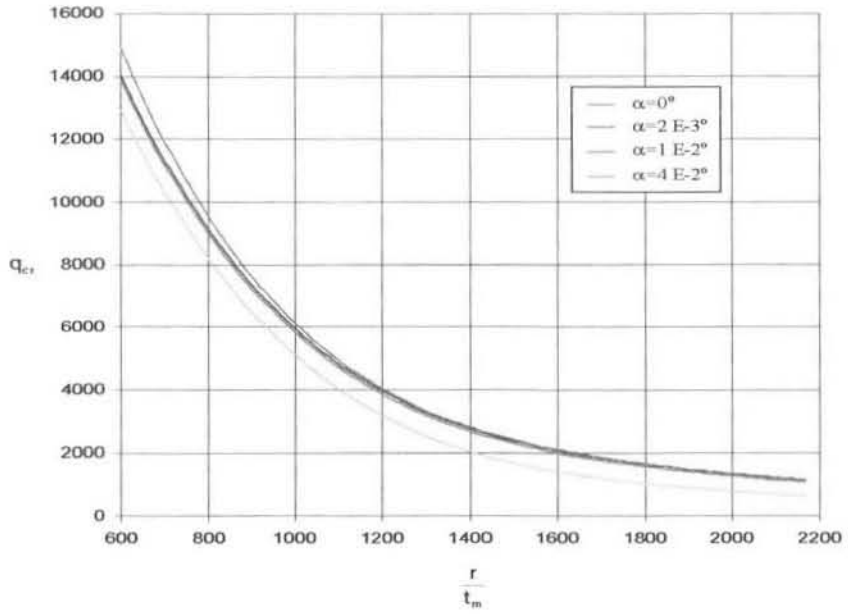

Figure 4-10: Graph of buckling pressure versus the radius to mean wall thickness ratio.

4.5 Combined loading

4.5.1 Literature survey

No research was found that covered the theoretical buckling of tapered cylinders subjected to combined loading.

4.5.2 Numerical analysis

The reduction in the buckling load is shown in figure 4-11, where the buckling loads for cylinder of various tapers are compared. It is evident that as the taper increases, the behaviour of the cylinder deviates more and more from that of the constant wall thickness cylinder.

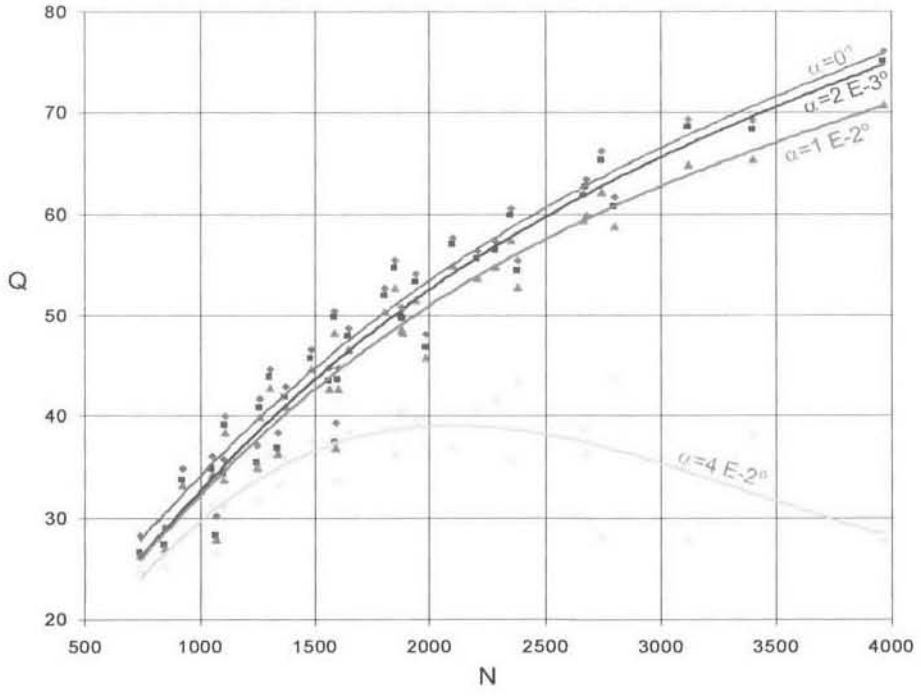

Figure 4-11: Q versus N for various tapers for the case of combined loading.

The interaction between the axial load and the hydrostatic buckling pressure is shown in the plot of Q versus $\widetilde{P}$ in figure 4-12, where $\widetilde{P} = \sqrt{3(1-\nu^2)}\frac{Pr^2}{Et_m^2}$.

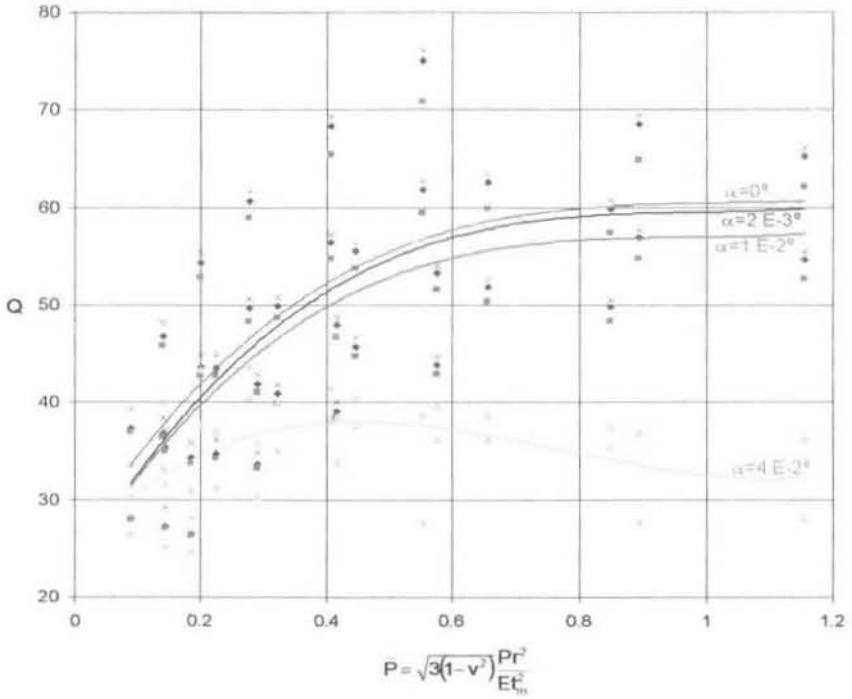

Figure 4-12: Q versus the load parameter for combined loading.

It is evident that as the cylinder radius to mean wall thickness ratio increases (and therefore $\widetilde{P}$ increases), the effect of the taper becomes asymptotic. The intial direct relationship is evident in figure 4-11.

But another trend is evident when the results are plotted as a reduction of buckling load versus $\widetilde{P}$ in figure 4-13. It was found that for small tapers, as an axial load is applied, the reduction of buckling pressure actually decreases.

The reduction in buckling pressure as a function of taper is shown in this figure, for a cylinder of Batdorf parameter, Z, of 2600.

Buckling due to hydrostatic pressure was found to be more sensitive to taper than lateral pressure as shown in figure 4-14. However, combined loading was found to be no more sensitive to taper than the case of hydrostatic pressure. It can also be seen that this difference in sensitivity to taper reduces as the taper increases.

For a specific taper of 0.01^o, the buckling loads for the various loading conditions

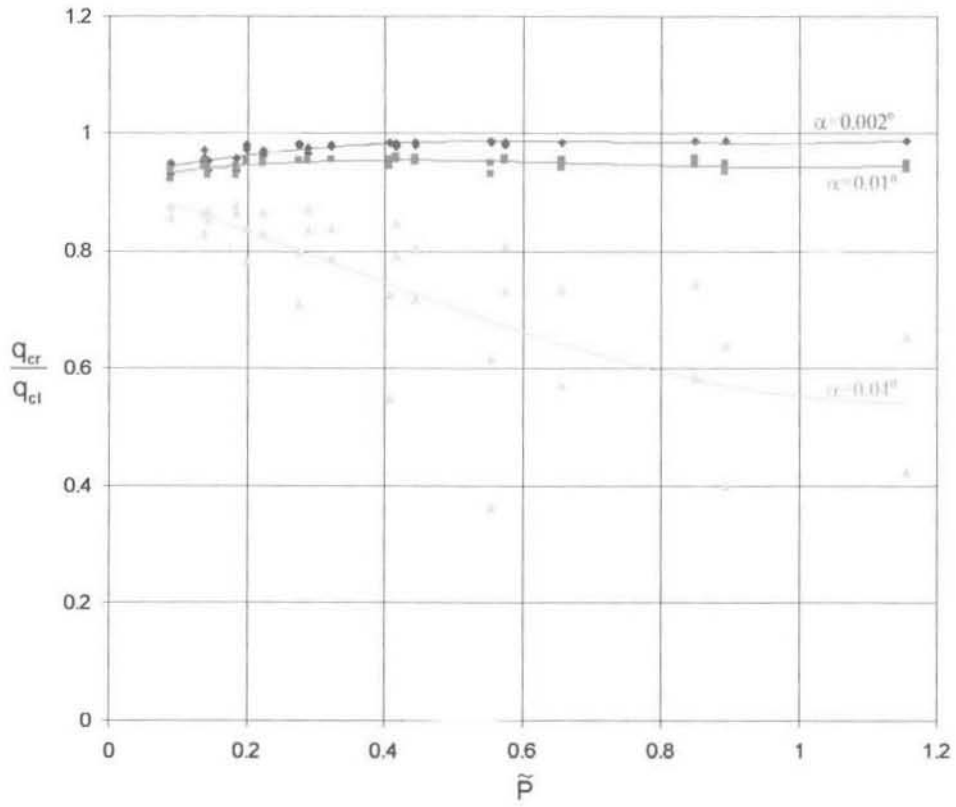

Figure 4-13: Reduction in buckling load versus the load parameter for a cylinder of Z=2600.

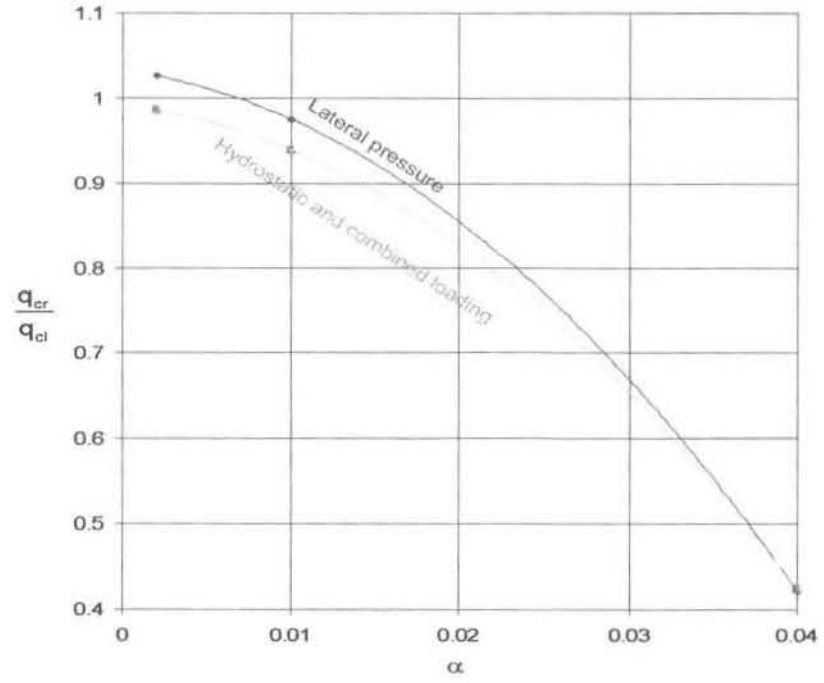

Figure 4-14: Reduction in buckling load versus taper for various loading conditions.

are shown in figure 4-15. It is evident that as the radius to wall thickness ratio increases, the buckling loads tend towards a common value.

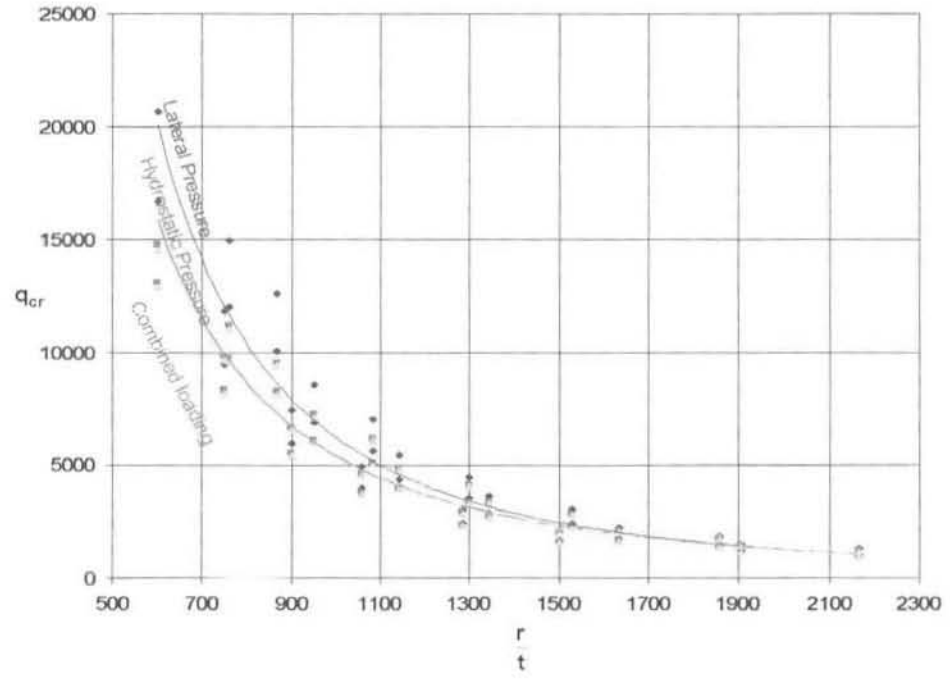

Figure 4-15: Buckling load versus r/t for various loading conditions for cylinder with taper α=0.01^o.

Chapter 5

IMPERFECT VARIABLE WALL THICKNESS CYLINDERS

5.1 Introduction

A great deal of literature spanning the last century has been devoted to the buckling of cylinders of constant wall thickness, and the buckling of cylinders with geometric imperfections has been explored for the past half-century. Even the buckling of cylinders with thickness variations has been briefly explored. However, no similar research seems to be available for the combined effect of thickness variations and geometric imperfections on the buckling of cylinders subjected to exteral pressure. It was found that in 1994, Koiter et al [56] studied the combined effect for cylinders subjected to axial loading.

In this study, the above-mentioned previous research will be reviewed and numerical analyses performed on the various cylinders for the various loading conditions. Geometric imperfections of the range $0.5\% \leq u \leq 2\%$ and tapers of the range $0.002^o \leq \alpha \leq 0.04^o$ will be considered for the cylinders of dimensions used in the previous studies. The analyses are performed using carbon steel as before.

5.2 Axial loading

5.2.1 Literature survey

The only published research, to best of the author's knowledge, that covers buckling of imperfect, variable wall thickness cylinders is that published by Koiter, Elishakoff, Li and Starnes [56]. They focused on axial loading of shells with small periodic axisymmetric thickness variations described by

$$t = t_m \left[1 - \varepsilon \cos \frac{px}{r} \right] \tag{5.1}$$

and axisymmetric initial geometric imperfections described by

$$w_0 = -\bar{A} \cos \frac{p_0 x}{r} \tag{5.2}$$

where

$$p_0 = \sqrt{\frac{\sqrt{3(1-\nu^2)}2r}{t_0}}.$$

Unfortunately for the purposes of this study, these imperfections are considered to be axisymmteric but, as this is the only research available, it will still be reviewed due to its similarity.

Koiter et al derived asymptotic formulae by means of the energy criteria and found a simple equation that related the reduction in buckling load, imperfection amplitude and mean wall thickness t_m, which is as follows

$$\left(1 - \frac{P_{cr}}{P_{cl}}\right)\left(1 - \frac{1}{2}\nu\varepsilon - \frac{P_{cr}}{P_{cl}}\right) - \frac{3}{2}\frac{P_{cr}}{P_{cl}}\frac{\bar{A}}{t_m}\sqrt{3(1-\nu^2)} = 0 \tag{5.3}$$

The relationship between these parameters can be seen in figure 5-1 as a 3-D plot, and in figure 5-2 for integral values of ε.

Koiter et al then compared these results to those obtained in a combined analytical-numerical technique and they were found to co-relate closely. They then introduced a thickness variation parameter, Ω, in order to assess the effect

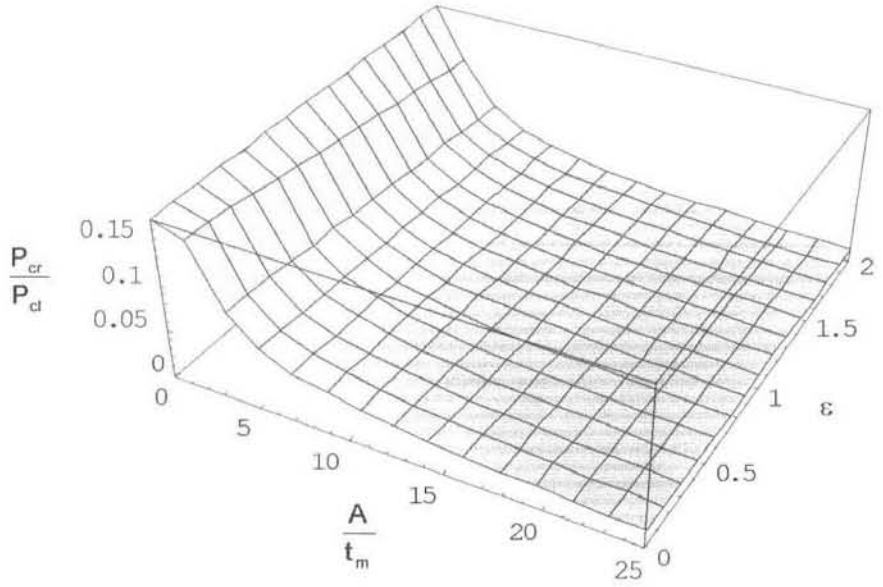

Figure 5-1: 3-D plot showing Koiter's aysmptotic formula for the reduction in buckling load.

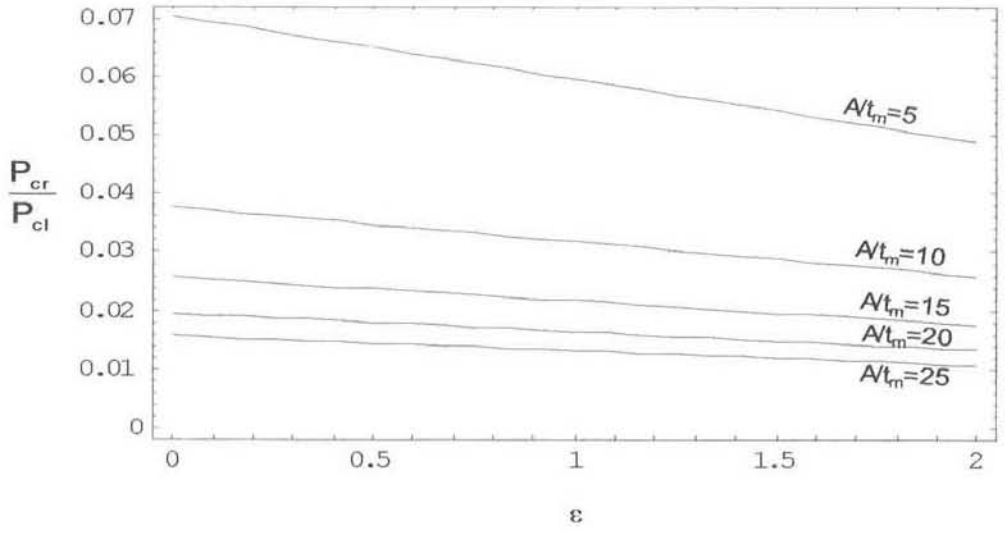

Figure 5-2: Plot of reduction values for integral values of ε.

of the thickness variation on the buckling load reduction. They defined it as follows

$$\Omega = \frac{P_u - P_{u,t}}{P_u} \times 100\% \tag{5.4}$$

where P_u is the buckling load of an imperfect shell of constant wall thickness, and $P_{u,t}$ is the buckling load of a shell of the same imperfection but, of variable wall thickness. A 3-D plot of this relationsship is shown in figure 5-3. Furthermore,

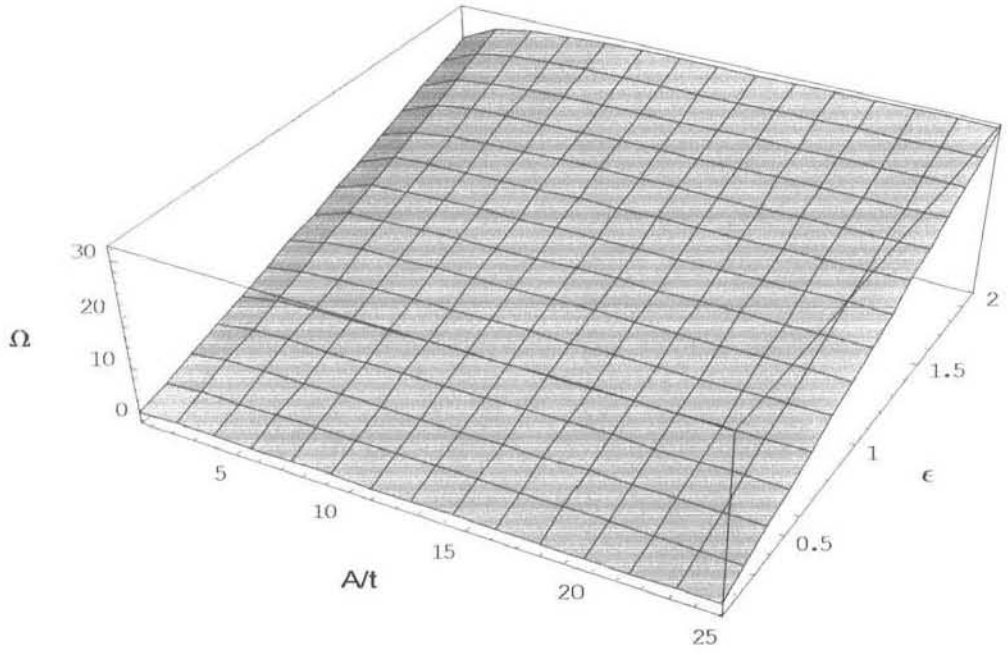

Figure 5-3: 3-D plot of the dependance of Ω on the imperfection amplitude and taper.

figure 5-4 shows the dependence of Ω on the imperfection amplitude for various integral values of ε.

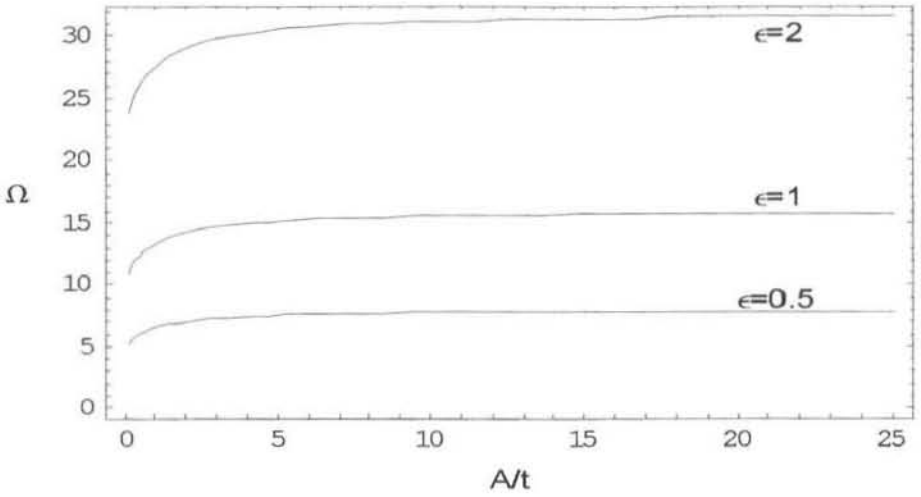

Figure 5-4: Plot showing the dependance of Ω on the imperfection amplitude for integral values of taper.

5.2.2 Numerical analysis

Plots showing how the reduction in buckling pressure depends on the degree of taper and imperfection are shown in figures 5-5 and 5-6.

The effect of the thickness variation on the buckling load reduction is shown using a plot of the thicknesss variation parameter versus imperfection for various values of taper. This is shown in figure 5-7. It is evident that the thickness variation parameter is fairly constant for increasing imperfection.

The effect of the individual imperfection and taper values were investigated and are shown in figure 5-8. It was found that the trends were similar for all cases.

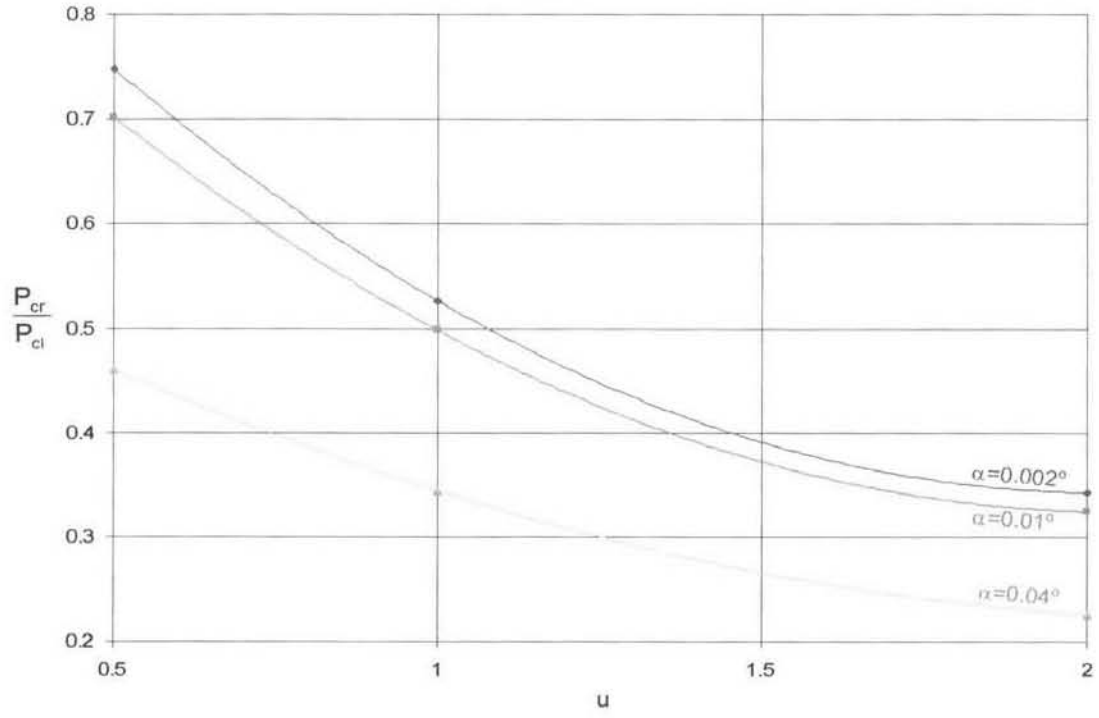

Figure 5-5: Plot showing the relationship between the reduction in buckling load and imperfection for cylinder l=12m, r=11.43m, and t=0.0085m

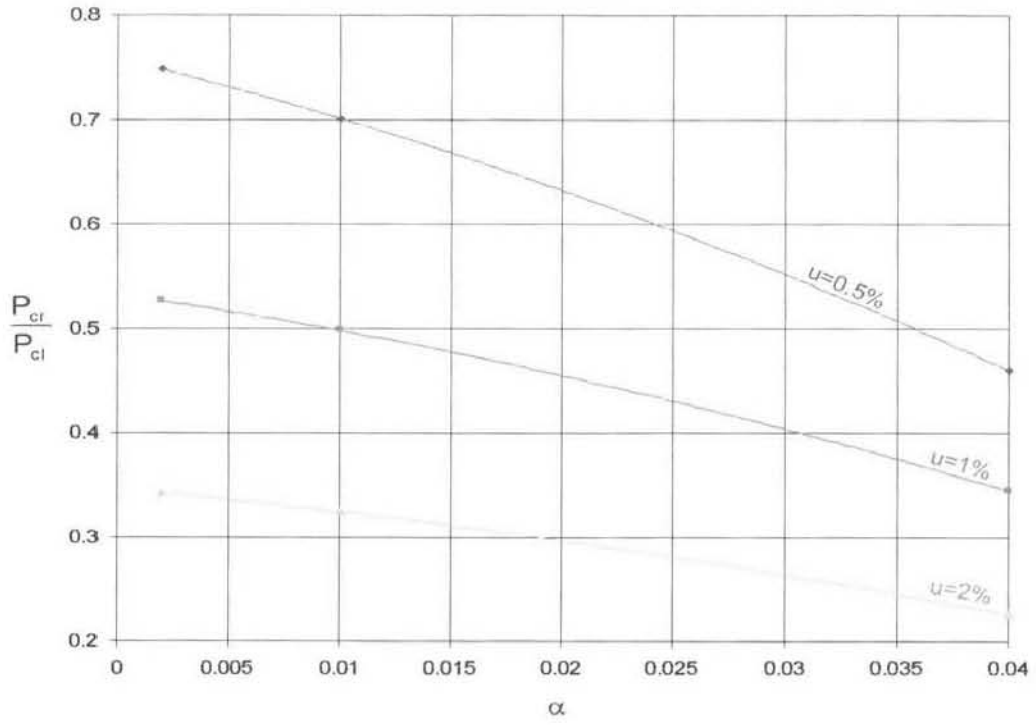

Figure 5-6: Plot showing the relationship between the reduction in buckling load and taper for cylinder l=12m, r=11.43m, and t=0.0085m

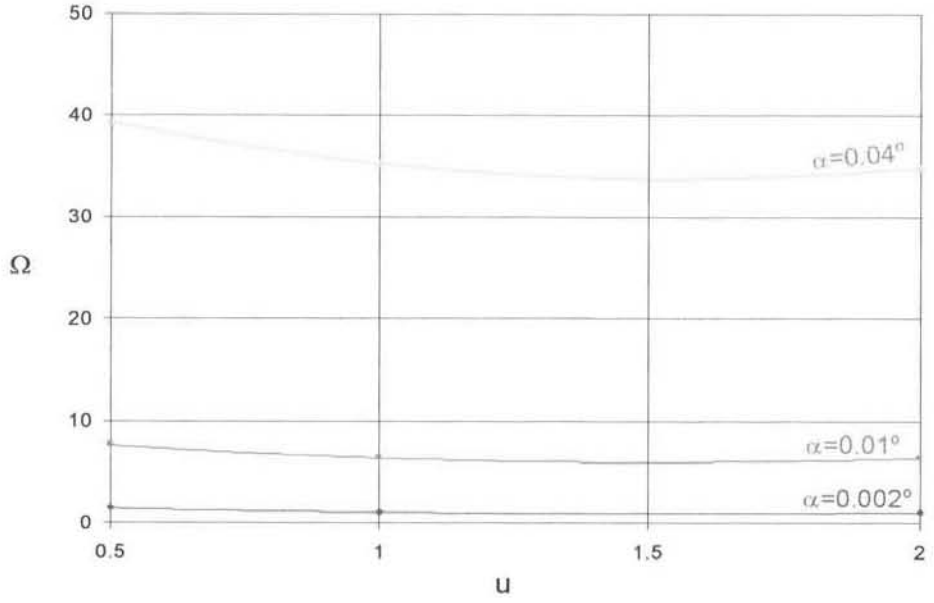

Figure 5-7: Plot showing the relationship between the thickness variation parameter and imperfection for cylinder l=12m, r=11.43m, and t=0.0085m

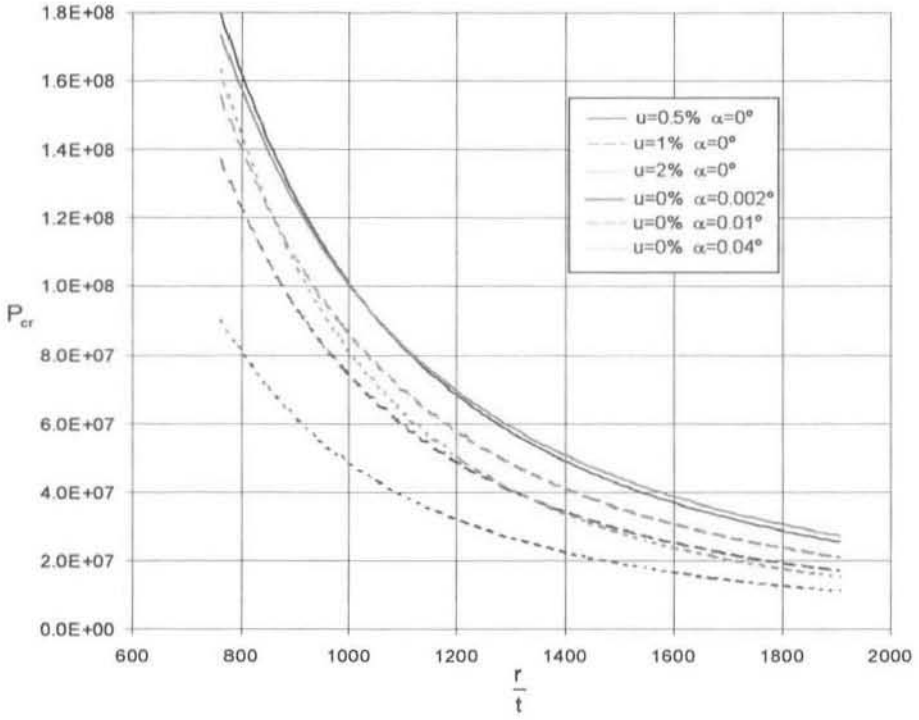

Figure 5-8: Various loading conditions for cylinder of parameters l=12m, r=11.43m, and t=0.0085m

5.3 Lateral external pressure

5.3.1 Literature survey

No research that covered the theoretical buckling pressures for imperfect tapered cylinders subjected to lateral external pressure was found.

5.3.2 Numerical analysis

The buckled form of the imperfect tapered wall is found to be a combination of the case of purely imperfect cylinders, and the case of purely tapered cylinders, whereby the buckling waves are concentrated on the minor radius and higher on the cylinder with the introduction of a taper. This can be seen in figures 5-9 to 5-11.

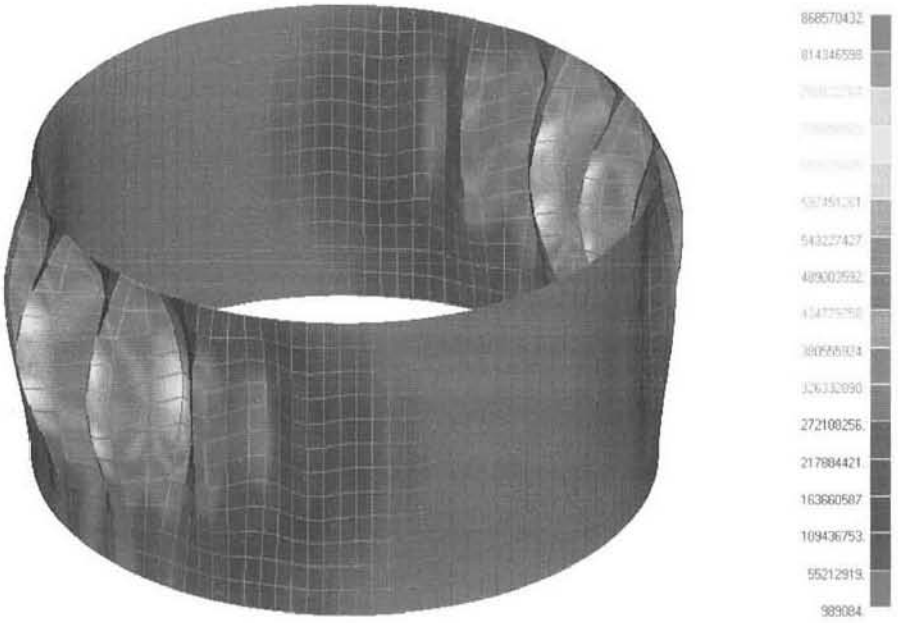

Figure 5-9: Isometric view of a buckled cylinder with parameters l=12m, r=11.43m, t=0.006m, u=1% and α=0.01^o

The effect of the imperfection and taper on the reduction in buckling load is shown in figure 5-12. It is evident that axial loading is far more imperfection

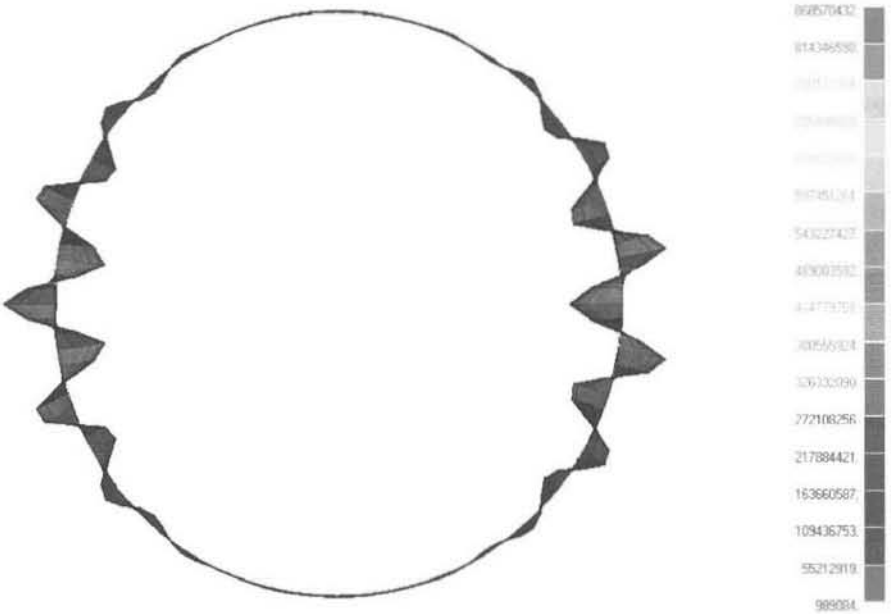

Figure 5-10: Top view of a buckled cylinder with parameters l=12m, r=11.43m, t=0.006m, u=1% and α=0.01^o

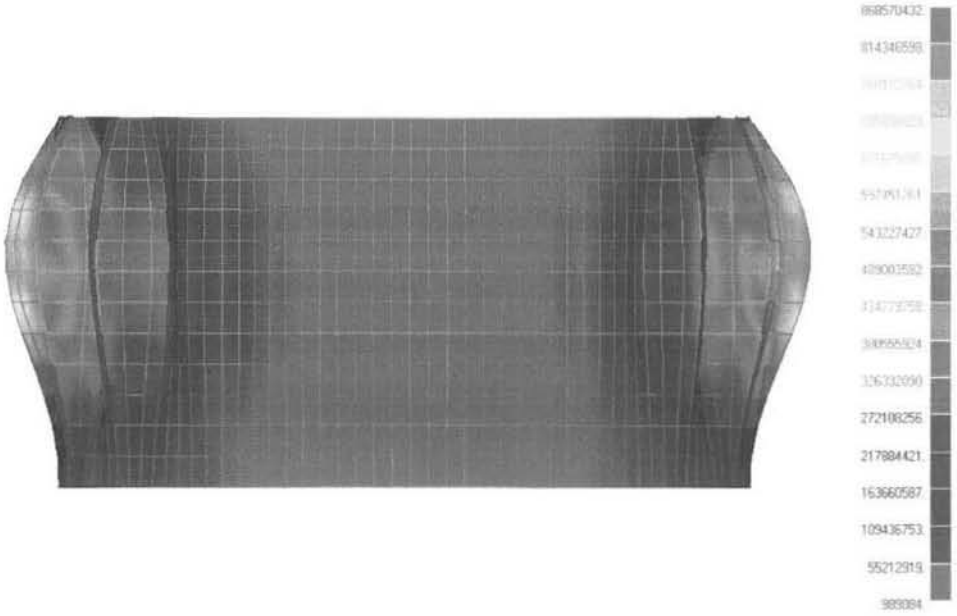

Figure 5-11: Side view of a buckled cylinder with parameters l=12m, r=11.43m, t=0.006m, u=1% and α=0.01^o

sensitive than lateral external pressure, where in the case of axial loading the buckling load is reduced by almost 80% for a taper of 0.004^o and 2% imperfection (refer to figure 5-6).

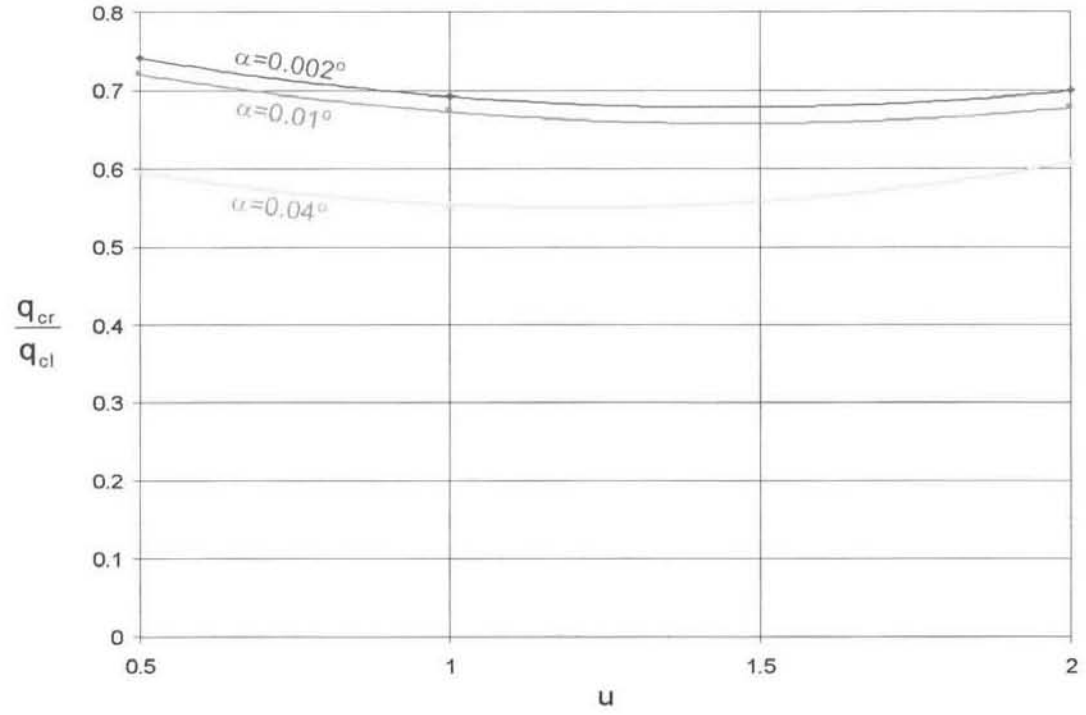

Figure 5-12: Graph showing the effect of taper and imperfection on the reduction of the buckling load of a cylinder subjected to lateral external pressure.

The thickness variation parameter in the case of lateral external pressure is fairly constant for all values of taper analysed as shown in figure 5-13, and was found to be far less than the case of axial pressure.

As in the case of axial loading, the effect of the individual imperfection and taper values analysed reduce the buckling load in the same manner.

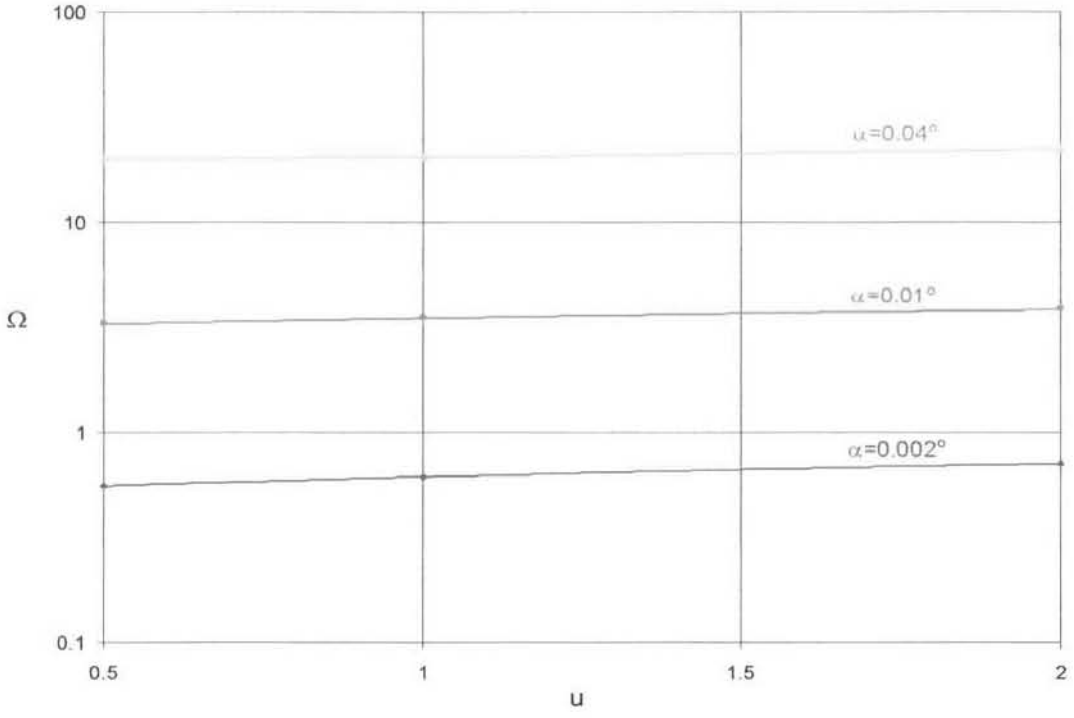

Figure 5-13: For l=12m, r=11.43m and t=0.0085m

5.4 Hydrostatic external pressure

5.4.1 Literature survey

No research that covered the theoretical analysis of buckling of imperfect tapered cylinders subjected to external hydrostatic pressure was found.

5.4.2 Numerical analysis

The effect of the imperfection and taper on the reduction of buckling load for the case of hydrostatic pressure is shown in figures 5-14 and 5-15. Hydrostatic pressure is also found to reduce the buckling load for increasing imperfection to a lesser degree than axial loading. The reduction in buckling load with increasing taper is also found to be more pronounced when subjected to axial loading than to hydrostatic pressure loading.

As before in the case of lateral external pressure, the thickness variation parameter is found to be constant with increasing imperfection. This plot is shown in figure 5-16.

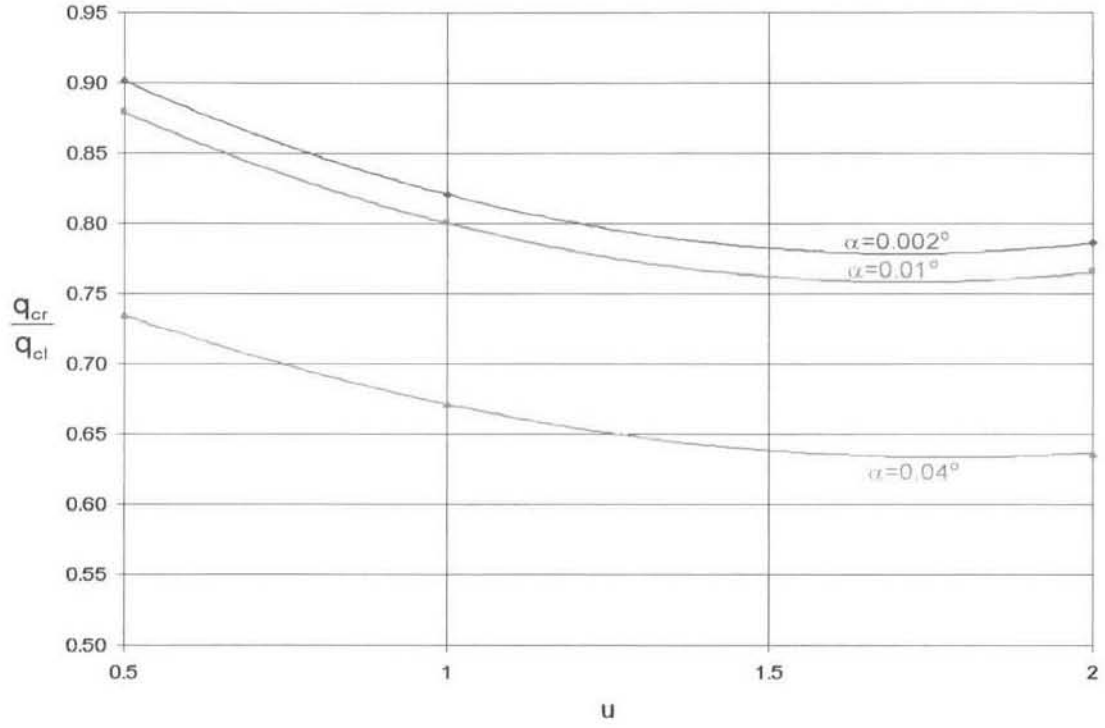

Figure 5-14: Plot showing the reduction in buckling load for cylinder l=12m, r=11.43m and t=0.0085m

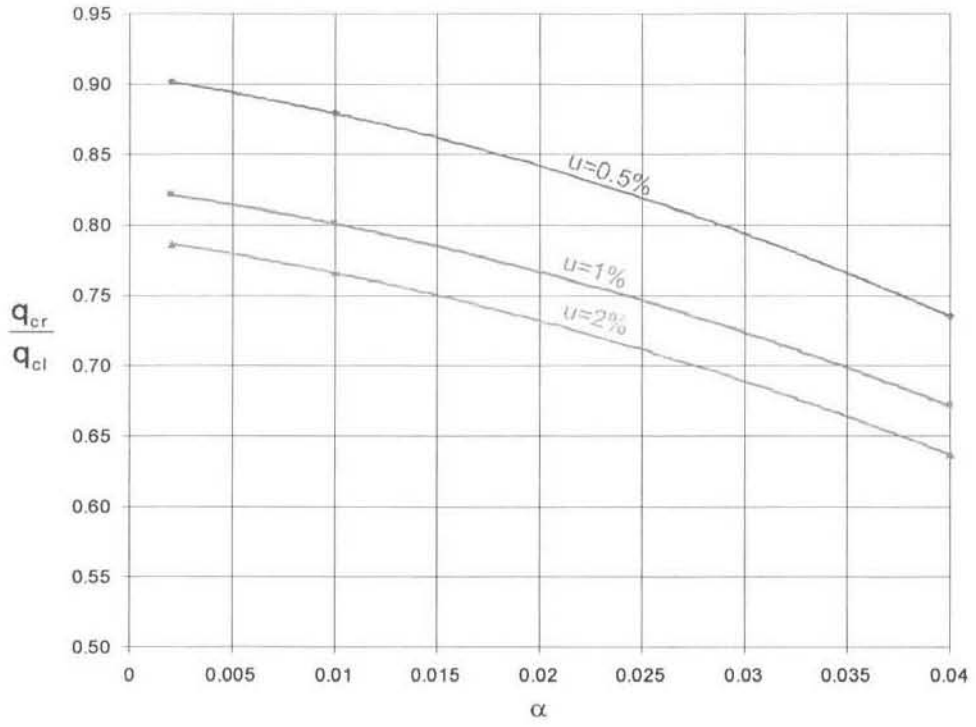

Figure 5-15: Plot showing the reduction in buckling load versus taper for cylinder l=12m, r=11.43m and t=0.0085m

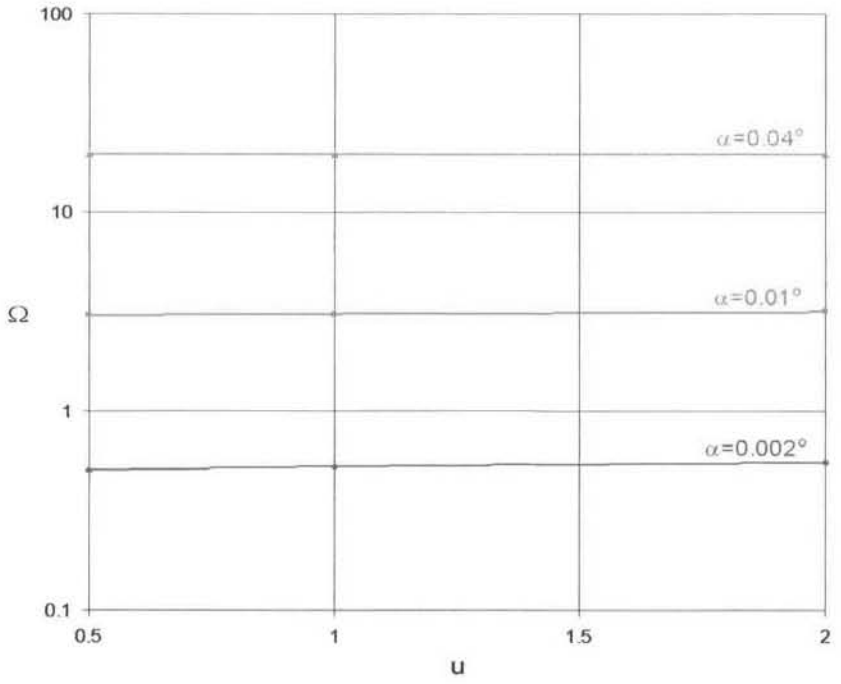

Figure 5-16: Plot showing the thickness variation parameter versus imperfection for the case of hydrostatic pressure for cylinder l=12m, r=11.43m and t=0.0085m

5.5 Combined loading

5.5.1 Literature survey

No research that theoretically investigated the buckling of imperfect tapered cylinders due to combined axial loading and external hydrostatic pressure was found.

5.5.2 Numerical analysis

The reduction in buckling load vesus imperfection and taper can be seen in figures 5-17 and 5-18. It is evident that the buckling load reduction is greater in the case of combined loading than in the case of hydrostatic pressure.

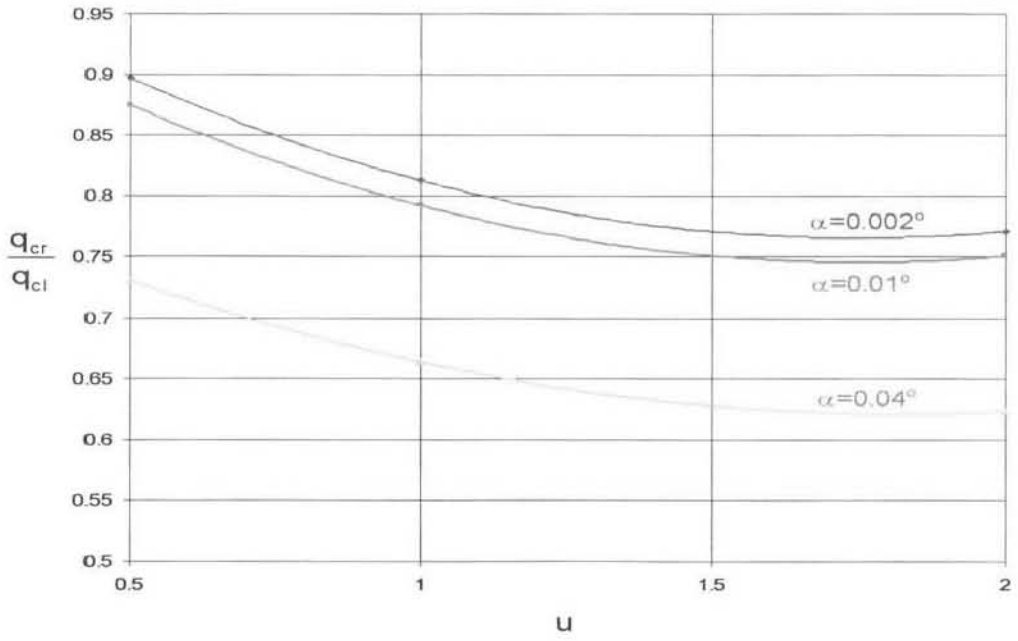

Figure 5-17: Plot showing the reduction in buckling load for increasing imperfection for cylinder l=12m, r=11.43m and t=0.0085m

As for hydrostatic and lateral pressure, the thickness variation parameter decreases with increasing taper, but remains fairly constant for increasing

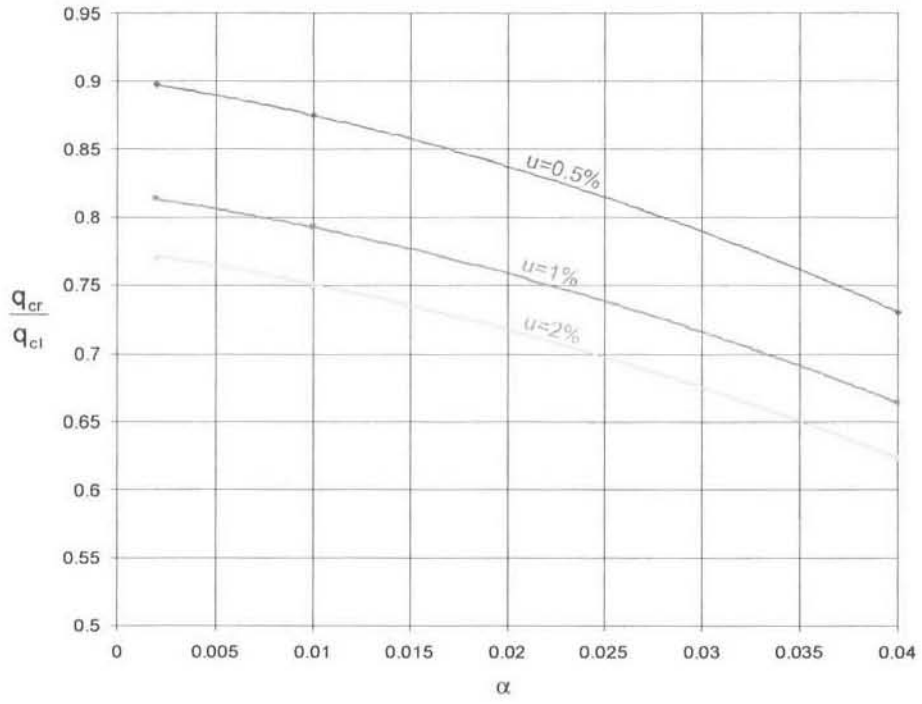

Figure 5-18: Plot showing the relationship between the reduction in buckling load, taper and imperfection for the case of combined loading for cylinder l=12m, r=11.43m and t=0.0085m

imperfection.

For the case of taper being 0.01^o and imperfection 1%, the buckling loads are compared for the various loading conditions in figure 5-20.

As in the previous chapters, there is a decreasing difference between the buckling loads for the various loading conditions as the radius to wall thickness ratio increases, i.e. as the wall thickness decreases.

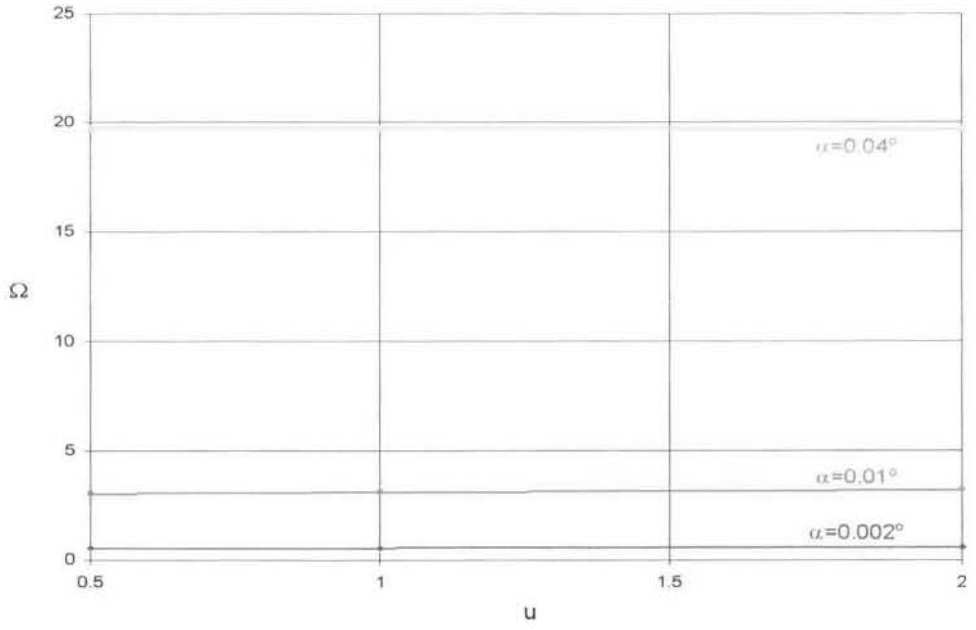

Figure 5-19: Plot showing the trends of the thickness varation parameter for cylinder l=12m, r=11.43m and t=0.0085m

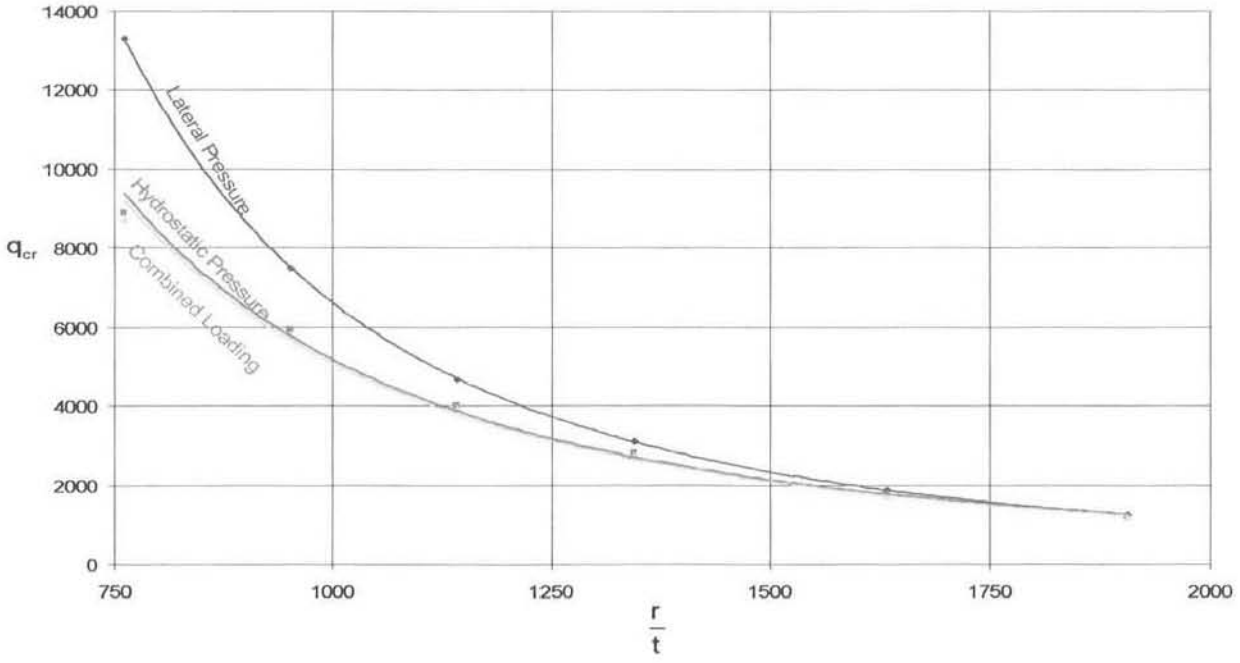

Figure 5-20: Plot showing a comparison of the reduction in buckling load for the various loading conditions for cylinder l=12m, r=11.43m and t=0.0085m

Chapter 6

DISCUSSION

Perfect cylinders have been thoroughly researched over the past century and present researchers in this field regard this research as complete in terms of buckling under static loads. When this research was reviewed and numerical analyses performed, it was found that although the trends are consistent with theory, the values of which are higher than that predicted theoretically. This behaviour was found to be constant across all loading conditions, the reason was discussed in chapter 1 where previous research using MSC Nastran for numerical analysis was reviewed. In the buckling of perfect cylinders subjected to axial loading, buckling equations were definitive and it was found that as the radius of the cylinder was increased or wall thickness decreased, the load carrying capability decreased. When lateral and hydrostatic external pressures were considered, it was found that a number of theories existed, some depending on the number of lobes into which the cylinder buckles and other theories were more simplified. It was found that the trends in lateral pressure buckling and hydrostatic pressure buckling were very similar but, as expected, cylinders subjected to hydrostatic pressure yielded lower buckling values than those subjected to lateral pressure. In the study of buckling under external pressure, it was found that as the length to radius ratio increases, the buckling load decreases. Furthermore, as the radius increases or wall thickness decreases, the buckling load also decreases. It was also found that as the radius increases, wall thickness decreases or length decreases, the

number of lobes into which the cylinder buckles increases almost exponentially. The prediction of the number of lobes was found to be good between theory and experiments conducted by other researchers of this field but, numerical analysis over-predicts the number of lobes at buckling. When the error between buckling pressure found by numerical analysis and theory was investigated, it was found that as the wall thickness decreases, this error increased slightly. This is due to the fact that as the cylinder becomes thinner the problem becomes more non-linear. The consequence of this is discussed in chapter 1 where it was shown that the version of the finite element package used in this study only had the linear buckling solution set available. The full version of the finite element method package also has a non-linear buckling solution set available, which has been shown by other researchers to be very accurate when compared to theory and experiments. Buckling of very thin shells is a non-linear problem.

When combined hydrostatic pressure and axial loading were considered, since a small axial load representing the roof, superstructure and live load (to accommodate a person walking on the roof) of SASOL's F7101b tank was used, the buckling load decreased by a small margin from the case of pure hydrostatic loading. When an investigation of the effect of varying axial loads was performed numerically, it was found that the pressure bearing capability of the cylinder decreased with an increasing axial load. It was also found that as the axial load increased, the bucking pressure decreased at a decreasing rate for increasing radius. This is best seen in figure 2-33 on page 62.

When imperfect cylinders were reviewed it was found that past research varied in their definitions of 'imperfect'. It was decided that the out-of-round definition of 'imperfect' were employed, as that is the measure of imperfection of SASOL's storage tanks. Therefore, tanks of a mid-length elliptical cross-section were used. Theory predicted that for increasing Batdorf parameter, Z, the buckling load would be reduced by a greater degree for a certain imperfection. In the case of axial loading it was seen that, as expected, the buckling load decreases for

increasing amplitude of imperfection and for a fixed imperfection the buckling load decreases for increasing Batdorf parameter. However, when numerical analysis was performed for lateral and hydrostatic pressure, it was found that as the imperfection was introduced, the reduction of the buckling load increases. Beyond some critical ratio of parameters, the reduction of the bucking load starts to decrease (ie. the ratio of buckling load to the classical buckling load begins to approach unity.) This trend was also prevalent in a previous study of bucking of imperfect cylinders executed by Guggenberger [61]. Numerical analysis also showed that the buckling lobes formed along the minor axis of the ellipse only.

Research on the buckling of variable wall thickness cylinders subjected to varying loading conditions proved to be elusive. As with imperfect cylinders, past research varied in their definition of 'variable'. Thickness imperfection definitions varied from sinusoidal to localised. This study considered a linearly tapered wall, where it was thickest at the base. The review of previous research showed that as the taper increases, the reduction in buckling load increased. When numerical analysis was executed, it was found that as the taper increased, the buckling lobes moved higher on the cylinder. In other words, as the gradient of the taper increased, the buckling waves shifted to where the cylinder is thinner. Numerical analysis confirmed the trend of decreasing buckling load for increased taper. Numerical analysis also showed that as the Batdorf parameter increased the effect of the taper on the buckling load increased, and vice versa. This was evident for both forms of external pressure. In a plot of the parameters Q and N, it can be seen that as the taper increases the buckling trend deviates increasingly from that of a perfect cylinder, until some critical imperfection, where the trend deviates completely. This behaviour is also seen in a plot of Q and the load parameter for the case of combined loading. When the reduction in buckling pressure for a specific size cylinder for increasing taper was considered, it was found that as the taper increased, the difference between the reduction in buckling load for external pressure and hydrostatic pressure were the same. At lower tapers the cylinder subjected to lateral external pressure was less effected by taper than the

hydrostatic case.

Existing research on the buckling of imperfect variable wall cylinders is virtually non-existent. This is because conversion from floating roof tanks to fixed roof tanks is not commonly undertaken. Therefore codes of practice do not cover this type of tank. The only research that was found considered axial loading exclusively. Their theoretical investigation concluded that the reduction in buckling load was inversely proportional to both imperfection and taper and derived a formula describing this relationship. They also introduced a thickness variation parameter in order to access the effect of the thickness variation on the buckling load reduction. Upon exploration of this parameter, it was found that as an imperfection is introduced, for a given taper, the thickness variation parameter increases, and then remains constant for increasing imperfection. In other words, as the imperfection increases, the specific taper has a constant effect. It was also found that for a given imperfection, increasing taper resulted in a higher thickness variation parameter as expected. Plots of numerical analysis results demonstrated that for a given taper, the reduction of buckling load decreases exponentially for increasing imperfection, and for a given imperfection decreases logarithmically for increasing taper. Numerical analysis confirmed the trends found theoretically of the thickness variation parameter. The buckled form of the variable wall thickness imperfect cylinder was found to be a combination of the two individual cases whereby the buckled waves were higher on the cylinder than mid-length (towards the thinner wall) and restricted to the minor axis of the ellipse.

Across all loading conditions and cylinder parameters a common result was that axial loading was far more sensitive to both imperfections and wall thickness variations where the bucking load was reduced to a greater degree than the external pressure cases for the same imperfection and/or taper.

Chapter 7

CONCLUSION

7.1 Overview

The investigation of buckling of cylinders was undertaken because SASOL had the need to predict the behaviour of cylinders that were converted from floating roof storage tanks to fixed roof tanks. The original floating roof tanks have tapered walls, and it is expected that tanks of large dimensions are impossible to construct perfectly. These tanks would also often be subjected to vacuums due to drastic ambient tempertature changes, which is characteristic of the extreme weather conditions experienced on the Highveld. Therefore, the buckling of variable wall imperfect cylinders due to combined loading had to be investigated.

The method of investigation was to review existing thoery and then to conduct numerical analyses on cylinders of a range of dimensions applicable to the tanks. The loading conditions considered were pure axial loading, lateral external pressure, hydrostatic external pressure, then finally the loading applicable to storage tanks : a combination of axial loading and hydrostatic external pressure. These loading conditions were considered for the case of perfect cylinders, imperfect (out-of-round) cylinders, tapered cylinders, and then finally the case in question : imperfect tapered cylinders. Due to the fact that little and sometimes no research has been conducted in the field of imperfect, tapered and imperfect

tapered cylinders, some of the relationships presented are based entirely on numerical analysis. The numerical analysis was performed using the finite element analysis software MSC Nastran for Windows.

The numerical analyses performed in this study is shown to be accurate in terms of trends, but over-predicted in terms of absolute values. This was found to be due to the fact that the MSC Nastran software implemented did not have the non-linear buckling solution set necessary to predict bucking of such thin-walled shells. It is therefore recognised that this study is merely a preliminary study from which definitive research in this field can be conducted in the future.

7.2 Recommendation for further work

Research in this field of imperfect variable wall thickness cylinders subjected to external pressure has just begun. The scope for work in this field is vast.

The next step in this research would be to perform numerical analyses of cylinders of various parameters using the non-linear buckling solution set. This would yield highly accurate results judging from the past research in buckling using this solution set of Nastran. From these curves, equations describing the behaviour of the cylinders could be determined for the imperfections and wall variations specific to SASOL's storage tanks.

Thereafter, this research could be extended to cover stiffened cylinders, which would then be of practical use to the designer of cylinders of SASOL's order of magnitude. Research would also have to cover the buckling of cones such that the roofs of these storage tanks are also taken into consideration.

Appendix A : Differential equations of a perfect cylindrical shell

This appendix shows how the differential equations of a perfect cylindrical shell can be used to derive the axial buckling load of a cylinder.

A general study of the buckling of a perfect cylinder under axial compression can be executed using equations 2.66 and 2.67.

In this case we will assume that all resultant forces, except N_x in figure 2-8, are very small. Therefore all the products of these forces with the derivatives of the displacements are also small, and can be neglected. Hence, the following equations result from equations 2.66 and 2.67

$$\begin{aligned} 0 &= rN'_x + \dot{N}_{yx} \\ 0 &= \dot{N}_y + rN'_{xy} + rN_x v'' - Q_y \\ 0 &= rQ'_x + \dot{Q}_y + rN_x w'' + N_y \end{aligned} \tag{A-1}$$

When the products of the moments and derivatives of the displacements are neglected, equations 2.67 become

$$\begin{aligned} Q_x &= M'_x + \frac{\dot{M}_{yx}}{r} \\ Q_y &= \frac{\dot{M}_y}{r} - M'_{xy} \end{aligned} \tag{A-2}$$

By combining these equations, the three equations of equilibrium for buckling of an axially compressed cylinder become

$$\begin{aligned} 0 &= rN'_x + \dot{N}_{yx} \\ 0 &= \dot{N}_y + rN'_{xy} + rN_x v'' - +M'_{xy} - \frac{\dot{M}_y}{r} \\ 0 &= rN_x w'' + N_y + rM''_x + \dot{M}'_{yx} + \frac{M''_y}{r} - \dot{M}'_{xy} \end{aligned} \tag{A-3}$$

If the values for forces and moments are then substituted into equations A–3 the following equations are obtained

$$\begin{aligned} 0 &= u'' + \frac{1+\nu}{2r}\dot{v}' - \frac{\nu}{r}w' + \frac{1-\nu}{2}\frac{\ddot{u}}{r^2} \\ 0 &= \frac{1+\nu}{2}\dot{u}' + \frac{r(1-\nu)}{2}v'' + \frac{\ddot{v}}{r} - \frac{\ddot{w}}{r} + \kappa\left[\frac{\ddot{v}}{r} + \frac{\dddot{w}}{r} + w\dot{w}'' + r(1-\nu)v''\right] \\ &\qquad - \frac{N_x r(1-\nu^2)}{Et}v'' \\ 0 &= -\frac{N_x r(1-\nu^2)}{Et}w'' + \nu u' + \frac{\dot{v}}{r} - \frac{w}{r} \\ &\qquad - \kappa\left[\frac{\dddot{v}}{r} + (2-\nu)r\dot{v}'' + r^3 w'''' + \frac{\dddot{w}}{r} + 2r\ddot{w}''\right] \end{aligned} \tag{A-4}$$

The general solution of these equations is taken as

$$\begin{aligned} u &= A \sin n\theta \cos \frac{m\pi x}{l} \\ v &= B \cos n\theta sin \frac{m\pi x}{l} \\ w &= C sinn\theta sin \frac{m\pi x}{l} \end{aligned} \tag{A–5}$$

which assumes that during buckling under axial loading, the length divides into m half waves, and the circumference into $2n$ half waves. At the ends $w = 0$ and $w'' = 0$, which are the conditions for simply supported edges. The results obtained in this manner can also be used for other edge conditions, since the effect of the edge conditions remain small for short cylinders too. Tests performed by Donnell in 1934 [7] showed that this is true for cylinders where the length-radius ratio is considerably less than unity.

If equations A–5 are substituted into equations A–4, the following expressions result

$$\begin{aligned} 0 &= A\left(m^2\chi^2 + \frac{1-\nu}{2}n^2\right) + B\frac{n(1+\nu)m\chi}{2} + C\nu m\chi \\ 0 &= A\frac{n(1+\nu)m\chi}{2} + B\left[\frac{(1-\nu)m^2\chi^2}{2} + n^2 + \kappa(1-\nu)m^2\chi^2 + \kappa n^2 - m^2\chi^2\frac{N_x(1-\nu^2)}{Et}\right] \\ &\qquad + C\left[n + \kappa n(n^2 + m^2\chi^2)\right] \\ 0 &= A\nu m\chi + Bn\left[1 + \kappa[n^2 + (2-\nu)m^2\chi^2]\right] \\ &\qquad + C\left[1 - m^2\chi^2\frac{N_x(1-\nu^2)}{Et} + \kappa(m^2\chi^2 + n^2)^2\right] \end{aligned} \tag{A–6}$$

where χ and κ are defined as for equation 2.103 on page 41.

Numerous experiments show that thin cylindrical shells under axial compression usually buckle into short longitudinal waves. Therefore m^2 and $m^2\chi^2$ are large numbers, and as in the section of the theoretical study of perfect cylinders subjected to lateral external pressure (see section 2.6.1, page 42), if the determinant is equated to zero, then the following is obtained

$$\frac{N_{cr}(1-\nu^2)}{Et} = \kappa\frac{n^2+m^2\chi^2)^2}{m^2\chi^2} + \frac{(1-\nu^2)m^2\chi^2}{(n^2+m^2\chi^2)^2} \tag{A-7}$$

This occurs at

$$\frac{n^2+m^2\chi^2)^2}{m^2\chi^2} = \frac{2r}{t}\sqrt{3(1-\nu^2)} \tag{A-8}$$

By substituting equation A–8 into equation A–7, an expression for the buckling load can be found as follows

$$N_{cr} = P_{cr} = \frac{2\pi Et^2}{\sqrt{3(1-\nu^2)}} \tag{A-9}$$

This is the same as equation 2.89 on page 34, where the buckling load was found by energy methods.

Appendix B : Cylinder parameters used in testing.

The cylinder parameters considered in this study are shown in the table overleaf.

The material considered was carbon steel, and the mechanical properties of carbon steel were taken to be as follows : $E = 200GPa$ $\nu = 0.32$ $S_Y = 350MPa$ $S_U = 450MPa$

l	r	t	α	u
12	9	0.006	0.002	0.5
14.63	11.43	0.007	0.01	1
	13	0.0085		
		0.01		
		0.012		
		0.015		

Table B–1: Table showing the cylinder parameters considered in numerical analysis.

Appendix C : Numerical results.

In the following tables all the numerical analysis results for the buckling of cylinders are shown for the various cylinders subjected to various loading conditions are recorded.

The imperfections and tapers are denoted as follows:

$$u1 = 0.5\%$$

$$u2 = 1\%$$

$$u3 = 2\%$$

$$a1 = \alpha = 0.002^o$$

$$a2 = \alpha = 0.01^o$$

$$a3 = \alpha = 0.04^o$$

C-1 : Axial loading

l	r	t	r/t	l/r	Pax cr TH	Pax cr NAS	Pax cr NAS	
						perfect	u1	u2
12	9	0.006	1500.0	1.333	2.76E+07	3.67E+07	2.82E+07	2.06E+07
12	9	0.007	1285.7	1.333	3.75E+07	4.91E+07	3.91E+07	2.92E+07
12	9	0.0085	1058.8	1.333	5.53E+07	7.09E+07	5.86E+07	4.51E+07
12	9	0.01	900.0	1.333	7.66E+07	9.65E+07	8.20E+07	6.48E+07
12	9	0.012	750.0	1.333	1.10E+08	1.37E+08	1.19E+08	9.68E+07
12	9	0.015	600.0	1.333	1.72E+08	2.05E+08	1.87E+08	1.57E+08
12	11.43	0.006	1905.0	1.050	2.76E+07	3.67E+07	2.53E+07	1.69E+07
12	11.43	0.007	1632.9	1.050	3.75E+07	4.91E+07	3.54E+07	2.41E+07
12	11.43	0.0085	1344.7	1.050	5.53E+07	7.09E+07	5.38E+07	3.77E+07
12	11.43	0.01	1143.0	1.050	7.66E+07	9.65E+07	7.61E+07	5.46E+07
12	11.43	0.012	952.5	1.050	1.10E+08	1.37E+08	1.12E+08	8.26E+07
12	11.43	0.015	762.0	1.050	1.72E+08	2.05E+08	1.78E+08	1.36E+08
12	13	0.006	2166.7	0.923	2.76E+07	3.67E+07	2.35E+07	1.52E+07
12	13	0.007	1857.1	0.923	3.75E+07	4.91E+07	3.30E+07	2.17E+07
12	13	0.0085	1529.4	0.923	5.53E+07	7.09E+07	5.05E+07	3.39E+07
12	13	0.01	1300.0	0.923	7.66E+07	9.65E+07	7.18E+07	4.92E+07
12	13	0.012	1083.3	0.923	1.10E+08	1.37E+08	1.06E+08	7.47E+07
12	13	0.015	866.7	0.923	1.72E+08	2.05E+08	1.71E+08	1.24E+08
14.63	9	0.006	1500.0	1.626	2.76E+07	3.67E+07	2.93E+07	2.26E+07
14.63	9	0.007	1285.7	1.626	3.75E+07	4.91E+07	4.03E+07	3.18E+07
14.63	9	0.0085	1058.8	1.626	5.53E+07	7.09E+07	6.01E+07	4.88E+07
14.63	9	0.01	900.0	1.626	7.66E+07	9.65E+07	3.36E+07	6.96E+07
14.63	9	0.012	750.0	1.626	1.10E+08	1.37E+08	1.21E+08	1.03E+08
14.63	9	0.015	600.0	1.626	1.72E+08	2.05E+08	1.89E+08	1.66E+08
14.63	11.43	0.006	1905.0	1.280	2.76E+07	3.67E+07	2.69E+07	1.88E+07
14.63	11.43	0.007	1632.9	1.280	3.75E+07	4.91E+07	3.74E+07	2.68E+07
14.63	11.43	0.0085	1344.7	1.280	5.53E+07	7.09E+07	5.65E+07	4.17E+07
14.63	11.43	0.01	1143.0	1.280	7.66E+07	9.65E+07	7.95E+07	6.01E+07
14.63	11.43	0.012	952.5	1.280	1.10E+08	1.37E+08	1.16E+08	9.04E+07
14.63	11.43	0.015	762.0	1.280	1.72E+08	2.05E+08	1.84E+08	1.48E+08
14.63	13	0.006	2166.7	1.125	2.76E+07	3.67E+07	2.53E+07	1.69E+07
14.63	13	0.007	1857.1	1.125	3.75E+07	4.91E+07	3.53E+07	2.41E+07
14.63	13	0.0085	1529.4	1.125	5.53E+07	7.09E+07	5.37E+07	3.76E+07
14.63	13	0.01	1300.0	1.125	7.66E+07	9.65E+07	7.60E+07	5.45E+07
14.63	13	0.012	1083.3	1.125	1.10E+08	1.37E+08	1.12E+08	8.25E+07
14.63	13	0.015	866.7	1.125	1.72E+08	2.05E+08	1.78E+08	1.36E+08

l	r	t	Pax cr NAS					
			u3	a1	a2	a3	u1a1	u1a2
12	9	0.006	1.32E+07	2.72E+07	2.11E+07	1.42E+07	2.77E+07	2.49E+07
12	9	0.007	1.89E+07	3.73E+07	2.92E+07	2.30E+07	3.83E+07	3.50E+07
12	9	0.0085	2.98E+07	5.52E+07	4.46E+07	3.94E+07	5.77E+07	5.34E+07
12	9	0.01	4.35E+07	7.67E+07	6.41E+07	5.97E+07	8.07E+07	7.49E+07
12	9	0.012	6.65E+07	1.11E+08	9.59E+07	9.25E+07	1.18E+08	1.10E+08
12	9	0.015	1.12E+08	1.73E+08	1.55E+08	1.54E+08	1.85E+08	1.76E+08
12	11.43	0.006	1.12E+07	2.72E+07	2.11E+07	1.42E+07	2.49E+07	2.28E+07
12	11.43	0.007	1.59E+07	3.73E+07	2.92E+07	2.30E+07	3.48E+07	3.23E+07
12	11.43	0.0085	2.46E+07	5.52E+07	4.46E+07	3.94E+07	5.30E+07	4.97E+07
12	11.43	0.01	3.56E+07	7.67E+07	6.41E+07	5.97E+07	7.50E+07	7.03E+07
12	11.43	0.012	5.41E+07	1.11E+08	9.59E+07	9.25E+07	1.11E+08	1.05E+08
12	11.43	0.015	9.06E+07	1.73E+08	1.55E+08	1.54E+08	1.77E+08	1.69E+08
12	13	0.006	1.06E+07	2.72E+07	2.11E+07	1.42E+07	2.31E+07	2.14E+07
12	13	0.007	1.48E+07	3.73E+07	2.92E+07	2.30E+07	3.25E+07	3.04E+07
12	13	0.0085	2.28E+07	5.52E+07	4.46E+07	3.94E+07	4.98E+07	4.70E+07
12	13	0.01	3.27E+07	7.67E+07	6.41E+07	5.97E+07	7.08E+07	6.67E+07
12	13	0.012	4.93E+07	1.11E+08	9.59E+07	9.25E+07	1.05E+08	9.97E+07
12	13	0.015	8.19E+07	1.73E+08	1.55E+08	1.54E+08	1.69E+08	1.62E+08
14.63	9	0.006	1.48E+07	2.72E+07	2.11E+07	1.42E+07	2.85E+07	2.45E+07
14.63	9	0.007	2.12E+07	3.73E+07	2.92E+07	2.30E+07	3.93E+07	3.45E+07
14.63	9	0.0085	3.34E+07	5.52E+07	4.46E+07	3.94E+07	5.88E+07	5.28E+07
14.63	9	0.01	4.87E+07	7.67E+07	6.41E+07	5.97E+07	8.28E+07	7.52E+07
14.63	9	0.012	7.43E+07	1.11E+08	9.59E+07	9.25E+07	1.20E+08	1.11E+08
14.63	9	0.015	1.24E+08	1.73E+08	1.55E+08	1.54E+08	1.88E+08	1.76E+08
14.63	11.43	0.006	1.21E+07	2.72E+07	2.11E+07	1.42E+07	2.63E+07	2.32E+07
14.63	11.43	0.007	1.72E+07	3.73E+07	2.92E+07	2.30E+07	3.67E+07	3.28E+07
14.63	11.43	0.0085	2.70E+07	5.52E+07	4.46E+07	3.94E+07	5.55E+07	5.06E+07
14.63	11.43	0.01	3.93E+07	7.67E+07	6.41E+07	5.97E+07	7.89E+07	7.25E+07
14.63	11.43	0.012	6.01E+07	1.11E+08	9.59E+07	9.25E+07	1.15E+08	1.07E+08
14.63	11.43	0.015	1.01E+08	1.73E+08	1.55E+08	1.54E+08	1.83E+08	1.72E+08
14.63	13	0.006	1.12E+07	2.72E+07	2.11E+07	1.42E+07	2.48E+07	2.21E+07
14.63	13	0.007	1.58E+07	3.73E+07	2.92E+07	2.30E+07	3.47E+07	3.14E+07
14.63	13	0.0085	2.44E+07	5.52E+07	4.46E+07	3.94E+07	5.28E+07	4.85E+07
14.63	13	0.01	3.54E+07	7.67E+07	6.41E+07	5.97E+07	7.55E+07	6.99E+07
14.63	13	0.012	5.39E+07	1.11E+08	9.59E+07	9.25E+07		1.04E+08
14.63	13	0.015	9.03E+07	1.73E+08	1.55E+08	1.54E+08	1.77E+08	1.68E+08

l	r	t	Pax cr NAS						
			u1a3	u2a1	u2a2	u2a3	u3a1	u3a2	u3a3
12	9	0.006	1.14E+07	2.02E+07	1.85E+07	8.90E+06	1.30E+07	1.20E+07	5.98E+06
12	9	0.007	1.89E+07	2.87E+07	2.66E+07	1.51E+07	1.86E+07	1.74E+07	1.03E+07
12	9	0.0085	3.33E+07	4.45E+07	4.17E+07	2.71E+07	2.94E+07	2.77E+07	1.89E+07
12	9	0.01	5.15E+07	6.38E+07	5.98E+07	4.27E+07	4.29E+07	4.04E+07	3.02E+07
12	9	0.012	8.16E+07	9.56E+07	9.03E+07	6.90E+07	6.57E+07	6.26E+07	4.97E+07
12	9	0.015	1.39E+08	1.56E+08	1.49E+08	1.20E+08	1.11E+08	1.06E+08	8.90E+07
12	11.43	0.006	1.14E+07	1.67E+07	1.55E+07	8.20E+06	1.10E+07	1.01E+07	5.20E+06
12	11.43	0.007	1.86E+07	2.38E+07	2.23E+07	1.37E+07	1.56E+07	1.46E+07	8.80E+06
12	11.43	0.0085	3.26E+07	3.73E+07	3.53E+07	2.44E+07	2.43E+07	2.30E+07	1.60E+07
12	11.43	0.01	5.04E+07	5.39E+07	5.10E+07	3.84E+07	3.51E+07	3.32E+07	2.54E+07
12	11.43	0.012	7.98E+07	8.17E+07	7.79E+07	6.20E+07	5.35E+07	5.11E+07	4.16E+07
12	11.43	0.015	1.36E+08	1.35E+08	1.30E+08	1.09E+08	8.99E+07	8.67E+07	7.43E+07
12	13	0.006	1.12E+07	1.50E+07	1.40E+07	7.80E+06	1.04E+07	9.40E+06	4.90E+06
12	13	0.007	1.83E+07	2.14E+07	2.01E+07	1.28E+07	1.46E+07	1.35E+07	8.20E+06
12	13	0.0085	3.18E+07	3.35E+07	3.19E+07	2.28E+07	2.25E+07	2.12E+07	1.47E+07
12	13	0.01	4.91E+07	4.87E+07	4.62E+07	3.56E+07	3.23E+07	3.05E+07	2.33E+07
12	13	0.012	7.78E+07	7.40E+07	7.08E+07	5.76E+07	4.88E+07	4.66E+07	3.80E+07
12	13	0.015	1.33E+08	1.23E+08	1.19E+08		8.13E+07	7.84E+07	6.75E+07
14.63	9	0.006	6.65E+06	2.20E+07	1.93E+07	5.50E+06	1.45E+07	1.29E+07	3.90E+06
14.63	9	0.007	1.30E+07	3.11E+07	2.78E+07	1.09E+07	2.08E+07	1.89E+07	7.90E+06
14.63	9	0.0085	2.58E+07	4.79E+07	4.36E+07	2.21E+07	3.29E+07	3.03E+07	1.64E+07
14.63	9	0.01	4.24E+07	6.90E+07	6.33E+07	3.68E+07	4.85E+07	4.51E+07	2.78E+07
14.63	9	0.012	7.05E+07	1.02E+08	9.52E+07	6.22E+07	7.40E+07	6.95E+07	4.79E+07
14.63	9	0.015	1.25E+08	1.65E+08	1.55E+08	1.12E+08	1.24E+08	1.17E+08	8.86E+07
14.63	11.43	0.006	6.90E+06	1.85E+07	1.66E+07	5.40E+06	1.19E+07	1.07E+07	3.50E+06
14.63	11.43	0.007	1.33E+07	2.64E+07	2.40E+07	1.04E+07	1.69E+07	1.55E+07	7.00E+06
14.63	11.43	0.0085	2.61E+07	4.11E+07	3.80E+07	2.08E+07	2.66E+07	2.47E+07	1.42E+07
14.63	11.43	0.01	4.26E+07	5.99E+07	5.57E+07	3.46E+07	3.92E+07	3.67E+07	2.40E+07
14.63	11.43	0.012	7.06E+07	9.00E+07	8.46E+07	5.83E+07	6.00E+07	5.68E+07	4.11E+07
14.63	11.43	0.015	1.25E+08	1.48E+08	1.40E+08	1.06E+08	1.01E+08	9.65E+07	7.59E+07
14.63	13	0.006	7.10E+06	1.66E+07	1.50E+07	5.30E+06	1.10E+07	9.80E+06	3.40E+06
14.63	13	0.007	1.35E+07	2.37E+07	2.18E+07	1.02E+07	1.55E+07	1.42E+07	6.60E+06
14.63	13	0.0085	2.61E+07	3.71E+07	3.46E+07	2.00E+07	2.41E+07	2.24E+07	1.32E+07
14.63	13	0.01	4.25E+07	5.44E+07	5.09E+07	3.30E+07	3.53E+07	3.31E+07	2.20E+07
14.63	13	0.012	7.01E+07	8.22E+07	7.77E+07	5.55E+07	5.38E+07	5.10E+07	3.75E+07
14.63	13	0.015	1.24E+08	1.36E+08	1.30E+08	1.00E+08	9.01E+07	8.65E+07	6.90E+07

C-2 : Lateral external pressure

l	r	t	r/t	l/r	qlat cr TH	qlat cr NAS		
						perfect	u1	u2
12	9	0.006	1500.0	1.333	1634.73	2160.3	2061.9	1932.4
12	9	0.007	1285.7	1.333	2408.21	3180.2	3040.8	2860.7
12	9	0.0085	1058.8	1.333	3923.87	6352.1	4956.9	4690
12	9	0.01	900.0	1.333	5905.97	7659.5	7452.6	7089.8
12	9	0.012	750.0	1.333	9346.09	12121.4	11803.8	11237.7
12	9	0.015	600.0	1.333	16398.45	21021.9	20660	19881
12	11.43	0.006	1905.0	1.050	1147.06	1553.4	1432.4	1334.2
12	11.43	0.007	1632.9	1.050	1690.42	2275.1	2112.5	1969.7
12	11.43	0.0085	1344.7	1.050	2755.74	4624.3	3446	3221.7
12	11.43	0.01	1143.0	1.050	4149.73	5478.6	5190.3	4867.7
12	11.43	0.012	952.5	1.050	6570.74	8590	8214.2	7737.8
12	11.43	0.015	762.0	1.050	11538.23	14934	14405.3	13650
12	13	0.006	2166.7	0.923	947.94	1306.4	1178.9	1108.2
12	13	0.007	1857.1	0.923	1397.27	1906.9	1738.2	1629.1
12	13	0.0085	1529.4	0.923	2278.50	3746	2835.1	2653.9
12	13	0.01	1300.0	0.923	3432.02	4594.2	4270.2	4000
12	13	0.012	1083.3	0.923	5436.12	7208.8	6761.4	6346.4
12	13	0.015	866.7	0.923	9550.26	12515.4	11865.4	11180.1
14.63	9	0.006	1500.0	1.626	1333.57	1749.8	1692.1	1598.6
14.63	9	0.007	1285.7	1.626	1963.63	2555.2	2489.3	2365.5
14.63	9	0.0085	1058.8	1.626	3197.41	4214.6	4059	3875.4
14.63	9	0.01	900.0	1.626	4809.65	6198.8	6096.1	5856.6
14.63	9	0.012	750.0	1.626	7605.52	9767.6	9632.3	9296.8
14.63	9	0.015	600.0	1.626	13330.78	17097.1	16908.2	16401.8
14.63	11.43	0.006	1905.0	1.280	935.25	1251.4	1174.3	1093.8
14.63	11.43	0.007	1632.9	1.280	1377.56	1827.8	1731.7	1618.3
14.63	11.43	0.0085	1344.7	1.280	2244.09	3019.8	2823.2	2651.9
14.63	11.43	0.01	1143.0	1.280	3377.00	4418.9	4250.2	4009.9
14.63	11.43	0.012	952.5	1.280	5342.76	6960.4	6731.1	6377.9
14.63	11.43	0.015	762.0	1.280	9371.18	12073.1	11786.9	11251.6
14.63	13	0.006	2166.7	1.125	772.63	1045.7	965	897.2
14.63	13	0.007	1857.1	1.125	1138.23	1531.2	1423.1	1324.6
14.63	13	0.0085	1529.4	1.125	1854.67	2545.9	2321.2	2166.8
14.63	13	0.01	1300.0	1.125	2791.63	3687.8	3496	3274
14.63	13	0.012	1083.3	1.125	4417.89	5781.7	5532.4	5204.8
14.63	13	0.015	866.7	1.125	7751.95	10050.6	9701.5	9182

l	r	t	qlat cr NAS					
			u3	a1	a2	a3	u1a1	u1a2
12	9	0.006	1858.7	2142.4	2059.4	1332.9	2044.3	1957.2
12	9	0.007	2724.8	3158.6	3042.8	2309.7	3019	2193
12	9	0.0085	4431.1	5096.8	4956.1	4130.3	4928	4791
12	9	0.01	6676.6	7625.9	7471.2	6528.5	7399	7162
12	9	0.012	10599.5	12082.1	11864.5	10702.9	11736	11435
12	9	0.015	18706.9	20960.6	20680.6	19183.5	20564	20148
12	11.43	0.006	1426.6	1592.6	1531.3	1043.5	1420	1361
12	11.43	0.007	2049.2	2326	2255.6	1728	2098	2052
12	11.43	0.0085	3255.9	3752.4	3661.1	3043	3427	3334
12	11.43	0.01	4825	5591.7	5473.1	4768.4	5153	4988
12	11.43	0.012	7544.3	8740.9	8600.3	7782	8167	7956
12	11.43	0.015	13127.7	15159.1	14980	13990	14341	14061
12	13	0.006	1280	1352.3	1300	909.9	1169	1121
12	13	0.007	1827.4	1894.4	1836.6	1418.1	1726	1667
12	13	0.0085	2869.7	3160.4	3083.7	2586	2819	2744
12	13	0.01	4205.1	4576.2	4488.6	3917.7	4240	4105
12	13	0.012	6493.3	7183.1	7062.2	6383.1	6722	6551
12	13	0.015	11144.9	12785.2	12635.8	11716.9	11813	11584
14.63	9	0.006	1498.7	1729.8	1633	634.8	1676	1579
14.63	9	0.007	2212.5	2532.6	2426.4	1404.3	2470	2355
14.63	9	0.0085	3622.2	4129.4	3986	2950.8	4035	3889
14.63	9	0.01	5481.2	6168	5986.2	4895.4	6126	5911
14.63	9	0.012	8728.1	9732.4	9525.7	8205.3	9674	9413
14.63	9	0.015	15443.6	17041.3	16714	15029.1	16968	16588
14.63	11.43	0.006	1088.6	1273.6	1207.4	551.4	1163.6	1097.7
14.63	11.43	0.007	1582.3	1861.5	1778.5	1100.6	1718.4	1637.9
14.63	11.43	0.0085	2550.2	2998.4	2896.9	2191.1	2806	2703
14.63	11.43	0.01	3819.8	4489.3	4372.1	3571.1	4271.8	4124.8
14.63	11.43	0.012	6033.6	7074.6	6904.2	6269.8	6760.6	6570.2
14.63	11.43	0.015	10602.4	12246.3	12031	10888.8	11830	11578.1
14.63	13	0.006	955.1	1072.8	1019.9	441	956.3	902.7
14.63	13	0.007	1371.6	1518.8	1452.9	895.3	1412.3	1346.9
14.63	13	0.0085	2179.4	2529.9	2446.4	1860.8	2307.2	2223.4
14.63	13	0.01	3230.4	3670.5	3565.9	2929.4	3513.8	3392.3
14.63	13	0.012	5052.7	5760.8	5635.3	4886.5	5557	5403.3
14.63	13	0.015	8795.3	10228.5	10064.4	9127.5	9737.7	9534.3

l	r	t	qlat cr NAS						
			u1a3	u2a1	u2a2	u2a3	u3a1	u3a2	u3a3
12	9	0.006	1259	1915	1830	1179	1840	1754	1093
12	9	0.007	2167	2839	2735	2029	2702	2596	1895
12	9	0.0085	3932	4662	4526	3695	4401	4264	3452
12	9	0.01	6259	7036	6799	5911	6623	6386	5513
12	9	0.012	10343	11205	10903	9831	10530	10226	9168
12	9	0.015	18809	19786	19374	18022	18612	18202	16850
12	11.43	0.006	911	1322	1264.5	844	1413	1346	812
12	11.43	0.007	1534	1955	1884	1424	2032	1952	1394
12	11.43	0.0085	2754	3202	3110	2561	3233	3132	2526
12	11.43	0.01	4372	4831	4668	4077	4786	4615	3983
12	11.43	0.012	7222	7690	7482	6764	7494	7276	6525
12	11.43	0.015	13149	13585	13305	12394	13059	12766	11818
12	13	0.006	768	1098	1051	714	1268	1207	711
12	13	0.007	1276	1617	1559	1189	1812	1740	1208
12	13	0.0085	2277		2562	2121	2850	2760	2192
12	13	0.01	3607	3970	3837	3361	4171	4022	3451
12	13	0.012	5952	6307	6137	5557	6449	6261	5601
12	13	0.015	10834	11127	10897	10160	11086	10835	10017
14.63	9	0.006	611	1583	1488.4	582.6	1482.8	1390.5	538.4
14.63	9	0.007	1344	2346.2	2230.8	1277.2	2192.7	2079.1	1179.3
14.63	9	0.0085	2815	3850.4	3702.5	2667.4	3596.3	3448.8	2464.4
14.63	9	0.01	4706	5884.7	5669.8	4473.8	5504.7	5292.5	4141.7
14.63	9	0.012	7989.4	9335.6	9066.7	7644.9	8761	8490.1	7104
14.63	9	0.015	14781.7	16459.6	16087.6	14267	15494	15129.9	13347.6
14.63	11.43	0.006	468.4	1083.1	1019.6	440.6	1077.1	1011.4	406.1
14.63	11.43	0.007	976.5	1605	1526.9	913.8	1568	1487.8	848.9
14.63	11.43	0.0085	1986.8	2634.5	2533.2	1855.6	2531.4	2427.9	1743.1
14.63	11.43	0.01	3294.3	4029.1	3883	3086	3834.6	3686.8	2902
14.63	11.43	0.012	5582.5	6404.5	6218.4	5257.1	6054.5	5865	4925.6
14.63	11.43	0.015	10343	11291.3	11040	9812.7	10634.4	10380.2	9172.2
14.63	13	0.006	410.5	888.5	837.3	382.8	945.2	887.4	356.7
14.63	13	0.007	826.1	1313.7	1250.6	768.5	1359.3	1290	725.3
14.63	13	0.0085	1648.9	2152.5	2070.4	1533.5	2163.3	2075	1475.3
14.63	13	0.01	2720.2	3289.5	3170.6	2534	3241.9	3117	2449.6
14.63	13	0.012	4600.5	5226.4	5074.2	4302	5068.7	4909.9	4126.1
14.63	13	0.015	8522.4	9214.3	9010.4	8018.6	8820	8607.3	7610.6

C-3 : Hydrostatic pressure

l	r	t	r/t	l/r	qhyd cr TH	qhyd cr NAS		
						perfect	u1	u2
12	9	0.006	1500.0	1.333	1616.99	2113.3	1989.5	1844.8
12	9	0.007	1285.7	1.333	2379.62	3071	2883	2673.4
12	9	0.0085	1058.8	1.333	3871.76	4859	4540.8	4201.3
12	9	0.01	900.0	1.333	5819.80	7009	6520.8	6012.4
12	9	0.012	750.0	1.333	9194.59	10391.8	9492.2	8699.6
12	9	0.015	600.0	1.333	16095.98	15952.1	14073.3	12737
12	11.43	0.006	1905.0	1.050	1131.59	1526.1	1369.8	1254.9
12	11.43	0.007	1632.9	1.050	1665.51	2213.3	1977.1	1801
12	11.43	0.0085	1344.7	1.050	2710.34	3510	3089.2	2787.5
12	11.43	0.01	1143.0	1.050	4074.69	5116.8	4395.5	3923
12	11.43	0.012	952.5	1.050	6438.81	7646.7	6302.4	5543.2
12	11.43	0.015	762.0	1.050	11274.80	12016.7	9105.3	7825.6
12	13	0.006	2166.7	0.923	933.79	1286.3	1120	1031.4
12	13	0.007	1857.1	0.923	1374.49	1862	1611.5	1466.6
12	13	0.0085	1529.4	0.923	2236.99	2951.5	2503.5	2240
12	13	0.01	1300.0	0.923	3363.39	4305.2	3537.6	3110.9
12	13	0.012	1083.3	0.923	5315.43	6474.1	5018.6	4318.7
12	13	0.015	866.7	0.923	9309.19	10235	7131.1	5948.5
14.63	9	0.006	1500.0	1.626	1323.34	1722	1644.0	1541.5
14.63	9	0.007	1285.7	1.626	1947.12	2491.8	2385.6	2244.1
14.63	9	0.0085	1058.8	1.626	3167.26	3977.9	3778.7	3557.0
14.63	9	0.01	900.0	1.626	4759.76	5821.9	5480.8	5149.6
14.63	9	0.012	750.0	1.626	7517.73	8754.4	8078.7	7583.0
14.63	9	0.015	600.0	1.626	13155.45	13954.3	12296.9	11459.3
14.63	11.43	0.006	1905.0	1.280	925.82	1233.7	1135.4	1046.4
14.63	11.43	0.007	1632.9	1.280	1362.37	1792.5	1648.1	1517.0
14.63	11.43	0.0085	1344.7	1.280	2216.41	2853.3	2602.0	2388.5
14.63	11.43	0.01	1143.0	1.280	3331.26	4188.1	3752.1	3427.4
14.63	11.43	0.012	952.5	1.280	5262.37	6380.9	5499.1	4985.8
14.63	11.43	0.015	762.0	1.280	9210.78	10332	8252.2	7371.3
14.63	13	0.006	2166.7	1.125	763.86	1032.9	928.61	851.43
14.63	13	0.007	1857.1	1.125	1124.11	1502.8	1344.47	1227.17
14.63	13	0.0085	1529.4	1.125	1828.95	2400.3	2113.34	1914.77
14.63	13	0.01	1300.0	1.125	2749.12	3526.2	3031.09	2721.08
14.63	13	0.012	1083.3	1.125	4343.19	5361.3	4400.96	3901.93
14.63	13	0.015	866.7	1.125	7602.92	8732.2	6493.46	5635.47

l	r	t	qhyd cr NAS					
			u3	a1	a2	a3	u1a1	u1a2
12	9	0.006	1737.6	2089.4	2005.7	1308.7	1973.4	1892.5
12	9	0.007	2473.9	3026.1	2930.4	2229.1	2863.9	2798.9
12	9	0.0085	3803.5	4786.6	4638.2	3891.6	4517.9	4404.3
12	9	0.01	5336.5	6836.3	6695.9	5893.6	6480	6295.1
12	9	0.012	7533.4	9974.5	9841.7	8989.4	9447.7	9247.2
12	9	0.015	10703.5	14908.5	14777	13971.3	14029.3	13830
12	11.43	0.006	1307.4	1506.4	1450.6	977.9	1374.3	1319.3
12	11.43	0.007	1802.7	2181.7	2118.4	1630	1998.2	1932.4
12	11.43	0.0085	2357.1	3444.9	3369.1	2828.4	3164.3	3086.5
12	11.43	0.01	3568.8	4994.6	4893	4303	4567.1	4439
12	11.43	0.012	4790.4	7377.8	7264.4	6640.8	6732.8	6591.5
12	11.43	0.015	6382.9	11310.3	11192.6	10482.3	10207	10062.4
12	13	0.006	1166.5	1270	1222.4	842	1132	1087.4
12	13	0.007	1584.5	1838.1	1738	1386	1646.7	1593.9
12	13	0.0085	2265.5	2899.8	2832.3	2391.6	2611.1	2547.6
12	13	0.01	2962.1	4212.7	4138.9	3651.7	3776.5	3671.1
12	13	0.012	3832.4	6267.1	6186.1	5642.4	5590	5472.9
12	13	0.015	4879.7	9645.2	9551.7	9037.4	8548.4	8427.9
14.63	9	0.006	1423.2	1697.1	1603.1	628.9	1635.7	1543.1
14.63	9	0.007	2055.3	2456.9	2355.6	1375.5	2382.6	2274.9
14.63	9	0.0085	3224.4	3913.1	3798.3	2827.3	3798	3668.5
14.63	9	0.01	4618.4	5710.9	5547.4	4572.5	5597.4	5413.9
14.63	9	0.012	6708.8	8506.5	8334.5	7283.4	8336	8131.4
14.63	9	0.015	9947.6	13274	13104.5	11964.7	12945.2	12731.1
14.63	11.43	0.006	1020.5	1218.3	1153.2	493.6	1137.4	1074.9
14.63	11.43	0.007	1441.6	1767.6	1690.6	1025.4	1662.6	1587.8
14.63	11.43	0.0085	2200.1	2809.4	2716.8	2055.9	2659.6	2567.6
14.63	11.43	0.01	3074.6	4112.8	4009.2	3304.3	3934.3	3809.4
14.63	11.43	0.012	4331.3	6210.5	6099.1	5293.5	5920.7	5777.7
14.63	11.43	0.015	6156.8	9877.7	9753.5	8855.0	9361.1	9202.8
14.63	13	0.006	886.48	1019.498	970.4039	438.3532	935.4	884.6
14.63	13	0.007	1229.57	1484.808	1424	882.1125	1367.9	1307.2
14.63	13	0.0085	1828.53	2366.663	2288.709	1740.146	2191.3	2116.5
14.63	13	0.01	2494.14	3471.325	3374.916	2790.317	3249	3146.3
14.63	13	0.012	3408.44	5243.602	5132.48	4487.992	4906.9	4787.5
14.63	13	0.015	4651.57	8390.883	8261.3	7574.103	7815.7	7681.6

l	r	t	qhyd cr NAS						
			u1a3	u2a1	u2a2	u2a3	u3a1	u3a2	u3a3
12	9	0.006	1231.8	1829.2	1752.4	1149.6	1722.1	1647.9	1059.5
12	9	0.007	2082.5	2654.9	2564.8	1933.8	2455.9	2370.3	1778.1
12	9	0.0085	3652.3	4179.3	4072.7	3380.1	3782.5	3683.9	3063.3
12	9	0.01	5557.1	5975.1	5805.4	5125.3	5303.4	5155.2	4564.9
12	9	0.012	8474.8	8653.6	8472.1	7766.2	7499.8	7348.4	6761.7
12	9	0.015	13048	12698.7	12523	11826.3	10673	10534.7	9994
12	11.43	0.006	893.1	1263.9	1212.3	824.2	1318	1261.3	788
12	11.43	0.007	1480.3	1831.1	1770.2	1360.9	1838.4	1774.3	1309.5
12	11.43	0.0085	2580.3	2883.2	2810.7	2356.2	2761	2688.8	2235
12	11.43	0.01	3935.4	4132.7	4016.6	3569.4	3804.9	3699.4	3284.4
12	11.43	0.012	6053.6	6026.7	5901.8	5435.2	5304.2	5197.8	4798.6
12	11.43	0.015	9514.1	8980.9	8858.9	8403.4	7485.6	7390.3	7036.2
12	13	0.006	753.6	1049.6	1007.5	696.6	1185.9	1132.6	690.2
12	13	0.007	1233.3	1514.3	1464.7	1137	1639.3	1580.8	1135.8
12	13	0.0085	2139.6		2317.1	1953.6	2422.6	2357.7	1936
12	13	0.01	3264.1	3401.4	3306.6	2949.6	3289.2	3197.3	2826.3
12	13	0.012	5037.2	4962.3	4860.2	4488.1	4511.9	4420.4	4076.5
12	13	0.015	7984	7423.9	7324.6	6964.3	6267.4	6186.7	5892
14.63	9	0.006	605.5	1534.6	1446.5	578.7	1419.9	1336.5	535.3
14.63	9	0.007	1315.2	2243.2	2138.4	1248.5	2061.1	1962.2	1148.2
14.63	9	0.0085	2685.6	3579.9	3452.5	2528	3260.4	3141.2	2304.2
14.63	9	0.01	4352.2	5271.5	5099.1	4087	4755.6	4599.7	3694.9
14.63	9	0.012	6996.5	7840	7645.4	6557.7	6992.6	6820.5	5863.2
14.63	9	0.015	11541.5	12095.4	11890	10757.1	10595.3	10418	9451.2
14.63	11.43	0.006	465.3	1051	991.9	437.7	1029.8	970.8	403.8
14.63	11.43	0.007	959.1	1537	1466.4	894.9	1471.2	1402.1	827.7
14.63	11.43	0.0085	1908.4	2458.7	2371.9	1767.5	2291.4	2208.7	1633.3
14.63	11.43	0.01	3079.7	3631.4	3514.3	2843.5	3311.3	3203.7	2595.8
14.63	11.43	0.012	4975.5	5440.9	5307.8	4575.9	4840.9	4723.1	4088.1
14.63	11.43	0.015	8336.5	8519.9	8376.4	7602.7	7337.6	7217.7	6584.1
14.63	13	0.006	407.8	862.1	814.6	380.3	902.9	851	354.7
14.63	13	0.007	812.1	1258.4	1201.6	753	1273.3	1213.7	707.4
14.63	13	0.0085	1588	2010.7	1940.5	1463.2	1953	1882.8	1382.8
14.63	13	0.01	2554.1	2970.6	2875.5	2341.7	2790.2	2699.9	2188.3
14.63	13	0.012	4131.2	4458.7	4350.4	3764.2	4038.1	3940.1	3418.2
14.63	13	0.015	6965.4	7016.8	6899.7	6277.2	6071	5972.3	5460.4

C-4 : Combined loading

l	r	t	r/t	l/r	qcomb cr TH	qcomb cr NAS		
						perfect	u1	u2
12	9	0.006	1500.0	1.333	1591.47	2089.4	1958.3	1805.4
12	9	0.007	1285.7	1.333	2339.96	3032.1	2835.7	2615.1
12	9	0.0085	1058.8	1.333	3801.95	4799.3	4462.4	4108.1
12	9	0.01	900.0	1.333	5707.15	6915.7	6406	5878.8
12	9	0.012	750.0	1.333	9001.10	10248.6	9321.9	8510
12	9	0.015	600.0	1.333	15719.50	15755.4	13827.5	12481.1
12	11.43	0.006	1905.0	1.050	1111.63	1514.2	1352.4	1231.9
12	11.43	0.007	1632.9	1.050	1634.40	2194.4	1951.2	1767.7
12	11.43	0.0085	1344.7	1.050	2655.48	3477.8	3047.3	2736.1
12	11.43	0.01	1143.0	1.050	3986.05	5072.2	4335.3	3852.1
12	11.43	0.012	952.5	1.050	6286.40	7580.2	6216.8	5448.2
12	11.43	0.015	762.0	1.050	10978.00	11930.6	8989.8	7708.2
12	13	0.006	2166.7	0.923	916.30	1278.3	1107.3	1013.9
12	13	0.007	1857.1	0.923	1347.19	1849.4	1592.6	1441.6
12	13	0.0085	1529.4	0.923	2188.79	2930.2	2473.6	2202.5
12	13	0.01	1300.0	0.923	3285.46	4272.8	3495.1	3060.4
12	13	0.012	1083.3	0.923	5181.38	6426.8	4959.8	4253.6
12	13	0.015	866.7	0.923	9048.02	10177.7	7055	5872.5
14.63	9	0.006	1500.0	1.626	1305.95	1706.4	1623.5	1516.6
14.63	9	0.007	1285.7	1.626	1920.21	2465.9	2355.0	2207.0
14.63	9	0.0085	1058.8	1.626	3120.10	3931.2	3726.8	3496.3
14.63	9	0.01	900.0	1.626	4683.81	5755.4	5404.1	5059.4
14.63	9	0.012	750.0	1.626	7387.52	8645.3	7961.3	7451.4
14.63	9	0.015	600.0	1.626	12902.47	13779.2	12117.0	11266.9
14.63	11.43	0.006	1905.0	1.280	912.24	1225.1	1122.9	1030.4
14.63	11.43	0.007	1632.9	1.280	1341.30	1780.1	1628.3	1492.6
14.63	11.43	0.0085	1344.7	1.280	2179.38	2831.7	2567.1	2346.6
14.63	11.43	0.01	1143.0	1.280	3271.55	4153.4	3695.8	3361.9
14.63	11.43	0.012	952.5	1.280	5159.87	6324.9	5403.1	4879.5
14.63	11.43	0.015	762.0	1.280	9011.46	10245.6	8075.9	7187.7
14.63	13	0.006	2166.7	1.125	751.97	1027.3	920.0	840.3
14.63	13	0.007	1857.1	1.125	1105.63	1493.7	1331.6	1210.9
14.63	13	0.0085	1529.4	1.125	1796.43	2384.5	2092.3	1889.1
14.63	13	0.01	1300.0	1.125	2696.65	3503.8	3000.2	2684.6
14.63	13	0.012	1083.3	1.125	4253.07	5326.0	4355.9	3851.6
14.63	13	0.015	866.7	1.125	7427.59	8679.3	6430.4	5569.5

l	r	t	qcomb cr NAS					
			u3	a1	a2	a3	u1a1	u1a2
12	9	0.006	1682	2061.1	1981.2	1290	1942.3	1862.3
12	9	0.007	2394.4	2986.2	2895.4	2196.4	2816.8	2751.8
12	9	0.0085	3682.6	4705.3	4577	3833.6	4439.6	4327.9
12	9	0.01	5172	6731.8	6598.7	5802.2	6365.7	6182.8
12	9	0.012	7315.8	9820.6	9687.2	8844.1	9277.8	9078.8
12	9	0.015	10435.8	14672.4	14539.5	13786.5	13783.5	13584.4
12	11.43	0.006	1271.6	1494.4	1438.6	968.5	1356.7	1302.3
12	11.43	0.007	1752.7	2162.4	2099.2	1613.9	1971.7	1906.6
12	11.43	0.0085	2578.6	3411.1	3335.5	2799.3	3120.7	3043.5
12	11.43	0.01	3476.8	4964.4	4844.7	4256.7	4502.4	4375.6
12	11.43	0.012	4678.9	7300.8	7187.1	6562.6	6636.2	6496.1
12	11.43	0.015	6261.7	11176	11068.8	10355.8	10064.5	9920.4
12	13	0.006	1138.8	1261.8	1214.2	835.5	1118.9	1074.7
12	13	0.007	1545.2	1825	1770	1374.9	1626.9	1574.6
12	13	0.0085	2209.6	2877.2	2809.8	2371.5	2578.8	2515.8
12	13	0.01	2893.1	4177	4103.1	3618.5	3728.7	3624.3
12	13	0.012	3753.4	6209.7	6128.5	5588.6	5518.5	5402.3
12	13	0.015	4800	9554	9460	8948	8442.2	8322.2
14.63	9	0.006	1389.4	1681.3	1587.4	621.2	1615.5	1523.6
14.63	9	0.007	2006.0	2430.9	2329.9	1356.7	2351.9	2244.7
14.63	9	0.0085	3147.1	3866.0	3751.2	2787.1	3745.4	3616.5
14.63	9	0.01	4509.0	5643.1	5479.7	4509.4	5518.1	5335.8
14.63	9	0.012	6555.8	8393.5	8221.6	7179.1	8212.3	8008.3
14.63	9	0.015	9743.0	13084.7	12914.8	11788.0	12474.8	12533.4
14.63	11.43	0.006	997.0	1209.5	1145.4	489.4	1126.1	1064.1
14.63	11.43	0.007	1407.1	1755.1	1678.1	1015.9	1645.5	1571.2
14.63	11.43	0.0085	2144.4	2787.1	2694.6	2036.4	2630.8	2539.4
14.63	11.43	0.01	2992.6	4076.3	3973.0	3272.4	3890	3765.9
14.63	11.43	0.012	4208.3	6149.4	6038.1	5239.9	5851.5	5709.3
14.63	11.43	0.015	6285.2	9770.5	9649.8	8756.7	9249.9	9092
14.63	13	0.006	869.0	1013.8	964.7	435.4	927.1	876.6
14.63	13	0.007	1204.9	1475.7	1415.6	875.6	1355.3	1295
14.63	13	0.0085	1792.5	2350.5	2273.9	1746.2	2170.2	2095.8
14.63	13	0.01	2446.6	3447.5	3351.1	2768.6	3216.5	3114.5
14.63	13	0.012	3348.6	5203.4	5092.4	4450.4	4856.5	4737.7
14.63	13	0.015	4827.1	8322.8	8193.1	7508.5	7733.9	7600.6

l	r	t	qcomb cr NAS						
			u1a3	u2a1	u2a2	u2a3	u3a1	u3a2	u3a3
12	9	0.006	1209.5	1790.1	1714.5	1123.5	1667	1594.6	1026.5
12	9	0.007	2042.7	2597	2508.2	1886.9	2376.9	2293.3	1716.9
12	9	0.0085	3581.6	4086.3	3981.2	3297.6	3662.2	3565.6	2957.9
12	9	0.01	5448.3	5842	5674.7	5001	5139.6	4994.1	4412.8
12	9	0.012	8308.2	8464.7	8285	7582.6	7282.5	7132.9	6550.8
12	9	0.015	12799	12442.5	12266.5	11568.3	10405.2	10266.6	9724.1
12	11.43	0.006	880.6	1240.5	1189.6	808.7	1281.4	1225.7	767.5
12	11.43	0.007	1458.5	1796.7	1736.7	1333.6	1786.4	1723.5	1270.9
12	11.43	0.0085	2541.4	2828.3	2756.8	2308.3	2683.1	2612.2	2167.2
12	11.43	0.01	3875.4	4054.3	3939.8	3497.3	3700.6	3596.8	3187.8
12	11.43	0.012	5960.7	5915.3	5791.7	5328.4	5168.2	5062.9	4667
12	11.43	0.015	9372.3	8828.2	8706.6	8251.2	7320.2	7224.8	6870
12	13	0.006	744.3	1031.4	990	684.6	1157.5	1104.7	674.2
12	13	0.007	1217.4	1487.8	1438.9	1116.1	1597.7	1539.9	1105.6
12	13	0.0085	2111.1		2275.9	1917.1	2359.6	2295.5	1881.6
12	13	0.01	3220	3341.6	3248.1	2894.9	3205.2	3114.6	2748.4
12	13	0.012	4968.8	4877.6	4776.5	4407.3	4403.8	4313.2	3971.8
12	13	0.015	7878.6	7307.7	7208.7	6849	6138.3	6057.6	5762.3
14.63	9	0.006	597.8	1509.6	1422.5	571.1	1385.9	1303.8	527.7
14.63	9	0.007	1293.8	2205.7	2101.9	1224.7	2011.1	1913.9	1119.7
14.63	9	0.0085	2639.4	3518	3391.7	2475.7	3180.8	3063.4	2240.1
14.63	9	0.01	4277.9	5177.8	5007.8	4003.2	4640.3	4486.5	3593.6
14.63	9	0.012	6877.3	7700.6	7507.3	6425.2	6827.8	6657.3	5708.8
14.63	9	0.015	11346.4	11885.3	11679.5	10547.8	10364.4	10187.6	9223
14.63	11.43	0.006	460.9	1036.4	977.9	433	1007.9	949.8	398.7
14.63	11.43	0.007	947.5	1515.2	1445.3	881.3	1439.5	1371.4	810.4
14.63	11.43	0.0085	1883.8	2422.8	2336.9	1738.2	2241.7	2160.2	1594.3
14.63	11.43	0.01	3039.9	3577.8	3641.8	2796.5	3240.2	3134.1	2534.2
14.63	11.43	0.012	4910.8	5360.3	5228.2	4501.1	4740.3	4623.7	3994.9
14.63	11.43	0.015	8228.2	8397.4	8254.4	7483.2	7197.6	7078.1	6447
14.63	13	0.006	404.4	851	804	376.5	885.3	834.1	350.6
14.63	13	0.007	803.6	1241.9	1185.5	742.6	1247.8	1189	693.9
14.63	13	0.0085	1570.2	1983.6	1914.2	1441.3	1913.4	1844.1	1352.3
14.63	13	0.01	2525.3	2930.2	2836	2306.7	2734	2644.9	2139.8
14.63	13	0.012	4084.2	4398.1	4290.7	3708.6	3959.4	3862.3	3345.4
14.63	13	0.015	6886.2	6924.7	6808.1	6188	5962.6	5864.2	5354.5

Appendix D : Values of γ for perfect cylinders.

This appendix shows the roots of γ for the purpose of finding the buckling equation of a perfect cylinder subjected to both axial loading and external hydrostatic pressure.

Note that because 'E' is a protected variable in Mathematica, 'E' is denoted as 'e' in the following calculations.

There are some equations for which it is mathematically impossible to find explicit formulae for the solutions. Mathematica uses *Root* objects to represent the solutions in this case. The first argument (#1) of *Root* is an irreducible polynomial expressed as a pure function and the second argument identifies the choice of root.

Although it cannot find explicit formulae, Mathematica can still find the solutions numerically once the values for the numerous variables are chosen.

```
Solve[Numerator[%31] == 0, γ]
```

$$\{\{\gamma \to 0\},$$

$$\{\gamma \to -\sqrt{\text{Root}\left[-30\,e\,\pi\,t^2 + 8\,P\,\sqrt{3-3\,\nu^2} - 17\,Pcl\,\sqrt{3-3\,\nu^2} + 8\,e\,\pi\,t^2\,\#1 + 24\,P\,\sqrt{3-3\,\nu^2}\,\#1 - 51\,Pcl\,\sqrt{3-3\,\nu^2}\,\#1 + 12\,e\,\pi\,t^2\,\#1^2 + 24\,P\,\sqrt{3-3\,\nu^2}\,\#1^2 - 2\,Pcl\,\sqrt{3-3\,\nu^2}\,\#1^2 + 8\,e\,\pi\,t^2\,\#1^3 + 8\,P\,\sqrt{3-3\,\nu^2}\,\#1^3 + 2\,Pcl\,\sqrt{3-3\,\nu^2}\,\#1^3 + 2\,e\,\pi\,t^2\,\#1^4 + 3\,Pcl\,\sqrt{3-3\,\nu^2}\,\#1^4 + Pcl\,\sqrt{3-3\,\nu^2}\,\#1^5 \&,\ 1\right]\},$$

$$\{\gamma \to \sqrt{\text{Root}\left[-30\,e\,\pi\,t^2 + 8\,P\,\sqrt{3-3\,\nu^2} - 17\,Pcl\,\sqrt{3-3\,\nu^2} + 8\,e\,\pi\,t^2\,\#1 + 24\,P\,\sqrt{3-3\,\nu^2}\,\#1 - 51\,Pcl\,\sqrt{3-3\,\nu^2}\,\#1 + 12\,e\,\pi\,t^2\,\#1^2 + 24\,P\,\sqrt{3-3\,\nu^2}\,\#1^2 - 2\,Pcl\,\sqrt{3-3\,\nu^2}\,\#1^2 + 8\,e\,\pi\,t^2\,\#1^3 + 8\,P\,\sqrt{3-3\,\nu^2}\,\#1^3 + 2\,Pcl\,\sqrt{3-3\,\nu^2}\,\#1^3 + 2\,e\,\pi\,t^2\,\#1^4 + 3\,Pcl\,\sqrt{3-3\,\nu^2}\,\#1^4 + Pcl\,\sqrt{3-3\,\nu^2}\,\#1^5 \&,\ 1\right]\},$$

$$\{\gamma \to -\sqrt{\text{Root}\left[-30\,e\,\pi\,t^2 + 8\,P\,\sqrt{3-3\,\nu^2} - 17\,Pcl\,\sqrt{3-3\,\nu^2} + 8\,e\,\pi\,t^2\,\#1 + 24\,P\,\sqrt{3-3\,\nu^2}\,\#1 - 51\,Pcl\,\sqrt{3-3\,\nu^2}\,\#1 + 12\,e\,\pi\,t^2\,\#1^2 + 24\,P\,\sqrt{3-3\,\nu^2}\,\#1^2 - 2\,Pcl\,\sqrt{3-3\,\nu^2}\,\#1^2 + 8\,e\,\pi\,t^2\,\#1^3 + 8\,P\,\sqrt{3-3\,\nu^2}\,\#1^3 + 2\,Pcl\,\sqrt{3-3\,\nu^2}\,\#1^3 + 2\,e\,\pi\,t^2\,\#1^4 + 3\,Pcl\,\sqrt{3-3\,\nu^2}\,\#1^4 + Pcl\,\sqrt{3-3\,\nu^2}\,\#1^5 \&,\ 2\right]\},$$

$$\{\gamma \to \sqrt{\text{Root}\left[-30\,e\,\pi\,t^2 + 8\,P\,\sqrt{3-3\,\nu^2} - 17\,Pcl\,\sqrt{3-3\,\nu^2} + 8\,e\,\pi\,t^2\,\#1 + 24\,P\,\sqrt{3-3\,\nu^2}\,\#1 - 51\,Pcl\,\sqrt{3-3\,\nu^2}\,\#1 + 12\,e\,\pi\,t^2\,\#1^2 + 24\,P\,\sqrt{3-3\,\nu^2}\,\#1^2 - 2\,Pcl\,\sqrt{3-3\,\nu^2}\,\#1^2 + 8\,e\,\pi\,t^2\,\#1^3 + 8\,P\,\sqrt{3-3\,\nu^2}\,\#1^3 + 2\,Pcl\,\sqrt{3-3\,\nu^2}\,\#1^3 + 2\,e\,\pi\,t^2\,\#1^4 + 3\,Pcl\,\sqrt{3-3\,\nu^2}\,\#1^4 + Pcl\,\sqrt{3-3\,\nu^2}\,\#1^5 \&,\ 2\right]\},$$

$$\{\gamma \to -\sqrt{\text{Root}\left[-30\,e\,\pi\,t^2 + 8\,P\,\sqrt{3-3\,\nu^2} - 17\,Pcl\,\sqrt{3-3\,\nu^2} + 8\,e\,\pi\,t^2\,\#1 + 24\,P\,\sqrt{3-3\,\nu^2}\,\#1 - 51\,Pcl\,\sqrt{3-3\,\nu^2}\,\#1 + 12\,e\,\pi\,t^2\,\#1^2 + 24\,P\,\sqrt{3-3\,\nu^2}\,\#1^2 - 2\,Pcl\,\sqrt{3-3\,\nu^2}\,\#1^2 + 8\,e\,\pi\,t^2\,\#1^3 + 8\,P\,\sqrt{3-3\,\nu^2}\,\#1^3 + 2\,Pcl\,\sqrt{3-3\,\nu^2}\,\#1^3 + 2\,e\,\pi\,t^2\,\#1^4 + 3\,Pcl\,\sqrt{3-3\,\nu^2}\,\#1^4 + Pcl\,\sqrt{3-3\,\nu^2}\,\#1^5 \&,\ 3\right]\},$$

$$\{\gamma \to \sqrt{\text{Root}\left[-30\,e\,\pi\,t^2 + 8\,P\,\sqrt{3-3\,\nu^2} - 17\,Pcl\,\sqrt{3-3\,\nu^2} + 8\,e\,\pi\,t^2\,\#1 + 24\,P\,\sqrt{3-3\,\nu^2}\,\#1 - 51\,Pcl\,\sqrt{3-3\,\nu^2}\,\#1 + 12\,e\,\pi\,t^2\,\#1^2 + 24\,P\,\sqrt{3-3\,\nu^2}\,\#1^2 - 2\,Pcl\,\sqrt{3-3\,\nu^2}\,\#1^2 + 8\,e\,\pi\,t^2\,\#1^3 + 8\,P\,\sqrt{3-3\,\nu^2}\,\#1^3 + 2\,Pcl\,\sqrt{3-3\,\nu^2}\,\#1^3 + 2\,e\,\pi\,t^2\,\#1^4 + 3\,Pcl\,\sqrt{3-3\,\nu^2}\,\#1^4 + Pcl\,\sqrt{3-3\,\nu^2}\,\#1^5 \&,\ 3\right]\},$$

$$\{\gamma \to -\sqrt{\text{Root}\left[-30\,e\,\pi\,t^2 + 8\,P\,\sqrt{3-3\,\nu^2} - 17\,Pcl\,\sqrt{3-3\,\nu^2} + 8\,e\,\pi\,t^2\,\#1 + 24\,P\,\sqrt{3-3\,\nu^2}\,\#1 - 51\,Pcl\,\sqrt{3-3\,\nu^2}\,\#1 + 12\,e\,\pi\,t^2\,\#1^2 + 24\,P\,\sqrt{3-3\,\nu^2}\,\#1^2 - 2\,Pcl\,\sqrt{3-3\,\nu^2}\,\#1^2 + 8\,e\,\pi\,t^2\,\#1^3 + 8\,P\,\sqrt{3-3\,\nu^2}\,\#1^3 + 2\,Pcl\,\sqrt{3-3\,\nu^2}\,\#1^3 + 2\,e\,\pi\,t^2\,\#1^4 + 3\,Pcl\,\sqrt{3-3\,\nu^2}\,\#1^4 + Pcl\,\sqrt{3-3\,\nu^2}\,\#1^5 \&,\ 4\right]\},$$

$$\{\gamma \to \sqrt{\text{Root}\left[-30\,e\,\pi\,t^2 + 8\,P\,\sqrt{3-3\,\nu^2} - 17\,Pcl\,\sqrt{3-3\,\nu^2} + 8\,e\,\pi\,t^2\,\#1 + 24\,P\,\sqrt{3-3\,\nu^2}\,\#1 - 51\,Pcl\,\sqrt{3-3\,\nu^2}\,\#1 + 12\,e\,\pi\,t^2\,\#1^2 + 24\,P\,\sqrt{3-3\,\nu^2}\,\#1^2 - 2\,Pcl\,\sqrt{3-3\,\nu^2}\,\#1^2 + 8\,e\,\pi\,t^2\,\#1^3 + 8\,P\,\sqrt{3-3\,\nu^2}\,\#1^3 + 2\,Pcl\,\sqrt{3-3\,\nu^2}\,\#1^3 + 2\,e\,\pi\,t^2\,\#1^4 + 3\,Pcl\,\sqrt{3-3\,\nu^2}\,\#1^4 + Pcl\,\sqrt{3-3\,\nu^2}\,\#1^5 \&,\ 4\right]\},$$

$$\{\gamma \to -\sqrt{\text{Root}\left[-30\,e\,\pi\,t^2 + 8\,P\,\sqrt{3-3\,\nu^2} - 17\,Pcl\,\sqrt{3-3\,\nu^2} + 8\,e\,\pi\,t^2\,\#1 + 24\,P\,\sqrt{3-3\,\nu^2}\,\#1 - 51\,Pcl\,\sqrt{3-3\,\nu^2}\,\#1 + 12\,e\,\pi\,t^2\,\#1^2 + 24\,P\,\sqrt{3-3\,\nu^2}\,\#1^2 - 2\,Pcl\,\sqrt{3-3\,\nu^2}\,\#1^2 + 8\,e\,\pi\,t^2\,\#1^3 + 8\,P\,\sqrt{3-3\,\nu^2}\,\#1^3 + 2\,Pcl\,\sqrt{3-3\,\nu^2}\,\#1^3 + 2\,e\,\pi\,t^2\,\#1^4 + 3\,Pcl\,\sqrt{3-3\,\nu^2}\,\#1^4 + Pcl\,\sqrt{3-3\,\nu^2}\,\#1^5 \&,\ 5\right]\},$$

$$\{\gamma \to \sqrt{\text{Root}\left[-30\,e\,\pi\,t^2 + 8\,P\,\sqrt{3-3\,\nu^2} - 17\,Pcl\,\sqrt{3-3\,\nu^2} + 8\,e\,\pi\,t^2\,\#1 + 24\,P\,\sqrt{3-3\,\nu^2}\,\#1 - 51\,Pcl\,\sqrt{3-3\,\nu^2}\,\#1 + 12\,e\,\pi\,t^2\,\#1^2 + 24\,P\,\sqrt{3-3\,\nu^2}\,\#1^2 - 2\,Pcl\,\sqrt{3-3\,\nu^2}\,\#1^2 + 8\,e\,\pi\,t^2\,\#1^3 + 8\,P\,\sqrt{3-3\,\nu^2}\,\#1^3 + 2\,Pcl\,\sqrt{3-3\,\nu^2}\,\#1^3 + 2\,e\,\pi\,t^2\,\#1^4 + 3\,Pcl\,\sqrt{3-3\,\nu^2}\,\#1^4 + Pcl\,\sqrt{3-3\,\nu^2}\,\#1^5 \&,\ 5\right]\}\}$$

Appendix E : Values of γ for imperfect cylinders.

This appendix shows the roots of γ for the purpose of finding the buckling equation of an imperfect cylinder subjected to both axial loading and external hydrostatic pressure.

Note that because 'E' is a protected variable in Mathematica, 'E' is denoted as 'e' in the following calculations.

There are some equations for which it is mathematically impossible to find explicit formulae for the solutions. Mathematica uses *Root* objects to represent the solutions in this case. The first argument (#1) of *Root* is an irreducible polynomial expressed as a pure function and the second argument identifies the choice of root.

Although it cannot find explicit formulae, Mathematica can still find the solutions numerically once the values for the numerous variables are chosen.

```
Solve[%, γ]
```

$$\{\{\gamma \to -\sqrt{\text{Root}\left[-5832\,\text{Pbar}^3 + 24057\,\text{Pbar}^2\,\text{Pcl} - 30618\,\text{Pbar}\,\text{Pcl}^2 + 12393\,\text{Pcl}^3 - 1944\,\text{Pbar}^3\,\#1 + 8019\,\text{Pbar}^2\,\text{Pcl}\,\#1 - 10206\,\text{Pbar}\,\text{Pcl}^2\,\#1 + 4131\,\text{Pcl}^3\,\#1 + 17280\,\text{Pbar}^3\,\#1^2 - 107001\,\text{Pbar}^2\,\text{Pcl}\,\#1^2 + 162162\,\text{Pbar}\,\text{Pcl}^2\,\#1^2 - 72441\,\text{Pcl}^3\,\#1^2 - 35424\,A^2\,\text{Pcl}^3\,\#1^2 + 35424\,A^2\,\text{Pcl}^3\,\nu^2\,\#1^2 - 46656\,A\,\text{Pbar}\,\text{Pcl}^2\sqrt{3-3\nu^2}\,\#1^2 + 46656\,A\,\text{Pcl}^3\sqrt{3-3\nu^2}\,\#1^2 + 5824\,\text{Pbar}^3\,\#1^3 + 57381\,\text{Pbar}^2\,\text{Pcl}\,\#1^3 - 132234\,\text{Pbar}\,\text{Pcl}^2\,\#1^3 + 69029\,\text{Pcl}^3\,\#1^3 + 128352\,A^2\,\text{Pcl}^3\,\#1^3 - 128352\,A^2\,\text{Pcl}^3\,\nu^2\,\#1^3 - 155520\,A\,\text{Pbar}\,\text{Pcl}^2\sqrt{3-3\nu^2}\,\#1^3 + 155520\,A\,\text{Pcl}^3\sqrt{3-3\nu^2}\,\#1^3 - 16848\,\text{Pbar}^3\,\#1^4 + 31482\,\text{Pbar}^2\,\text{Pcl}\,\#1^4 - 12420\,\text{Pbar}\,\text{Pcl}^2\,\#1^4 - 2214\,\text{Pcl}^3\,\#1^4 - 163296\,A^2\,\text{Pcl}^3\,\#1^4 + 163296\,A^2\,\text{Pcl}^3\,\nu^2\,\#1^4 - 188352\,A\,\text{Pbar}\,\text{Pcl}^2\sqrt{3-3\nu^2}\,\#1^4 + 188352\,A\,\text{Pcl}^3\sqrt{3-3\nu^2}\,\#1^4 - 5808\,\text{Pbar}^3\,\#1^5 + 4766\,\text{Pbar}^2\,\text{Pcl}\,\#1^5 + 7892\,\text{Pbar}\,\text{Pcl}^2\,\#1^5 - 6850\,\text{Pcl}^3\,\#1^5 + 74976\,A^2\,\text{Pcl}^3\,\#1^5 - 74976\,A^2\,\text{Pcl}^3\,\nu^2\,\#1^5 - 98560\,A\,\text{Pbar}\,\text{Pcl}^2\sqrt{3-3\nu^2}\,\#1^5 + 98560\,A\,\text{Pcl}^3\sqrt{3-3\nu^2}\,\#1^5 + 5184\,\text{Pbar}^3\,\#1^6 - 14290\,\text{Pbar}^2\,\text{Pcl}\,\#1^6 + 13028\,\text{Pbar}\,\text{Pcl}^2\,\#1^6 - 3922\,\text{Pcl}^3\,\#1^6 + 2784\,A^2\,\text{Pcl}^3\,\#1^6 - 2784\,A^2\,\text{Pcl}^3\,\nu^2\,\#1^6 - 20928\,A\,\text{Pbar}\,\text{Pcl}^2\sqrt{3-3\nu^2}\,\#1^6 + 20928\,A\,\text{Pcl}^3\sqrt{3-3\nu^2}\,\#1^6 + 1920\,\text{Pbar}^3\,\#1^7 - 4854\,\text{Pbar}^2\,\text{Pcl}\,\#1^7 + 3948\,\text{Pbar}\,\text{Pcl}^2\,\#1^7 - 1014\,\text{Pcl}^3\,\#1^7 - 6624\,A^2\,\text{Pcl}^3\,\#1^7 + 6624\,A^2\,\text{Pcl}^3\,\nu^2\,\#1^7 - 1920\,A\,\text{Pbar}\,\text{Pcl}^2\sqrt{3-3\nu^2}\,\#1^7 + 1920\,A\,\text{Pcl}^3\sqrt{3-3\nu^2}\,\#1^7 + 216\,\text{Pbar}^3\,\#1^8 + 189\,\text{Pbar}^2\,\text{Pcl}\,\#1^8 - 1026\,\text{Pbar}\,\text{Pcl}^2\,\#1^8 + 621\,\text{Pcl}^3\,\#1^8 - 672\,A^2\,\text{Pcl}^3\,\#1^8 + 672\,A^2\,\text{Pcl}^3\,\nu^2\,\#1^8 - 64\,A\,\text{Pbar}\,\text{Pcl}^2\sqrt{3-3\nu^2}\,\#1^8 + 64\,A\,\text{Pcl}^3\sqrt{3-3\nu^2}\,\#1^8 + 8\,\text{Pbar}^3\,\#1^9 + 223\,\text{Pbar}^2\,\text{Pcl}\,\#1^9 - 470\,\text{Pbar}\,\text{Pcl}^2\,\#1^9 + 239\,\text{Pcl}^3\,\#1^9 - 96\,A^2\,\text{Pcl}^3\,\#1^9 + 96\,A^2\,\text{Pcl}^3\,\nu^2\,\#1^9 + 27\,\text{Pbar}^2\,\text{Pcl}\,\#1^{10} - 54\,\text{Pbar}\,\text{Pcl}^2\,\#1^{10} + 27\,\text{Pcl}^3\,\#1^{10} + \text{Pbar}^2\,\text{Pcl}\,\#1^{11} - 2\,\text{Pbar}\,\text{Pcl}^2\,\#1^{11} + \text{Pcl}^3\,\#1^{11}\,\&,\,1\right]\},$$

$$\{\gamma \to \sqrt{\text{Root}\left[-5832\,\text{Pbar}^3 + 24057\,\text{Pbar}^2\,\text{Pcl} - 30618\,\text{Pbar}\,\text{Pcl}^2 + 12393\,\text{Pcl}^3 - 1944\,\text{Pbar}^3\,\#1 + 8019\,\text{Pbar}^2\,\text{Pcl}\,\#1 - 10206\,\text{Pbar}\,\text{Pcl}^2\,\#1 + 4131\,\text{Pcl}^3\,\#1 + 17280\,\text{Pbar}^3\,\#1^2 - 107001\,\text{Pbar}^2\,\text{Pcl}\,\#1^2 + 162162\,\text{Pbar}\,\text{Pcl}^2\,\#1^2 - 72441\,\text{Pcl}^3\,\#1^2 - 35424\,A^2\,\text{Pcl}^3\,\#1^2 + 35424\,A^2\,\text{Pcl}^3\,\nu^2\,\#1^2 - 46656\,A\,\text{Pbar}\,\text{Pcl}^2\sqrt{3-3\nu^2}\,\#1^2 + 46656\,A\,\text{Pcl}^3\sqrt{3-3\nu^2}\,\#1^2 + 5824\,\text{Pbar}^3\,\#1^3 + 57381\,\text{Pbar}^2\,\text{Pcl}\,\#1^3 - 132234\,\text{Pbar}\,\text{Pcl}^2\,\#1^3 + 69029\,\text{Pcl}^3\,\#1^3 + 128352\,A^2\,\text{Pcl}^3\,\#1^3 - 128352\,A^2\,\text{Pcl}^3\,\nu^2\,\#1^3 - 155520\,A\,\text{Pbar}\,\text{Pcl}^2\sqrt{3-3\nu^2}\,\#1^3 + 155520\,A\,\text{Pcl}^3\sqrt{3-3\nu^2}\,\#1^3 - 16848\,\text{Pbar}^3\,\#1^4 + 31482\,\text{Pbar}^2\,\text{Pcl}\,\#1^4 - 12420\,\text{Pbar}\,\text{Pcl}^2\,\#1^4 - 2214\,\text{Pcl}^3\,\#1^4 - 163296\,A^2\,\text{Pcl}^3\,\#1^4 + 163296\,A^2\,\text{Pcl}^3\,\nu^2\,\#1^4 - 188352\,A\,\text{Pbar}\,\text{Pcl}^2\sqrt{3-3\nu^2}\,\#1^4 + 188352\,A\,\text{Pcl}^3\sqrt{3-3\nu^2}\,\#1^4 - 5808\,\text{Pbar}^3\,\#1^5 + 4766\,\text{Pbar}^2\,\text{Pcl}\,\#1^5 + 7892\,\text{Pbar}\,\text{Pcl}^2\,\#1^5 - 6850\,\text{Pcl}^3\,\#1^5 + 74976\,A^2\,\text{Pcl}^3\,\#1^5 - 74976\,A^2\,\text{Pcl}^3\,\nu^2\,\#1^5 - 98560\,A\,\text{Pbar}\,\text{Pcl}^2\sqrt{3-3\nu^2}\,\#1^5 + 98560\,A\,\text{Pcl}^3\sqrt{3-3\nu^2}\,\#1^5 + 5184\,\text{Pbar}^3\,\#1^6 - 14290\,\text{Pbar}^2\,\text{Pcl}\,\#1^6 + 13028\,\text{Pbar}\,\text{Pcl}^2\,\#1^6 - 3922\,\text{Pcl}^3\,\#1^6 + 2784\,A^2\,\text{Pcl}^3\,\#1^6 - 2784\,A^2\,\text{Pcl}^3\,\nu^2\,\#1^6 - 20928\,A\,\text{Pbar}\,\text{Pcl}^2\sqrt{3-3\nu^2}\,\#1^6 + 20928\,A\,\text{Pcl}^3\sqrt{3-3\nu^2}\,\#1^6 + 1920\,\text{Pbar}^3\,\#1^7 - 4854\,\text{Pbar}^2\,\text{Pcl}\,\#1^7 + 3948\,\text{Pbar}\,\text{Pcl}^2\,\#1^7 - 1014\,\text{Pcl}^3\,\#1^7 - 6624\,A^2\,\text{Pcl}^3\,\#1^7 + 6624\,A^2\,\text{Pcl}^3\,\nu^2\,\#1^7 - 1920\,A\,\text{Pbar}\,\text{Pcl}^2\sqrt{3-3\nu^2}\,\#1^7 + 1920\,A\,\text{Pcl}^3\sqrt{3-3\nu^2}\,\#1^7 + 216\,\text{Pbar}^3\,\#1^8 + 189\,\text{Pbar}^2\,\text{Pcl}\,\#1^8 - 1026\,\text{Pbar}\,\text{Pcl}^2\,\#1^8 + 621\,\text{Pcl}^3\,\#1^8 - 672\,A^2\,\text{Pcl}^3\,\#1^8 + 672\,A^2\,\text{Pcl}^3\,\nu^2\,\#1^8 - 64\,A\,\text{Pbar}\,\text{Pcl}^2\sqrt{3-3\nu^2}\,\#1^8 + 64\,A\,\text{Pcl}^3\sqrt{3-3\nu^2}\,\#1^8 + 8\,\text{Pbar}^3\,\#1^9 + 223\,\text{Pbar}^2\,\text{Pcl}\,\#1^9 - 470\,\text{Pbar}\,\text{Pcl}^2\,\#1^9 + 239\,\text{Pcl}^3\,\#1^9 - 96\,A^2\,\text{Pcl}^3\,\#1^9 + 96\,A^2\,\text{Pcl}^3\,\nu^2\,\#1^9 + 27\,\text{Pbar}^2\,\text{Pcl}\,\#1^{10} - 54\,\text{Pbar}\,\text{Pcl}^2\,\#1^{10} + 27\,\text{Pcl}^3\,\#1^{10} + \text{Pbar}^2\,\text{Pcl}\,\#1^{11} - 2\,\text{Pbar}\,\text{Pcl}^2\,\#1^{11} + \text{Pcl}^3\,\#1^{11}\,\&,\,1\right]\},$$

$$\{\gamma \to -\sqrt{\text{Root}\left[-5832\,\text{Pbar}^3 + 24057\,\text{Pbar}^2\,\text{Pcl} - 30618\,\text{Pbar}\,\text{Pcl}^2 + 12393\,\text{Pcl}^3 - 1944\,\text{Pbar}^3\,\#1 + 8019\,\text{Pbar}^2\,\text{Pcl}\,\#1 - 10206\,\text{Pbar}\,\text{Pcl}^2\,\#1 + 4131\,\text{Pcl}^3\,\#1 + 17280\,\text{Pbar}^3\,\#1^2 - 107001\,\text{Pbar}^2\,\text{Pcl}\,\#1^2 + 162162\,\text{Pbar}\,\text{Pcl}^2\,\#1^2 - 72441\,\text{Pcl}^3\,\#1^2 - 35424\,A^2\,\text{Pcl}^3\,\#1^2 + 35424\,A^2\,\text{Pcl}^3\,\nu^2\,\#1^2 - 46656\,A\,\text{Pbar}\,\text{Pcl}^2\sqrt{3-3\nu^2}\,\#1^2 + 46656\,A\,\text{Pcl}^3\sqrt{3-3\nu^2}\,\#1^2 + 5824\,\text{Pbar}^3\,\#1^3 + 57381\,\text{Pbar}^2\,\text{Pcl}\,\#1^3 - 132234\,\text{Pbar}\,\text{Pcl}^2\,\#1^3 + 69029\,\text{Pcl}^3\,\#1^3 + 128352\,A^2\,\text{Pcl}^3\,\#1^3 - 128352\,A^2\,\text{Pcl}^3\,\nu^2\,\#1^3 - 155520\,A\,\text{Pbar}\,\text{Pcl}^2\sqrt{3-3\nu^2}\,\#1^3 + 155520\,A\,\text{Pcl}^3\sqrt{3-3\nu^2}\,\#1^3 - 16848\,\text{Pbar}^3\,\#1^4 + 31482\,\text{Pbar}^2\,\text{Pcl}\,\#1^4 - 12420\,\text{Pbar}\,\text{Pcl}^2\,\#1^4 - 2214\,\text{Pcl}^3\,\#1^4 - 163296\,A^2\,\text{Pcl}^3\,\#1^4 + 163296\,A^2\,\text{Pcl}^3\,\nu^2\,\#1^4 -$$

```
188352 A Pbar Pcl^2 Sqrt[3 - 3 v^2] #1^4 + 188352 A Pcl^3 Sqrt[3 - 3 v^2] #1^4 - 5808 Pbar^3 #1^5 +
4766 Pbar^2 Pcl #1^5 + 7892 Pbar Pcl^2 #1^5 - 6850 Pcl^3 #1^5 + 74976 A^2 Pcl^3 #1^5 -
74976 A^2 Pcl^3 v^2 #1^5 - 98560 A Pbar Pcl^2 Sqrt[3 - 3 v^2] #1^5 + 98560 A Pcl^3 Sqrt[3 - 3 v^2] #1^5 +
5184 Pbar^3 #1^6 - 14290 Pbar^2 Pcl #1^6 + 13028 Pbar Pcl^2 #1^6 - 3922 Pcl^3 #1^6 +
2784 A^2 Pcl^3 #1^6 - 2784 A^2 Pcl^3 v^2 #1^6 - 20928 A Pbar Pcl^2 Sqrt[3 - 3 v^2] #1^6 +
20928 A Pcl^3 Sqrt[3 - 3 v^2] #1^6 + 1920 Pbar^3 #1^7 - 4854 Pbar^2 Pcl #1^7 + 3948 Pbar Pcl^2 #1^7 -
1014 Pcl^3 #1^7 - 6624 A^2 Pcl^3 #1^7 + 6624 A^2 Pcl^3 v^2 #1^7 - 1920 A Pbar Pcl^2 Sqrt[3 - 3 v^2] #1^7 +
1920 A Pcl^3 Sqrt[3 - 3 v^2] #1^7 + 216 Pbar^3 #1^8 + 189 Pbar^2 Pcl #1^8 - 1026 Pbar Pcl^2 #1^8 +
621 Pcl^3 #1^8 - 672 A^2 Pcl^3 #1^8 + 672 A^2 Pcl^3 v^2 #1^8 - 64 A Pbar Pcl^2 Sqrt[3 - 3 v^2] #1^8 +
64 A Pcl^3 Sqrt[3 - 3 v^2] #1^8 + 8 Pbar^3 #1^9 + 223 Pbar^2 Pcl #1^9 - 470 Pbar Pcl^2 #1^9 +
239 Pcl^3 #1^9 - 96 A^2 Pcl^3 #1^9 + 96 A^2 Pcl^3 v^2 #1^9 + 27 Pbar^2 Pcl #1^10 -
54 Pbar Pcl^2 #1^10 + 27 Pcl^3 #1^10 + Pbar^2 Pcl #1^11 - 2 Pbar Pcl^2 #1^11 + Pcl^3 #1^11 &, 2]},
{γ → Sqrt[Root[-5832 Pbar^3 + 24057 Pbar^2 Pcl - 30618 Pbar Pcl^2 + 12393 Pcl^3 -
1944 Pbar^3 #1 + 8019 Pbar^2 Pcl #1 - 10206 Pbar Pcl^2 #1 + 4131 Pcl^3 #1 + 17280 Pbar^3 #1^2 -
107001 Pbar^2 Pcl #1^2 + 162162 Pbar Pcl^2 #1^2 - 72441 Pcl^3 #1^2 - 35424 A^2 Pcl^3 #1^2 +
35424 A^2 Pcl^3 v^2 #1^2 - 46656 A Pbar Pcl^2 Sqrt[3 - 3 v^2] #1^2 + 46656 A Pcl^3 Sqrt[3 - 3 v^2] #1^2 +
5824 Pbar^3 #1^3 + 57381 Pbar^2 Pcl #1^3 - 132234 Pbar Pcl^2 #1^3 + 69029 Pcl^3 #1^3 +
128352 A^2 Pcl^3 #1^3 - 128352 A^2 Pcl^3 v^2 #1^3 - 155520 A Pbar Pcl^2 Sqrt[3 - 3 v^2] #1^3 +
155520 A Pcl^3 Sqrt[3 - 3 v^2] #1^3 - 16848 Pbar^3 #1^4 + 31482 Pbar^2 Pcl #1^4 -
12420 Pbar Pcl^2 #1^4 - 2214 Pcl^3 #1^4 - 163296 A^2 Pcl^3 #1^4 + 163296 A^2 Pcl^3 v^2 #1^4 -
188352 A Pbar Pcl^2 Sqrt[3 - 3 v^2] #1^4 + 188352 A Pcl^3 Sqrt[3 - 3 v^2] #1^4 - 5808 Pbar^3 #1^5 +
4766 Pbar^2 Pcl #1^5 + 7892 Pbar Pcl^2 #1^5 - 6850 Pcl^3 #1^5 + 74976 A^2 Pcl^3 #1^5 -
74976 A^2 Pcl^3 v^2 #1^5 - 98560 A Pbar Pcl^2 Sqrt[3 - 3 v^2] #1^5 + 98560 A Pcl^3 Sqrt[3 - 3 v^2] #1^5 +
5184 Pbar^3 #1^6 - 14290 Pbar^2 Pcl #1^6 + 13028 Pbar Pcl^2 #1^6 - 3922 Pcl^3 #1^6 +
2784 A^2 Pcl^3 #1^6 - 2784 A^2 Pcl^3 v^2 #1^6 - 20928 A Pbar Pcl^2 Sqrt[3 - 3 v^2] #1^6 +
20928 A Pcl^3 Sqrt[3 - 3 v^2] #1^6 + 1920 Pbar^3 #1^7 - 4854 Pbar^2 Pcl #1^7 + 3948 Pbar Pcl^2 #1^7 -
1014 Pcl^3 #1^7 - 6624 A^2 Pcl^3 #1^7 + 6624 A^2 Pcl^3 v^2 #1^7 - 1920 A Pbar Pcl^2 Sqrt[3 - 3 v^2] #1^7 +
1920 A Pcl^3 Sqrt[3 - 3 v^2] #1^7 + 216 Pbar^3 #1^8 + 189 Pbar^2 Pcl #1^8 - 1026 Pbar Pcl^2 #1^8 +
621 Pcl^3 #1^8 - 672 A^2 Pcl^3 #1^8 + 672 A^2 Pcl^3 v^2 #1^8 - 64 A Pbar Pcl^2 Sqrt[3 - 3 v^2] #1^8 +
64 A Pcl^3 Sqrt[3 - 3 v^2] #1^8 + 8 Pbar^3 #1^9 + 223 Pbar^2 Pcl #1^9 - 470 Pbar Pcl^2 #1^9 +
239 Pcl^3 #1^9 - 96 A^2 Pcl^3 #1^9 + 96 A^2 Pcl^3 v^2 #1^9 + 27 Pbar^2 Pcl #1^10 -
54 Pbar Pcl^2 #1^10 + 27 Pcl^3 #1^10 + Pbar^2 Pcl #1^11 - 2 Pbar Pcl^2 #1^11 + Pcl^3 #1^11 &, 2]},
{γ → -Sqrt[Root[-5832 Pbar^3 + 24057 Pbar^2 Pcl - 30618 Pbar Pcl^2 + 12393 Pcl^3 - 1944 Pbar^3 #1 +
8019 Pbar^2 Pcl #1 - 10206 Pbar Pcl^2 #1 + 4131 Pcl^3 #1 + 17280 Pbar^3 #1^2 -
107001 Pbar^2 Pcl #1^2 + 162162 Pbar Pcl^2 #1^2 - 72441 Pcl^3 #1^2 - 35424 A^2 Pcl^3 #1^2 +
35424 A^2 Pcl^3 v^2 #1^2 - 46656 A Pbar Pcl^2 Sqrt[3 - 3 v^2] #1^2 + 46656 A Pcl^3 Sqrt[3 - 3 v^2] #1^2 +
5824 Pbar^3 #1^3 + 57381 Pbar^2 Pcl #1^3 - 132234 Pbar Pcl^2 #1^3 + 69029 Pcl^3 #1^3 +
128352 A^2 Pcl^3 #1^3 - 128352 A^2 Pcl^3 v^2 #1^3 - 155520 A Pbar Pcl^2 Sqrt[3 - 3 v^2] #1^3 +
155520 A Pcl^3 Sqrt[3 - 3 v^2] #1^3 - 16848 Pbar^3 #1^4 + 31482 Pbar^2 Pcl #1^4 -
12420 Pbar Pcl^2 #1^4 - 2214 Pcl^3 #1^4 - 163296 A^2 Pcl^3 #1^4 + 163296 A^2 Pcl^3 v^2 #1^4 -
188352 A Pbar Pcl^2 Sqrt[3 - 3 v^2] #1^4 + 188352 A Pcl^3 Sqrt[3 - 3 v^2] #1^4 - 5808 Pbar^3 #1^5 +
4766 Pbar^2 Pcl #1^5 + 7892 Pbar Pcl^2 #1^5 - 6850 Pcl^3 #1^5 + 74976 A^2 Pcl^3 #1^5 -
74976 A^2 Pcl^3 v^2 #1^5 - 98560 A Pbar Pcl^2 Sqrt[3 - 3 v^2] #1^5 + 98560 A Pcl^3 Sqrt[3 - 3 v^2] #1^5 +
5184 Pbar^3 #1^6 - 14290 Pbar^2 Pcl #1^6 + 13028 Pbar Pcl^2 #1^6 - 3922 Pcl^3 #1^6 +
2784 A^2 Pcl^3 #1^6 - 2784 A^2 Pcl^3 v^2 #1^6 - 20928 A Pbar Pcl^2 Sqrt[3 - 3 v^2] #1^6 +
20928 A Pcl^3 Sqrt[3 - 3 v^2] #1^6 + 1920 Pbar^3 #1^7 - 4854 Pbar^2 Pcl #1^7 + 3948 Pbar Pcl^2 #1^7 -
1014 Pcl^3 #1^7 - 6624 A^2 Pcl^3 #1^7 + 6624 A^2 Pcl^3 v^2 #1^7 - 1920 A Pbar Pcl^2 Sqrt[3 - 3 v^2] #1^7 +
1920 A Pcl^3 Sqrt[3 - 3 v^2] #1^7 + 216 Pbar^3 #1^8 + 189 Pbar^2 Pcl #1^8 - 1026 Pbar Pcl^2 #1^8 +
621 Pcl^3 #1^8 - 672 A^2 Pcl^3 #1^8 + 672 A^2 Pcl^3 v^2 #1^8 - 64 A Pbar Pcl^2 Sqrt[3 - 3 v^2] #1^8 +
64 A Pcl^3 Sqrt[3 - 3 v^2] #1^8 + 8 Pbar^3 #1^9 + 223 Pbar^2 Pcl #1^9 - 470 Pbar Pcl^2 #1^9 +
239 Pcl^3 #1^9 - 96 A^2 Pcl^3 #1^9 + 96 A^2 Pcl^3 v^2 #1^9 + 27 Pbar^2 Pcl #1^10 -
```

```
    54 Pbar Pcl^2 #1^10 + 27 Pcl^3 #1^10 + Pbar^2 Pcl #1^11 - 2 Pbar Pcl^2 #1^11 + Pcl^3 #1^11 &, 3]},
{γ → √Root[-5832 Pbar^3 + 24057 Pbar^2 Pcl - 30618 Pbar Pcl^2 + 12393 Pcl^3 -
    1944 Pbar^3 #1 + 8019 Pbar^2 Pcl #1 - 10206 Pbar Pcl^2 #1 + 4131 Pcl^3 #1 +
    17280 Pbar^3 #1^2 - 107001 Pbar^2 Pcl #1^2 + 162162 Pbar Pcl^2 #1^2 - 72441 Pcl^3 #1^2 -
    35424 A^2 Pcl^3 #1^2 + 35424 A^2 Pcl^3 ν^2 #1^2 - 46656 A Pbar Pcl^2 √(3 - 3 ν^2) #1^2 +
    46656 A Pcl^3 √(3 - 3 ν^2) #1^2 + 5824 Pbar^3 #1^3 + 57381 Pbar^2 Pcl #1^3 -
    132234 Pbar Pcl^2 #1^3 + 69029 Pcl^3 #1^3 + 128352 A^2 Pcl^3 #1^3 - 128352 A^2 Pcl^3 ν^2 #1^3 -
    155520 A Pbar Pcl^2 √(3 - 3 ν^2) #1^3 + 155520 A Pcl^3 √(3 - 3 ν^2) #1^3 -
    16848 Pbar^3 #1^4 + 31482 Pbar^2 Pcl #1^4 - 12420 Pbar Pcl^2 #1^4 - 2214 Pcl^3 #1^4 -
    163296 A^2 Pcl^3 #1^4 + 163296 A^2 Pcl^3 ν^2 #1^4 - 188352 A Pbar Pcl^2 √(3 - 3 ν^2) #1^4 +
    188352 A Pcl^3 √(3 - 3 ν^2) #1^4 - 5808 Pbar^3 #1^5 + 4766 Pbar^2 Pcl #1^5 +
    7892 Pbar Pcl^2 #1^5 - 6850 Pcl^3 #1^5 + 74976 A^2 Pcl^3 #1^5 - 74976 A^2 Pcl^3 ν^2 #1^5 -
    98560 A Pbar Pcl^2 √(3 - 3 ν^2) #1^5 + 98560 A Pcl^3 √(3 - 3 ν^2) #1^5 + 5184 Pbar^3 #1^6 -
    14290 Pbar^2 Pcl #1^6 + 13028 Pbar Pcl^2 #1^6 - 3922 Pcl^3 #1^6 + 2784 A^2 Pcl^3 #1^6 -
    2784 A^2 Pcl^3 ν^2 #1^6 - 20928 A Pbar Pcl^2 √(3 - 3 ν^2) #1^6 + 20928 A Pcl^3 √(3 - 3 ν^2) #1^6 +
    1920 Pbar^3 #1^7 - 4854 Pbar^2 Pcl #1^7 + 3948 Pbar Pcl^2 #1^7 - 1014 Pcl^3 #1^7 -
    6624 A^2 Pcl^3 #1^7 + 6624 A^2 Pcl^3 ν^2 #1^7 - 1920 A Pbar Pcl^2 √(3 - 3 ν^2) #1^7 +
    1920 A Pcl^3 √(3 - 3 ν^2) #1^7 + 216 Pbar^3 #1^8 + 189 Pbar^2 Pcl #1^8 - 1026 Pbar Pcl^2 #1^8 +
    621 Pcl^3 #1^8 - 672 A^2 Pcl^3 #1^8 + 672 A^2 Pcl^3 ν^2 #1^8 - 64 A Pbar Pcl^2 √(3 - 3 ν^2) #1^8 +
    64 A Pcl^3 √(3 - 3 ν^2) #1^8 + 8 Pbar^3 #1^9 + 223 Pbar^2 Pcl #1^9 - 470 Pbar Pcl^2 #1^9 +
    239 Pcl^3 #1^9 - 96 A^2 Pcl^3 #1^9 + 96 A^2 Pcl^3 ν^2 #1^9 + 27 Pbar^2 Pcl #1^10 -
    54 Pbar Pcl^2 #1^10 + 27 Pcl^3 #1^10 + Pbar^2 Pcl #1^11 - 2 Pbar Pcl^2 #1^11 + Pcl^3 #1^11 &, 3]},
{γ → -√Root[-5832 Pbar^3 + 24057 Pbar^2 Pcl - 30618 Pbar Pcl^2 + 12393 Pcl^3 - 1944 Pbar^3 #1 +
    8019 Pbar^2 Pcl #1 - 10206 Pbar Pcl^2 #1 + 4131 Pcl^3 #1 + 17280 Pbar^3 #1^2 -
    107001 Pbar^2 Pcl #1^2 + 162162 Pbar Pcl^2 #1^2 - 72441 Pcl^3 #1^2 - 35424 A^2 Pcl^3 #1^2 +
    35424 A^2 Pcl^3 ν^2 #1^2 - 46656 A Pbar Pcl^2 √(3 - 3 ν^2) #1^2 + 46656 A Pcl^3 √(3 - 3 ν^2) #1^2 +
    5824 Pbar^3 #1^3 + 57381 Pbar^2 Pcl #1^3 - 132234 Pbar Pcl^2 #1^3 + 69029 Pcl^3 #1^3 +
    128352 A^2 Pcl^3 #1^3 - 128352 A^2 Pcl^3 ν^2 #1^3 - 155520 A Pbar Pcl^2 √(3 - 3 ν^2) #1^3 +
    155520 A Pcl^3 √(3 - 3 ν^2) #1^3 - 16848 Pbar^3 #1^4 + 31482 Pbar^2 Pcl #1^4 -
    12420 Pbar Pcl^2 #1^4 - 2214 Pcl^3 #1^4 - 163296 A^2 Pcl^3 #1^4 + 163296 A^2 Pcl^3 ν^2 #1^4 -
    188352 A Pbar Pcl^2 √(3 - 3 ν^2) #1^4 + 188352 A Pcl^3 √(3 - 3 ν^2) #1^4 - 5808 Pbar^3 #1^5 +
    4766 Pbar^2 Pcl #1^5 + 7892 Pbar Pcl^2 #1^5 - 6850 Pcl^3 #1^5 + 74976 A^2 Pcl^3 #1^5 -
    74976 A^2 Pcl^3 ν^2 #1^5 - 98560 A Pbar Pcl^2 √(3 - 3 ν^2) #1^5 + 98560 A Pcl^3 √(3 - 3 ν^2) #1^5 +
    5184 Pbar^3 #1^6 - 14290 Pbar^2 Pcl #1^6 + 13028 Pbar Pcl^2 #1^6 - 3922 Pcl^3 #1^6 +
    2784 A^2 Pcl^3 #1^6 - 2784 A^2 Pcl^3 ν^2 #1^6 - 20928 A Pbar Pcl^2 √(3 - 3 ν^2) #1^6 +
    20928 A Pcl^3 √(3 - 3 ν^2) #1^6 + 1920 Pbar^3 #1^7 - 4854 Pbar^2 Pcl #1^7 + 3948 Pbar Pcl^2 #1^7 -
    1014 Pcl^3 #1^7 - 6624 A^2 Pcl^3 #1^7 + 6624 A^2 Pcl^3 ν^2 #1^7 - 1920 A Pbar Pcl^2 √(3 - 3 ν^2) #1^7 +
    1920 A Pcl^3 √(3 - 3 ν^2) #1^7 + 216 Pbar^3 #1^8 + 189 Pbar^2 Pcl #1^8 - 1026 Pbar Pcl^2 #1^8 +
    621 Pcl^3 #1^8 - 672 A^2 Pcl^3 #1^8 + 672 A^2 Pcl^3 ν^2 #1^8 - 64 A Pbar Pcl^2 √(3 - 3 ν^2) #1^8 +
    64 A Pcl^3 √(3 - 3 ν^2) #1^8 + 8 Pbar^3 #1^9 + 223 Pbar^2 Pcl #1^9 - 470 Pbar Pcl^2 #1^9 +
    239 Pcl^3 #1^9 - 96 A^2 Pcl^3 #1^9 + 96 A^2 Pcl^3 ν^2 #1^9 + 27 Pbar^2 Pcl #1^10 -
    54 Pbar Pcl^2 #1^10 + 27 Pcl^3 #1^10 + Pbar^2 Pcl #1^11 - 2 Pbar Pcl^2 #1^11 + Pcl^3 #1^11 &, 4]},
{γ → √Root[-5832 Pbar^3 + 24057 Pbar^2 Pcl - 30618 Pbar Pcl^2 + 12393 Pcl^3 -
    1944 Pbar^3 #1 + 8019 Pbar^2 Pcl #1 - 10206 Pbar Pcl^2 #1 + 4131 Pcl^3 #1 +
    17280 Pbar^3 #1^2 - 107001 Pbar^2 Pcl #1^2 + 162162 Pbar Pcl^2 #1^2 - 72441 Pcl^3 #1^2 -
    35424 A^2 Pcl^3 #1^2 + 35424 A^2 Pcl^3 ν^2 #1^2 - 46656 A Pbar Pcl^2 √(3 - 3 ν^2) #1^2 +
    46656 A Pcl^3 √(3 - 3 ν^2) #1^2 + 5824 Pbar^3 #1^3 + 57381 Pbar^2 Pcl #1^3 -
    132234 Pbar Pcl^2 #1^3 + 69029 Pcl^3 #1^3 + 128352 A^2 Pcl^3 #1^3 - 128352 A^2 Pcl^3 ν^2 #1^3 -
    155520 A Pbar Pcl^2 √(3 - 3 ν^2) #1^3 + 155520 A Pcl^3 √(3 - 3 ν^2) #1^3 -
    16848 Pbar^3 #1^4 + 31482 Pbar^2 Pcl #1^4 - 12420 Pbar Pcl^2 #1^4 - 2214 Pcl^3 #1^4 -
    163296 A^2 Pcl^3 #1^4 + 163296 A^2 Pcl^3 ν^2 #1^4 - 188352 A Pbar Pcl^2 √(3 - 3 ν^2) #1^4 +
```

$$
\begin{aligned}
&188352\,A\,Pcl^3\sqrt{3-3\nu^2}\,\#1^4 - 5808\,Pbar^3\,\#1^5 + 4766\,Pbar^2\,Pcl\,\#1^5 + \\
&7892\,Pbar\,Pcl^2\,\#1^5 - 6850\,Pcl^3\,\#1^5 + 74976\,A^2\,Pcl^3\,\#1^5 - 74976\,A^2\,Pcl^3\,\nu^2\,\#1^5 - \\
&98560\,A\,Pbar\,Pcl^2\sqrt{3-3\nu^2}\,\#1^5 + 98560\,A\,Pcl^3\sqrt{3-3\nu^2}\,\#1^5 + 5184\,Pbar^3\,\#1^6 - \\
&14290\,Pbar^2\,Pcl\,\#1^6 + 13028\,Pbar\,Pcl^2\,\#1^6 - 3922\,Pcl^3\,\#1^6 + 2784\,A^2\,Pcl^3\,\#1^6 - \\
&2784\,A^2\,Pcl^3\,\nu^2\,\#1^6 - 20928\,A\,Pbar\,Pcl^2\sqrt{3-3\nu^2}\,\#1^6 + 20928\,A\,Pcl^3\sqrt{3-3\nu^2}\,\#1^6 + \\
&1920\,Pbar^3\,\#1^7 - 4854\,Pbar^2\,Pcl\,\#1^7 + 3948\,Pbar\,Pcl^2\,\#1^7 - 1014\,Pcl^3\,\#1^7 - \\
&6624\,A^2\,Pcl^3\,\#1^7 + 6624\,A^2\,Pcl^3\,\nu^2\,\#1^7 - 1920\,A\,Pbar\,Pcl^2\sqrt{3-3\nu^2}\,\#1^7 + \\
&1920\,A\,Pcl^3\sqrt{3-3\nu^2}\,\#1^7 + 216\,Pbar^3\,\#1^8 + 189\,Pbar^2\,Pcl\,\#1^8 - 1026\,Pbar\,Pcl^2\,\#1^8 + \\
&621\,Pcl^3\,\#1^8 - 672\,A^2\,Pcl^3\,\#1^8 + 672\,A^2\,Pcl^3\,\nu^2\,\#1^8 - 64\,A\,Pbar\,Pcl^2\sqrt{3-3\nu^2}\,\#1^8 + \\
&64\,A\,Pcl^3\sqrt{3-3\nu^2}\,\#1^8 + 8\,Pbar^3\,\#1^9 + 223\,Pbar^2\,Pcl\,\#1^9 - 470\,Pbar\,Pcl^2\,\#1^9 + \\
&239\,Pcl^3\,\#1^9 - 96\,A^2\,Pcl^3\,\#1^9 + 96\,A^2\,Pcl^3\,\nu^2\,\#1^9 + 27\,Pbar^2\,Pcl\,\#1^{10} - \\
&54\,Pbar\,Pcl^2\,\#1^{10} + 27\,Pcl^3\,\#1^{10} + Pbar^2\,Pcl\,\#1^{11} - 2\,Pbar\,Pcl^2\,\#1^{11} + Pcl^3\,\#1^{11}\,\&,\,4\big]\big\},
\end{aligned}
$$

$$
\begin{aligned}
&\{\gamma \to -\sqrt{\text{Root}\big[-5832\,Pbar^3 + 24057\,Pbar^2\,Pcl - 30618\,Pbar\,Pcl^2 + 12393\,Pcl^3 - 1944\,Pbar^3\,\#1 + \\
&8019\,Pbar^2\,Pcl\,\#1 - 10206\,Pbar\,Pcl^2\,\#1 + 4131\,Pcl^3\,\#1 + 17280\,Pbar^3\,\#1^2 - \\
&107001\,Pbar^2\,Pcl\,\#1^2 + 162162\,Pbar\,Pcl^2\,\#1^2 - 72441\,Pcl^3\,\#1^2 - 35424\,A^2\,Pcl^3\,\#1^2 + \\
&35424\,A^2\,Pcl^3\,\nu^2\,\#1^2 - 46656\,A\,Pbar\,Pcl^2\sqrt{3-3\nu^2}\,\#1^2 + 46656\,A\,Pcl^3\sqrt{3-3\nu^2}\,\#1^2 + \\
&5824\,Pbar^3\,\#1^3 + 57381\,Pbar^2\,Pcl\,\#1^3 - 132234\,Pbar\,Pcl^2\,\#1^3 + 69029\,Pcl^3\,\#1^3 + \\
&128352\,A^2\,Pcl^3\,\#1^3 - 128352\,A^2\,Pcl^3\,\nu^2\,\#1^3 - 155520\,A\,Pbar\,Pcl^2\sqrt{3-3\nu^2}\,\#1^3 + \\
&155520\,A\,Pcl^3\sqrt{3-3\nu^2}\,\#1^3 - 16848\,Pbar^3\,\#1^4 + 31482\,Pbar^2\,Pcl\,\#1^4 - \\
&12420\,Pbar\,Pcl^2\,\#1^4 - 2214\,Pcl^3\,\#1^4 - 163296\,A^2\,Pcl^3\,\#1^4 + 163296\,A^2\,Pcl^3\,\nu^2\,\#1^4 - \\
&188352\,A\,Pbar\,Pcl^2\sqrt{3-3\nu^2}\,\#1^4 + 188352\,A\,Pcl^3\sqrt{3-3\nu^2}\,\#1^4 - 5808\,Pbar^3\,\#1^5 + \\
&4766\,Pbar^2\,Pcl\,\#1^5 + 7892\,Pbar\,Pcl^2\,\#1^5 - 6850\,Pcl^3\,\#1^5 + 74976\,A^2\,Pcl^3\,\#1^5 - \\
&74976\,A^2\,Pcl^3\,\nu^2\,\#1^5 - 98560\,A\,Pbar\,Pcl^2\sqrt{3-3\nu^2}\,\#1^5 + 98560\,A\,Pcl^3\sqrt{3-3\nu^2}\,\#1^5 + \\
&5184\,Pbar^3\,\#1^6 - 14290\,Pbar^2\,Pcl\,\#1^6 + 13028\,Pbar\,Pcl^2\,\#1^6 - 3922\,Pcl^3\,\#1^6 + \\
&2784\,A^2\,Pcl^3\,\#1^6 - 2784\,A^2\,Pcl^3\,\nu^2\,\#1^6 - 20928\,A\,Pbar\,Pcl^2\sqrt{3-3\nu^2}\,\#1^6 + \\
&20928\,A\,Pcl^3\sqrt{3-3\nu^2}\,\#1^6 + 1920\,Pbar^3\,\#1^7 - 4854\,Pbar^2\,Pcl\,\#1^7 + 3948\,Pbar\,Pcl^2\,\#1^7 - \\
&1014\,Pcl^3\,\#1^7 - 6624\,A^2\,Pcl^3\,\#1^7 + 6624\,A^2\,Pcl^3\,\nu^2\,\#1^7 - 1920\,A\,Pbar\,Pcl^2\sqrt{3-3\nu^2}\,\#1^7 + \\
&1920\,A\,Pcl^3\sqrt{3-3\nu^2}\,\#1^7 + 216\,Pbar^3\,\#1^8 + 189\,Pbar^2\,Pcl\,\#1^8 - 1026\,Pbar\,Pcl^2\,\#1^8 + \\
&621\,Pcl^3\,\#1^8 - 672\,A^2\,Pcl^3\,\#1^8 + 672\,A^2\,Pcl^3\,\nu^2\,\#1^8 - 64\,A\,Pbar\,Pcl^2\sqrt{3-3\nu^2}\,\#1^8 + \\
&64\,A\,Pcl^3\sqrt{3-3\nu^2}\,\#1^8 + 8\,Pbar^3\,\#1^9 + 223\,Pbar^2\,Pcl\,\#1^9 - 470\,Pbar\,Pcl^2\,\#1^9 + \\
&239\,Pcl^3\,\#1^9 - 96\,A^2\,Pcl^3\,\#1^9 + 96\,A^2\,Pcl^3\,\nu^2\,\#1^9 + 27\,Pbar^2\,Pcl\,\#1^{10} - \\
&54\,Pbar\,Pcl^2\,\#1^{10} + 27\,Pcl^3\,\#1^{10} + Pbar^2\,Pcl\,\#1^{11} - 2\,Pbar\,Pcl^2\,\#1^{11} + Pcl^3\,\#1^{11}\,\&,\,5\big]\big\},
\end{aligned}
$$

$$
\begin{aligned}
&\{\gamma \to \sqrt{\text{Root}\big[-5832\,Pbar^3 + 24057\,Pbar^2\,Pcl - 30618\,Pbar\,Pcl^2 + 12393\,Pcl^3 - \\
&1944\,Pbar^3\,\#1 + 8019\,Pbar^2\,Pcl\,\#1 - 10206\,Pbar\,Pcl^2\,\#1 + 4131\,Pcl^3\,\#1 + \\
&17280\,Pbar^3\,\#1^2 - 107001\,Pbar^2\,Pcl\,\#1^2 + 162162\,Pbar\,Pcl^2\,\#1^2 - 72441\,Pcl^3\,\#1^2 - \\
&35424\,A^2\,Pcl^3\,\#1^2 + 35424\,A^2\,Pcl^3\,\nu^2\,\#1^2 - 46656\,A\,Pbar\,Pcl^2\sqrt{3-3\nu^2}\,\#1^2 + \\
&46656\,A\,Pcl^3\sqrt{3-3\nu^2}\,\#1^2 + 5824\,Pbar^3\,\#1^3 + 57381\,Pbar^2\,Pcl\,\#1^3 - \\
&132234\,Pbar\,Pcl^2\,\#1^3 + 69029\,Pcl^3\,\#1^3 + 128352\,A^2\,Pcl^3\,\#1^3 - 128352\,A^2\,Pcl^3\,\nu^2\,\#1^3 - \\
&155520\,A\,Pbar\,Pcl^2\sqrt{3-3\nu^2}\,\#1^3 + 155520\,A\,Pcl^3\sqrt{3-3\nu^2}\,\#1^3 - \\
&16848\,Pbar^3\,\#1^4 + 31482\,Pbar^2\,Pcl\,\#1^4 - 12420\,Pbar\,Pcl^2\,\#1^4 - 2214\,Pcl^3\,\#1^4 - \\
&163296\,A^2\,Pcl^3\,\#1^4 + 163296\,A^2\,Pcl^3\,\nu^2\,\#1^4 - 188352\,A\,Pbar\,Pcl^2\sqrt{3-3\nu^2}\,\#1^4 + \\
&188352\,A\,Pcl^3\sqrt{3-3\nu^2}\,\#1^4 - 5808\,Pbar^3\,\#1^5 + 4766\,Pbar^2\,Pcl\,\#1^5 + \\
&7892\,Pbar\,Pcl^2\,\#1^5 - 6850\,Pcl^3\,\#1^5 + 74976\,A^2\,Pcl^3\,\#1^5 - 74976\,A^2\,Pcl^3\,\nu^2\,\#1^5 - \\
&98560\,A\,Pbar\,Pcl^2\sqrt{3-3\nu^2}\,\#1^5 + 98560\,A\,Pcl^3\sqrt{3-3\nu^2}\,\#1^5 + 5184\,Pbar^3\,\#1^6 - \\
&14290\,Pbar^2\,Pcl\,\#1^6 + 13028\,Pbar\,Pcl^2\,\#1^6 - 3922\,Pcl^3\,\#1^6 + 2784\,A^2\,Pcl^3\,\#1^6 - \\
&2784\,A^2\,Pcl^3\,\nu^2\,\#1^6 - 20928\,A\,Pbar\,Pcl^2\sqrt{3-3\nu^2}\,\#1^6 + 20928\,A\,Pcl^3\sqrt{3-3\nu^2}\,\#1^6 + \\
&1920\,Pbar^3\,\#1^7 - 4854\,Pbar^2\,Pcl\,\#1^7 + 3948\,Pbar\,Pcl^2\,\#1^7 - 1014\,Pcl^3\,\#1^7 - \\
&6624\,A^2\,Pcl^3\,\#1^7 + 6624\,A^2\,Pcl^3\,\nu^2\,\#1^7 - 1920\,A\,Pbar\,Pcl^2\sqrt{3-3\nu^2}\,\#1^7 + \\
&1920\,A\,Pcl^3\sqrt{3-3\nu^2}\,\#1^7 + 216\,Pbar^3\,\#1^8 + 189\,Pbar^2\,Pcl\,\#1^8 - 1026\,Pbar\,Pcl^2\,\#1^8 + \\
&621\,Pcl^3\,\#1^8 - 672\,A^2\,Pcl^3\,\#1^8 + 672\,A^2\,Pcl^3\,\nu^2\,\#1^8 - 64\,A\,Pbar\,Pcl^2\sqrt{3-3\nu^2}\,\#1^8 + \\
&64\,A\,Pcl^3\sqrt{3-3\nu^2}\,\#1^8 + 8\,Pbar^3\,\#1^9 + 223\,Pbar^2\,Pcl\,\#1^9 - 470\,Pbar\,Pcl^2\,\#1^9 +
\end{aligned}
$$

```
239 Pcl^3 #1^9 - 96 A^2 Pcl^3 #1^9 + 96 A^2 Pcl^3 v^2 #1^9 + 27 Pbar^2 Pcl #1^10 -
    54 Pbar Pcl^2 #1^10 + 27 Pcl^3 #1^10 + Pbar^2 Pcl #1^11 - 2 Pbar Pcl^2 #1^11 + Pcl^3 #1^11 &, 5]},
{γ → -√Root[-5832 Pbar^3 + 24057 Pbar^2 Pcl - 30618 Pbar Pcl^2 + 12393 Pcl^3 - 1944 Pbar^3 #1 +
    8019 Pbar^2 Pcl #1 - 10206 Pbar Pcl^2 #1 + 4131 Pcl^3 #1 + 17280 Pbar^3 #1^2 -
    107001 Pbar^2 Pcl #1^2 + 162162 Pbar Pcl^2 #1^2 - 72441 Pcl^3 #1^2 - 35424 A^2 Pcl^3 #1^2 +
    35424 A^2 Pcl^3 v^2 #1^2 - 46656 A Pbar Pcl^2 √(3 - 3 v^2) #1^2 + 46656 A Pcl^3 √(3 - 3 v^2) #1^2 +
    5824 Pbar^3 #1^3 + 57381 Pbar^2 Pcl #1^3 - 132234 Pbar Pcl^2 #1^3 + 69029 Pcl^3 #1^3 +
    128352 A^2 Pcl^3 #1^3 - 128352 A^2 Pcl^3 v^2 #1^3 - 155520 A Pbar Pcl^2 √(3 - 3 v^2) #1^3 +
    155520 A Pcl^3 √(3 - 3 v^2) #1^3 - 16848 Pbar^3 #1^4 + 31482 Pbar^2 Pcl #1^4 -
    12420 Pbar Pcl^2 #1^4 - 2214 Pcl^3 #1^4 - 163296 A^2 Pcl^3 #1^4 + 163296 A^2 Pcl^3 v^2 #1^4 -
    188352 A Pbar Pcl^2 √(3 - 3 v^2) #1^4 + 188352 A Pcl^3 √(3 - 3 v^2) #1^4 - 5808 Pbar^3 #1^5 +
    4766 Pbar^2 Pcl #1^5 + 7892 Pbar Pcl^2 #1^5 - 6850 Pcl^3 #1^5 + 74976 A^2 Pcl^3 #1^5 -
    74976 A^2 Pcl^3 v^2 #1^5 - 98560 A Pbar Pcl^2 √(3 - 3 v^2) #1^5 + 98560 A Pcl^3 √(3 - 3 v^2) #1^5 +
    5184 Pbar^3 #1^6 - 14290 Pbar^2 Pcl #1^6 + 13028 Pbar Pcl^2 #1^6 - 3922 Pcl^3 #1^6 +
    2784 A^2 Pcl^3 #1^6 - 2784 A^2 Pcl^3 v^2 #1^6 - 20928 A Pbar Pcl^2 √(3 - 3 v^2) #1^6 +
    20928 A Pcl^3 √(3 - 3 v^2) #1^6 + 1920 Pbar^3 #1^7 - 4854 Pbar^2 Pcl #1^7 + 3948 Pbar Pcl^2 #1^7 -
    1014 Pcl^3 #1^7 - 6624 A^2 Pcl^3 #1^7 + 6624 A^2 Pcl^3 v^2 #1^7 - 1920 A Pbar Pcl^2 √(3 - 3 v^2) #1^7 +
    1920 A Pcl^3 √(3 - 3 v^2) #1^7 + 216 Pbar^3 #1^8 + 189 Pbar^2 Pcl #1^8 - 1026 Pbar Pcl^2 #1^8 +
    621 Pcl^3 #1^8 - 672 A^2 Pcl^3 #1^8 + 672 A^2 Pcl^3 v^2 #1^8 - 64 A Pbar Pcl^2 √(3 - 3 v^2) #1^8 +
    64 A Pcl^3 √(3 - 3 v^2) #1^8 + 8 Pbar^3 #1^9 + 223 Pbar^2 Pcl #1^9 - 470 Pbar Pcl^2 #1^9 +
    239 Pcl^3 #1^9 - 96 A^2 Pcl^3 #1^9 + 96 A^2 Pcl^3 v^2 #1^9 + 27 Pbar^2 Pcl #1^10 -
    54 Pbar Pcl^2 #1^10 + 27 Pcl^3 #1^10 + Pbar^2 Pcl #1^11 - 2 Pbar Pcl^2 #1^11 + Pcl^3 #1^11 &, 6]},
{γ → √Root[-5832 Pbar^3 + 24057 Pbar^2 Pcl - 30618 Pbar Pcl^2 + 12393 Pcl^3 -
    1944 Pbar^3 #1 + 8019 Pbar^2 Pcl #1 - 10206 Pbar Pcl^2 #1 + 4131 Pcl^3 #1 +
    17280 Pbar^3 #1^2 - 107001 Pbar^2 Pcl #1^2 + 162162 Pbar Pcl^2 #1^2 - 72441 Pcl^3 #1^2 -
    35424 A^2 Pcl^3 #1^2 + 35424 A^2 Pcl^3 v^2 #1^2 - 46656 A Pbar Pcl^2 √(3 - 3 v^2) #1^2 +
    46656 A Pcl^3 √(3 - 3 v^2) #1^2 + 5824 Pbar^3 #1^3 + 57381 Pbar^2 Pcl #1^3 -
    132234 Pbar Pcl^2 #1^3 + 69029 Pcl^3 #1^3 + 128352 A^2 Pcl^3 #1^3 - 128352 A^2 Pcl^3 v^2 #1^3 -
    155520 A Pbar Pcl^2 √(3 - 3 v^2) #1^3 + 155520 A Pcl^3 √(3 - 3 v^2) #1^3 -
    16848 Pbar^3 #1^4 + 31482 Pbar^2 Pcl #1^4 - 12420 Pbar Pcl^2 #1^4 - 2214 Pcl^3 #1^4 -
    163296 A^2 Pcl^3 #1^4 + 163296 A^2 Pcl^3 v^2 #1^4 - 188352 A Pbar Pcl^2 √(3 - 3 v^2) #1^4 +
    188352 A Pcl^3 √(3 - 3 v^2) #1^4 - 5808 Pbar^3 #1^5 + 4766 Pbar^2 Pcl #1^5 +
    7892 Pbar Pcl^2 #1^5 - 6850 Pcl^3 #1^5 + 74976 A^2 Pcl^3 #1^5 - 74976 A^2 Pcl^3 v^2 #1^5 -
    98560 A Pbar Pcl^2 √(3 - 3 v^2) #1^5 + 98560 A Pcl^3 √(3 - 3 v^2) #1^5 + 5184 Pbar^3 #1^6 -
    14290 Pbar^2 Pcl #1^6 + 13028 Pbar Pcl^2 #1^6 - 3922 Pcl^3 #1^6 + 2784 A^2 Pcl^3 #1^6 -
    2784 A^2 Pcl^3 v^2 #1^6 - 20928 A Pbar Pcl^2 √(3 - 3 v^2) #1^6 + 20928 A Pcl^3 √(3 - 3 v^2) #1^6 +
    1920 Pbar^3 #1^7 - 4854 Pbar^2 Pcl #1^7 + 3948 Pbar Pcl^2 #1^7 - 1014 Pcl^3 #1^7 -
    6624 A^2 Pcl^3 #1^7 + 6624 A^2 Pcl^3 v^2 #1^7 - 1920 A Pbar Pcl^2 √(3 - 3 v^2) #1^7 +
    1920 A Pcl^3 √(3 - 3 v^2) #1^7 + 216 Pbar^3 #1^8 + 189 Pbar^2 Pcl #1^8 - 1026 Pbar Pcl^2 #1^8 +
    621 Pcl^3 #1^8 - 672 A^2 Pcl^3 #1^8 + 672 A^2 Pcl^3 v^2 #1^8 - 64 A Pbar Pcl^2 √(3 - 3 v^2) #1^8 +
    64 A Pcl^3 √(3 - 3 v^2) #1^8 + 8 Pbar^3 #1^9 + 223 Pbar^2 Pcl #1^9 - 470 Pbar Pcl^2 #1^9 +
    239 Pcl^3 #1^9 - 96 A^2 Pcl^3 #1^9 + 96 A^2 Pcl^3 v^2 #1^9 + 27 Pbar^2 Pcl #1^10 -
    54 Pbar Pcl^2 #1^10 + 27 Pcl^3 #1^10 + Pbar^2 Pcl #1^11 - 2 Pbar Pcl^2 #1^11 + Pcl^3 #1^11 &, 6]},
{γ → -√Root[-5832 Pbar^3 + 24057 Pbar^2 Pcl - 30618 Pbar Pcl^2 + 12393 Pcl^3 - 1944 Pbar^3 #1 +
    8019 Pbar^2 Pcl #1 - 10206 Pbar Pcl^2 #1 + 4131 Pcl^3 #1 + 17280 Pbar^3 #1^2 -
    107001 Pbar^2 Pcl #1^2 + 162162 Pbar Pcl^2 #1^2 - 72441 Pcl^3 #1^2 - 35424 A^2 Pcl^3 #1^2 +
    35424 A^2 Pcl^3 v^2 #1^2 - 46656 A Pbar Pcl^2 √(3 - 3 v^2) #1^2 + 46656 A Pcl^3 √(3 - 3 v^2) #1^2 +
    5824 Pbar^3 #1^3 + 57381 Pbar^2 Pcl #1^3 - 132234 Pbar Pcl^2 #1^3 + 69029 Pcl^3 #1^3 +
    128352 A^2 Pcl^3 #1^3 - 128352 A^2 Pcl^3 v^2 #1^3 - 155520 A Pbar Pcl^2 √(3 - 3 v^2) #1^3 +
    155520 A Pcl^3 √(3 - 3 v^2) #1^3 - 16848 Pbar^3 #1^4 + 31482 Pbar^2 Pcl #1^4 -
    12420 Pbar Pcl^2 #1^4 - 2214 Pcl^3 #1^4 - 163296 A^2 Pcl^3 #1^4 + 163296 A^2 Pcl^3 v^2 #1^4 -
```

$$188352\,A\,Pbar\,Pcl^2\sqrt{3-3\nu^2}\,\#1^4 + 188352\,A\,Pcl^3\sqrt{3-3\nu^2}\,\#1^4 - 5808\,Pbar^3\,\#1^5 +$$
$$4766\,Pbar^2\,Pcl\,\#1^5 + 7892\,Pbar\,Pcl^2\,\#1^5 - 6850\,Pcl^3\,\#1^5 + 74976\,A^2\,Pcl^3\,\#1^5 -$$
$$74976\,A^2\,Pcl^3\,\nu^2\,\#1^5 - 98560\,A\,Pbar\,Pcl^2\sqrt{3-3\nu^2}\,\#1^5 + 98560\,A\,Pcl^3\sqrt{3-3\nu^2}\,\#1^5 +$$
$$5184\,Pbar^3\,\#1^6 - 14290\,Pbar^2\,Pcl\,\#1^6 + 13028\,Pbar\,Pcl^2\,\#1^6 - 3922\,Pcl^3\,\#1^6 +$$
$$2784\,A^2\,Pcl^3\,\#1^6 - 2784\,A^2\,Pcl^3\,\nu^2\,\#1^6 - 20928\,A\,Pbar\,Pcl^2\sqrt{3-3\nu^2}\,\#1^6 +$$
$$20928\,A\,Pcl^3\sqrt{3-3\nu^2}\,\#1^6 + 1920\,Pbar^3\,\#1^7 - 4854\,Pbar^2\,Pcl\,\#1^7 + 3948\,Pbar\,Pcl^2\,\#1^7 -$$
$$1014\,Pcl^3\,\#1^7 - 6624\,A^2\,Pcl^3\,\#1^7 + 6624\,A^2\,Pcl^3\,\nu^2\,\#1^7 - 1920\,A\,Pbar\,Pcl^2\sqrt{3-3\nu^2}\,\#1^7 +$$
$$1920\,A\,Pcl^3\sqrt{3-3\nu^2}\,\#1^7 + 216\,Pbar^3\,\#1^8 + 189\,Pbar^2\,Pcl\,\#1^8 - 1026\,Pbar\,Pcl^2\,\#1^8 +$$
$$621\,Pcl^3\,\#1^8 - 672\,A^2\,Pcl^3\,\#1^8 + 672\,A^2\,Pcl^3\,\nu^2\,\#1^8 - 64\,A\,Pbar\,Pcl^2\sqrt{3-3\nu^2}\,\#1^8 +$$
$$64\,A\,Pcl^3\sqrt{3-3\nu^2}\,\#1^8 + 8\,Pbar^3\,\#1^9 + 223\,Pbar^2\,Pcl\,\#1^9 - 470\,Pbar\,Pcl^2\,\#1^9 +$$
$$239\,Pcl^3\,\#1^9 - 96\,A^2\,Pcl^3\,\#1^9 + 96\,A^2\,Pcl^3\,\nu^2\,\#1^9 + 27\,Pbar^2\,Pcl\,\#1^{10} -$$
$$54\,Pbar\,Pcl^2\,\#1^{10} + 27\,Pcl^3\,\#1^{10} + Pbar^2\,Pcl\,\#1^{11} - 2\,Pbar\,Pcl^2\,\#1^{11} + Pcl^3\,\#1^{11}\,\&,\ 7\Big]\Big\},$$

$$\Big\{\gamma \to \sqrt{\text{Root}\Big[-5832\,Pbar^3 + 24057\,Pbar^2\,Pcl - 30618\,Pbar\,Pcl^2 + 12393\,Pcl^3 -$$
$$1944\,Pbar^3\,\#1 + 8019\,Pbar^2\,Pcl\,\#1 - 10206\,Pbar\,Pcl^2\,\#1 + 4131\,Pcl^3\,\#1 +$$
$$17280\,Pbar^3\,\#1^2 - 107001\,Pbar^2\,Pcl\,\#1^2 + 162162\,Pbar\,Pcl^2\,\#1^2 - 72441\,Pcl^3\,\#1^2 -$$
$$35424\,A^2\,Pcl^3\,\#1^2 + 35424\,A^2\,Pcl^3\,\nu^2\,\#1^2 - 46656\,A\,Pbar\,Pcl^2\sqrt{3-3\nu^2}\,\#1^2 +$$
$$46656\,A\,Pcl^3\sqrt{3-3\nu^2}\,\#1^2 + 5824\,Pbar^3\,\#1^3 + 57381\,Pbar^2\,Pcl\,\#1^3 -$$
$$132234\,Pbar\,Pcl^2\,\#1^3 + 69029\,Pcl^3\,\#1^3 + 128352\,A^2\,Pcl^3\,\#1^3 - 128352\,A^2\,Pcl^3\,\nu^2\,\#1^3 -$$
$$155520\,A\,Pbar\,Pcl^2\sqrt{3-3\nu^2}\,\#1^3 + 155520\,A\,Pcl^3\sqrt{3-3\nu^2}\,\#1^3 -$$
$$16848\,Pbar^3\,\#1^4 + 31482\,Pbar^2\,Pcl\,\#1^4 - 12420\,Pbar\,Pcl^2\,\#1^4 - 2214\,Pcl^3\,\#1^4 -$$
$$163296\,A^2\,Pcl^3\,\#1^4 + 163296\,A^2\,Pcl^3\,\nu^2\,\#1^4 - 188352\,A\,Pbar\,Pcl^2\sqrt{3-3\nu^2}\,\#1^4 +$$
$$188352\,A\,Pcl^3\sqrt{3-3\nu^2}\,\#1^4 - 5808\,Pbar^3\,\#1^5 + 4766\,Pbar^2\,Pcl\,\#1^5 +$$
$$7892\,Pbar\,Pcl^2\,\#1^5 - 6850\,Pcl^3\,\#1^5 + 74976\,A^2\,Pcl^3\,\#1^5 - 74976\,A^2\,Pcl^3\,\nu^2\,\#1^5 -$$
$$98560\,A\,Pbar\,Pcl^2\sqrt{3-3\nu^2}\,\#1^5 + 98560\,A\,Pcl^3\sqrt{3-3\nu^2}\,\#1^5 + 5184\,Pbar^3\,\#1^6 -$$
$$14290\,Pbar^2\,Pcl\,\#1^6 + 13028\,Pbar\,Pcl^2\,\#1^6 - 3922\,Pcl^3\,\#1^6 + 2784\,A^2\,Pcl^3\,\#1^6 -$$
$$2784\,A^2\,Pcl^3\,\nu^2\,\#1^6 - 20928\,A\,Pbar\,Pcl^2\sqrt{3-3\nu^2}\,\#1^6 + 20928\,A\,Pcl^3\sqrt{3-3\nu^2}\,\#1^6 +$$
$$1920\,Pbar^3\,\#1^7 - 4854\,Pbar^2\,Pcl\,\#1^7 + 3948\,Pbar\,Pcl^2\,\#1^7 - 1014\,Pcl^3\,\#1^7 -$$
$$6624\,A^2\,Pcl^3\,\#1^7 + 6624\,A^2\,Pcl^3\,\nu^2\,\#1^7 - 1920\,A\,Pbar\,Pcl^2\sqrt{3-3\nu^2}\,\#1^7 +$$
$$1920\,A\,Pcl^3\sqrt{3-3\nu^2}\,\#1^7 + 216\,Pbar^3\,\#1^8 + 189\,Pbar^2\,Pcl\,\#1^8 - 1026\,Pbar\,Pcl^2\,\#1^8 +$$
$$621\,Pcl^3\,\#1^8 - 672\,A^2\,Pcl^3\,\#1^8 + 672\,A^2\,Pcl^3\,\nu^2\,\#1^8 - 64\,A\,Pbar\,Pcl^2\sqrt{3-3\nu^2}\,\#1^8 +$$
$$64\,A\,Pcl^3\sqrt{3-3\nu^2}\,\#1^8 + 8\,Pbar^3\,\#1^9 + 223\,Pbar^2\,Pcl\,\#1^9 - 470\,Pbar\,Pcl^2\,\#1^9 +$$
$$239\,Pcl^3\,\#1^9 - 96\,A^2\,Pcl^3\,\#1^9 + 96\,A^2\,Pcl^3\,\nu^2\,\#1^9 + 27\,Pbar^2\,Pcl\,\#1^{10} -$$
$$54\,Pbar\,Pcl^2\,\#1^{10} + 27\,Pcl^3\,\#1^{10} + Pbar^2\,Pcl\,\#1^{11} - 2\,Pbar\,Pcl^2\,\#1^{11} + Pcl^3\,\#1^{11}\,\&,\ 7\Big]\Big\},$$

$$\Big\{\gamma \to -\sqrt{\text{Root}\Big[-5832\,Pbar^3 + 24057\,Pbar^2\,Pcl - 30618\,Pbar\,Pcl^2 + 12393\,Pcl^3 - 1944\,Pbar^3\,\#1 +$$
$$8019\,Pbar^2\,Pcl\,\#1 - 10206\,Pbar\,Pcl^2\,\#1 + 4131\,Pcl^3\,\#1 + 17280\,Pbar^3\,\#1^2 -$$
$$107001\,Pbar^2\,Pcl\,\#1^2 + 162162\,Pbar\,Pcl^2\,\#1^2 - 72441\,Pcl^3\,\#1^2 - 35424\,A^2\,Pcl^3\,\#1^2 +$$
$$35424\,A^2\,Pcl^3\,\nu^2\,\#1^2 - 46656\,A\,Pbar\,Pcl^2\sqrt{3-3\nu^2}\,\#1^2 + 46656\,A\,Pcl^3\sqrt{3-3\nu^2}\,\#1^2 +$$
$$5824\,Pbar^3\,\#1^3 + 57381\,Pbar^2\,Pcl\,\#1^3 - 132234\,Pbar\,Pcl^2\,\#1^3 + 69029\,Pcl^3\,\#1^3 +$$
$$128352\,A^2\,Pcl^3\,\#1^3 - 128352\,A^2\,Pcl^3\,\nu^2\,\#1^3 - 155520\,A\,Pbar\,Pcl^2\sqrt{3-3\nu^2}\,\#1^3 +$$
$$155520\,A\,Pcl^3\sqrt{3-3\nu^2}\,\#1^3 - 16848\,Pbar^3\,\#1^4 + 31482\,Pbar^2\,Pcl\,\#1^4 -$$
$$12420\,Pbar\,Pcl^2\,\#1^4 - 2214\,Pcl^3\,\#1^4 - 163296\,A^2\,Pcl^3\,\#1^4 + 163296\,A^2\,Pcl^3\,\nu^2\,\#1^4 -$$
$$188352\,A\,Pbar\,Pcl^2\sqrt{3-3\nu^2}\,\#1^4 + 188352\,A\,Pcl^3\sqrt{3-3\nu^2}\,\#1^4 - 5808\,Pbar^3\,\#1^5 +$$
$$4766\,Pbar^2\,Pcl\,\#1^5 + 7892\,Pbar\,Pcl^2\,\#1^5 - 6850\,Pcl^3\,\#1^5 + 74976\,A^2\,Pcl^3\,\#1^5 -$$
$$74976\,A^2\,Pcl^3\,\nu^2\,\#1^5 - 98560\,A\,Pbar\,Pcl^2\sqrt{3-3\nu^2}\,\#1^5 + 98560\,A\,Pcl^3\sqrt{3-3\nu^2}\,\#1^5 +$$
$$5184\,Pbar^3\,\#1^6 - 14290\,Pbar^2\,Pcl\,\#1^6 + 13028\,Pbar\,Pcl^2\,\#1^6 - 3922\,Pcl^3\,\#1^6 +$$
$$2784\,A^2\,Pcl^3\,\#1^6 - 2784\,A^2\,Pcl^3\,\nu^2\,\#1^6 - 20928\,A\,Pbar\,Pcl^2\sqrt{3-3\nu^2}\,\#1^6 +$$
$$20928\,A\,Pcl^3\sqrt{3-3\nu^2}\,\#1^6 + 1920\,Pbar^3\,\#1^7 - 4854\,Pbar^2\,Pcl\,\#1^7 + 3948\,Pbar\,Pcl^2\,\#1^7 -$$
$$1014\,Pcl^3\,\#1^7 - 6624\,A^2\,Pcl^3\,\#1^7 + 6624\,A^2\,Pcl^3\,\nu^2\,\#1^7 - 1920\,A\,Pbar\,Pcl^2\sqrt{3-3\nu^2}\,\#1^7 +$$
$$1920\,A\,Pcl^3\sqrt{3-3\nu^2}\,\#1^7 + 216\,Pbar^3\,\#1^8 + 189\,Pbar^2\,Pcl\,\#1^8 - 1026\,Pbar\,Pcl^2\,\#1^8 +$$
$$621\,Pcl^3\,\#1^8 - 672\,A^2\,Pcl^3\,\#1^8 + 672\,A^2\,Pcl^3\,\nu^2\,\#1^8 - 64\,A\,Pbar\,Pcl^2\sqrt{3-3\nu^2}\,\#1^8 +$$
$$64\,A\,Pcl^3\sqrt{3-3\nu^2}\,\#1^8 + 8\,Pbar^3\,\#1^9 + 223\,Pbar^2\,Pcl\,\#1^9 - 470\,Pbar\,Pcl^2\,\#1^9 +$$

```
    239 Pcl^3 #1^9 - 96 A^2 Pcl^3 #1^9 + 96 A^2 Pcl^3 v^2 #1^9 + 27 Pbar^2 Pcl #1^10 -
    54 Pbar Pcl^2 #1^10 + 27 Pcl^3 #1^10 + Pbar^2 Pcl #1^11 - 2 Pbar Pcl^2 #1^11 + Pcl^3 #1^11 &, 8]},
{γ → √Root[-5832 Pbar^3 + 24057 Pbar^2 Pcl - 30618 Pbar Pcl^2 + 12393 Pcl^3 -
    1944 Pbar^3 #1 + 8019 Pbar^2 Pcl #1 - 10206 Pbar Pcl^2 #1 + 4131 Pcl^3 #1 +
    17280 Pbar^3 #1^2 - 107001 Pbar^2 Pcl #1^2 + 162162 Pbar Pcl^2 #1^2 - 72441 Pcl^3 #1^2 -
    35424 A^2 Pcl^3 #1^2 + 35424 A^2 Pcl^3 v^2 #1^2 - 46656 A Pbar Pcl^2 √(3 - 3 v^2) #1^2 +
    46656 A Pcl^3 √(3 - 3 v^2) #1^2 + 5824 Pbar^3 #1^3 + 57381 Pbar^2 Pcl #1^3 -
    132234 Pbar Pcl^2 #1^3 + 69029 Pcl^3 #1^3 + 128352 A^2 Pcl^3 #1^3 - 128352 A^2 Pcl^3 v^2 #1^3 -
    155520 A Pbar Pcl^2 √(3 - 3 v^2) #1^3 + 155520 A Pcl^3 √(3 - 3 v^2) #1^3 -
    16848 Pbar^3 #1^4 + 31482 Pbar^2 Pcl #1^4 - 12420 Pbar Pcl^2 #1^4 - 2214 Pcl^3 #1^4 -
    163296 A^2 Pcl^3 #1^4 + 163296 A^2 Pcl^3 v^2 #1^4 - 188352 A Pbar Pcl^2 √(3 - 3 v^2) #1^4 +
    188352 A Pcl^3 √(3 - 3 v^2) #1^4 - 5808 Pbar^3 #1^5 + 4766 Pbar^2 Pcl #1^5 +
    7892 Pbar Pcl^2 #1^5 - 6850 Pcl^3 #1^5 + 74976 A^2 Pcl^3 #1^5 - 74976 A^2 Pcl^3 v^2 #1^5 -
    98560 A Pbar Pcl^2 √(3 - 3 v^2) #1^5 + 98560 A Pcl^3 √(3 - 3 v^2) #1^5 + 5184 Pbar^3 #1^6 -
    14290 Pbar^2 Pcl #1^6 + 13028 Pbar Pcl^2 #1^6 - 3922 Pcl^3 #1^6 + 2784 A^2 Pcl^3 #1^6 -
    2784 A^2 Pcl^3 v^2 #1^6 - 20928 A Pbar Pcl^2 √(3 - 3 v^2) #1^6 + 20928 A Pcl^3 √(3 - 3 v^2) #1^6 +
    1920 Pbar^3 #1^7 - 4854 Pbar^2 Pcl #1^7 + 3948 Pbar Pcl^2 #1^7 - 1014 Pcl^3 #1^7 -
    6624 A^2 Pcl^3 #1^7 + 6624 A^2 Pcl^3 v^2 #1^7 - 1920 A Pbar Pcl^2 √(3 - 3 v^2) #1^7 +
    1920 A Pcl^3 √(3 - 3 v^2) #1^7 + 216 Pbar^3 #1^8 + 189 Pbar^2 Pcl #1^8 - 1026 Pbar Pcl^2 #1^8 +
    621 Pcl^3 #1^8 - 672 A^2 Pcl^3 #1^8 + 672 A^2 Pcl^3 v^2 #1^8 - 64 A Pbar Pcl^2 √(3 - 3 v^2) #1^8 +
    64 A Pcl^3 √(3 - 3 v^2) #1^8 + 8 Pbar^3 #1^9 + 223 Pbar^2 Pcl #1^9 - 470 Pbar Pcl^2 #1^9 +
    239 Pcl^3 #1^9 - 96 A^2 Pcl^3 #1^9 + 96 A^2 Pcl^3 v^2 #1^9 + 27 Pbar^2 Pcl #1^10 -
    54 Pbar Pcl^2 #1^10 + 27 Pcl^3 #1^10 + Pbar^2 Pcl #1^11 - 2 Pbar Pcl^2 #1^11 + Pcl^3 #1^11 &, 8]},
{γ → -√Root[-5832 Pbar^3 + 24057 Pbar^2 Pcl - 30618 Pbar Pcl^2 + 12393 Pcl^3 - 1944 Pbar^3 #1 +
    8019 Pbar^2 Pcl #1 - 10206 Pbar Pcl^2 #1 + 4131 Pcl^3 #1 + 17280 Pbar^3 #1^2 -
    107001 Pbar^2 Pcl #1^2 + 162162 Pbar Pcl^2 #1^2 - 72441 Pcl^3 #1^2 - 35424 A^2 Pcl^3 #1^2 +
    35424 A^2 Pcl^3 v^2 #1^2 - 46656 A Pbar Pcl^2 √(3 - 3 v^2) #1^2 + 46656 A Pcl^3 √(3 - 3 v^2) #1^2 +
    5824 Pbar^3 #1^3 + 57381 Pbar^2 Pcl #1^3 - 132234 Pbar Pcl^2 #1^3 + 69029 Pcl^3 #1^3 +
    128352 A^2 Pcl^3 #1^3 - 128352 A^2 Pcl^3 v^2 #1^3 - 155520 A Pbar Pcl^2 √(3 - 3 v^2) #1^3 +
    155520 A Pcl^3 √(3 - 3 v^2) #1^3 - 16848 Pbar^3 #1^4 + 31482 Pbar^2 Pcl #1^4 -
    12420 Pbar Pcl^2 #1^4 - 2214 Pcl^3 #1^4 - 163296 A^2 Pcl^3 #1^4 + 163296 A^2 Pcl^3 v^2 #1^4 -
    188352 A Pbar Pcl^2 √(3 - 3 v^2) #1^4 + 188352 A Pcl^3 √(3 - 3 v^2) #1^4 - 5808 Pbar^3 #1^5 +
    4766 Pbar^2 Pcl #1^5 + 7892 Pbar Pcl^2 #1^5 - 6850 Pcl^3 #1^5 + 74976 A^2 Pcl^3 #1^5 -
    74976 A^2 Pcl^3 v^2 #1^5 - 98560 A Pbar Pcl^2 √(3 - 3 v^2) #1^5 + 98560 A Pcl^3 √(3 - 3 v^2) #1^5 +
    5184 Pbar^3 #1^6 - 14290 Pbar^2 Pcl #1^6 + 13028 Pbar Pcl^2 #1^6 - 3922 Pcl^3 #1^6 +
    2784 A^2 Pcl^3 #1^6 - 2784 A^2 Pcl^3 v^2 #1^6 - 20928 A Pbar Pcl^2 √(3 - 3 v^2) #1^6 +
    20928 A Pcl^3 √(3 - 3 v^2) #1^6 + 1920 Pbar^3 #1^7 - 4854 Pbar^2 Pcl #1^7 + 3948 Pbar Pcl^2 #1^7 -
    1014 Pcl^3 #1^7 - 6624 A^2 Pcl^3 #1^7 + 6624 A^2 Pcl^3 v^2 #1^7 - 1920 A Pbar Pcl^2 √(3 - 3 v^2) #1^7 +
    1920 A Pcl^3 √(3 - 3 v^2) #1^7 + 216 Pbar^3 #1^8 + 189 Pbar^2 Pcl #1^8 - 1026 Pbar Pcl^2 #1^8 +
    621 Pcl^3 #1^8 - 672 A^2 Pcl^3 #1^8 + 672 A^2 Pcl^3 v^2 #1^8 - 64 A Pbar Pcl^2 √(3 - 3 v^2) #1^8 +
    64 A Pcl^3 √(3 - 3 v^2) #1^8 + 8 Pbar^3 #1^9 + 223 Pbar^2 Pcl #1^9 - 470 Pbar Pcl^2 #1^9 +
    239 Pcl^3 #1^9 - 96 A^2 Pcl^3 #1^9 + 96 A^2 Pcl^3 v^2 #1^9 + 27 Pbar^2 Pcl #1^10 -
    54 Pbar Pcl^2 #1^10 + 27 Pcl^3 #1^10 + Pbar^2 Pcl #1^11 - 2 Pbar Pcl^2 #1^11 + Pcl^3 #1^11 &, 9]},
{γ → √Root[-5832 Pbar^3 + 24057 Pbar^2 Pcl - 30618 Pbar Pcl^2 + 12393 Pcl^3 -
    1944 Pbar^3 #1 + 8019 Pbar^2 Pcl #1 - 10206 Pbar Pcl^2 #1 + 4131 Pcl^3 #1 +
    17280 Pbar^3 #1^2 - 107001 Pbar^2 Pcl #1^2 + 162162 Pbar Pcl^2 #1^2 - 72441 Pcl^3 #1^2 -
    35424 A^2 Pcl^3 #1^2 + 35424 A^2 Pcl^3 v^2 #1^2 - 46656 A Pbar Pcl^2 √(3 - 3 v^2) #1^2 +
    46656 A Pcl^3 √(3 - 3 v^2) #1^2 + 5824 Pbar^3 #1^3 + 57381 Pbar^2 Pcl #1^3 -
    132234 Pbar Pcl^2 #1^3 + 69029 Pcl^3 #1^3 + 128352 A^2 Pcl^3 #1^3 - 128352 A^2 Pcl^3 v^2 #1^3 -
    155520 A Pbar Pcl^2 √(3 - 3 v^2) #1^3 + 155520 A Pcl^3 √(3 - 3 v^2) #1^3 -
    16848 Pbar^3 #1^4 + 31482 Pbar^2 Pcl #1^4 - 12420 Pbar Pcl^2 #1^4 - 2214 Pcl^3 #1^4 -
```

$$163296\,A^2\,Pcl^3\,\#1^4 + 163296\,A^2\,Pcl^3\,\nu^2\,\#1^4 - 188352\,A\,Pbar\,Pcl^2\,\sqrt{3-3\,\nu^2}\,\#1^4 +$$
$$188352\,A\,Pcl^3\,\sqrt{3-3\,\nu^2}\,\#1^4 - 5808\,Pbar^3\,\#1^5 + 4766\,Pbar^2\,Pcl\,\#1^5 +$$
$$7892\,Pbar\,Pcl^2\,\#1^5 - 6850\,Pcl^3\,\#1^5 + 74976\,A^2\,Pcl^3\,\#1^5 - 74976\,A^2\,Pcl^3\,\nu^2\,\#1^5 -$$
$$98560\,A\,Pbar\,Pcl^2\,\sqrt{3-3\,\nu^2}\,\#1^5 + 98560\,A\,Pcl^3\,\sqrt{3-3\,\nu^2}\,\#1^5 + 5184\,Pbar^3\,\#1^6 -$$
$$14290\,Pbar^2\,Pcl\,\#1^6 + 13028\,Pbar\,Pcl^2\,\#1^6 - 3922\,Pcl^3\,\#1^6 + 2784\,A^2\,Pcl^3\,\#1^6 -$$
$$2784\,A^2\,Pcl^3\,\nu^2\,\#1^6 - 20928\,A\,Pbar\,Pcl^2\,\sqrt{3-3\,\nu^2}\,\#1^6 + 20928\,A\,Pcl^3\,\sqrt{3-3\,\nu^2}\,\#1^6 +$$
$$1920\,Pbar^3\,\#1^7 - 4854\,Pbar^2\,Pcl\,\#1^7 + 3948\,Pbar\,Pcl^2\,\#1^7 - 1014\,Pcl^3\,\#1^7 -$$
$$6624\,A^2\,Pcl^3\,\#1^7 + 6624\,A^2\,Pcl^3\,\nu^2\,\#1^7 - 1920\,A\,Pbar\,Pcl^2\,\sqrt{3-3\,\nu^2}\,\#1^7 +$$
$$1920\,A\,Pcl^3\,\sqrt{3-3\,\nu^2}\,\#1^7 + 216\,Pbar^3\,\#1^8 + 189\,Pbar^2\,Pcl\,\#1^8 - 1026\,Pbar\,Pcl^2\,\#1^8 +$$
$$621\,Pcl^3\,\#1^8 - 672\,A^2\,Pcl^3\,\#1^8 + 672\,A^2\,Pcl^3\,\nu^2\,\#1^8 - 64\,A\,Pbar\,Pcl^2\,\sqrt{3-3\,\nu^2}\,\#1^8 +$$
$$64\,A\,Pcl^3\,\sqrt{3-3\,\nu^2}\,\#1^8 + 8\,Pbar^3\,\#1^9 + 223\,Pbar^2\,Pcl\,\#1^9 - 470\,Pbar\,Pcl^2\,\#1^9 +$$
$$239\,Pcl^3\,\#1^9 - 96\,A^2\,Pcl^3\,\#1^9 + 96\,A^2\,Pcl^3\,\nu^2\,\#1^9 + 27\,Pbar^2\,Pcl\,\#1^{10} -$$
$$54\,Pbar\,Pcl^2\,\#1^{10} + 27\,Pcl^3\,\#1^{10} + Pbar^2\,Pcl\,\#1^{11} - 2\,Pbar\,Pcl^2\,\#1^{11} + Pcl^3\,\#1^{11}\,\&,\,9\Big]\Big\},$$

$$\Big\{\gamma \to -\sqrt{\text{Root}\Big[-5832\,Pbar^3 + 24057\,Pbar^2\,Pcl - 30618\,Pbar\,Pcl^2 + 12393\,Pcl^3 - 1944\,Pbar^3\,\#1 +$$
$$8019\,Pbar^2\,Pcl\,\#1 - 10206\,Pbar\,Pcl^2\,\#1 + 4131\,Pcl^3\,\#1 + 17280\,Pbar^3\,\#1^2 -$$
$$107001\,Pbar^2\,Pcl\,\#1^2 + 162162\,Pbar\,Pcl^2\,\#1^2 - 72441\,Pcl^3\,\#1^2 - 35424\,A^2\,Pcl^3\,\#1^2 +$$
$$35424\,A^2\,Pcl^3\,\nu^2\,\#1^2 - 46656\,A\,Pbar\,Pcl^2\,\sqrt{3-3\,\nu^2}\,\#1^2 + 46656\,A\,Pcl^3\,\sqrt{3-3\,\nu^2}\,\#1^2 +$$
$$5824\,Pbar^3\,\#1^3 + 57381\,Pbar^2\,Pcl\,\#1^3 - 132234\,Pbar\,Pcl^2\,\#1^3 + 69029\,Pcl^3\,\#1^3 +$$
$$128352\,A^2\,Pcl^3\,\#1^3 - 128352\,A^2\,Pcl^3\,\nu^2\,\#1^3 - 155520\,A\,Pbar\,Pcl^2\,\sqrt{3-3\,\nu^2}\,\#1^3 +$$
$$155520\,A\,Pcl^3\,\sqrt{3-3\,\nu^2}\,\#1^3 - 16848\,Pbar^3\,\#1^4 + 31482\,Pbar^2\,Pcl\,\#1^4 -$$
$$12420\,Pbar\,Pcl^2\,\#1^4 - 2214\,Pcl^3\,\#1^4 - 163296\,A^2\,Pcl^3\,\#1^4 + 163296\,A^2\,Pcl^3\,\nu^2\,\#1^4 -$$
$$188352\,A\,Pbar\,Pcl^2\,\sqrt{3-3\,\nu^2}\,\#1^4 + 188352\,A\,Pcl^3\,\sqrt{3-3\,\nu^2}\,\#1^4 - 5808\,Pbar^3\,\#1^5 +$$
$$4766\,Pbar^2\,Pcl\,\#1^5 + 7892\,Pbar\,Pcl^2\,\#1^5 - 6850\,Pcl^3\,\#1^5 + 74976\,A^2\,Pcl^3\,\#1^5 -$$
$$74976\,A^2\,Pcl^3\,\nu^2\,\#1^5 - 98560\,A\,Pbar\,Pcl^2\,\sqrt{3-3\,\nu^2}\,\#1^5 + 98560\,A\,Pcl^3\,\sqrt{3-3\,\nu^2}\,\#1^5 +$$
$$5184\,Pbar^3\,\#1^6 - 14290\,Pbar^2\,Pcl\,\#1^6 + 13028\,Pbar\,Pcl^2\,\#1^6 - 3922\,Pcl^3\,\#1^6 +$$
$$2784\,A^2\,Pcl^3\,\#1^6 - 2784\,A^2\,Pcl^3\,\nu^2\,\#1^6 - 20928\,A\,Pbar\,Pcl^2\,\sqrt{3-3\,\nu^2}\,\#1^6 +$$
$$20928\,A\,Pcl^3\,\sqrt{3-3\,\nu^2}\,\#1^6 + 1920\,Pbar^3\,\#1^7 - 4854\,Pbar^2\,Pcl\,\#1^7 + 3948\,Pbar\,Pcl^2\,\#1^7 -$$
$$1014\,Pcl^3\,\#1^7 - 6624\,A^2\,Pcl^3\,\#1^7 + 6624\,A^2\,Pcl^3\,\nu^2\,\#1^7 - 1920\,A\,Pbar\,Pcl^2\,\sqrt{3-3\,\nu^2}\,\#1^7 +$$
$$1920\,A\,Pcl^3\,\sqrt{3-3\,\nu^2}\,\#1^7 + 216\,Pbar^3\,\#1^8 + 189\,Pbar^2\,Pcl\,\#1^8 - 1026\,Pbar\,Pcl^2\,\#1^8 +$$
$$621\,Pcl^3\,\#1^8 - 672\,A^2\,Pcl^3\,\#1^8 + 672\,A^2\,Pcl^3\,\nu^2\,\#1^8 - 64\,A\,Pbar\,Pcl^2\,\sqrt{3-3\,\nu^2}\,\#1^8 +$$
$$64\,A\,Pcl^3\,\sqrt{3-3\,\nu^2}\,\#1^8 + 8\,Pbar^3\,\#1^9 + 223\,Pbar^2\,Pcl\,\#1^9 - 470\,Pbar\,Pcl^2\,\#1^9 +$$
$$239\,Pcl^3\,\#1^9 - 96\,A^2\,Pcl^3\,\#1^9 + 96\,A^2\,Pcl^3\,\nu^2\,\#1^9 + 27\,Pbar^2\,Pcl\,\#1^{10} -$$
$$54\,Pbar\,Pcl^2\,\#1^{10} + 27\,Pcl^3\,\#1^{10} + Pbar^2\,Pcl\,\#1^{11} - 2\,Pbar\,Pcl^2\,\#1^{11} + Pcl^3\,\#1^{11}\,\&,\,10\Big]\Big\},$$

$$\Big\{\gamma \to \sqrt{\text{Root}\Big[-5832\,Pbar^3 + 24057\,Pbar^2\,Pcl - 30618\,Pbar\,Pcl^2 + 12393\,Pcl^3 -$$
$$1944\,Pbar^3\,\#1 + 8019\,Pbar^2\,Pcl\,\#1 - 10206\,Pbar\,Pcl^2\,\#1 + 4131\,Pcl^3\,\#1 +$$
$$17280\,Pbar^3\,\#1^2 - 107001\,Pbar^2\,Pcl\,\#1^2 + 162162\,Pbar\,Pcl^2\,\#1^2 - 72441\,Pcl^3\,\#1^2 -$$
$$35424\,A^2\,Pcl^3\,\#1^2 + 35424\,A^2\,Pcl^3\,\nu^2\,\#1^2 - 46656\,A\,Pbar\,Pcl^2\,\sqrt{3-3\,\nu^2}\,\#1^2 +$$
$$46656\,A\,Pcl^3\,\sqrt{3-3\,\nu^2}\,\#1^2 + 5824\,Pbar^3\,\#1^3 + 57381\,Pbar^2\,Pcl\,\#1^3 -$$
$$132234\,Pbar\,Pcl^2\,\#1^3 + 69029\,Pcl^3\,\#1^3 + 128352\,A^2\,Pcl^3\,\#1^3 - 128352\,A^2\,Pcl^3\,\nu^2\,\#1^3 -$$
$$155520\,A\,Pbar\,Pcl^2\,\sqrt{3-3\,\nu^2}\,\#1^3 + 155520\,A\,Pcl^3\,\sqrt{3-3\,\nu^2}\,\#1^3 -$$
$$16848\,Pbar^3\,\#1^4 + 31482\,Pbar^2\,Pcl\,\#1^4 - 12420\,Pbar\,Pcl^2\,\#1^4 - 2214\,Pcl^3\,\#1^4 -$$
$$163296\,A^2\,Pcl^3\,\#1^4 + 163296\,A^2\,Pcl^3\,\nu^2\,\#1^4 - 188352\,A\,Pbar\,Pcl^2\,\sqrt{3-3\,\nu^2}\,\#1^4 +$$
$$188352\,A\,Pcl^3\,\sqrt{3-3\,\nu^2}\,\#1^4 - 5808\,Pbar^3\,\#1^5 + 4766\,Pbar^2\,Pcl\,\#1^5 +$$
$$7892\,Pbar\,Pcl^2\,\#1^5 - 6850\,Pcl^3\,\#1^5 + 74976\,A^2\,Pcl^3\,\#1^5 - 74976\,A^2\,Pcl^3\,\nu^2\,\#1^5 -$$
$$98560\,A\,Pbar\,Pcl^2\,\sqrt{3-3\,\nu^2}\,\#1^5 + 98560\,A\,Pcl^3\,\sqrt{3-3\,\nu^2}\,\#1^5 +$$
$$5184\,Pbar^3\,\#1^6 - 14290\,Pbar^2\,Pcl\,\#1^6 + 13028\,Pbar\,Pcl^2\,\#1^6 - 3922\,Pcl^3\,\#1^6 +$$
$$2784\,A^2\,Pcl^3\,\#1^6 - 2784\,A^2\,Pcl^3\,\nu^2\,\#1^6 - 20928\,A\,Pbar\,Pcl^2\,\sqrt{3-3\,\nu^2}\,\#1^6 +$$
$$20928\,A\,Pcl^3\,\sqrt{3-3\,\nu^2}\,\#1^6 + 1920\,Pbar^3\,\#1^7 - 4854\,Pbar^2\,Pcl\,\#1^7 +$$
$$3948\,Pbar\,Pcl^2\,\#1^7 - 1014\,Pcl^3\,\#1^7 - 6624\,A^2\,Pcl^3\,\#1^7 + 6624\,A^2\,Pcl^3\,\nu^2\,\#1^7 -$$
$$1920\,A\,Pbar\,Pcl^2\,\sqrt{3-3\,\nu^2}\,\#1^7 + 1920\,A\,Pcl^3\,\sqrt{3-3\,\nu^2}\,\#1^7 + 216\,Pbar^3\,\#1^8 +$$
$$189\,Pbar^2\,Pcl\,\#1^8 - 1026\,Pbar\,Pcl^2\,\#1^8 + 621\,Pcl^3\,\#1^8 - 672\,A^2\,Pcl^3\,\#1^8 +$$

```
672 A^2 Pcl^3 v^2 #1^8 - 64 A Pbar Pcl^2 Sqrt[3 - 3 v^2] #1^8 + 64 A Pcl^3 Sqrt[3 - 3 v^2] #1^8 +
8 Pbar^3 #1^9 + 223 Pbar^2 Pcl #1^9 - 470 Pbar Pcl^2 #1^9 + 239 Pcl^3 #1^9 -
96 A^2 Pcl^3 #1^9 + 96 A^2 Pcl^3 v^2 #1^9 + 27 Pbar^2 Pcl #1^10 - 54 Pbar Pcl^2 #1^10 +
27 Pcl^3 #1^10 + Pbar^2 Pcl #1^11 - 2 Pbar Pcl^2 #1^11 + Pcl^3 #1^11 &, 10]},
{γ → -Sqrt[Root[-5832 Pbar^3 + 24057 Pbar^2 Pcl - 30618 Pbar Pcl^2 + 12393 Pcl^3 - 1944 Pbar^3 #1 +
8019 Pbar^2 Pcl #1 - 10206 Pbar Pcl^2 #1 + 4131 Pcl^3 #1 + 17280 Pbar^3 #1^2 -
107001 Pbar^2 Pcl #1^2 + 162162 Pbar Pcl^2 #1^2 - 72441 Pcl^3 #1^2 - 35424 A^2 Pcl^3 #1^2 +
35424 A^2 Pcl^3 v^2 #1^2 - 46656 A Pbar Pcl^2 Sqrt[3 - 3 v^2] #1^2 + 46656 A Pcl^3 Sqrt[3 - 3 v^2] #1^2 +
5824 Pbar^3 #1^3 + 57381 Pbar^2 Pcl #1^3 - 132234 Pbar Pcl^2 #1^3 + 69029 Pcl^3 #1^3 +
128352 A^2 Pcl^3 #1^3 - 128352 A^2 Pcl^3 v^2 #1^3 - 155520 A Pbar Pcl^2 Sqrt[3 - 3 v^2] #1^3 +
155520 A Pcl^3 Sqrt[3 - 3 v^2] #1^3 - 16848 Pbar^3 #1^4 + 31482 Pbar^2 Pcl #1^4 -
12420 Pbar Pcl^2 #1^4 - 2214 Pcl^3 #1^4 - 163296 A^2 Pcl^3 #1^4 + 163296 A^2 Pcl^3 v^2 #1^4 -
188352 A Pbar Pcl^2 Sqrt[3 - 3 v^2] #1^4 + 188352 A Pcl^3 Sqrt[3 - 3 v^2] #1^4 - 5808 Pbar^3 #1^5 +
4766 Pbar^2 Pcl #1^5 + 7892 Pbar Pcl^2 #1^5 - 6850 Pcl^3 #1^5 + 74976 A^2 Pcl^3 #1^5 -
74976 A^2 Pcl^3 v^2 #1^5 - 98560 A Pbar Pcl^2 Sqrt[3 - 3 v^2] #1^5 + 98560 A Pcl^3 Sqrt[3 - 3 v^2] #1^5 +
5184 Pbar^3 #1^6 - 14290 Pbar^2 Pcl #1^6 + 13028 Pbar Pcl^2 #1^6 - 3922 Pcl^3 #1^6 +
2784 A^2 Pcl^3 #1^6 - 2784 A^2 Pcl^3 v^2 #1^6 - 20928 A Pbar Pcl^2 Sqrt[3 - 3 v^2] #1^6 +
20928 A Pcl^3 Sqrt[3 - 3 v^2] #1^6 + 1920 Pbar^3 #1^7 - 4854 Pbar^2 Pcl #1^7 + 3948 Pbar Pcl^2 #1^7 -
1014 Pcl^3 #1^7 - 6624 A^2 Pcl^3 #1^7 + 6624 A^2 Pcl^3 v^2 #1^7 - 1920 A Pbar Pcl^2 Sqrt[3 - 3 v^2] #1^7 +
1920 A Pcl^3 Sqrt[3 - 3 v^2] #1^7 + 216 Pbar^3 #1^8 + 189 Pbar^2 Pcl #1^8 - 1026 Pbar Pcl^2 #1^8 +
621 Pcl^3 #1^8 - 672 A^2 Pcl^3 #1^8 + 672 A^2 Pcl^3 v^2 #1^8 - 64 A Pbar Pcl^2 Sqrt[3 - 3 v^2] #1^8 +
64 A Pcl^3 Sqrt[3 - 3 v^2] #1^8 + 8 Pbar^3 #1^9 + 223 Pbar^2 Pcl #1^9 - 470 Pbar Pcl^2 #1^9 +
239 Pcl^3 #1^9 - 96 A^2 Pcl^3 #1^9 + 96 A^2 Pcl^3 v^2 #1^9 + 27 Pbar^2 Pcl #1^10 -
54 Pbar Pcl^2 #1^10 + 27 Pcl^3 #1^10 + Pbar^2 Pcl #1^11 - 2 Pbar Pcl^2 #1^11 + Pcl^3 #1^11 &, 11]},
{γ → Sqrt[Root[-5832 Pbar^3 + 24057 Pbar^2 Pcl - 30618 Pbar Pcl^2 + 12393 Pcl^3 -
1944 Pbar^3 #1 + 8019 Pbar^2 Pcl #1 - 10206 Pbar Pcl^2 #1 + 4131 Pcl^3 #1 +
17280 Pbar^3 #1^2 - 107001 Pbar^2 Pcl #1^2 + 162162 Pbar Pcl^2 #1^2 - 72441 Pcl^3 #1^2 -
35424 A^2 Pcl^3 #1^2 + 35424 A^2 Pcl^3 v^2 #1^2 - 46656 A Pbar Pcl^2 Sqrt[3 - 3 v^2] #1^2 +
46656 A Pcl^3 Sqrt[3 - 3 v^2] #1^2 + 5824 Pbar^3 #1^3 + 57381 Pbar^2 Pcl #1^3 -
132234 Pbar Pcl^2 #1^3 + 69029 Pcl^3 #1^3 + 128352 A^2 Pcl^3 #1^3 - 128352 A^2 Pcl^3 v^2 #1^3 -
155520 A Pbar Pcl^2 Sqrt[3 - 3 v^2] #1^3 + 155520 A Pcl^3 Sqrt[3 - 3 v^2] #1^3 -
16848 Pbar^3 #1^4 + 31482 Pbar^2 Pcl #1^4 - 12420 Pbar Pcl^2 #1^4 - 2214 Pcl^3 #1^4 -
163296 A^2 Pcl^3 #1^4 + 163296 A^2 Pcl^3 v^2 #1^4 - 188352 A Pbar Pcl^2 Sqrt[3 - 3 v^2] #1^4 +
188352 A Pcl^3 Sqrt[3 - 3 v^2] #1^4 - 5808 Pbar^3 #1^5 + 4766 Pbar^2 Pcl #1^5 +
7892 Pbar Pcl^2 #1^5 - 6850 Pcl^3 #1^5 + 74976 A^2 Pcl^3 #1^5 - 74976 A^2 Pcl^3 v^2 #1^5 -
98560 A Pbar Pcl^2 Sqrt[3 - 3 v^2] #1^5 + 98560 A Pcl^3 Sqrt[3 - 3 v^2] #1^5 +
5184 Pbar^3 #1^6 - 14290 Pbar^2 Pcl #1^6 + 13028 Pbar Pcl^2 #1^6 - 3922 Pcl^3 #1^6 +
2784 A^2 Pcl^3 #1^6 - 2784 A^2 Pcl^3 v^2 #1^6 - 20928 A Pbar Pcl^2 Sqrt[3 - 3 v^2] #1^6 +
20928 A Pcl^3 Sqrt[3 - 3 v^2] #1^6 + 1920 Pbar^3 #1^7 - 4854 Pbar^2 Pcl #1^7 +
3948 Pbar Pcl^2 #1^7 - 1014 Pcl^3 #1^7 - 6624 A^2 Pcl^3 #1^7 + 6624 A^2 Pcl^3 v^2 #1^7 -
1920 A Pbar Pcl^2 Sqrt[3 - 3 v^2] #1^7 + 1920 A Pcl^3 Sqrt[3 - 3 v^2] #1^7 + 216 Pbar^3 #1^8 +
189 Pbar^2 Pcl #1^8 - 1026 Pbar Pcl^2 #1^8 + 621 Pcl^3 #1^8 - 672 A^2 Pcl^3 #1^8 +
672 A^2 Pcl^3 v^2 #1^8 - 64 A Pbar Pcl^2 Sqrt[3 - 3 v^2] #1^8 + 64 A Pcl^3 Sqrt[3 - 3 v^2] #1^8 +
8 Pbar^3 #1^9 + 223 Pbar^2 Pcl #1^9 - 470 Pbar Pcl^2 #1^9 + 239 Pcl^3 #1^9 -
96 A^2 Pcl^3 #1^9 + 96 A^2 Pcl^3 v^2 #1^9 + 27 Pbar^2 Pcl #1^10 - 54 Pbar Pcl^2 #1^10 +
27 Pcl^3 #1^10 + Pbar^2 Pcl #1^11 - 2 Pbar Pcl^2 #1^11 + Pcl^3 #1^11 &, 11]}}
```

Bibliography

[1] Southwell R.V. (1913) "On the General Theory of Elastic Stability." *Philosophical Transactions* v. 213, p187-244

[2] Von Mises R. (1914) "Der Kritische Aussendruck Zylindrischer Rohre." *Z. Vereins Deutch Ing.* v. 58(19), p750-755

[3] Southwell R.V. (1915) "On the collapse of Tubes by External Pressure." *Philosophical Magazine* p67-77

[4] Von Mises R. (1929) "Der Kritische Aussendruck für Allseits Belastete Zylindrische Rohre." *StodolaFestchrift* p418-430

[5] Saunders H.E. and Windenburg D.F (1931) "Strength of Thin Cylindrical Shells under External Pressure." *Transactions of the ASME.* v. 53, p207-218

[6] Windenburg D.F. and Trilling C. (1934) "Collapse by Instability of Thin Cylindrical Shells under External Pressure." *Transactions of the ASME.* v. 56, p819-825

[7] Donnell L.H. (1934) "A New Theory for the Buckling of Thin Cylinders Under Axial Compression and Bending." *Transactions of the ASME.* v. 56, p795-806

[8] Timoshenko S. (1936) *Theory of Elastic Stability.* 1st Edition. McGraw-Hill Book Company, USA

[9] Biezeno C.B. and Koch J.J. (1938) "The Buckling of a Cylindrical Tank of Variable Wall Thickness Under External Pressure." *Proceedings of the Fifth International Congress for Applied Mechanics.*

[10] Donnell L.H. and Wan C.C. (1950) "Effect of Imperfections on the Buckling of Thin Cylinders and Columns Under Axial Compression." *ASME - Journal of Applied Mechanics.* v. 17(1), p73-83

[11] Holt M. (1952) "A Procedure for Determining the Allowable Out-of-Roundness for Vessels Under External Pressure." *Transactions of the ASME.* v. 74(7), p1225-1230

[12] Kennard E.H. (1953) "The New Approach to Shell Theory : Circular Cylindrical Shells." *Journal of Applied Mechanics.* v. 20(3), p33-40

[13] Galletly G.D. and Bart R. (1956) "Effects of Boundary Conditions and Intial Out-of-Roundness of the Strength of Thin-Walled Cylinders Subject to External Hydrostatic Pressure." *Journal of Applied Mechanics*, p351-358

[14] Donnell L.H. (1956) "Effect of Imperfections of Thin Cylinders under External Pressure." *Journal of Applied Mechanics.* v. 23(4), p569-575

[15] Lunchick M.E. and Short R.D.Jnr (1957) "Behaviour of Cylinders with Initial Shell Deflection." *Journal of Applied Mechanics.* v. 24(4), p559-564

[16] Timoshenko S. and Woinowsky-Krieger S. (1959) *Theory of Plates and Shells.* 2nd Edition. McGraw-Hill Book Company, Tokyo

[17] Sharman P.W. (1962) "Theoretical Interaction Equation for the Buckling of Circular Shells under Axial Compression and External Pressure." *Journal of the Aerospace Sciences.* v. 29, p878-879

[18] Flügge W. (1962) *Stresses in Shells.* 2nd Edition. Springer-Verlag, Germany

[19] Armenakàs A.E. and Herrmann G. (1963) "Buckling of Thin Shells under External Pressure." *Journal of Engineering Mechanics.* v. 89(EM3), p131-146

[20] Koiter (1963) "Elastic Stability and Postbuckling Behaviour." *Procedure on the Symposium on Non-linear Problems.* University of Winsconsin Press, p257-275

[21] Weingarten V.I. and Seide P. (1965) "Elastic Stability of Thin-Walled Cylindrical and Conical Shells under Axial Compression." *AIAA Journal* v. 3(3), p500-505

[22] Weingarten V.I. and Seide P. (1965) "Elastic Stability of Thin-Walled Cylindrical and Conical Shells under Combined External Pressure and Axial Compression." *AIAA Journal* v. 3(5), p913-920

[23] Hutchinson J. (1965) "Axial Buckling of Pressurized Imperfect Cylindrical Shells." *AIAA Journal.* v. 3(8), p1461-1466

[24] Hutchinson J. (1965) "Buckling of Imperfect Cylindrical Shells under Axial Compression and External Pressure." *AIAA Journal.* v. 3(10), p1968-1970

[25] Turner C.E. (1965) *Introduction to Plate and Shell Theory.* 1st Edition. Longmans, UK

[26] Bickell M.B. and Ruiz C. (1967) *Pressure Vessel Design and Analysis.* Macmillan

[27] Koiter (1967) "On the Stability of the Elastic Equilibrium." *NASA* v. F10, p833

[28] Arbocz J. and Babcock C.D.Jnr. (1969) "The Effect of General Imperfections on the Buckling of Cylindrical Shells." *Transactions of the ASME.* v. 36(1), p28-38

[29] Gill S.S. (1970) *The Stress Analysis of Pressure Vessels and Pressure Vessel Components.* Pergamon Press

[30] Babcock C.D.Jnr (1974) "Experiments in Shell Buckling." *Thin Shell Structures - Thoery, Experiment and Design.* Edited by Fung Y.C. and Sechler E.E. Prentice-Hall

[31] Seide P. (1974) "A Re-examination of Koiter's Theory of Initial Postbuckling Behaviour and Imperfection Sensitivity of Structures." *Thin Shell Structures - Thoery, Experiment and Design.* Edited by Fung Y.C. and Sechler E.E. Prentice-Hall

[32] Arbocz J. (1974) "The Effect of Initial Imperfections on Shell Stability." *Thin Shell Structures : Theory, Experiment and Design.* Edited by Fung Y.C. and Sechler E.E. Prentice-Hall

[33] Fung Y.C. and Sechler E.E. (1974) *Thin-Shell Structures : Theory, Experiment and Design.* Prentice-Hall, New-Jersey

[34] Brush D.O. and Almroth B.O. (1975) *Buckling of bars, Plates, and Shells.* McGraw-Hill Book Company, USA

[35] Donnell L.H. (1976) *Beams, Plates and Shells.* 1st Edition. McGraw-Hill Book Company, USA

[36] Tennyson R.C., Booton M. and Chan K.H. (1978) "Buckling of Short Cylinders Under Combined Loading." *Transactions of the ASME.* v. 45, p574-578

[37] Allen H.G. and Bulson P.S. (1980) *Background to Buckling.* 1st Edition. McGraw-Hill Book Company, USA

[38] ASME (1980) *Pressure Vessels.* ASME Boiler and Pressure Vessel Code, Section VIII.

[39] Arbocz J. (1982) "The Imperfection Data Bank, A Mean to Obtain Realistic Buckling Loads." *Buckling of Shells : Proceedings from a State-of-the-Art Coloquium.*

[40] Galletly G.D. and Pemsing K. (1982) "Buckling of Cylinders under Combined External Pressure and Axial Compression." *Collapse : The Buckling of Structures in Theory and Practice.* p505-527, Cambridge University Press.

[41] Reis A.J., Walker A.C. and Virtuoso F.E. (1982) "Externally Pressurized Cylindrical Shells : Buckling and Collapse under Combined Loading." *Collapse : The Buckling of Structures in Theory and Practice.* p481-491, Cambridge University Press

[42] Thompson J.M.T. and Hunt G.W. (1983) *Collapse : The Buckling of Structures in Theory and Practice. International Union of Theoretical and Applied Mechanics Symposium 1982* Cambridge University Press

[43] Kollár L. and Dulácska E. (1984) *Buckling of Shells for Engineers.* 1st Edition. John-Wiley and Sons, Hungary

[44] Harvey J.F. (1985) *Theory and Design of Pressure Vessels.* P.E. van Nostrand Reinhold Company

[45] Hunt G.W., Williams K.A.J. and Cowell R.G. (1986) "Hidden Symmetry Concepts in the Elastic Buckling of Axially-Loaded Cylinders." *International Journal of Solids and Structures.* v. 22(12), p1501-1515

[46] Yamada S. and Croll J.G.A. (1989) "Buckling Behaviour of Pressure Loaded Cylindrical Panels." *ASCE Journal of Engineering Mechanics.* v. 115(2), p327-344

[47] Jawad M.H. and Farr J.R. (1989) *Structural Analysis and Design of Process Equipment.* John-Wiley and Sons

[48] Rajagopalan K. (1990) *Storage Structures.* AA Balkema

[49] Mazurkiewicz Z.E. and Nagórski R.T. (1991) *Shells of Revolution.* Elsevier PWN-Polish Scientific Publishers, Warsaw

[50] Shen H. and Chen T. (1991) "Buckling and Postbuckling Behaviour of Cylindrical Shells under Combined External Pressure and Axial Compression." *Thin-Walled Structures.* v. 12, p321-334

[51] Abdelmoula R., Damil N. and Potier-Ferry M. (1992) "Influence of Distributed and Localised Imperfections on the Buckling of Cylindrical Shells under External Pressure." *International Journal of Solids and Structures.* v. 28(1), p1-25

[52] Joseph Stanley A. and Ganesan N. (1993) "Deformation of Cylindrical Shells with Discontinuity in Thickness Subjected to Axisymmetric Loading." *Journal of Computers and Structures.* v. 49(3), p495-505

[53] Joseph Stanley A. and Ganesan N. (1993) "Comparison of Shell Theories in the Analysis of Cylindrical Shells with Discontinuity in Thickness." *Journal of Computers and Structures.* v. 48(6), p1057-1071

[54] Yamada S. and Croll J.G.A. (1993) "Buckling and Postbuckling Characteristics of Pressure-Loaded Cylinders." *Journal of Applied Mechancis.* v. 60, p290-299

[55] Koiter W.T., Elishakoff I., Li Y.W. and Starnes J.H. (1994) "Buckling of an Axially Compressed Cylindrical Shell of Variable Thickness," *International Journal of Solids and Structures.* v. 31(6), p797-805

[56] Koiter W.T., Elishakoff I., Li Y.W. and Starnes J.H. (1994) "Buckling of an Axially Compressed Imperfect Cylindrical Shell of Variable Thickness," *Proceedings of the 35th AIAA/ASME/ASCE/AHS/ASC Structures, Structural Dynamics and Materials Conference.* v. 1, p277-289

[57] AD-Merkblatt (1995) *Design of Pressure Vessels.* B 0 and *Cylindrical Shells Subjected to External Overpressure.* B 6

[58] Schneider M.H., Feldes R.J., Halcomb J.R. and Hoff C.C (1995) "Stability Analysis of Perfect and Imperfect Cylinders using MSC Nastran Linear and Non-Linear Buckling." *MSC 1995 World User's Conference Proceedings.* Paper No. 27

[59] Arbocz J. and Hol J.M.A.M. (1995) "Collapse of Axially Compressed Cylindrical Shells with Random Imperfections." *Journal of Thin-Walled Structures.* v. 23, p131-158

[60] Croll J.G.A. (1995) "Towards a Rationally Based Elastic-Plastic Shell Buckling Design Methodology." *Journal of Thin-Walled Structures.* v. 23, p67-84

[61] Guggenberger W. (1995) "Buckling and postbuckling of Imperfect Cylindrical Shells Under External Pressure" *Journal of Thin-Walled Structures.* v. 23, p351-366

[62] Gere J.M. and Timoshenko S.P. (1995) *Mechanics of Materials.* 3rd Edition. Chapman and Hall, London

[63] Showkati H. and Ansourian P. (1996) "Influence of Primary Boundary Conditions on the Buckling of Shallow Cylindrical Shells." *Journal of Constructional Steel Research.* v. 36(1), p53-75

[64] Benham P.P., Crawford R.J. and Armstrong C.G. (1996) *Mechanics of Engineering Materials.* 2nd Edition. Longman, UK

[65] Jamal M., Midani M., Damil N. and Potier-Ferry M. (1999) "Influence of Localised Imperfections on the Buckling of Cylindrical Shells under Axial Compression." *International Journal of Solids and Structures.* v. 36, p441-464

[66] Yamada S. and Croll J.G.A. (1999) "Contributions to Understanding the Behaviour of Axially Compressed Cylinders." *International Journal of Applied Mechanics.* v. 66, p299-309

[67] Gusic G., Combescure A. and Jullien J.F. (2000) "The Influence of Thickness Variations on the Buckling of Cylindrical Shells under External Pressure." *International Journal of Computers and Structures.* v. 74, p461-477